INTERNATIONAL DOCTORAL
SCHOOL OF THE USC

Martina
Migliavacca

PhD Thesis

Engineering smart biomimetic nanocarriers for biomedical applications

Santiago de Compostela, 2023

Doctoral Programme in Materials Science

ESCOLA DE DOUTORAMENTO
INTERNACIONAL DA USC

DOCTORAL THESIS

ENGINEERING SMART BIOMIMETIC NANOCARRIERS FOR BIOMEDICAL APPLICATIONS

Author

Martina Migliavacca

Supervisor/s: Ester Polo, Beatriz Pelaz

Tutor: Ester Polo

PHD PROGRAMME IN MATERIALS SCIENCE

SANTIAGO DE COMPOSTELA

DECLARACIÓN DEL AUTOR/A DE LA TESIS

D./Dña. Martina Migliavacca

Título de la tesis: Engineering smart biomimetic nanocarriers for biomedical applications

Presento mi tesis, siguiendo el procedimiento adecuado al Reglamento y declaro que:

1) La tesis abarca los resultados de la elaboración de mi trabajo.
2) De ser el caso, en la tesis se hace referencia a las colaboraciones que tuvo este trabajo.
3) Confirmo que la tesis no incurre en ningún tipo de plagio de otros autores ni de trabajos presentados por mí para la obtención de otros títulos.
4) La tesis es la versión definitiva presentada para su defensa y coincide la versión impresa con la presentada en formato electrónico.

Y me comprometo a presentar el Compromiso Documental de Supervisión en el caso que el original no esté depositado en la Escuela.

En **Santiago de Compostela**, **01 de octubre de 2023**.

Firma electrónica

Acknowledgments

I would like to thank Ester Polo, Beatriz Pelaz, and Pablo del Pino (mis jefes) for giving me the opportunity to be part of the BioNanoTools team and for guiding me through all this journey not only professionally, but also from a personal point of view.

I am also thankful to each member of the BioNanoTools group. All of you have helped me, sometimes with ICP measurements, sometimes with nanoparticles, and sometimes with just a simple smile, making every day “un día maravilloso”.

I would like to extend my gratitude to the PLATMED project (Biomimetic platelet-derived nanomedicines for the treatment of thromboembolic stroke AC20/0041, 2021-2023, ISC III-AES 2020 Euronanomed III, USC, IDIS, University Caen-Normandy, GIP Cyceron of France, and McGill University of Canada), and in particular to Dr. F. Campos and Dr. C. Correa-Paz (IDIS, Spain), to Dr. D. Maysinger (McGill University, Canada), and to Dr. D. Vivien and Dr. M. Rubio (University Caen-Normandy, GIP Cyceron of France) for allowing me to contribute to the results achieved.

Moreover, I would like to thank Dr. M. Collado, P. Picallos (IDIS, Spain), Dr. M. A. Moreno Mateos, Dr. I. Moreno Sánchez (CABD/CSIC, Seville, Spain), Dr. D. Rodríguez Aguirre, and Dr. L. Montoliu (CNB/CSIC, Madrid, Spain) for contributing to enhancing the scientific value of this doctoral thesis.

Martina Migliavacca

Contents

List of abbreviations

AAV	Adeno-associated virus
ACE2	Angiotensin-converting enzyme 2
AKT	Protein kinase B
AP	Acute pancreatitis
ATTR	Transthyretin amyloidosis
AuNP	Gold nanoparticle
BBB	Blood-brain barrier
BCL-2	B-cell lymphoma-2
BMV	Bacterial membrane vesicle
CAR	Chimeric antigen receptor
Cas	CRISPR-associated
CBF	Cerebral blood flow
CDN	Cell-derived nanovesicle
COVID-19	Coronavirus disease 19
CP	Chlorpromazine
CPP	Cell-penetrating peptide
CQ	Chloroquine
CRDDS	Controlled release drug delivery system
CRISPR	Clustered regularly interspaced short palindromic repeat
CSM	Cellsome
CTC	Circulating tumor cell
DC	Dendritic cell
DDS	Drug delivery system
DLS	Dynamic light scattering
DMEM	Dulbecco's modified eagle medium
DOPE	1,2-dioleoyl-sn-glycero-3-phosphoethanolamine
DOTAP	1,2-dioleoyl-3-trimethylammonium-propane
DOX	Doxorubicin
DSB	Double-strand break
DSPC	1,2-distearoyl-sn-glycero-3-phosphocholine
DYN	Dynasore
ECM	Extracellular matrix
EDTA	Ethylenediaminetetraacetic acid
ENM	Engineered nanomaterial
EPR	Enhanced permeability and retention
EV	Extracellular vesicle

FBS	Fetal bovine serum
FC	Flow cytometry
FCSM	Fusogenic cellsome
FDA	Food and drug administration
FITC	Fluorescein isothiocyanate
GIT	Gastrointestinal tract
GSH	Glutathione
HA	Hemagglutinin
HEPES	4-(2-hydroxyethyl)-1-piperazineethanesulfonic acid
HEPN domain	Higher eukaryotes and prokaryotes nucleotide-binding domain
HR	Homologous recombination
ICP-OES	Inductively coupled plasma optical emission spectroscopy
IgG	Immunoglobulin G
iNP	Inorganic nanoparticle
MCA	Middle cerebral artery
MERS	Middle East respiratory syndrome
MES	2-(N-morpholino) ethanesulfonic acid
MBCD	Methyl-β-cyclodextrin
MOF	Metal-organic framework
MPS	Mononuclear phagocyte system
MRI	Magnetic resonance imaging
MTT	3-(4,5-dimethylthiazol-2-yl)-2,5-diphenyl-tetrazolium bromide

NHEJ	Non-homologous end joining
NNI	National nanotechnology initiative
NP	Nanoparticle
NSTC	National science and technology council
NTA	Nanoparticle tracking analysis
NYS	Nystatin
oNP	Organic nanoparticle
PAI-1	Plasminogen activator inhibitor-1
PAM	Protospacer-adjacent motif
PAMAM	Poly(amidoamine)
PBS	Phosphate buffer saline
PEI	Polyethyleneimine
PEG	Polyethylene Glycol
PI3K	Phosphatidylinositol 3-kinase
PIC	Proteases inhibitor cocktail
PLGA	Poly(lactic-co-glycolic acid)
PSF	Phagolysosomal Simulant Fluid
PSNP	Polystyrene nanoparticle
PTX	Paclitaxel
QD	Quantum dot
RBC	Red blood cell
RES	Reticuloendothelial system
ROS	Reactive oxygen species

rtPA	Recombinant tissue plasminogen activator
S protein	Spike glycoprotein
SARS	Severe acute respiratory syndrome
SARS-CoV-2	Severe acute respiratory syndrome coronavirus 2
SCAP	Senescent cell anti-apoptotic pathway
sgRNA	Single guide RNA
siRNA	Small interfering RNA
SLN	Solid lipid nanoparticle
SNARE	SNAP receptor
SNAP	Soluble *N*-ethylmaleimide-sensitive factor attachment proteins
TALEN	Transcription activator-like effector nuclease
UiO	Universitetet i Oslo (University of Oslo)
VSVG	Vesicular stomatitis virus G-protein
WHO	World health organization
ZFN	Zinc-finger nuclease

Summary

Nanotechnologies play a crucial role in the biomedical field, enabling significant advancements in disease diagnosis, therapy, and monitoring. The nanoscale dimensions of structures allow precise interaction with cells and tissues, enhancing treatment selectivity and efficacy. Nanoparticles (NPs) serve as drug delivery vehicles, enabling controlled and targeted release, thereby reducing side effects. Moreover, NPs can be functionalized for early biomarker detection, improving diagnostic accuracy. Nanotechnologies open new avenues for personalized medicine, tailoring treatments to individual characteristics. However, it is essential to consider safety and regulatory aspects, ensuring ethical and safe utilization of these innovations in the medical area.

Biomimetic nanocarriers are emerging as a pivotal innovation in the field of drug delivery, revolutionizing the precision, efficiency, and safety of therapeutic interventions. Drawing inspiration from natural systems, these nanoscale vehicles replicate cellular structures, optimizing interactions with biological components and overcoming traditional drug delivery limitations. Their pivotal role lies in their ability to overcome obstacles that hinder optimal drug transport within the body. These nanocarriers offer a multifaceted approach: encapsulating drugs to protect them from degradation, enhancing stability and bioavailability. This safeguarding effect extends to the controlled release of payloads, fostering sustained therapeutic concentrations over extended periods.

Biomimetic nanocarriers exhibit an inherent ability to target specific cells or tissues with remarkable accuracy, mitigating systemic side effects and enhancing drug efficacy. By mimicking the biological attributes of their source cells, these nanosystems circumvent immune detection, ensuring prolonged circulation and greater chances of reaching the intended site of action. The dynamic potential of biomimetic nanocarriers transcends conventional drug delivery constraints, promising a transformative impact across diverse medical fields. They enable tailored treatments for cancer, neurological disorders, and infections, capitalizing on their ability to reach the target site and evade the immune response.

Furthermore, biomimetic nanocarriers may facilitate personalized medicine by accommodating patient-specific characteristics. Customized modifications can fine-tune these carriers for individual requirements, optimizing drug dosage and minimizing adverse effects. The field of gene therapy also stands to benefit, as biomimetic nanocarriers allow precise delivery of gene-editing tools to target cells.

Although these advancements hold immense promises, challenges remain. Developing scalable and reproducible synthetic methods and ensuring long-term safety are crucial. Nevertheless, biomimetic nanocarriers represent a transformative paradigm in drug delivery. Their emulation of nature’s complexities grants unparalleled precision, elevating therapeutic outcomes while minimizing risks. The potential to tailor treatments, enhance drug stability, and target specific sites of action places biomimetic nanocarriers as a keystone of modern medicine, leading to a new era of precision and effectiveness in patient care.

Considering all of this, the main objective of this doctoral thesis is the design, development, and optimization of cell-derived nanovesicles employed for biomedical applications.

In the initial phase of this work (Chapter 1), nanovesicles were designed and developed from the plasma membrane of various cell lines (tumoral cells, cells from healthy tissues, and immune cells, etc.). This enabled the creation of a collection of cell-derived nanosystems (here called cellsomes, or CSMs), which, following comprehensive physicochemical and biological characterization, demonstrated the versatile nature of the obtained CSMs and thereby underscored the universality of the developed protocol. Specifically, the plasma membrane of both tumoral and non-tumoral cells was employed for the fabrication of these CSMs using a protocol that utilizes a key step of extrusion through nanosized polycarbonate membranes. This approach generates highly monodisperse solutions of biomimetic nanovesicles, ensuring uniformity in their final size distribution.

In Chapter 1, besides the optimization of the preparation protocol, one of the focuses was on investigating the ability of CSMs to retain cargos within their structures and how these cargos were released over extended time inside cells. This was achieved through the encapsulation of fluorescent molecules, such as Hoechst, facilitating the visualization of the release process through confocal microscopy. This approach allowed for a comprehensive understanding of the mechanisms governing cargo retention and controlled release dynamics of CSMs within cells.

However, the primary emphasis of this initial chapter revolved around characterizing the physicochemical properties of CSMs from various perspectives. One of these aspects is the homotypic targeting ability, enabling the precise interaction and recognition of CSMs with cells of the same origin. This intrinsic property has significant implications for enhancing the specificity and effectiveness of cellular interactions, serving as a foundation for their potential applications in targeted drug delivery and therapeutic interventions. Through an extensive study of the uptake of CSMs derived from various tumoral cell lines, it was possible to explore their interactions with different cell lines, encompassing both tumoral and non-tumoral cells, as well as a macrophage cell line. The comprehensive investigation shed light on the versatility and selectivity of CSMs interactions with diverse cell types, thereby enriching the understanding of their potential applications in tailored drug delivery and immune-related therapeutic strategies. The homotypic capabilities were remarkably demonstrated among the tumoral cell lines. The macrophage cell line also provided insights into the interaction between these biomimetic nanovesicles and cells of the immune system. The results indicate that cells of the immune system exhibit limited internalization of both tumoral-derived and non-tumoral-derived CSMs. This observation reinforces the hypothesis that, in addition to their biomimetic characteristics, these CSMs also possess stealth properties. The reduced uptake by immune cells suggests that the CSMs can effectively evade immune recognition, potentially enhancing their circulation time and allowing for more targeted interactions with desired cell types. This dual attribute of biomimicry and stealth properties further underscores the potential of CSMs as versatile carriers for drug delivery applications, minimizing unintended immune responses while optimizing therapeutic outcomes.

In Chapter 1, the endocytic mechanism of CSMs within cells was also explored. Various inhibitors targeting individual endocytic pathways were employed to specifically block distinct routes. However, these preliminary investigations provided only partial insights into the internalization mechanism of CSMs. Further studies are imperative to determine the precise internalization pathway.

Nevertheless, the obtained results suggest that the predominantly utilized mechanism for these nanovesicles is likely to be a clathrin-dependent endocytosis, a typical pathway among many other NPs. While these findings offer a glimpse into the cellular uptake mechanisms of CSMs, they underscore the need for more comprehensive investigations to unravel the intricate dynamics underlying their interactions with cells. This exploration contributes to the evolving understanding of CSMs behavior, paving the way for informed design strategies and tailored applications in the field of targeted drug delivery and nanomedicine.

In addition to investigating homotypic targeting between cells of different origins, this first chapter also explored a relatively understudied area in the literature: leveraging CSMs characteristics for targeting and drug delivery to senescent cells. Specifically, the study examined the potential application of senescent derived-CSMs in targeting and delivering therapeutic agents to senescent A549 tumoral cells, considering their unique cell cycle state. This exploration offered insights into the prospect of harnessing senescent derived CSMs as novel nanocarriers to target senescent cells, a promising avenue with implications for innovative therapeutic strategies and detection in cancer and aging-related conditions.

In the final part of this chapter, an initial attempt into the prospect of engineering CSMs was undertaken. CSMs were manufactured from modified cells that expressed the spike protein of SARS-CoV-2 on their surface. These cells underwent plasma membrane extraction, serving as the foundation for generating the resulting spike protein enhanced-CSMs. The primary objective of this study was to explore the enhancement of active targeting inherent to CSMs by leveraging spike protein expression. This innovative approach presents a chance to increasing the selective interactions of CSMs with specific target cells, paving the way for refined and sophisticated drug delivery systems. The integration of bioengineering principles into CSMs fabrication holds considerable promise for advancing the field of targeted drug delivery and personalized medicine.

The second chapter focuses on harnessing nanovesicles derived from platelets to address ischemic stroke treatment. Several critical factors need consideration, particularly the existing use of tissue plasminogen activator (tPA), an enzyme capable of dissolving blood clots. However, tPA encounters multiple issues, such as its inherent instability and propensity to degrade rapidly, limiting its therapeutic effectiveness. Moreover, despite its established clinical use, tPA short half-life and potential adverse effects raise concerns about its practical application. This chapter explores the potential of platelet-derived CSMs with rtPA encapsulated as a novel approach for ischemic stroke therapy, offering the prospect of overcoming the limitations associated with free tPA. By encapsulating therapeutic agents within these nanovesicles and capitalizing on their biomimetic nature, targeted drug delivery to stroke-affected regions becomes a viable strategy. This research represents a pivotal step towards addressing the challenges posed by traditional ischemic stroke treatments, fostering hope for improved therapeutic outcomes in stroke patients.

Specifically, platelet-derived CSMs were manufactured by optimizing the protocol, particularly in the critical steps, such as the purification method to remove the excess of the non-encapsulated tPA. This refinement ensured the production of CSMs with enhanced purity and stability, crucial for their successful application as drug carriers. Then, a comprehensive array of experiments was undertaken, encompassing both *in vitro* and *in vivo* evaluations.

Moreover, throughout the optimization process of the synthesis protocol, meticulous assessments of drug activity were conducted at each step. By addressing challenges associated with purification and encapsulation, the chapter aimed to establish a robust foundation for using platelet-derived CSMs as an innovative and effective strategy for ischemic stroke treatment. The optimization process not only enhances the therapeutic potential of these nanovesicles but also paves the way for more reliable and reproducible applications in the complex landscape of ischemic stroke therapy.

Furthermore, a particular emphasis was placed on assessing the most suitable storage condition for the encapsulated drug. The results demonstrated that lyophilization (freeze-drying) process facilitated the attainment of stable nanovesicles while maintaining the activity of the encapsulated rtPA over time. This achievement serves as a fundamental aspect for ensuring the prolonged shelf-life and therapeutic efficacy of the platelet-derived CSMs. The investigation into effective preservation techniques contributes significantly to the feasibility of translating this innovative approach into clinical applications. By maintaining the stability and functionality of the encapsulated drug, the potential for successful and impactful ischemic stroke treatment using platelet-derived CSMs might be heightened, offering new avenues for improving patient care and outcomes.

After refining the synthesis protocol, evaluating different purification methods, and conducting an initial biomedical application assessment, the second part of the doctoral thesis (Chapters 3 and 4) explore the potential surface modification of CSMs to modulate their properties. This was achieved by introducing a specific combination of lipids, imparting fusogenic properties to the nanovesicles. This strategic modification enhances the ability of CSMs to fuse with cell membranes, enabling direct release of cargo into the cytosol and bypassing endocytic pathways. This innovative engineering approach opens new possibilities for targeted drug delivery and gene therapy applications, harnessing the dynamic fusion capabilities of CSMs to amplify their therapeutic potential.

Specifically, drawing inspiration from literature about fusogenic liposomes, a distinct lipid combination was employed in the study. This combination comprised a cationic lipid, a neutral lipid, and a lipid with a fluorescent aromatic head group. This strategic mixture was utilized to create fusogenic CSMs (FCSMs). By capitalizing on the synergistic interactions of these lipids, the resulting FCSMs exhibited enhanced fusogenic properties, facilitating efficient fusion with cell membranes. This innovative approach leverages the fusion capabilities of FCSMs to promote cargo delivery directly into the cytosol, bypassing conventional endocytic processes. The incorporation of these specialized lipids signifies a paradigm shift in the design and functionality of CSMs, opening new avenues for targeted intracellular delivery and gene therapy applications. The integration of established principles from the field of fusogenic liposomes into the context of nanocarrier technology exhibits the dynamic evolution of cell-derived nanovesicles for advanced biomedical applications.

In Chapter 3, these FCSMs were utilized with the primary objective of releasing the gene editing tool, CRISPR/Cas complex, within the cellular environment. Leveraging the fusogenic nature of these nanovesicles, the cargo was effectively liberated directly into the cytoplasm, circumventing entrapment within the endolysosomal system. This breakthrough approach represents a significant advancement in gene delivery strategies, eliminating the hindrances posed by conventional endocytic pathways.

By enabling the direct delivery of the CRISPR/Cas complex to the cytoplasm, FCSMs hold immense promise for enhancing the precision and efficiency of gene therapy applications. This innovative utilization of FCSMs exemplifies their transformative potential in the field of molecular medicine, where precise intracellular cargo delivery plays a pivotal role in unlocking new frontiers of therapeutic interventions. For this purpose, two Cas proteins were selected. Cas9, a widely studied and commercially available protein, was chosen to optimize the encapsulation process within FCSMs and validate the functionality of this fusogenic nanosystems. Its DNA-targeting ability allowed for refinement and validation of the nanosystem, establishing the efficacy of the FCSM platform. Then, Cas13d, which targets RNA instead of DNA, was employed to develop a fusogenic nanocarrier with the aim of generating antiviral nanotherapeutics. Its RNA-targeting potential was harnessed for its distinct application in antiviral strategies, aligning with the evolving landscape of gene therapy and nanomedicine. Moreover, this differential utilization of Cas proteins within the context of FCSMs highlights the versatility of this platform, offering tailored solutions for diverse therapeutic challenges.

The final chapter of this doctoral thesis (Chapter 4) leverages the wealth of information acquired from the preceding studies to explore a slightly divergent biomedical application. In this context, CSMs and FCSMs were employed not as standalone nanovesicles for encapsulating molecules or drugs, as observed in the earlier chapters, but as biomimetic coatings for other type of synthetic NPs. This innovative approach capitalizes on the unique characteristics of CSMs and FCSMs to enhance the functionality of other types of synthetic nanomaterials. By utilizing CSMs and FCSMs as coatings, the surface properties of synthetic NPs can be fine-tuned, optimizing their interactions with biological systems. This novel approach combines insights from various aspects of this doctoral thesis, offering a versatile platform for designing enhanced nanomaterials for diverse biomedical applications. This culmination highlights the adaptability and transformative potential of CSMs and FCSMs in shaping the future landscape of advanced nanomedicine and targeted therapies.

For this purpose, two types of NPs were studied: polystyrene NPs (PSNPs) and metal-organic frameworks (MOFs). The former served as a foundational model to establish and refine the coating protocol, elucidate the endocytic mechanism of these biomimetic nanosystems, and conduct preliminary *in vitro* studies to confirm the functionality of the engineered fusogenic coating for intracellular delivery of PSNPs. By utilizing PSNPs as a model system, the coating methodology was optimized, laying the groundwork for subsequent studies with more complex NPs. Subsequently, MOFs were chosen due to their distinctive porous structures and controlled release properties. These MOFs were integrated as the core of the resulting core-shell nanostructures, facilitating the encapsulation and targeted delivery of therapeutic agents. The dual application of PSNPs and MOFs underscores the versatility of CSMs and FCSMs as coatings for enhancing the performance of various nanomaterials.

The utilization of these diverse NPs amplifies the potential for developing tailored and multifunctional nanosystems with intricate capabilities for precision drug delivery and therapeutic interventions. Within this chapter, nanometric-sized UiO-67 MOFs (nanoMOFs) NPs were employed as the solid core to construct core-shell structures, with these NPs being cloaked by either CSMs or FCSMs. A series of uptake studies were conducted to assess the efficiency of FCSMs in comparison to both CSMs and uncoated UiO-67 nanoMOFs.

These investigations aimed to determine the differential cellular interactions and uptake behaviors of these various nanosystems. By evaluating the uptake efficiency, the chapter elucidated the distinct advantages offered by FCSMs over CSMs and bare UiO-67 nanoMOFs, shedding light on the enhanced capabilities of the fusogenic coating in facilitating fast and efficient intracellular internalization. This comprehensive evaluation contributes to a deeper understanding of the potential benefits of utilizing biomimetic coatings for synthetic NPs, underscoring their role in advancing the field of nanomedicine and targeted drug delivery.

In the last part of this chapter, and indeed the entire doctoral thesis, this biomimetic and fusogenic nanosystem was employed as a coating for UiO-67 nanoMOFs. These MOF NPs, in turn, encapsulated a therapeutic drug, carboplatin. By capitalizing on the inherent properties of the biomimetic coating, the nanosystem aimed to enhance the targeted delivery and release of carboplatin. This core-shell strategy embodies a promising avenue for developing advanced drug delivery platforms, where the fusogenic coating facilitates controlled and targeted drug release, increasing the therapeutic potential of the encapsulated drug. The successful integration of the biomimetic cell-derived coating and the fusogenic surface modification with the UiO-67 core is the result of different studies conducted within this work to engineer innovative nanocarriers that hold immense promise for precise drug delivery strategies. This culmination underlines the significance of this research in paving the way for advancements in nanomedicine and personalized therapeutic interventions.

In conclusion, the work conducted throughout this doctoral thesis have revealed the versatility of cell membrane-derived nanovesicles, their tissue-specific targeting capabilities, and their innovative role cloaking NPs. Nevertheless, it is important to acknowledge that the findings presented are preliminary studies, serving as a foundation upon which more extensive investigations can be built.

Designing, producing, and optimizing fusogenic nanovesicles present a transformative opportunity for intracellular drug delivery. The integration of fusogenic properties not only enhances cellular uptake but also allows for direct cytoplasmic cargo release, bypassing endosomal entrapment. This innovation is aimed at enabling precise therapeutic targeting and maximizing efficient drug delivery while mitigating potential drug degradation. As coatings for synthetic NPs, these fusogenic nanovesicles amplify the NPs cellular interactions and internalization, optimizing their therapeutic potential. Moreover, as standalone nanovesicles, they offer the unique ability to encapsulate and deliver diverse cargos with tailored physicochemical features. This multifaceted approach capitalizes on the synergistic combination of biomimetic cell membrane components and fusogenic attributes, paving the way for revolutionary advancements in personalized medicine and targeted therapies.

While these preliminary studies have provided valuable insights into the behavior, functionality, and interactions of the developed nanosystems, further in-depth investigations are warranted. The transition to *in vivo* experiments, for instance, could offer a more comprehensive understanding of the nanosystems performance within living organisms, providing insights into their biodistribution, biocompatibility, and therapeutic efficacy.

These promising results highlight the exciting potential of this innovative approach, laying the groundwork for future research endeavors. By investigating deeper into the complexities of cellular interactions, cargo release dynamics, and *in vivo* responses, a more refined understanding of these biomimetic and fusogenic nanosystems can be attained. Such advancements are meant to contribute significantly to the field of nanomedicine, revolutionizing drug delivery strategies and offering tailored therapeutic solutions for a myriad of biomedical applications.

Resumo

As nanotecnoloxías desempeñan un papel crucial no campo biomédico, permitindo avances significativos no diagnóstico, a terapia e a vixilancia de enfermidades. As dimensións nanométricas das estruturas permiten unha interacción precisa coas células e os tecidos, mellorando a selectividade e eficacia do tratamento. As nanopartículas actúan como vehículos de administración de medicamentos, posibilitando a liberación controlada e dirixida, reducindo así os efectos secundarios. Ademais, as nanopartículas poden ser funcionalizadas para a detección temperá de biomarcadores, mellorando a precisión diagnóstica. As nanotecnoloxías abren novas vías para a medicina personalizada, adaptando os tratamentos ás características individuais. Con todo, é esencial considerar os aspectos de seguridade e regulación, asegurando a utilización ética e segura destas innovacións no ámbito médico.

Os nanocarriers biomiméticos están a emerxer como unha innovación crucial no campo da administración de medicamentos, revolucionando a precisión, eficiencia e seguridade das intervencións terapéuticas. Inspirados en sistemas naturais, estes vehículos a escala nanométrica replican estruturas celulares, optimizando as interaccións con compoñentes biolóxicos e superando as limitacións tradicionais da administración de medicamentos. O seu papel fundamental radica na súa capacidade para superar obstáculos que dificultan o transporte óptimo de medicamentos no corpo. Os nanocarriers ofrecen un enfoque multifacético: a encapsulación de medicamentos protéxeos da degradación, mellorando a estabilidade e a biodisponibilidad. Este efecto protector esténdese á liberación controlada de cargas terapéuticas, fomentando concentracións terapéuticas sostidas durante períodos prolongados.

Os nanocarriers biomiméticos exhiben unha capacidade inherente para dirixirse a células ou tecidos específicos cunha precisión notable, mitigando os efectos secundarios sistémicos e mellorando a eficacia dos medicamentos. Ao imitar os atributos biolóxicos das súas células de orixe, estes nanosistemas evitan a detección inmunológica, garantindo unha circulación prolongada e maiores posibilidades de chegar ao sitio de acción previsto. O potencial dinámico dos nanocarriers biomiméticos transcende as limitacións convencionais da administración de medicamentos, prometendo un impacto transformador en diversos ámbitos médicos. Permiten tratamentos personalizados para o cancro, trastornos neurolóxicos e infeccións, aproveitando a súa capacidade para chegar ao sitio obxectivo e evadir a resposta inmunológica.

Ademais, os nanocarriers biomiméticos poden facilitar a medicina personalizada ao adaptarse ás características específicas de cada paciente. As modificacións personalizadas poden afinar estes transportadores segundo os requisitos individuais, optimizando a dose de medicamentos e minimizando os efectos adversos. O campo da terapia génica tamén se beneficia, xa que os nanocarriers biomiméticos permiten a entrega precisa de ferramentas de edición xenética ás células obxectivo.

A pesar destas prometedoras innovacións, persisten desafíos. O desenvolvemento de métodos de sínteses escalables e reproducibles, así como garantir a seguridade a longo prazo, son cruciais. Con todo, os nanocarriers biomiméticos representan un paradigma transformador na entrega de medicamentos. A súa emulación das complexidades da natureza outorga unha precisión sen igual, elevando os resultados terapéuticos á vez que se minimizan os riscos. A capacidade de adaptar tratamentos, mellorar a estabilidade dos medicamentos e dirixirse a sitios específicos de acción posiciona aos nanocarriers biomiméticos como un piar da medicina moderna, inaugurando unha nova era de precisión e eficacia na atención ao paciente.

Considerando todo isto, o obxectivo principal desta tese doutoral é o deseño, desenvolvemento e optimización de nanovesículas derivadas de células empregadas para aplicacións biomédicas.

Na fase inicial deste traballo (Capítulo 1), deseñáronse e desenvolveron nanovesículas a partir da membrana plasmática de diversas liñas celulares. Isto permitiu a creación dunha colección de nanosistemas derivados de células (aquí chamados "cellsome" ou CSMs), que, tras unha caracterización físico-química e biolóxica exhaustiva, demostraron a natureza universal dos CSMs obtidos e, por tanto, subliñaron a universalidade do protocolo empregado. Especificamente, a membrana plasmática de células tanto tumorais como non tumorais utilizouse para a fabricación destes CSMs mediante un protocolo que emprega un paso crave de extrusión a través de membranas de policarbonato de tamaño nanométrico. Este enfoque xera solucións altamente monodispersas de nanovesículas biomiméticas, asegurando uniformidade nas súas características.

No Capítulo 1, ademais da optimización do protocolo de preparación, un dos enfoques centrouse en investigar a capacidade dos CSMs para reter cargas dentro das súas estruturas e como estas cargas liberábanse ao longo do tempo dentro das células. Isto logrouse mediante a encapsulación de moléculas fluorescentes como o Hoechst, facilitando a visualización do proceso de liberación a través da microscopía confocal. Este enfoque permitiu unha comprensión integral dos mecanismos que gobernan a retención de carga e a dinámica de liberación controlada dentro dos CSMs.

Con todo, a énfase principal deste primeiro capítulo virou ao redor da caracterización dos CSMs desde varias perspectivas. Un destes aspectos é a capacidade de direccionamiento homotípico, que permite a interacción e recoñecemento precisos dos CSMs con células do mesma orixe. Esta propiedade intrínseca ten implicacións significativas para mellorar a especificidade e a efectividade das interaccións celulares, servindo como base para as súas posibles aplicacións na entrega dirixida de fármacos e intervencións terapéuticas. A través dun estudo exhaustivo da captación de CSMs derivados de diversas liñas celulares tumorais, foi factible explorar as súas interaccións con diferentes liñas celulares, que abarcan tanto células tumorais como non tumorais, así como unha liña de células de macrófagos. A investigación exhaustiva lanzou luz sobre a versatilidade e selectividade das interaccións dos CSMs con diversos tipos celulares, enriquecendo así a comprensión das súas posibles aplicacións na entrega de fármacos personalizada e estratexias terapéuticas relacionadas co sistema inmunolóxico.

A liña celular de macrófagos tamén proporcionou información sobre a interacción entre estas nanovesículas biomiméticas e as células do sistema inmunolóxico. Os resultados indican que as células do sistema inmunolóxico mostran unha captación limitada tanto dos CSMs derivados de tumores como dos non tumorais. Esta observación reforza a hipótese de que, ademais das súas características biomiméticas, estes CSMs tamén posúen propiedades de evasión. A captación reducida polas células inmunitarias suxire que os CSMs poden evadir eficazmente o recoñecemento inmunolóxico, potenciando así o seu tempo de circulación e permitindo interaccións máis específicas cos tipos celulares desexados. Este atributo dual de biomimetismo e propiedades de evasión subliña aínda máis o potencial dos CSMs como transportadores versátiles para aplicacións de entrega de fármacos, minimizando respostas inmunitarias non desexadas mentres se optimizan os resultados terapéuticos.

No Capítulo 1, tamén se explorou o mecanismo endocítico dos CSMs dentro das células. Empregáronse diversos inhibidores que apuntaban a roteiros endocíticas individuais para bloquear especificamente roteiros distintos. Con todo, estas investigacións preliminares só proporcionaron perspectivas parciais sobre o mecanismo de internalización dos CSMs. Estudos adicionais son imperativos para determinar a vía de internalización precisa.

Con todo, os resultados obtidos suxiren que o mecanismo predominante empregado para estas nanovesículas probablemente sexa unha endocitosis dependente da clatrina, unha vía típica entre moitas outras nanopartículas. Aínda que estes achados ofrecen unha visión dos mecanismos de captación celular dos CSMs, subliñan a necesidade de investigacións máis exhaustivas para desentrañar a dinámica intrincada que subxace nas súas interaccións coas células. Esta exploración contribúe á comprensión en evolución do comportamento dos CSMs, achandando o camiño para estratexias de deseño informadas e aplicacións personalizadas no campo da administración dirixida de fármacos e a nanomedicina.

Ademais de investigar o direccionamiento homotípico entre células de diferentes orixes, este primeiro capítulo tamén explorou unha área relativamente pouca estudada na literatura: aproveitar as características dos CSMs para o direccionamiento e a administración de medicamentos a células senescentes. Especificamente, o estudo examinou a posible aplicación dos CSMs no direccionamiento e a entrega de axentes terapéuticos a células tumorais senescentes (A54), considerando o seu estado único no ciclo celular. Esta exploración ofreceu perspicacias sobre a perspectiva de aproveitar os CSMs como medio para abordar patoloxías asociadas á senescencia, unha vía prometedora con implicacións para estratexias terapéuticas innovadoras e intervencións en condicións relacionadas co cancro e o envellecemento.

Na parte final deste capítulo, levou a cabo un intento inicial para explorar a posibilidade de enxeñería dos CSMs. Os CSMs foron fabricados a partir de células modificadas que expresaban a proteína spike na súa superficie. Estas células sometéronse a unha extracción de membrana plasmática, servindo como base para xerar os CSMs resultantes. O obxectivo principal deste estudo foi explorar a mellora do direccionamiento activo inherente aos CSMs mediante a utilización da expresión da proteína spike. Este enfoque innovador ofrece a oportunidade de aumentar as interaccións selectivas dos CSMs con células obxectivo específicas, achandando o camiño para sistemas de administración de medicamentos refinados e sofisticados. A integración dos principios da bioenxeñaría na fabricación dos CSMs ten un gran potencial para avanzar no campo da administración de medicamentos dirixida e a medicina personalizada.

O segundo capítulo céntrase en aproveitar as nanovesículas derivadas das plaquetas para abordar o tratamento do accidente cerebrovascular isquémico. Varios factores críticos deben considerarse, particularmente o uso existente do activador de plasminógeno tisular (tPA), unha encima capaz de disolver coágulos sanguíneos. Con todo, o tPA enfronta múltiples problemas, como a súa inestabilidade inherente e a súa propensión para degradarse rapidamente, o que limita a súa eficacia terapéutica. Ademais, a pesar do seu uso clínico establecido, a curta vida media do tPA e os posibles efectos adversos expoñen preocupacións sobre a súa aplicación práctica. Este capítulo explora o potencial das nanovesículas derivadas de plaquetas como un enfoque novo para a terapia do accidente cerebrovascular isquémico, ofrecendo a posibilidade de superar as limitacións asociadas co tPA. Ao encapsular axentes terapéuticos dentro destas nanovesículas e aproveitar a súa natureza biomimética, a administración dirixida de medicamentos ás rexións afectadas polo accidente cerebrovascular convértese nunha estratexia viable. Esta investigación representa un paso fundamental para abordar os desafíos expostos polos tratamentos tradicionais do accidente cerebrovascular isquémico, fomentando a esperanza de mellorar os resultados terapéuticos nos pacientes con accidente cerebrovascular. Especificamente, fabricáronse CSMs derivados de plaquetas optimizando o protocolo, especialmente nos pasos críticos, como o método de purificación para eliminar o exceso de tPA encapsulado. Esta refinación garantiu a produción de CSMs cunha maior pureza e estabilidade, crucial para a súa aplicación exitosa como transportadores de medicamentos. Logo, levou a cabo unha ampla variedade de experimentos, que abarcaron avaliacións tanto in vitro como in vivo.

Ademais, ao longo do proceso de optimización do protocolo de síntese, levaron a cabo meticulosas avaliacións da actividade do medicamento en cada paso. Ao abordar os desafíos asociados coa purificación e a encapsulación, o capítulo tivo como obxectivo establecer unha base sólida para utilizar CSMs derivados de plaquetas como unha estratexia innovadora e efectiva para o tratamento do accidente cerebrovascular isquémico. O proceso de optimización non só mellora o potencial terapéutico destas nanovesículas, senón que tamén achanda o camiño para aplicacións máis confiables e reproducibles no complexo panorama da terapia do accidente cerebrovascular isquémico.

Ademais, fíxose fincapé en avaliar a condición de almacenamento máis adecuada para o medicamento encapsulado. Os resultados demostraron que a liofilización facilitou a obtención de nanovesículas estables á vez que mantiña a actividade do tPA encapsulado ao longo do tempo. Este logro é un aspecto fundamental para garantir a vida útil prolongada e a eficacia terapéutica dos CSMs derivados de plaquetas. A investigación sobre técnicas efectivas de preservación contribúe de maneira significativa á viabilidade de traducir este enfoque innovador en aplicacións clínicas. Ao manter a estabilidade e funcionalidade do medicamento encapsulado, poderíase aumentar o potencial dunha terapia exitosa e cun grande impacto no tratamento do accidente cerebrovascular isquémico mediante CSMs derivados de plaquetas, ofrecendo novas oportunidades para mellorar a atención e os resultados dos pacientes.

Despois de refinar o protocolo de síntese, avaliar diferentes métodos de purificación e levar a cabo unha avaliación inicial de aplicación biomédica, a segunda parte da tese doutoral (Capítulos 3 e 4) explora a potencial modificación superficial dos CSMs.

Isto logrouse introducindo unha combinación específica de lípidos, outorgando propiedades fusoxénicas ás nanovesículas. Esta modificación estratéxica mellora a capacidade dos CSMs para fusionarse coas membranas celulares, permitindo a liberación directa da carga no citosol e evitando as vías de endocitosis. Este enfoque de enxeñería innovador abre novas posibilidades para a entrega dirixida de fármacos e as aplicacións de terapia xénica, aproveitando as capacidades dinámicas de fusión dos CSMs para amplificar o seu potencial terapéutico.

Especificamente, tomando inspiración da literatura sobre liposomas fusoxénicos, empregouse unha combinación única de lípidos no estudo. Esta combinación consistiu nun lípido catiónico, un lípido neutro e un lípido cun grupo aromático fluorescente na súa cabeza. Esta mestura estratéxica utilizouse para crear CSMs fusoxénicos (FCSMs). Aproveitando as interaccións sinérxicas destes lípidos, os FCSMs resultantes exhibiron propiedades fusoxénicas melloradas, facilitando a fusión eficiente coas membranas celulares. Este enfoque innovador aproveita as capacidades de fusión dos FCSMs para axilizar a entrega de carga directamente ao citosol, evitando os procesos endocíticos convencionais. A incorporación destes lípidos especializados representa un cambio de paradigma no deseño e funcionalidade dos CSMs, abrindo novas vías para a entrega intracelular dirixida e as aplicacións de terapia xénica. A integración de principios establecidos no campo dos liposomas fusoxénicos no contexto da tecnoloxía de nanovehículos mostra a evolución dinámica das nanovesículas derivadas de células para aplicacións biomédicas avanzadas.

No Capítulo 3, estes FCSMs utilizáronse co obxectivo principal de liberar o complexo CRISPR/Cas na contorna celular. Aproveitando a natureza fusoxénica destas nanovesículas, a carga liberouse eficazmente directamente no citoplasma, evitando a retención no sistema endolisosomal. Este enfoque innovador representa un avance significativo nas estratexias de entrega de xenes, eliminando os obstáculos expostos polas vías endocíticas convencionais.

Ao permitir a entrega directa do complexo CRISPR/Cas ao citoplasma, os FCSMs teñen un inmenso potencial para mellorar a precisión e eficiencia das aplicacións de terapia xénica. Esta utilización innovadora dos FCSMs exemplifica o seu potencial transformador no campo da medicina molecular, onde a entrega precisa de cargas intracelulares desempeña un papel fundamental para abrir novas fronteiras nas intervencións terapéuticas. Con este propósito, seleccionáronse dúas proteínas Cas: Cas9, unha proteína amplamente estudada e comercialmente dispoñible, elixiuse para optimizar o proceso de encapsulación dentro dos FCSMs e validar a funcionalidade deste nanosistema fusoxénico. A súa capacidade de dirixirse ao ADN permitiu o refinamento e a validación do nanosistema, establecendo a eficacia da plataforma FCSMs. Logo, utilizouse Cas13d, que se dirixe ao ARN en lugar do ADN, para desenvolver un nanocarrier fusoxénico co obxectivo de xerar nanoterapéuticos antivirais. O seu potencial de dirixirse ao ARN aproveitouse para a súa aplicación específica en estratexias antivirais, en liña co panorama en constante evolución da terapia xénica e a nanomedicina. Ademais, esta utilización diferencial das proteínas Cas no contexto dos FCSMs resalta a versatilidade desta plataforma, ofrecendo solucións adaptadas para diversos desafíos terapéuticos.

O capítulo final desta tese doutoral (Capítulo 4) aproveita a abundante información obtida dos estudos anteriores para explorar unha aplicación biomédica lixeiramente diverxente. Neste contexto, os CSMs e FCSMs utilizáronse non como nanovesículas independentes para encapsular moléculas ou fármacos, como se observou nos capítulos anteriores, senón como recubrimentos biomiméticos para nanopartículas inorgánicas. Este enfoque innovador capitaliza as características únicas dos CSMs e FCSMs para mellorar a funcionalidade dos nanomateriales inorgánicos. Ao utilizar os CSMs e FCSMs como recubrimentos, as propiedades superficiais das nanopartículas inorgánicas pódense axustar finamente, optimizando as súas interaccións cos sistemas biolóxicos. Este enfoque novo combina coñecementos de diversos aspectos desta tese doutoral, ofrecendo unha plataforma versátil para deseñar nanomateriales mellorados para diversas aplicacións biomédicas. Esta culminación destaca a adaptabilidade e o potencial transformador dos CSMs e FCSMs na configuración do futuro da nanomedicina avanzada e as terapias dirixidas.

Con este propósito, empregáronse dous tipos de nanopartículas: as nanopartículas de poliestireno (PSNPs) e os estruturas metaloorgánicas (MOFs). As primeiras serviron como modelo fundamental para establecer e refinar o protocolo de recubrimento, dilucidar o mecanismo endocítico destes nanosistemas biomiméticos e levar a cabo estudos *in vitro* preliminares para confirmar a funcionalidade do recubrimento fusoxénico deseñado para a liberación intracelular das PSNPs. Ao utilizar as PSNPs como sistema modelo, optimizouse a metodoloxía de recubrimento, sentando as bases para estudos posteriores con nanopartículas máis complexas. Posteriormente, elixíronse os MOFs debido ás súas estruturas porosas distintivas e propiedades de liberación controlada. Estes MOFs integráronse como o núcleo das nanoestructuras de tipo núcleo-cuberta resultantes, facilitando a encapsulación e entrega dirixida de axentes terapéuticos. A dobre aplicación das PSNPs e os MOFs subliña a versatilidade dos CSMs e FCSMs como recubrimentos para mellorar o rendemento de varios nanomateriales. A utilización destas diversas nanopartículas amplifica o potencial para desenvolver nanosistemas adaptados e multifuncionais con capacidades intricadas para a entrega precisa de fármacos e as intervencións terapéuticas. Dentro deste capítulo, empregáronse nanopartículas UiO-67 como o núcleo inorgánico para construír estruturas de tipo núcleo-cuberta, con estas nanopartículas sendo envolvidas xa sexa por CSMs ou FCSMs. levaron a cabo unha serie de estudos de captación para avaliar a eficiencia de FCSMs en comparación con CSMs e nanopartículas UiO-67 sen recubrir.

Estas investigacións tiveron como obxectivo determinar as interaccións celulares diferenciais e os comportamentos de captación destes diversos nanosistemas. Ao avaliar a eficiencia de captación, o capítulo dilucidou as vantaxes distintas ofrecidas por FCSMs en comparación con CSMs e as nanopartículas UiO-67 sen recubrir, lanzando luz sobre as capacidades melloradas do recubrimento fusoxénico para facilitar a internalización intracelular eficiente. Esta avaliación integral contribúe a unha comprensión máis profunda dos beneficios potenciais de utilizar recubrimentos biomiméticos para nanopartículas inorgánicas, subliñando o seu papel no avance do campo da nanomedicina e a entrega de medicamentos dirixida.

Na última parte deste capítulo, e de feito en toda a tese doutoral, este nanosistema biomimético e fusoxénico utilizouse como recubrimento para as nanopartículas UiO-67. Estas nanopartículas MOF, á súa vez, encapsularon un fármaco terapéutico, o carboplatino.

Aproveitando as propiedades inherentes do recubrimento biomimético, o nanosistema tiña como obxectivo mellorar a entrega e liberación dirixida do carboplatino. Esta estratexia de núcleo-cuberta encarna un prometedor enfoque para desenvolver plataformas avanzadas de entrega de medicamentos, onde o recubrimento fusoxénico facilita a liberación controlada e dirixida do fármaco, aumentando o potencial terapéutico do fármaco encapsulado. A exitosa integración do recubrimento biomimético derivado de células e a modificación da superficie fusoxénica co núcleo UiO-67 é o resultado de diferentes estudos realizados neste traballo para deseñar nanocarriers innovadores que teñen un inmenso potencial para estratexias de entrega de medicamentos precisas. Esta culminación resalta a importancia desta investigación para abrir camiño a avances na nanomedicina e as intervencións terapéuticas personalizadas.

En conclusión, o traballo realizado ao longo dos capítulos revelou a versatilidade das nanovesículas derivadas de membranas celulares, as súas capacidades de targeting específico a tecidos e o seu papel innovador como recubrimentos para nanopartículas inorgánicas. Con todo, é importante recoñecer que os descubrimentos presentados son estudos preliminares, que serven como base sobre a cal se poden construír investigacións máis extensas.

Deseñar, producir e optimizar nanovesículas fusoxénicas representa unha oportunidade transformadora para a entrega de fármacos intracelulares. A integración de propiedades fusoxénicas non só mellora a captación celular, senón que tamén permite a liberación directa da carga no citoplasma, evitando o atrapamiento nos endosomas. Esta innovación ten como obxectivo posibilitar un targeting terapéutico preciso e maximizar a entrega eficiente de fármacos, á vez que mitiga a posible degradación dos fármacos. Como recubrimentos para nanopartículas inorgánicas, estas nanovesículas fusoxénicas amplifican as interaccións celulares e a internalización das nanopartículas, optimizando o seu potencial terapéutico. Ademais, como nanovesículas independentes, ofrecen a capacidade única de encapsular e entregar diversas cargas con características físico-químicas adaptadas. Este enfoque multifacético aproveita a combinación sinérxica de compoñentes de membrana celular biomiméticos e atributos fusoxénicos, achandando o camiño para avances revolucionarios en medicina personalizada e terapias dirixidas.

Aínda que estes estudos preliminares han proporcionado coñecementos valiosos sobre o comportamento, a funcionalidade e as interaccións dos nanosistemas desenvolvidos, requírense investigacións máis exhaustivas en profundidade. A transición a experimentos *in vivo*, por exemplo, podería ofrecer unha comprensión máis completa do rendemento dos nanosistemas dentro de organismos vivos, brindando información sobre a súa biodistribución, biocompatibilidade e eficacia terapéutica.

Estes resultados prometedores resaltan o emocionante potencial deste enfoque innovador, sentando as bases para futuros proxectos de investigación. Ao investigar máis a fondo nas complexidades das interaccións celulares, a dinámica de liberación de cargas e as respostas *in vivo*, pódese lograr unha comprensión máis refinada destes nanosistemas biomiméticos e fusoxénicos. Tales avances están destinados a contribuír significativamente ao campo da nanomedicina, revolucionando as estratexias de entrega de fármacos e ofrecendo solucións terapéuticas personalizadas para unha variedade de aplicacións biomédicas.

1. Introduction

2

1.1. NANOBIOTECHNOLOGY IN BIOMEDICAL APPLICATIONS

Nanoscience represents the intersection of physics, materials science, and biology, focusing on the manipulation of materials at the atomic and molecular level[1]. On the other hand, nanotechnology involves the planning, creation, and utilization of materials and devices at the nanometer scale,[2] typically ranging from 1 to 100 nm in size (**Figure 1-1**).

Considered as one of the most promising technologies in the 21st century, nanotechnology applies the principles of nanoscience to practical applications across various domains. These applications span fields such as chemistry, physics, biology, medicine, engineering, and electronics. [1]

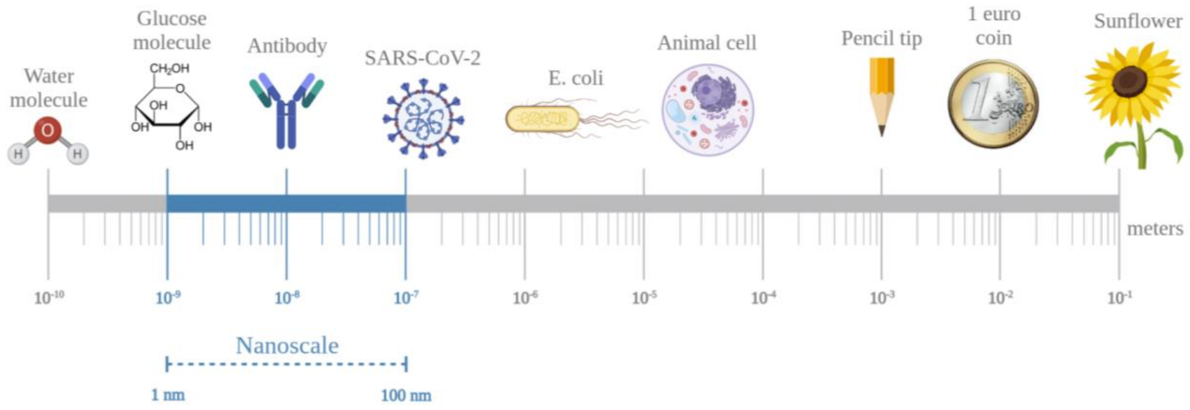

Figure 1-1 *Nanometer scale (in blue).*

Nanotechnology's idea was first brought to attention in 1959 by Richard Phillips Feynman, who, in his lecture "There's plenty of room at the bottom", explained the process of developing the ability to manipulate individual atoms and molecules. He discussed matter scaling concerns that would inevitably change the magnitude of several physical phenomena, such as gravity, which would become less important, or surface tension and Van der Waals attraction, that would acquire much more significance.[3]

The concept of nanobiotechnology was developed when the unique physicochemical properties of nanosized materials were applied to biological systems. These characteristics encompass dimensions, surface area, solubility, chemical makeup, form, agglomeration status, crystal structure, surface energy, surface charge, surface structure, and surface coating.[4] Since many of the biological machineries inside cells naturally occur at the nanoscale, it seemed straightforward for biomedical researchers to focus their efforts on the same natural scale. Thanks to nanobiotechnology it is now possible to improve, or even revolutionize, many technology and industry sectors.[5]

Over the last two decades enormous advances have been made in nanotechnology field, turning early possibilities into reality and contributing to economic growth and public health.[6]

Nanotechnologies have been shown to be advantageous for different disciplines that include data management, purification of water, drug delivery, and the creation of nanomaterials for healthcare and other industrial applications.[7] Among all, nanomedicine, defined as the application of nanotechnology and nanoscience to the prevention and treatment of human diseases, is surely one of the most challenging.

1.1.1. Nanomedicine

Nanomedicine is a particular branch of nanotechnology within the healthcare field, focused on diagnosis, treatment, and monitoring of current (including diabetes, cardiovascular diseases, neurodegenerative disorders, and cancer) and emerging (such as coronavirus disease 2019, COVID-19) diseases.[8]

Nanomedicine has progressed and evolved significantly since its conception in the 1990s.[9] Research in this scientific area has led to the development of novel nanobiomaterials and nanotherapeutics,[10] and improvements in diagnostics,[11] contrast reagents,[12] and medical devices.[13]

Nevertheless, nanomedicine progression during years led to a different trend which evolves further than its initial goal. If originally nanomedicine's aim was restricted to overcome the challenges of traditional drug delivery, limited to longer circulation times and reduced toxicities, now it seems to be much more sophisticated and innovative. Complex particles systems have been designed for controlled drug release, active targeting of diseases, and diversification of drug approaches beyond traditional therapeutics.[14-15]

The merging of therapeutic and diagnostic modalities is known as "theranostics" and there are several examples of products in pre-clinical and clinical trials. In the past decade, nanotheranostic industry exhibited great growth and development of emerging nanotherapeutics, which offer huge opportunities (but also face greater challenges) compared to traditional drugs.[10]

1.1.2. Drug delivery systems

Drug delivery systems (DDSs) refer to techniques employed to safely transport drugs to specific tissues, organs, cells, and subcellular organelles, with the aim of facilitating drug release and absorption using a range of drug carriers.[16]

Once the DDS enters the body, it follows a precise pharmacokinetic pathway, generally divided into five main steps: liberation, absorption, distribution, metabolism, and excretion. The liberation is the drug dissolution and release from its dosage form into the organism; the absorption dictates how the drug moves from the site of administration to circulation; the metabolism is the drug modification by liver enzymes rendering drug ineffective; the excretion is the elimination of the drug and/or the metabolites produced by the metabolism step.[17]

Conventional DDSs are usually eliminated from the body very quickly and the dose is barely maintained within the therapeutic window, which is the range of drug concentrations that provide therapeutic response without significant adverse effects. While controlled release DDSs (CRDDSs) are supposed to maintain the drug plasma levels at a constant concentration within the therapeutic window, therefore extending the desired therapeutic effect for a longer time.[17] Thus, CRDDSs offer many advantages compared to conventional DDSs, such as enhanced efficiency, reduced side effects and adverse reactions, which leads to greater drug potential. CRDDSs exploit vehicles for the delivery of drugs to the desired target sites, improving both the movement across biological membranes and the interactions with the biological environment.[18]

However, in designing a CRDDS, various factors and parameters need to be considered. For instance, biochemical properties such as the stability (half-life), the hepatic metabolism, the solubility, the partition coefficient, and the number of doses needed to reach the desired effect, are crucial for designing suitable CRDDS. These parameters can be both formulation-related and drug-related and their main function is to maximize the pharmacological response, while minimizing the drug toxicity.[18]

As mentioned, CRDDS require to be supported by vehicles (mostly in the nanoscale range) to carry out their functions. The need to deliver drugs to specific target sites led to the study and the development of engineered nanomaterials (ENMs), which may offer exciting opportunities in a wide range of applications for the diagnosis and treatment of human diseases. Due to their small size, ENMs are able to enter cells, interact with organelles, and significantly contribute to the improvement of not only CRDDS, but also contrast agents, photothermal mediators, and imaging effectors.[19] ENMs features have provided advantageous benefits over conventional methods for theranostics, such as the decrease of unwanted side effects and cytotoxicity of healthy cells, and their ability to reach target cells or tissues without diffusing to the adjacent areas. Yet, it is mandatory to address whether undesirable interactions occur between nanomaterials and the nanoscale machineries of biological systems.[20-21]

1.1.2.1. Biological barriers

Biological barriers serve as the primary biological impediments, with the purpose of thwarting unwanted access to delicate organs while permitting controlled and selective passage. These barriers primarily consist of closely interconnected cells, complemented by additional cells engaged in tasks such as clearance, immune responses, and other vital processes.[22]

Biological barriers such as skin,[23] air-blood lung barrier,[24] barriers in circulation,[25] blood-brain barrier,[26] and barriers of the reproductive system (**Figure 1-2**).[27] These barriers have a dual purpose: they defend their organ systems and enable the selective passage of specific substances like nutrients and signaling molecules.[28] The functioning of these barriers primarily relies on cells, which serve as the fundamental functional units. Within these cells, various organelles oversee the regulation of extracellular and intracellular access, as well as the transport of foreign substances.[29-30]

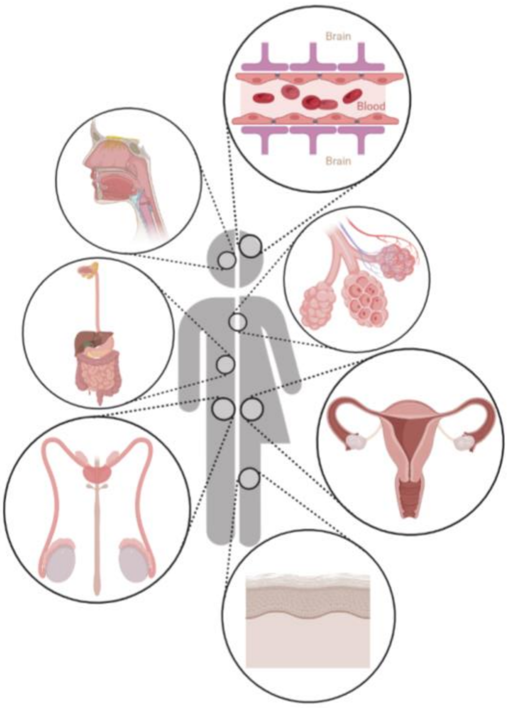

Figure 1-2 *Biological barriers. From the top, clockwise: blood-brain barrier, air-blood barrier, barrier of female reproductive system, skin, barrier of the male reproductive system, gastrointestinal tract, olfactory mucosa.*

In contrast to bulk materials, engineered nanomaterials (ENMs) display intricate physicochemical characteristics, encompassing factors such as size, shape, surface area, charge, chemical composition, crystalline structure, mechanical attributes, colloidal stability, porosity, and more. These individual or combined properties can influence how ENMs interact with a particular biological barrier.[31]

One of the first defenses that ENMs encounter is skin. Depending on their size and surface features, ENMs may gain entry through the intracellular pathway, involving the lipid channels between corneocytes, allowing them to penetrate deeper into the skin. Alternatively, they might utilize the appendage route by hitching a ride through hair follicles and sweat glands.[23] In specific instances, dermal exposure to ENMs could potentially enable their entry into the bloodstream and subsequently reach secondary organs. This process may lead to sub-lethal effects, including the induction of oxidative stress, inflammation, and photosensitization.[32]

ENMs may also face another significant obstacle in the form of the gastrointestinal tract (GIT). Entering this system can occur through various mechanisms, such as endocytosis by epithelial cells, transcytosis via the M-cell-rich layer of Peyer's Patches, persorption through openings in the gut lumen, and paracellular uptake, particularly in pathological conditions.[33-34]

Extensive research has been conducted on the air-blood barrier in the lungs. The manner in which particles are distributed within the lungs depends on their physicochemical attributes, predominantly their size and charge.[35-36] The size-dependent influence on distribution can be partially elucidated by considering the interaction of particles with lipids and proteins in the alveolar capillary membrane.

Micro-sized particles are efficiently recognized by alveolar macrophages.[37] On the other hand, smaller non-cationic particles, particularly those measuring less than 6 nm, can swiftly infiltrate the lymph nodes and the bloodstream, ultimately undergoing removal through renal elimination.[38]

The blood-brain barrier (BBB) achieves its remarkable selectivity primarily through the presence of tight junctions in the endothelial cells, further reinforced by interactions with astrocytes and pericytes. This collaboration results in a notably impermeable barrier, preventing the unregulated entry of substances into the brain. This rigorous control of influx is complemented by an efficient efflux transport system, promptly removing common foreign substances and particles that may accumulate in the brain. Together, these mechanisms safeguard the functionality of the central nervous system from external disturbances.[26] Engineered nanomaterials (ENMs) are known to penetrate the BBB through a transcytosis-mediated route.[39] An illustrative example of this is the transportation of transferrin across the BBB,[40] which is frequently employed as a surface modification to facilitate the delivery of therapeutic payloads through the BBB.[41-42]

Studies have revealed that delivering drugs through the olfactory mucosa represents an effective method to circumvent the BBB and enhance drug dispersion in the brain. This approach provides an alternative means of delivering drugs to the brain.[43]

In terms of the biological barriers within the reproductive system, dedicated cells and structures function as dynamic safeguards against dangerous agents. In the male reproductive system, Sertoli cells play a dual role: they support spermatogenesis within the seminiferous tubules and also serve as a crucial protective shield, preventing harmful substances from reaching germ cells.[37]

The female reproductive system comprises mucosal and epithelial barriers, with the addition of the placental barrier during pregnancy, serving as a complex and crucial component of the reproductive defense system. The permeability of the placental barrier varies depending on the stage of pregnancy, gradually increasing from the first to the third trimester.[44] Consequently, as pregnancy progresses, there may be an elevated likelihood for ENMs to cross the placenta.[37]

Gaining the ability to regulate biological barriers for the control of ENMs access is essential not only for deciphering the delicate balance between nanotoxicity and therapeutic possibilities but also for its growing importance in the field of nanomedicine. Given the multifaceted nature of nanosystems, it becomes crucial to adopt a nano-engineered strategy to address the structural and functional aspects of biological barriers. This approach aims to either prevent undesired access for potentially harmful particles or facilitate restricted access for therapeutic ENMs.[31]

1.1.2.2. Interactions with the immune system

The immune system has the ability to detect recurring patterns that resemble those found on pathogens like viruses. This remarkable capability enables the immune system to potentially produce antibodies against various chemical species, whether they come from natural or synthetic origin.[45]

Gaining a deeper understanding of how ENMs interact with the immune system is of utmost importance. This knowledge serves to comprehend the potential risks associated with these interactions and to harness them for the purpose of designing more effective nanotherapeutic interventions.[46]

The body's inherent biological barriers and elimination processes typically do a commendable job of preventing the entry of ENMs, and this usually does not trigger immune recognition mechanisms. Nonetheless, in numerous instances, ENMs can stimulate an immune response, leading to the removal of the foreign material. The key cellular actors in this response are predominantly phagocytes, which efficiently dispose of ENMs by engulfing and degrading them.[46]

As an example, injectable nanocarriers for cancer drugs administered intravenously are often referred to as “magic bullets” due to their remarkable ability to selectively target diseased tissues and cells while bypassing healthy ones.[47] Even so, the reality is that a significant portion of these cancer drug nanocarriers are identified and captured by the mononuclear phagocytic cells of the reticuloendothelial system (RES) found in the liver and spleen. This sequestration is often increased by the surface coating of ENMs with a protein corona, which can lead to opsonization and heightened phagocytosis by the RES.[48] The opsonization process of ENMs serves as the initial step in their sequestration, carried out by the mononuclear phagocyte system (MPS), primarily composed of phagocytic cells, including resident macrophages located in the spleen, lymph nodes, and liver. This leads to a substantial accumulation of ENMs in organs such as the spleen and liver, thus contributing to the non-specific distribution of nanotherapeutics to healthy organs.

Indeed, once ENMs are introduced into any biological environment, they undergo numerous chemical and physical transformations. They may agglomerate, which is a reversible process, or aggregate, which is irreversible, contingent on their surface chemistry and the environmental conditions at play. Aggregated nanomaterials are readily identified by phagocytes and are immediately taken up. When in contact with body’ fluids, nanomaterials typically adsorb proteins and other molecules from the plasma, giving rise to a bio-corona (or protein-corona) on their surface.[49-51]

An alternative situation to consider is that the binding of plasma proteins to the surface of ENMs could modify the conformation of these proteins. Consequently, these altered proteins may be perceived by innate immune cells as warning signals, leading to a notable inflammatory response.[46]

Modifications to the surface of ENMs, like the incorporation of polyethylene glycol (PEGylation), represent significant design elements aimed at mitigating non-specific uptake by macrophages. However, it is important to take into account their immunogenicity and other potential performance constraints.[52-53] Additionally, novel polysaccharides, whether of natural or synthetic origin, and reconstituted cellular membranes are emerging as promising alternatives for evading the RES.[54-55]

Nevertheless, the same ENMs interactions with the immune cells could potentially be exploited in a clinical setting. For instance, targeting ENMs to monocytes or macrophages could enable innovative therapeutic and diagnostic approaches.[56]

In addition, ENMs may be employed in vaccination strategies, as they can be considered as adjuvants or delivery vehicles for antigens, taking advantage of their propensity for dendritic cells (DCs) and other antigen-presenting cells uptake.[57]

1.1.2.3. ENMs-cells interactions

As mentioned above, the protein corona formation may lead to the process of opsonization. ENMs surface coating is composed by opsonins, particularly immunoglobulin G (IgG), via hydrophilic/hydrophobic, electrostatic, and van der Waals interactions, which effectively label them for phagocytosis ("eat me" signal). Otherwise, ENMs surface may be coated with CD47 glycoprotein and other self-peptides, making them able to bypass phagocytic recognition and clearance ("don't eat me" signal).[58]

ENMs encounter a sequence of cellular barriers, with cells often serving as the fundamental functional unit within these various barriers.[29] The outcomes of the interaction between ENMs and cells can be categorized into two phases: the initial particle-cell association and the subsequent internalization of the particles. As mentioned previously, the interaction between ENMs and cells is commonly facilitated by the formation of a protein corona within biological environments, and these interactions play a crucial role in determining the bioactivity of ENMs.[48] Moreover, the surface of ENMs itself can influence the structure and function of the adsorbed proteins, thereby affecting the recognition and cellular uptake of ENMs by cells.[59]

The protein corona essentially constitutes the biological identity of a NP. The process of protein adsorption on the NP's surface is primarily governed by the affinity interactions between proteins and the surface of the ENMs, as well as by interactions between proteins themselves, based on their affinity.[60] The composition of the protein corona can be classified into two categories based on the speed of exchange: hard and soft (**Figure 1-3**). Hard corona proteins directly adhere to the particle surface due to their strong binding affinity. This hard corona represents the initial layer of tightly bound proteins with a slow exchange rate, taking many hours to change. On the other hand, the soft corona comprises the second layer of proteins that associate with the hard corona through weaker protein-protein interactions (without direct binding to the ENMs), and these proteins undergo rapid exchanges over time, typically in seconds or minutes.[61]

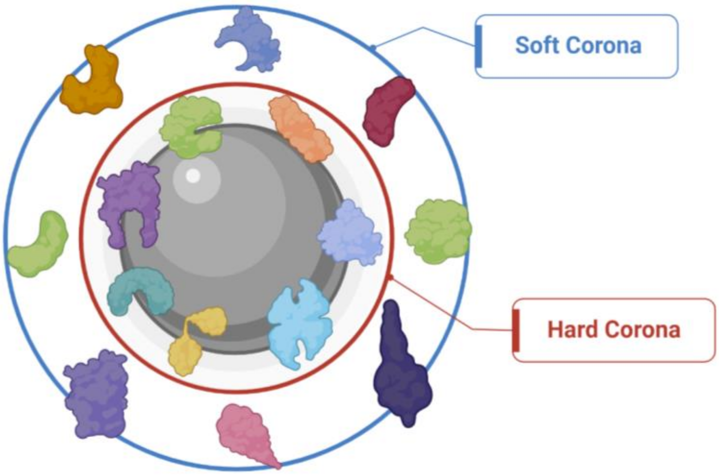

Figure 1-3 *Protein corona composition: hard corona proteins are directly adsorbed on the particle surface and show strong binding affinity and slow exchange time; while soft corona proteins are not directly bound to the particle surface because of their weak binding affinity for it, thus exhibiting shorter residence time.*

Surface properties, such as charge, play a crucial role in protein adsorption, which in turn affects ENMs pharmacokinetics and biodistribution. Highly cationic ENMs are rapidly cleared from circulation,[62] compared to highly anionic ENMs. In contrast, neutral ENMs, as well as those with a slight negative charge, show significantly extended circulating half-lives. This translates to improved accumulation in tumors, leading to recent research efforts aimed at functionalizing ENMs with zwitterionic surfaces.[63]

Despite their lower circulation time, positively charged ENMs show increased cellular uptake, therefore affecting ENMs bioavailability and cell membrane stability. Increased cellular uptake may affect the delicate balance between toxicity and therapeutic potential, given that effective drug delivery is reliant on efficient cellular uptake.[59]

ENMs with positively charged groups at their surface can induce disruption of plasma membrane. Such disruption is responsible for nanoholes formation.[64] In addition to holes formation, ENMs have been found to precipitate at the cell surface. Sometimes, this kind of ENMs agglomeration at the cell surface results in the disruption of cell function.[65]

Regarding the size, smaller ENMs interact with cell membrane by forming holes, whereas larger ENMs wrap a lipid bilayer around themselves.[66]

1.1.2.4. Passive and active targeting

At present, most nanotherapeutics are tailored for the treatment of cancer, and a significant portion of them is systemically administered to specifically target solid tumor sites, leveraging the enhanced permeability and retention (EPR) effect. The EPR effect theory is based on the observation that substances within the nanoscale range tend to exit the bloodstream and accumulate in tumor tissues to a greater extent compared to healthy tissues.

This phenomenon is attributed to the presence of enlarged fenestrated vasculature commonly found in many tumor tissues.[67] In fact, under certain conditions (inflammation/hypoxia, typical of tumoral environment), the endothelium of blood vessels becomes more permeable than in healthy state.[68]

The efficacy of the enhanced permeability and retention (EPR) effect, particularly in clinical applications, remains a subject of ongoing discussion. The success of the EPR effect varies from one case to another, with this diversity being partially attributed to the presence of the tumor stroma. The tumor stroma acts as both a physical and functional barrier that impedes the access of engineered nanomaterials (ENMs).[31] Recent studies conducted by Chan's group revealed that the dominant mechanism of NPs transport is an active process and not a passive trafficking into solid tumors.[69]

While demonstrating promise in preclinical studies, the effectiveness of the EPR effect for early-stage ENMs is greatly contingent on the specific type of cancer. Generally, the ideal "magic bullet" effect has not yet been consistently realized in patients.[70] The underlying principle of "leaky tumor blood vessels" remains incompletely understood from a cancer biology perspective. Vascular irregularities that contribute to the EPR effect include factors like enlarged tumor fenestrations, irregular angiogenic branching, and atypical vessel density, which have been frequently observed in various solid tumor models, as noted in reference.[71]

Studies have shown that in certain cancer types characterized by a dense dysplastic stroma, such as pancreatic cancer, the tumor vasculature is hindered by low perfusion due to the presence of pericytes and collagen deposition covering the blood vessels within the tumor. Therefore, apart from structural irregularities, factors like lymphatic drainage impairment, stromal effects, and non-cellular elements also contribute to the variability in the effectiveness of the EPR effect.[72]

In the case of non-permeable tumor types, it is yet to be established whether ENMs primarily enter through tumor fenestrations or employ an alternate mechanism.[72-74]

Nevertheless, research findings over the past decade concerning the effectiveness of ENMs in drug delivery reveal that merely 0.7% of the administered particle dose accumulates within solid tumors, with marginal improvement observed over time.[75] While a low accumulation rate may suggest reduced efficiency, scientists contend that the accumulation of ENMs at the tumor site does not necessarily imply that the active pharmaceutical ingredient is not effectively delivered or is not functioning within the tumor cells.[76]

From a physicochemical standpoint, the ideal hydrodynamic size for ENMs to exploit the enhanced permeability and retention (EPR) effect typically falls within the range of approximately 50-200 nm. Nevertheless, this optimal size can vary depending on the specific cancer type. ENMs carrying a negative charge or remaining neutral tend to exhibit fewer non-specific interactions with negatively charged biological membranes. However, a slight positive charge on the surface of the particles can be strategically utilized to enhance cellular uptake and promote efficient escape from lysosomes without causing any toxicity.[31]

The discovery and exploitation of EPR effect is commonly known as passive targeting. Since its theory only relies on greater extravasation towards tumor tissue, it lacks specificity. This limitation can be overcome by targeting tumors actively. ENMs can be targeted to the specific region of capillary endothelium to concentrate the drug and allow it to diffuse from the carrier to the target tissue. Hence, active targeting facilitates the active uptake of ENMs by the tumor cells themselves.[77]

Active targeting is typically achieved by aiming for the preferential accumulation of drugs within tumor tissues, individual cancer cells, specific intracellular organelles, or particular molecules. The inclusion of ligands on the surface of ENMs plays a pivotal role in determining their behavior within the body. ENMs equipped with specific recognition ligands attached to their surface demonstrate considerable potential for selective uptake at designated sites and enhanced precision in drug targeting.[78] This approach has been effectively employed to guide ENMs towards cell surface carbohydrates, receptors, and antigens.[79] The ligands affixed to the surface can encompass any molecule capable of selectively recognizing and binding to molecules present on target cells.[80] It is essential to utilize only those ligands that correspond to antigens or receptors that are overexpressed on cancer cells. Hormones such as estrogens,[81-82] glycoproteins like transferrin,[83] and folic acid[84-85] are the most widely used ligands for actively targeting different organs and tissues.

The combination of active and passive drug targeting, perhaps together with an imaging or diagnostic agent, would generate “smart” theranostic systems, able to monitor diseases progression and evaluate therapeutic efficacy in real time.[86]

1.1.2.5. Intracellular trafficking

When in contact with biological aqueous solutions, ENMs interact with a huge number of biological components, such as phospholipids, nucleic acids, proteins, cellular compartments, etc.[87]

After site-specific extravasation, ENMs undergo cellular internalization, enabling the cargo they carry to be released and exert therapeutic effects on cytoplasmic and nuclear targets. While low molecular weight hydrophobic molecules can simply diffuse through the cell’s plasma membrane, microscale and nanoscale supramolecular structures necessitate active uptake mechanisms.[88]

The discovery that positively charged ENMs are more readily uptaken by cells than their negatively charged counterparts has prompted the exploration of novel strategies for charge conversion. These approaches aim to modify the charge of particles in response to environmental triggers, such as fluctuations in pH.[89-90]

Endocytosis is a process by which cells absorb external molecules.[91] This process is commonly divided into two primary phenomena: phagocytosis and pinocytosis (**Figure 1-4**). Phagocytosis is a cellular process that outlines the mechanisms through which phagocytes eliminate foreign particles like ENMs present in the bloodstream.[92] While pinocytosis occurs by four different mechanisms: macropinocytosis, caveolin-dependent endocytosis, clathrin-dependent endocytosis, and clathrin/caveolin-independent endocytosis.[93-95]

Macropinocytosis is involved in the formation of lamellipodia-like plasma membrane extensions. ENMs of 200 nm in size can enter cells through macropinocytosis.[96]

Receptor-mediated endocytic mechanism is one of the main processes involved in ENMs uptake performed by cells. Briefly, cellular plasma membrane binds to ENMs through receptors, wraps around these particles and then cleaves to form vesicles. It is assisted by specific proteins, either clathrin or caveolae.[97] Clathrin coats and spherical caveolae have diameters of 100-200 nm and 50-80 nm, respectively. Clathrin-coated pits have the ability to collect only particles up to 100 nm and the uptake of ENMs in clathrin-dependent endocytosis is limited to receptor-bound ligands.[98-99] While in the case of caveolae-mediated endocytosis, the internalization of ENMs is more efficient for particles smaller than the caveolae, therefore restricting the internalization of larger particles.[100]

In typical mammalian cells without specialized functions, the process of clathrin-mediated endocytosis serves as the conventional mechanism that governs the cellular uptake of ENMs.[101] The endocytosis of ENMs encompasses their engulfment within membrane invaginations, leading to the creation of intracellular vesicles, known as endosomes. These endosomes ultimately fuse with lysosomes.[102] The lysosomes, characterized by their highly acidic environment and enzyme-rich content, play a significant role in breaking down organic particles, drugs, and, notably, genetic material degradation.[103]

Phagosomes and endosomes that are part of the clathrin-mediated endocytic pathways are ultimately directed toward lysosomes. In contrast, the caveolae-mediated mechanism of endocytosis leads to the creation of caveolae structures that detach from the plasma membrane and merge with caveosomes characterized by a neutral pH. In certain cases, this pathway has been demonstrated to bypass the route to lysosomes.[104]

Besides the caveolae-mediated endocytic pathway, it has been frequently hypothesized that cargo molecules associated with clathrin-independent uptake are endocytosed through lipid rafts-based mechanisms. Rafts are suggested to be lipid-based platforms for sorting and signaling that are particularly rich in cholesterol and sphingolipids.[105] The lipid raft hypothesis suggests that interactions between lipids can lead to the lateral organization of biological membranes, forming domains with unique structures, compositions, and functions, such as those involved in endocytosis.[106]

Caveolar and lipid rafts trafficking are strictly related. The two key pieces of evidence for this relationship are the enrichment of raft components in caveolae and the sensitivity of caveolae-mediated traffic to perturbation of raft lipids.[107] Similarly, several raft-associated proteins were shown to be included in caveolae[108] and to induce the genesis of caveolar trafficking intermediates upon their cross-linking, which stabilizes and fuse raft domains.[109] This crosslink-mediated raft blending might be the mechanism responsible for the internalization of pathogens or bacterial toxins.[110]

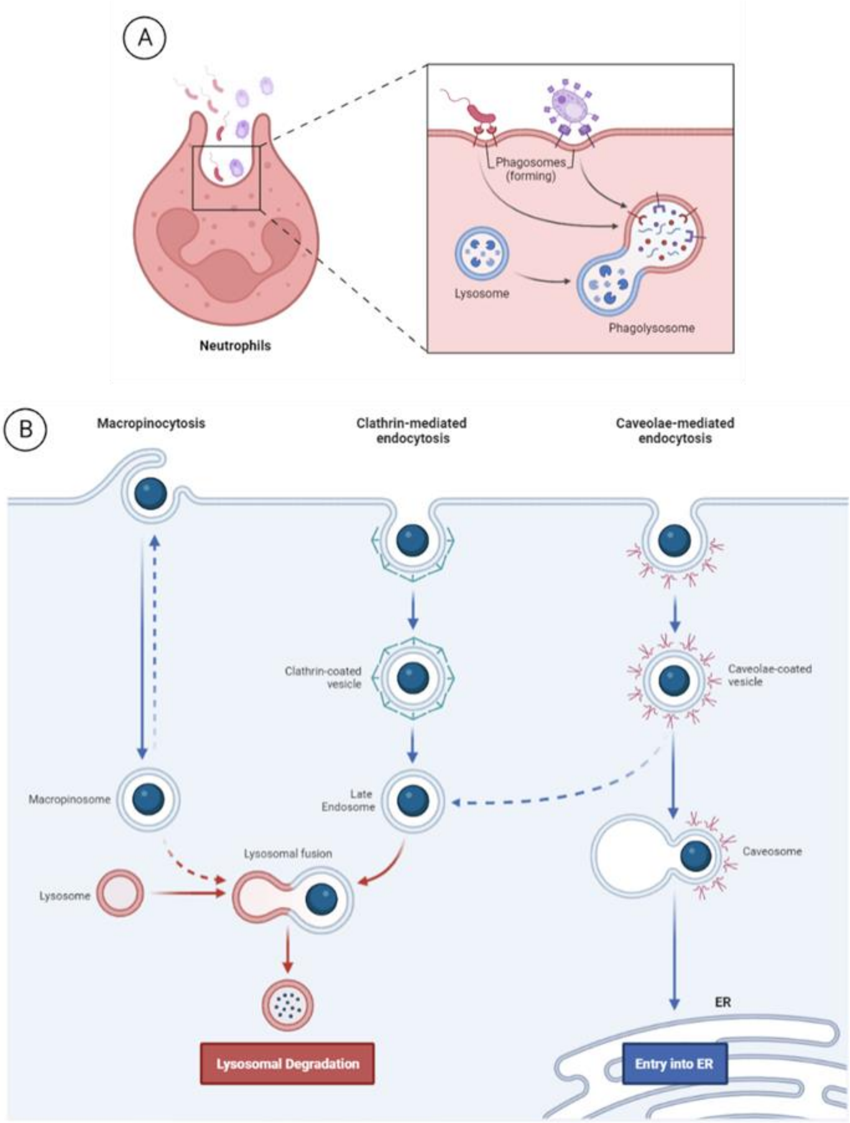

Figure 1-4 *Endocytosis processes: (A) phagocytosis versus (B) pinocytosis.*

Cellular internalization of ENMs could happen through any of these pathways depending on their size, shape, and nature. Endocytosed ENMs are usually confined to endosomes. However, endosomal uptake of ENMs can be avoided for instance by modifying their surface with cell-penetrating peptides (CPPs).[111]

In the light of highly degradative environment of the endosomes/lysosomes internalization, recent studies have focused on strategies aimed at promoting endosomal escape or lysosomal avoidance altogether.[112-114] Currently, the understanding of the different endosomal escape mechanisms is limited and still subjected to considerable debate, although it remains key to the rational design of efficient and nontoxic DDSs.[115]

One of the standard mechanisms through which ENMs can escape the endosomes is using osmotic pressure. According to the proton sponge effect proposed mechanism, during the acidification of the endosomes, ENMs can inhibit the drop in pH, causing the cell to continue pumping protons into the endosome in order to reach the desired pH. This results in an influx of chloride counterions and water molecules, which increases the pressure and eventually lyses the endosome.[116]

NPs have been designed to expand or swell in response to the decreased pH that occurs in the endo/lysosomes following endocytosis. There is evidence to suggest that these particles can aid in endosomal escape. However, the precise impact of this swelling phenomenon is still not fully understood.[117]

Endosomal escape can also be accomplished by inducing membrane destabilization. Directly disrupting the plasma membrane can significantly affect cell viability. To minimize cytotoxicity, it is vital to induce the destabilization of ENMs within the endo/lysosomal pathway. Typically, ENMs undergo a pH-induced transformation within the endo/lysosomal compartment, leading to the interaction of a hydrophobic region of the carrier with the lipid membrane.[118]

Nevertheless, perhaps the most efficient way to directly reach cytoplasmatic or nucleic targets is avoiding the endo/lysosomal entrapment. Some viruses are able to facilitate endosomal escape through fusion with the lipidic cell plasma membrane.[119] This mechanism can also be exploited by ENMs.[120] The challenge associated with this approach is to precisely regulate the fusion process, ensuring that it targets a specific cell or occurs exclusively within the endo/lysosomal compartment.

1.1.3. ENMs in drug delivery systems

ENMs have the potential to enhance drugs safety and efficacy by promoting solubility and stability of the encapsulated cargos, the transport across biological membranes, and prolonged circulation times.[88, 121] Thanks to the extensive research initiated and motivated by the National Nanotechnology Initiative (NNI) launched in 2000 by the US National Science and Technology Council (NSTC), the fabrication and clinical translation of promising nano-based drug formulations were facilitated within the market. Liposomes, lipid NPs, polymeric nanodrugs, and protein-based NPs are currently some of the nanoformulations available on the market, even though they only represent a small part compared to all the potential nano-based drugs designed and developed during the last 20 years.[122] Nanotechnology and nanomedicine, indeed, still need huge investigation efforts before actually reaching patients.[123]

This is mainly caused by a lack of understanding of the differences between animal models and humans, mostly how these differences influence the behavior and functionality of nanomedicine in the organism.[124] Another great limitation of nanomedicine success is heterogeneity among patients, both in disease biological settings and regarding patients themselves. This heterogeneity affects ENMs efficacy because the growth and physiology of diseased tissue alter particles functionality and distribution.[125]

1.1.3.1. Nanoparticles (iNPs vs oNPs)

NPs can be classified based on different criteria: considering the origin (natural or anthropogenic), the size (1-10 nm, 10-100 nm, over 100 nm), or the material. The latter is the most common criterium used in literature and also the one that better explains the correlation between matter composition and physicochemical properties.[126]

NPs are generally divided into inorganic and organic NPs (iNPs and oNPs), even though novel classes of nanostructured materials are emerging as promising alternatives for therapeutic applications (**Figure 1-5**).

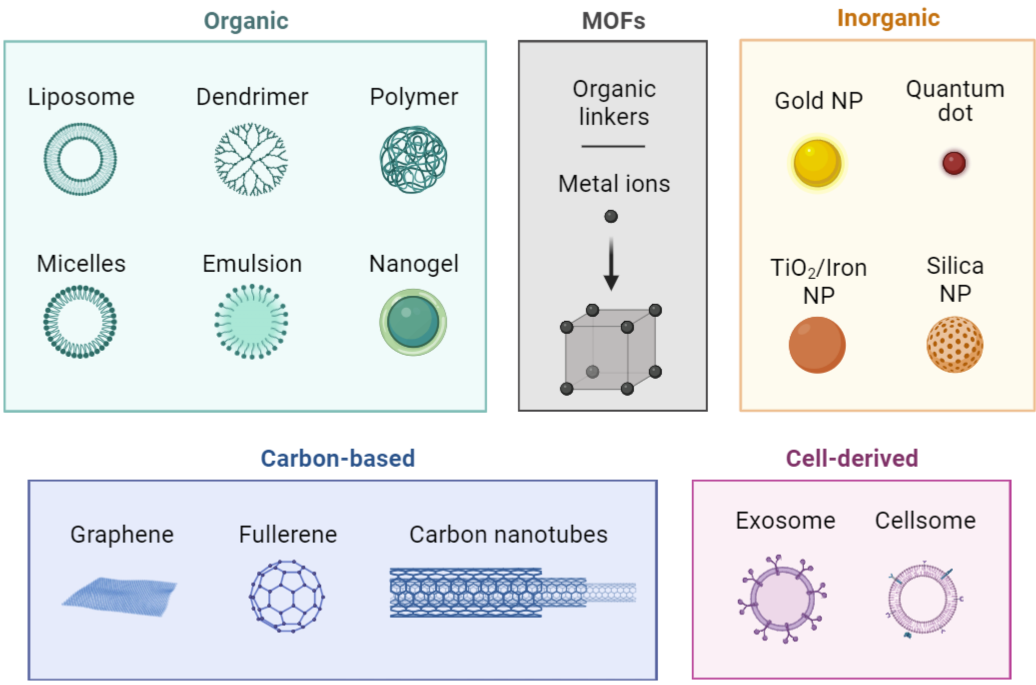

Figure 1-5 *Different types of NPs for therapeutic applications.*

Inorganic materials like gold, iron, and silica have been employed in the synthesis of ENMs for a wide range of drug delivery and imaging applications.[127] These iNPs are formulated *ad hoc* for the specific application and can be engineered to have a wide range of sizes, structures, and geometries. Additionally, iNPs have unique physical, electrical, magnetic, and optical properties, due to the characteristics of the base material they are made of.

Gold NPs (AuNPs), among the most studied, are synthesized and used in various geometries such as nanospheres, nanorods, nanostars, nanoshells, and nanocages.[128] AuNPs have free electrons at their surface that undergo continuous oscillation at a frequency determined by their size and shape, imparting photothermal properties to them.[129] AuNPs are also easily functionalized, conferring them great delivery capabilities.[128]

Iron oxide is another commonly researched material for iNPs synthesis and NPs made of iron oxide constitute the majority of Food and Drug Administration (FDA)-approved inorganic nanomedicines.[14] Magnetic iron oxide nanoparticles, often consisting of materials like magnetite (Fe_3O_4) or maghemite (Fe_2O_3), display superparamagnetic properties when they reach certain sizes. These nanoparticles have proven to be highly effective as contrast agents, drug delivery carriers, and for applications in thermal-based therapeutics.[130]

Calcium phosphate and mesoporous silica NPs are other deeply studied iNPs, which have been used successfully for gene and drug delivery.[131-132]

Quantum dots (QDs), typically composed of semiconducting materials like silicon, are distinctive nanoparticles widely utilized in *in vitro* imaging applications and hold potential for *in vivo* diagnostics.[133-134]

Due to their magnetic, radioactive, or plasmonic properties, iNPs are uniquely qualified for applications such as diagnostic, imaging, and therapy (e.g. photothermal). Despite their generally good biocompatibility, most are limited in clinical application because of low solubility and toxicity concerns, especially in formulations using heavy metals.[130, 135]

Metal-organic frameworks (MOFs) are a subgroup of coordination polymers. MOFs represent an appealing category of hybrid materials that blend inorganic and organic components. These materials consist of nodes containing metals (metal ions or clusters) and organic ligands, which can come together to create one-, two-, or three-dimensional structures,[136] theoretically generating infinite combination of structures (**Figure 1-6**). The other main feature of MOFs is their porosity, which occupy 90% of the free volume due to the structures present in the different pores, tunnels, and cages.[137] Compared to other porous materials, MOFs offer a notable advantage in that they can finely tune the host-guest interaction. This can be achieved not only by adjusting the pore size but also by functionalizing the building blocks with chemical groups, which allows for precise control over the kinetics of cargo release.[138]

MOFs have been recently investigated as potential nanocarriers in biomedical applications, acting as new therapeutic and/or diagnostic materials, among others. Even though clinical applications may not be accomplished in the near future, great progress in synthetic methodologies has already been achieved. Deep exploration of MOFs has yielded suitable stability and functionality, providing numerous advantages, including controlled delivery, sensing capacity, and biocatalytic activity.[139]

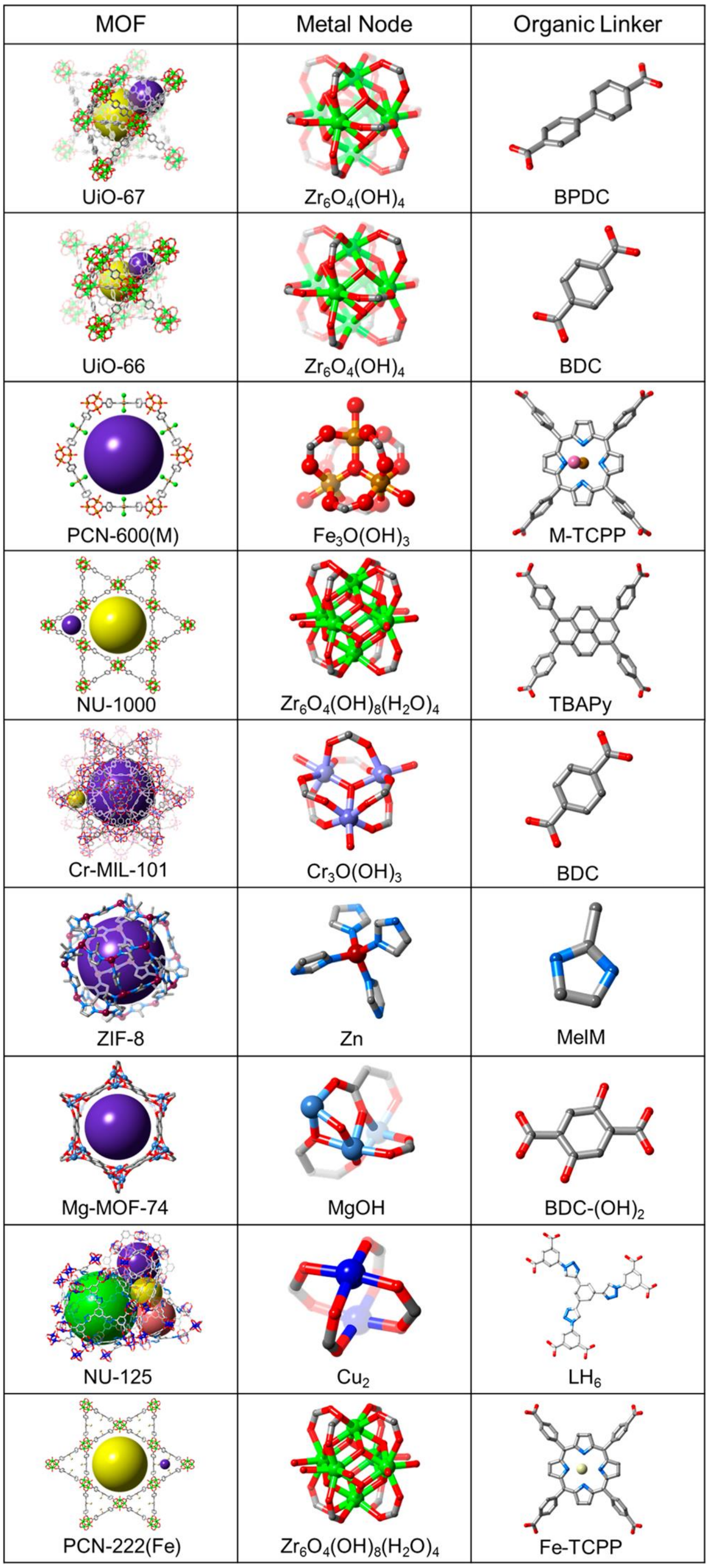

Figure 1-6 *Examples of different metal-organic frameworks (MOFs) structures with their corresponding metallic clusters and organic linkers (Zr: green; Fe: yellow; Cr: light purple; Zn: dark red; Mg: blue; Cu: royal blue; C: grey; O: red; N: light blue; Cl: pink).*[140]

Regarding organic NPs, polymeric NPs have been proved to be ideal candidates for drug delivery because they are biocompatible, water soluble, biodegradable, biomimetic, and stable during storage. Moreover, their surface can be easily modified for additional targeting.[141] They can be synthesized either from natural or synthetic materials, as well as monomers or preformed polymers, resulting in a wide variety of possible structures and properties.[125] They are considered as good vehicles because of their biocompatibility and simple formulation parameters. As carriers, they have several options: therapeutics can be encapsulated within the polymeric NP core, entrapped in the polymer matrix, chemically conjugated to the polymer, or bound to the NP surface. This advantage allows the delivery of different payloads including hydrophobic and hydrophilic compounds, as well as cargos with different molecular weights such as small molecules,[142] biological macromolecules,[143] proteins,[144] and vaccines,[145] making polymeric NPs ideal for co-delivery applications.[146] Properties such as composition, stability, responsivity, and surface charge can be properly modulated, therefore granting precise control of therapeutics loading efficacies and release kinetics.[147] Common structures of polymeric NPs are nanocapsules (cavities surrounded by a polymeric membrane or shell) and nanospheres (solid matrix systems). Polymeric NPs are further divided into shapes: polymersomes, micelles, and dendrimers.

Polymersomes are artificial vesicles similar to liposomes, whose membranes are made of amphiphilic block copolymers. They are reported to have improved stability and cargo-retention efficiency,[148] making them effective nanocarriers for therapeutics delivery to the cytosol.[149]

Polymeric micelles, which are also typically responsive block copolymers, tend to self-assemble to form nanospheres with a hydrophobic core and a hydrophilic coating. Thanks to this property they are able to protect drugs and improve circulation times. Micelles can load various therapeutic types, from small molecules to proteins,[150] and have been used for the delivery of cancer therapeutics in clinical trials.[151]

Dendrimers are highly structured hyperbranched polymers with intricate three-dimensional architectures that allow for precise control over their mass, size, shape, and surface chemistry. These dendrimers feature active functional groups on their exterior, which facilitate the attachment of biomolecules and contrast agents to the surface, while the core can be loaded with drugs. Dendrimers are versatile carriers capable of accommodating various types of cargo, although they are typically studied for the delivery of nucleic acids and small molecules.[152] Though, disadvantages of polymeric NPs may include toxicity and an increased risk of particle aggregation.[125]

Among organic NPs, lipid-based NPs comprise various structures but are typically spherical platforms composed by at least one lipid monolayer (in the case of solid lipid NPs) or one lipid bilayer (liposomes). In drug delivery, lipid-based NPs offer many advantages including biocompatibility, self-assembly, bioavailability, formulation simplicity, ability to load large cargos, and a range of physicochemical properties that can be controlled to modulate their biological characteristics.[153]

For these reasons, lipid-based NPs are within the most common class of FDA-approved nanomedicines.[154] For instance, due to the recent COVID-19 outbreak, lipid-based NPs have been deeply investigated and successfully reached the clinic for the delivery of small molecules such as mRNA.[155] Therefore, lipid-based NPs represent a promising nanocarrier platform to deliver a variety of therapeutic agents. However, their beneficial features have not only been extended to the pharmaceutical industry, but also to other fields, such as cosmetics.[156]

1.1.3.2. Lipid-based NPs

The diversity of lipid-based NPs applied in different research areas has grown over the last decade.[157] Liposomes, for instance, have had great impact on drug development and biomedical research, being one of the most promising nanocarriers for efficient drug and gene delivery.[158]

The term "liposome" was used for the first time in 1960s to name the structure that formed spontaneously in aqueous media and have been widely exploited since then, besides constituting the earliest nanomedicine used in drug delivery field.[157]

Liposomes are mainly composed by phospholipids and have a size that may range between 30 nm and 2 µm.[159] Phospholipids have an amphiphilic nature which trigger the formation of closed spherical vesicles in aqueous solutions. In presence of water, in fact, lipids tend to aggregate together (self-assemble) into a variety of structures, such as lipid bilayers, micelles, and/or vesicles. The geometry of these aggregates depends on the lipid structure.[160] Generally, single-chain lipids are known to form spherical micelles, whereas double-chain lipids having large head group area may form bilayers (or membranes) with all of their hydrophobic tails pointing towards the center of the membranes.[161]

Because of the amphiphilic nature of phospholipids, liposomes can be used as versatile tools regarding the molecules that can be encapsulated. While hydrophilic drugs are usually soluble in the aqueous core, hydrophobic ones are more likely inserted within the lipid bilayers. One of the most famous examples of liposomal nanoformulation is Doxil®, the first FDA-approved nano-drug (1995).[162] Doxil®, whose patent expired in 2010 (in US), is known to be a PEGylated unilamellar liposome encapsulating the precipitated compound Doxorubicin (DOX), a chemotherapeutic drug which intercalates DNA and inhibits the biosynthesis dynamics.

Cargo encapsulation in liposomal formulations can be achieved through passive or active loading. In passive targeting the encapsulation of the cargo takes place during the formation of the liposome and the use of hydrophobic molecules is advisable, leading to encapsulation efficiencies up to 100%.[159] Whereas, higher trapping effectiveness of hydrophilic molecules can be achievable with active loading using pH gradients. Following this strategy, pH-sensitive liposomes are designed to be stable at physiological pH but to lose their structural integrity at weakly acidic conditions. Therefore, cargo release can also be controlled based on pH values. Nevertheless, the capacity to either release the cargo in acidic environments or to fuse with other liposomes and endosome-like liposomes is reduced in PEGylated pH-sensitive liposomes, causing a significant reduction in the process effectiveness.[163]

Liposomes properties vary depending on several factors, such as lipidic composition, surface charge or even the preparation method.

Despite the numerous advantages that liposomes offer as DDSs compared to non-encapsulated drugs, other types of nanocarriers have emerged as alternatives to circumvent the challenges imposed by the use of liposomes.

Solid lipid NPs (SLNs), for instance, are composed by lipids that are solid at room and body temperature, being colloidal carrier nanosystems developed for the delivery of water-soluble drugs and nucleic acid therapeutics.[164] One of the main advantages of SLNs is their capability to protect the encapsulated drugs from proteolytic degradation before it reaches its target sites,[165] enhancing the drug release profile and increasing its therapeutic effect.

The choice of the lipidic composition not only permits to select between solid or soluble lipids, but also to tune the surface features of the NP, thus modulating the interactions between the nanosystem and the biological environment. For example, cationic lipid-based NPs (with ionizable groups) are emerging as promising non-viral vectors for nucleic acid delivery.[166] The first non-viral gene delivery system, Onpattro® (approved by the FDA in 2018), is a lipid-based nanosystem which delivers short interference RNA (siRNA) to the liver to silence the expression of the protein transthyretin in transthyretin amyloidosis (ATTR). Following the successful path of Onpattro®, lipid-based vaccines against the more recent COVID-19 (Comirnaty® from Pfizer/BioNTech and Spikevax® from Moderna) have surely contributed to demonstrate the enormous potential of lipid NPs in delivering nucleic acid cargos.

To date, all the current FDA-approved lipid-based nanoformulations exhibit a similar lipidic combination consisting of four main components: an ionizable cationic lipid, helper lipids including 1,2-distearoyl-sn-glycero-3-phosphocholine (DSPC) and cholesterol, and a PEG-lipid conjugate (**Figure 1-7**).[167]

Due to their acid-dissociation constant (pK_a between 6 and 7 for FDA-approved therapeutics), ionizable cationic lipids usually maintain a neutral charge in systemic circulation (pH = ~7.5) and become positively charged when the pH decrease. This key feature not only facilitate nucleic acid encapsulation (because of DNA/RNA negative charge), but also mediates the interaction with biological membranes (typically negatively charged). In particular, ionizable cationic lipids are designed both to mediate endosomal membrane disruption, thus enabling the nucleic acid release into the cytosol, and to promote the uptake of the lipid-based NP, either interacting directly with the negatively charged plasma membrane, or supporting cellular internalization through the binding to plasma proteins.[167]

PEG-lipids are reported to have different functions within the FDA-approved lipid-based NPs, such as particle monodispersity and stability,[168] encapsulation efficiency,[169] immune response,[170] and circulation half-life[169] by reducing renal- and macrophage-mediated hepatic clearance.

Regarding helper lipids, the hypothesis spread among researchers is that they would support stability during storage and systemic circulation.[171]

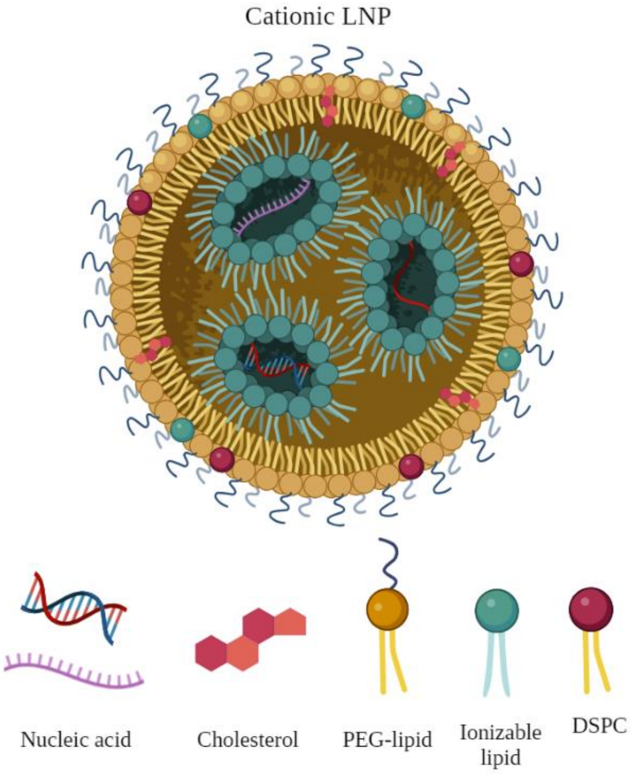

***Figure 1-7** Chemical composition of ionizable LNPs.*

1.1.3.3. Cell-derived nanoparticles

Despite the high number of preclinical studies that use synthetic complex NPs, their clinical trials performance remains inadequate. This is mainly due to the formation of a protein corona around the NPs complex, which triggers the immunological response before reaching its therapeutic target, limiting NPs surface ligands exposition to the biological environment. The components of this protein corona vary among the different animal models, making its detection quite challenging. Additionally, the ligands used to functionalize synthetic nanosystems may exhibit diverse orientations, distribution patterns, and concentrations, which can ultimately lower the efficiency of targeting.

While the inclusion of PEG in lipid-based NPs has been effective in extending their circulation half-life and has demonstrated its efficacy in mRNA vaccines against SARS-CoV-2, it is worth noting that at higher doses, it may trigger immunogenic responses and accelerate clearance, potentially leading to off-target release. Still, therapeutics such as Doxil®, Abraxane® or Myocet® remain the gold standard treatments in oncology.

Current approaches for cancer treatment based on bottom-up conjugation and delivery face challenges related to low specificity and efficacy due to the heterogeneity of tumors and the associated physiological barriers. In contrast, top-down systems, which involve biological exosomes and natural membrane-coated nanosystems, hold the potential to address these issues by maintaining and expressing structural and functional self-recognition markers.

Natural nanocarriers derived from biological sources inspired the fabrication of new structures that help to build biomimetic nanosystems mimicking the natural biological processes. Various bioinspired and biomimetic delivery systems for drug and gene delivery applications have been deeply investigated.

Among these, bacterial membrane vesicles (BMVs) are extracted from bacteria and can be used as smart drug delivery nanosystems due to their biomimetic properties and versatile functions. The advantages of BMVs are the possibility of scaling-up the production at lower costs compared to other biomimetic DDSs and the ease of modifying the surface either with specific ligands or via genetic manipulation, thus obtaining tailor-made BMVs able to reach the therapeutic target.[172]

Extracellular vesicles (EVs) are particles at the nanometer range (30-5000 nm) endogenously secreted by cells in a constitutive or inducible manner.[173-174] They include apoptotic bodies, which are released from cells undergoing apoptotic cell death, microvesicles, generated via membrane budding and shedding, and exosomes, the smallest EVs (30-100 nm) formed as multivesicular bodies.

EVs consist of membrane proteins, lipid materials, and various cytoplasmic components. The composition of EVs is influenced by both their formation pathway and the physiological condition of the originating cells.[175-176] EVs have the capability to transport various materials, including proteins, lipids, mRNAs, and miRNAs, making them a means of short to long-distance intercellular communication.[177] Once released, EVs can be uptaken by cells located both nearby and at a distance, facilitating the transmission of information through homotypic or heterotypic transfer.[178-179]

Because of their biomimetic and homing capabilities, EVs, and in particular exosomes, have been widely studied as potential nanocarriers in drug delivery.[180] They are currently considered to be main physiological actors, as they are mediators in coagulation,[181] pregnancy,[182] and immune response processes.[183]

Nonetheless, exosomes are also produced in abundance under pathological conditions such as infection[184] or cancer,[185-186] whereby they sustain and modulate the disease development.[187] Cancerous cells actively release exosomes as part of the tumor progression process. These exosomes convey molecular signals to neighboring healthy cells, potentially promoting processes like angiogenesis, immune suppression, and tumor growth.[188]

Beyond their physiological and pathological roles, extracellular vesicles (EVs) can exhibit regenerative properties. For instance, exosomes have been observed to play a significant part in the paracrine effects of transplanted cells. They supply the microenvironment with various trophic and survival signals, including cytokines, aimed at restoring tissue function and homeostasis.[189]

EVs also have the potential to serve as diagnostic biomarkers. This potential arises from their capacity to be examined for specific cargo profiles associated with different diseases and their surface protein markers, which can be analyzed to identify the organ, tissue, or cell type of their origin.[190]

Considering these advantages, exosomes have the potential to be harnessed for targeted drug delivery to specific cells within the body. Unmodified exosomes can be absorbed by nearby cells through various mechanisms, including clathrin-dependent endocytosis, caveolin-mediated uptake, phagocytosis, micropinocytosis, and lipid raft-mediated internalization.[191]

Exosomes can be generated via multiple mechanisms. Despite the variations among these pathways, a crucial common feature of all released exosomes is that their lipid-bound membrane closely resembles that of their host cell.[190, 192]

Nevertheless, exosomes beneficial effects may be limited by their scarce scalable manufacturing methods due to the low yield obtained from their production processes.[193]

To overcome these limitations, an innovative yet still challenging biomimetic approach is the use of cell membrane-derived nanovesicles for therapeutic purposes (**Figure 1-8**). Biomimetic nanosystems such as cell-derived nanocarriers are able to mimic the natural composition and biological functions of cells, thus offering the opportunity to avoid potential side effects occurring from systemic administration of therapeutic or imaging tools.[194] Moreover, cell membrane-derived nanovesicles may be used as NPs surface coating, overcoming both the drawbacks derived from natural exosomes, such as low drug loading and retention, and the ones resulting from the potential use of synthetic NPs as DDSs (e.g. low biocompatibility, rapid clearance, toxicity, etc.).

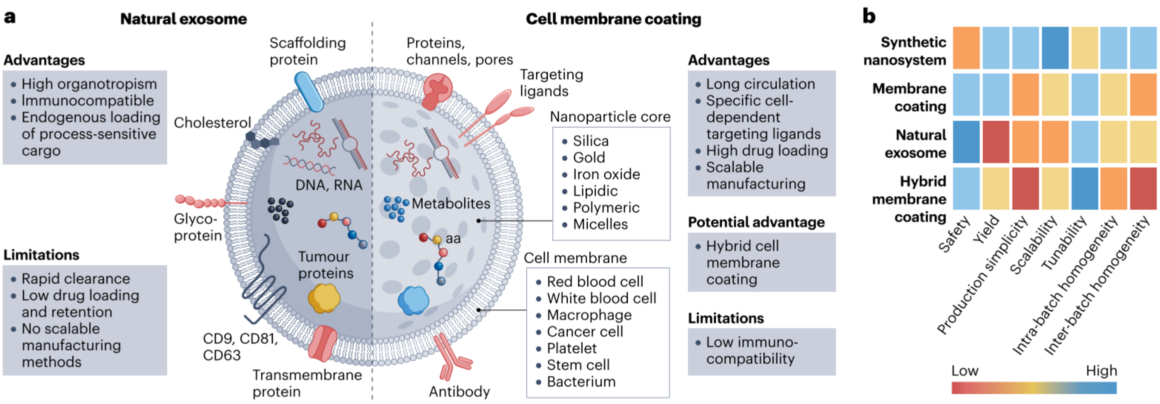

Figure 1-8 Comparison of naturally secreted exosomes and engineered cell membrane-coated nanosystems.[193]

1.2. CELL MEMBRANE-DERIVED NANOVESICLES

Aiming at moving towards personalized medicine, nanostructures increasingly similar to what is naturally present in our organism have been widely explored during the last decade. In this perspective, the idea of isolating cell plasma membranes to synthesize cell membrane-derived nanovesicles is emerging as a promising strategy in nanomedicine field.

Cell-derived nanovesicles (CDNs) are basically formed by the plasma membranes of the source cells used for their synthesis, although additional components can be included. These nanovesicles are expected to maintain the plasma membrane surface properties of the cell type from which they derive.[195] In addition to the enhanced biomimicry, several advantages have been attributed to CDNs, including prolonged circulation time, immune evasion, homotypic targeting capabilities, among others (**Figure 1-9**).[196]

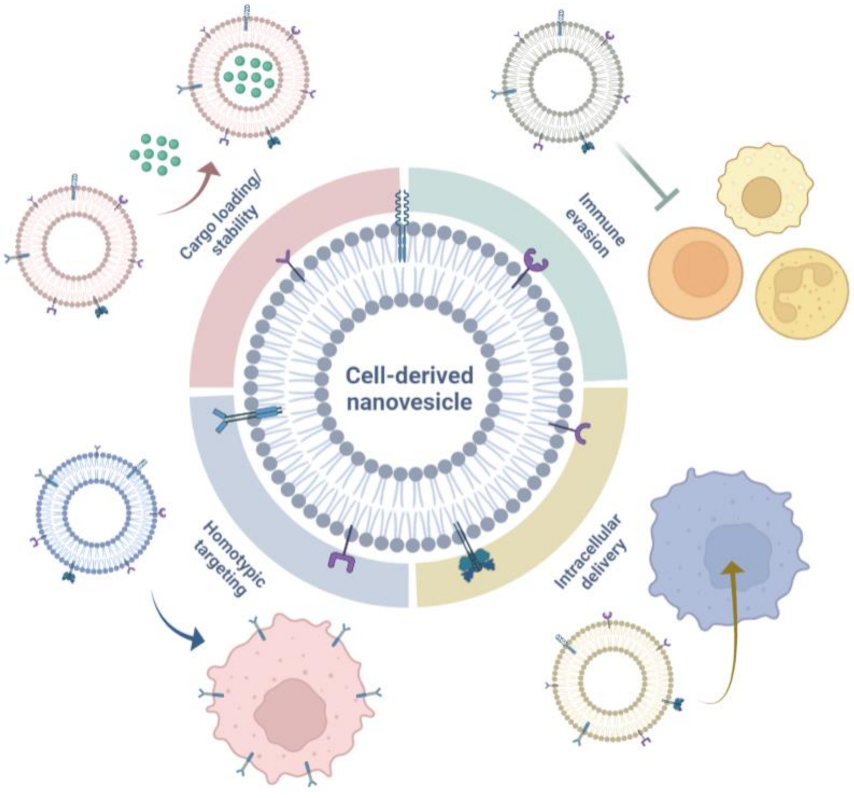

Figure 1-9 *Main biomimetic features.*

1.2.1. Biomimetic features

Cell plasma membrane is a thin semipermeable lipidic bilayer consisting of phospholipids (mainly phosphatidylcholine, phosphatidylethanolamine, phosphatidylserine),[197] receptors, ion channels, proteins, and carbohydrates. Different cells have different membrane compositions, which are mostly associated with their cellular functions.[198] Plasma membrane's main function is to protect the cell with selective permeability, which allows required substances to enter the cell while keeping unnecessary substances out. Another essential function is the process of information transmission and reception, which permits cellular communication involved in different biological processes.[199]

Cell plasma membrane can be extracted from cells and additionally used to coat nanomaterials. Thus, the attributes and functions of cell membrane can be transferred to cell membrane-coated nanomaterials.[198] During the last decade, researchers focused on producing nanovesicles able to mimic different cellular compositions (such as leukocytes, platelets, erythrocytes, macrophages, or tumoral cells) that can potentially be programmed to carry out distinct biological functions, such as evading the immune system, activating lymphocytes and dendritic cells, adhering to endothelial cells, and targeting cells of the same type.

Pioneering studies by Zhang's group involved the use of red blood cells (RBCs) to fabricate RBC membrane-coated NPs (either polymeric or gold NPs) capable of prolonged blood circulation time by evading the immune system.[200-201] The same group also developed platelets membrane-cloaked NPs with the aim of displaying platelet-mimicking properties such as selective adhesion to damaged human and rodent vasculatures as well as enhanced binding to platelet-adhering pathogens.[202]

A significant research study conducted by Tasciotti's group demonstrated that biomimetic camouflage based on leukocytes offers a competitive advantage in surmounting vascular barriers. This is achieved by reducing the opsonization process, leveraging self-recognition mechanisms to delay phagocytic uptake, and aiding in the passage through the endothelial layer while evading the lysosomal pathway.[203]

1.2.1.1. Cargo loading/stability

Similar to liposomes and lipid-based nanostructures, cell membrane-based vesicles serve as natural drug carriers for both hydrophilic and hydrophobic agents. In contrast, synthetic nanomaterials, which have the ability to load drugs with high capacity and co-deliver drugs with varying hydrophilic properties, are constrained by their biocompatibility. Therefore, by combining the benefits of synthetic nanomaterials and cell membranes, it is possible to enhance drug loading capacity, protect drugs from degradation, and achieve active targeting.[204-205]

For instance, doxorubicin (DOX) can be loaded into RBC membrane-coated polymeric NPs and released at an increased rate compared to PEG-coated NPs, showing that RBCs membrane can behave as a diffusion barrier for DOX release.[206] Cell membrane-coated nanomaterials have been used to load and delivery not only chemotherapeutic drugs, such as DOX, but also photosensitizers,[207] fluorescent dyes,[208] and immunologic adjuvants.[209] In addition, the use of cell membrane as NPs coating offers enormous translational benefit as it maintains both the natural properties of cells plasma membrane and the stability and tailored features of synthetic NPs.[210] Moreover, besides the capability to load different types of cargo, the employment of cell membrane-derived nanosystems offer the advantage of enhanced stability and biocompatibility compared to conventional DDSs.[211]

1.2.1.2. Immune evasion

To evade immune clearance and improve drug circulation time, PEG and other hydrophilic polymers have been frequently used as NPs coating. However, the polymer incorporation into the NPs surface requires elaborate procedures and conjugation chemistries that, despite their general consideration of being non-immunogenic, have often been proved to fail in animal models,[210] especially following repeat administration.[170] PEG's stealth properties, in fact, have shown prominent protein adsorption around the NPs surface and increase circulation time. However, there is a lack of effective targeting due to a loss of disease site targeting, accelerated clearance from the blood stream, and acute hypersensitivity.[170]

Nevertheless, significant advances have been made to develop more suitable biomimetic coating able to resist both immune response and rapid clearance. Cells membranes have specific surface molecules that, functioning in cellular recognition, activation, and migration, resemble camouflage to protect NPs from the attack of immune system, providing cell membrane-coated nanomaterials with prolonged blood circulation.[198] Nanomaterials with properties of prolonged circulation time and immune escape ability may have considerable clinical impact.[212]

For example, a series of NPs (such as polymeric nanomaterials,[213] metal nanomaterials,[214] inorganic nonmetal nanomaterials, etc.) have been coated with RBCs membrane to extend their circulation time. This feature is attributed to the natural markers on the RBCs membrane.[215]

The mechanism of RBC membrane-coated nanomaterials long circulation is not completely clear. The integrin associated protein CD47 (the "don't eat me" marker) on the RBC surface is thought to be responsible for the long circulation time and immune escape capability through the interaction with the signal regulatory protein-alpha (SIRP-alpha) receptor.[216] CD47-conjugated polystyrene beads have demonstrated that CD47 surface modification prolong the circulation time and reduce macrophage engulfment.[217] However, there may be other mechanisms controlling the RBC membrane coating properties.

Many researchers mainly focused on RBC membranes. However, nanomaterials camouflaged with plasma membrane derived from other cell types may be favorable for some specific diseases.

1.2.1.3. Homotypic targeting

The ultimate goal of nanomedicine, specifically for cancer therapy and diagnosis, is to develop the well-known “magic bullet” nanosystem able to evade the immune system and reach specific targeting to tumor cells.

Natural entities possess special features that are scarcely recreated by synthetic materials. The effective strategy of biomimicry provides to nanomaterials new and improved functionalities beyond any expectation.[218] Such nanosystems focus on exploiting naturally occurring interactions (including with other cells, the extracellular matrix (ECM), and a wide range of biomolecules) that have already been highly optimized by the process of evolution, combining them with optimized bioengineering tools.[219]

Cell membrane-coated nanomaterials can be tailored for specific delivery applications by selecting the source of the membrane coating. For example, using cancer cell membranes has demonstrated improved homotypic targeting, where nanoparticles exhibit a preference for binding to the cells from which the membrane is sourced.[220] Homotypic targeting of membrane-coated NPs can be remarkably achieved *in vivo*, even in the presence of a competing heterologous tumor,[195] and this strategy has been used across different tumor types.[205, 221] Cancer cell membrane coating strategy has been used not only across different tumor types, but also to relieve tumor hypoxia, which promotes tumor progression and drug resistance.[222]

In addition to cancer cell membrane, other cell types that play a key role in tumorigenesis have been used for tumor targeting. For example, chemotherapeutics loaded in white blood cells membrane-cloaked NPs have been successfully employed in tumors targeting.[223-224] Since various surface moieties of mesenchymal stem cells also participate in the interaction with tumor cells, they have also been exploited as well for biomimetic NP-based cancer therapy.[225]

In addition to tumors, various types of cells can hold significant therapeutic potential. Dysregulation in T cells and B cells can contribute to autoimmune diseases, and the only distinguishing feature among these cells is their antigen-specific receptors. Consequently, diseases resulting from aberrant T cells and B cells populations are particularly challenging to target, often necessitating the use of broad immunosuppressive agents in the treatment of autoimmunity, despite potential side effects.[226] Since the targets of these immune cells are often other cells within the body, this has created an ideal opportunity for the development of biomimetic nanoformulations.[227]

Moreover, immune cells display a variety of intrinsic homing capabilities, which can be exploited for therapeutic purposes. For example, leukocytes express specific proteins on their surface that can promote the moving across biological barriers to reach specific regions like tumors and inflammation; dendritic cells activate T cells and together with natural killer cells are themselves significant contributors to immune defense and can facilitate immune stimulation via cell membrane immunotherapy; macrophages are able to target tumor microenvironment regulating the immune response; myeloid-derived suppressor cells (MDSCs) show affinity towards the tumor site, being potential cell membrane coating for cancer therapy.[228]

An emergent and innovative application of cell membrane coating technology relies on the exploitation of immune cells membrane for nanovaccine development. As cancer vaccines, white blood cells (WBCs)-coated NPs can mimic host WBC-tumor interactions that modulate and boost anti-cancer immunity. As antibacterial vaccines, WBCs-coated NPs are able to adsorb bacterial virulence factors, leading to inactivated toxins that confer adequate immune protection.[229]

The utilization of biomimetic targeting through cell membrane coatings has proven to be effective in the treatment of bacterial infections as well.[230] It is well-established that a significant mechanism of action in many types of bacterial infections centers around the adhesion of bacteria to host cells.[231] Platelets are able to bind to certain types of bacteria through their surface receptors[232] and, along with this line, they have been employed likewise.[202]

Platelets also play a key role in maintaining homeostasis as a result of their unique ability to target various components of the ECM.[233] Due to this biological affinity, platelet membranes have been used to design nanoformulations capable of addressing certain vascular disorders. In addition, platelets membrane has been used to coat NPs loaded with different types of therapeutics, such as magnetic resonance imaging (MRI) contrast agents,[234] chemotherapy medications such as docetaxel,[202] or enzymes capable of lysing fibrin-containing clots.[235]

1.2.1.4. Intracellular delivery

Nanomaterials have been engineered to be capable of reaching their biological targets in a specific and efficient manner. Targeting and delivering therapeutics at the subcellular level has recently become imperative as complex events occurring within living cells are yet to be understood and modulating such processes (including gene regulation, signaling and transport) is crucial in order to design efficient therapies.[114]

The intracellular environment is physically isolated by the plasma membrane and in order to deliver nanotherapeutics into cells and to their subcellular targets, nanovehicles should first be able to traverse this plasma membrane. As previously mentioned, ENMs may be internalized through different pathways (see Section 1.1.2.5). Controlling the route of ENMs internalization pathway is important for mediating their intracellular fate and biological response.[236]

To target the endolysosomal network (for example to treat lysosomal storage disorders), the most common endocytic pathway provides immediate access to the therapeutic target.[237] Nonetheless, in many other applications, the entrapment of nanoparticles within endosomes is not desirable. Achieving subcellular targeting of nanotherapeutics has become crucial. For example, precise targeting of mitochondria can enhance photo-sensitizer-induced damage in photodynamic therapies, or nanocarriers carrying oligonucleotides for gene therapy must reach the cytosol and nuclei to be therapeutically effective.[238]

Biochemical delivery strategies to overcome the endosomal entrapment could be use membrane-based envelopes with the ability to fuse with plasma or endosomal membranes. Cationic molecules can interact strongly with negatively charged cell plasma membrane and induce membrane permeability. Various types of cationic coatings have been explored as transfection agents to deliver nanotherapeutics into cells, including cationic liposomes,[239] polypeptides,[240] amine-containing polymers,[241] and superchaotropic carriers such as cluster anions.[242]

NPs can be functionalized with amine-containing polymers, such as polyethyleneimine (PEI), through standard conjugation chemistries. PEI has been widely studied for gene delivery because of its ability to complex with DNA and enter efficiently in different cell lines.

In general, NPs can reach their intracellular target using two main strategies: the direct internalization, bypassing the endolysosomal entrapment following the endocytosis process, or through endosomal escape.[236]

Endosomal lysis by cationic NPs, membrane pores formation, and proton sponge effect are classical routes for triggering endosomal escape, used by cationic materials, such as PEI, that can potentially be limited by toxicity. Cationic polymers, in fact, are generally cytotoxic and instable in biological buffers, including culture media.[243]

Direct cytosolic delivery may be a safer alternative for intracellular delivery of cargos. Different strategies have been proposed mainly involving the fusion of the nanomaterial with cells plasma membrane to directly release the encapsulated cargo inside the cytosol, thus avoiding the endolysosomal entrapment.

Artificial membrane-fusion strategies have recently been developed to manipulate cell behavior and avoid the entrapment in the endolysosomal pathway. These emerging nanosystems can perform a biomimetic membrane-fusion process with the targeted cellular plasma membrane to transport the encapsulated cargo directly to the cellular cytosol. Thus, inner cargo transfer mediated by membrane fusion is able to maximize the transportation efficiency, emerging as a unique cytoplasmic delivery platform.[244]

Furthermore, this could be a cell membrane bioengineering approach, as the membrane fusion may allow the lipid bilayers mixing between lipid-based particles and cells. When the membrane fusion occurs, the merging of lipids favor the contact of the substances contained in both membranes. This innovative feature of the fusion-based strategy can be exploited for membrane editing to achieve some specific therapeutic goals, such as intramembranous cargo transfer, exterior and interior membrane engineering, etc. (**Figure 1-10**).[244]

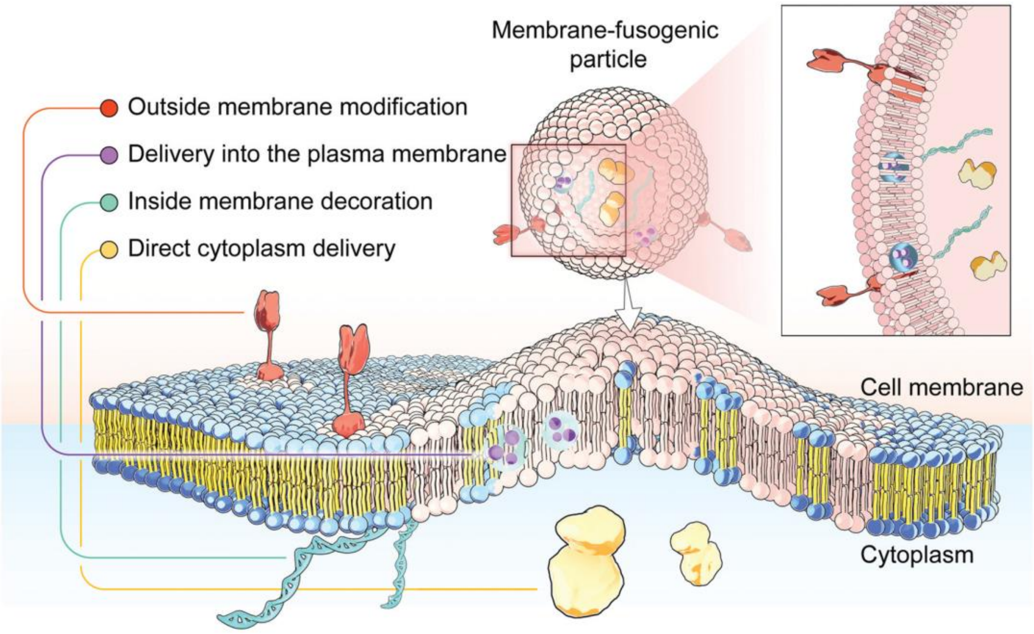

Figure 1-10 *Possible promising applications of membrane-fusogenic systems: direct inner cargo delivery into the cytoplasm, extracellular and intracellular bioengineering.[244]*

One of the earliest investigated systems for achieving artificial membrane fusion involves the modification of the molecules engaged in the fusion process present on both particle and cell surfaces. This modification allows the particles to adhere to the targeted cells and facilitates the fusion process.[245] This approach draws inspiration from the concept of complementary soluble N-ethylmaleimide-sensitive factor attachment protein receptor (SNARE) complexes, which play a key role in mediating fusion during neuronal exocytosis. These complementary SNARE protein subunits, found on opposing membrane surfaces, have the ability to form a coiled-coil structure. This structure brings the two membranes into close proximity, leading to subsequent lipid mixing, pore formation, and the concurrent transfer of contents (**Figure 1-11**).[246]

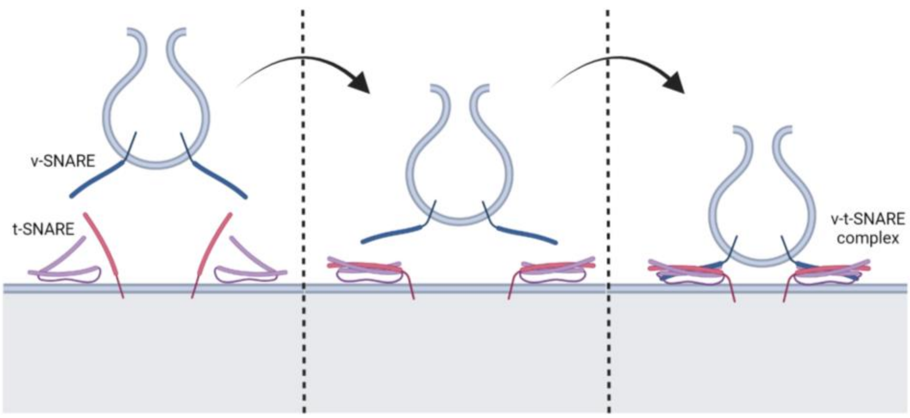

Figure 1-11 *SNARE proteins coiled-coil structure formation driving membranes to proximity.*

Inspired by the SNARE machinery, Kros and colleagues discovered a pair of synthetic peptides with complementary properties, capable of interacting and forming a SNARE-like coiled-coil structure. This coiled-coil structure played a crucial role in mediating the fusion between liposomes and cell membranes. By attaching these peptides to cholesterol-PEG, they successfully replicated the formation of the dimeric coiled-coil, which encouraged the contact and fusion of liposomal and cellular membranes.[247] Building upon this achievement, the Kros research group also explored the potential of dual modification of these complementary peptides as the basis for a membrane fusion-mediated platform for delivering therapeutic drugs into the cytoplasm for therapeutic purposes.[248]

Various other approaches for surface modification have been devised to generate artificial membrane integration. For instance, Sun and colleagues introduced DNA-lipid hybrids for the purpose of achieving targeted and programmable fusion with cellular plasma membranes.[249] They observed that the hybridization of single-stranded DNA with 3’ cholesterol functionalization on cell membranes and complementary single-stranded DNA with 5’ cholesterol functionalization on liposomes could create a zipper-like structure, leading to membrane tethering and facilitating the fusion process.

The process of membrane fusion between viruses and host cells is a pathophysiological event mediated by specific glycoproteins expressed on the virus’s surface, such as the vesicular stomatitis virus G-protein (VSVG) and hemagglutinin (HA), which have been demonstrated to trigger membrane fusion at acidic pH.[250] To harness these specific viral proteins for the purpose of membrane engineering, they have been expressed on the surface of particles, typically genetically engineered cell-derived vesicles and exosomes, to develop virus-like particles capable of facilitating plasma membrane fusion. For example, Yang and colleagues engineered VSVG-expressing exosomes derived from 293T cells to modify membrane proteins on target cells.[250] Fusogenic vesicles engineered with VSVG and HA have also been developed as platforms for delivering therapeutic agents into cells. For instance, Montagna et al. reported the efficient delivery of VSVG-decorated vesicles carrying CRISPR/Cas9 ribonucleoproteins through fusion-based transport.[251] Nonetheless, the translation of these virus-like particles into *in vivo* applications raises three primary concerns: the efficiency of delivery, the absence of tissue or cellular specificity, and the potential for undesired immune responses due to the introduction of foreign viral fusogens.

Developing a nanosystem based on membrane fusion using artificial materials relies on platforms like liposomes and lipid-based particles, which are well-suited to imitating the membrane fusion process. Lipid-based nanomaterials share a chemical structure, fluidity, and phase-transition characteristics similar to the lipid bilayers of cell membranes. Hence, it is anticipated that the appropriate lipid components can serve as mimics of regulators to induce non-physiological fusion.[252] For instance, Shen’s research group designed a fusogenic lipo-polyplex coating to initiate membrane fusion-mediated DNA delivery.[253]

Specific types of fusogenic liposomes have been documented to undergo hybridization with natural cell membranes or membrane proteins to enhance their targeting abilities. For example, Ge’s research team hybridized fusogenic liposomes with platelet cell membranes, enabling the delivery of anti-inflammatory microRNA-21 for myocardial remodeling in the context of cardiac healing.[254]

Likewise, the same group integrated membrane proteins derived from neutrophils onto the surfaces of fusogenic liposomes, thereby mimicking the homotypic targeting capability of neutrophils, aiming to reach the injured heart following myocardial infarction.[255]

Overall, the similar structure of lipid bilayers and appropriate preparations of selective lipidic materials are crucial for the preparation of fusogenic nanosystems with significant functional optimizations.[244]

1.2.2. Applications

The biomimetic technology and bioinspired membrane-coated nanoformulations could make nanomedicine's early promise of developing enhanced therapeutic and vaccination approaches a potentially improved competitor among other nanosystems.[256]

1.2.2.1. Cell-derived nanocarriers for cancer therapy

As mentioned, cell plasma membranes maintain their source cells surface features as a result of the optimized membrane extraction process. Thus, cell membranes are able to endow coated NPs with improved biological functions, which include active targeting, immune escape capability, and longer circulation time.

Cell surface interactions in cancer cell membranes, including Thomsen-Friedenreich antigens and E-cadherin, are thought to be responsible for their homotypic targeting capability. Cancer cell membranes can facilitate the infiltration of NPs into tissue and tumor due to cancer cell self-adherence exhibition. This property offers cancer cell membrane-derived NPs the possibility to actively target tumors. Moreover, self-adherence and the presence of CD47 molecule overexpressed by cancer cells play a major role in immune clearance evasion.

The "nanoghost" strategy, through which NPs can be camouflaged by cell membranes, takes advantage on different cell types of membranes, including cancer cells, RBCs cells, and immune cells.

Since cancer cell membrane inherits the functionalities of the antigen pool and homologous targeting from their source cells, it has been applied in cancer therapy and immunotherapy. In cancer therapy, cancer cell membranes have been used as coating for different NPs and further integrated with therapeutics to achieve targeting of the tumor region.

For example, chemotherapeutics like Paclitaxel (PTX) was loaded into FDA-approved PLGA NPs coated with 4T1 cell membrane. The effectiveness of tumor targeting and the blood half-life of PTX following administration exhibited a 4.3-fold improvement and a 2-fold increase when compared to the use of uncoated nanoparticles.[221] In another study, hyperthermia-responsive gold nanocages were loaded with DOX and incorporated within 4T1 cancer cell membrane to form a core-shell nanostructure. Under laser irradiation, roughly 75% of the encapsulated DOX was rapidly released within the initial 8 hours. Conversely, without laser irradiation, DOX release was notably sustained, with a cumulative release of 38% over 8 hours. The synergistic combination of chemo/photothermal therapy demonstrated a significant inhibition of tumor growth and metastasis.[257]

The improved efficacy of cancer therapy facilitated by the coating of cancer cell membrane is also bolstered by its impact on the regulation of the tumor microenvironment. To address the challenges posed by drug resistance and the typically poor outcomes of chemotherapy, MnO2 nanoparticles were enveloped with the 4T1 tumor cell membrane. This innovative approach was demonstrated to neutralize the surplus of glutathione (GSH) within the tumor environment. Additionally, the nanosystem was loaded with an antiangiogenic drug, Apatinib, to counteract proangiogenic responses in the tumor. Consequently, this multifunctional nanosystem offered an integrated solution to tackle both the excess GSH and the proangiogenic effects during the photodynamic therapy process.[258]

Furthermore, the “nanoghost” approach has gained rapid attention in the field of cancer immunotherapy. The targeted delivery of antigens to dendritic cells (DCs) is a critical challenge in the development of an effective cancer vaccine. To address this challenge, red blood cell (RBC) membrane was utilized to coat polymeric nanoparticles (NPs) that were anchored with mannose and carried the ovalbumin antigen. This engineered system provided a specific ligand for the recognition and uptake of DCs. The well-thought-out design of this nanovaccine facilitated the transport of antigens to draining lymph nodes and effectively suppressed tumor growth, inhibiting tumor metastasis in prophylactic, therapeutic, and metastatic melanoma models.[259]

Platelet cell membrane-based nanosystems have demonstrated promise in addressing tumor metastasis due to the distinctive hallmarks present on cell plasma membranes. These nanosystems leverage the specific P-Selectin receptor found on platelets' surface, which can bind specifically to CD44, a protein that is overexpressed on tumor cells. This mechanism is a recent discovery and plays a crucial role in tumor metastasis.[260] The specific recognition between platelets and circulating tumor cells (CTCs) plays a crucial role in promoting the aggregation of platelets around CTCs and facilitating their circulation through the bloodstream to reach sites of tumor metastasis. For example, a study by Gu et al. involved the development of a platelet membrane-coated core-shell nanovehicle designed to target both primary tumor sites and CTCs. Inside this nanovehicle, nanoparticles loaded with the anticancer drug DOX were encapsulated within the platelet membrane, and the external surface of the membrane was adorned with the protein drug TRAIL (tumor necrosis factor (TNF)-related apoptosis inducing ligand). TRAIL has the ability to activate the apoptosis signaling pathway. This multifaceted drug-loaded nanosystem, cleverly disguised with platelet membrane coating, demonstrated synergistic antitumor efficacy and the capacity to eliminate tumor cells with potential metastatic properties.[261]

1.2.2.2. Cells-derived nanovesicles to target senescence

Aging is a multifaceted biological process influenced, in part, by various hallmarks of aging, which encompass cellular senescence, genomic instability, mitochondrial dysfunction, telomere attrition, and other factors.[262] One of the key driver of age-related diseases has been directly attributed to cellular senescence. Senescent cells are defined by their permanent withdrawal from the cell cycle and their inability to proliferate, even when exposed to mitogenic stimuli.[263] Aside from replicative senescence, which results from telomeric shortening and the initiation of DNA damage responses, cellular senescence can also be triggered by various other factors. These include reactive metabolites, epigenetic alterations, oxidative stress, the inactivation of tumor suppressor genes, and viral infections.[264]

Senescent cells tend to accumulate in various organs and produce a mix of senescence-associated factors collectively known as the senescence-associated secretory phenotype (SASP). This phenomenon is linked to the development of several age-related diseases, including cancer.[265]

Addressing senescence appears to be a hopeful strategy for both the treatment and prevention of aging, with the aim of promoting extended health and longevity.[265] Researchers attempts to develop strategies designed for targeting senescent cells result unsuccessful. Therefore, they moved to a hypothesis-driven drug discovery paradigm to try to understand the senescence mechanism. They found that senescent cells may prevent their own removal through protective senescent cell anti-apoptotic pathway (SCAP) networks, using RNA interference.[266]

Cellular senescence is a stress response that directly activates innate immune cells, whereas the interplay with the adaptive immune system is yet to be understood.[267] Research involving various animal models suggests that various components of the immune system, such as NK cells, T cells, and macrophages, play a role in regulating the presence of senescent cells in tissues.

Two main strategies have been proposed to develop therapeutics against senescence and its age-related diseases. On the one hand, senolytic drugs have been employed to target senescent cells, not a single receptor, enzyme, or biochemical pathway. Compared with candidates that act on a single molecule, senolytic agents act on multiple SCAP network nodes, reducing off-target effects on non-senescent cells and increasing efficiency. On the other hand, senomorphic compounds, have been designed to reduce the senescence-associated factors (SASP), mitigating their deleterious effects.

Drug candidates that do act upon single or limited targets, for example Navitoclax[268] or Nutlin-3a,[269] have substantial off-target apoptotic effects on non-senescent cells types, such as platelets and immune cells.[270]

Traditional drug discovery methods are being used to identify a second generation of senolytic agents.[271] New strategies have been employed to develop potential senolytic interventions, such as using galacto-oligosaccharide-coated nanoparticles with toxic cargos that can be taken up by senescent cells.[272-273]

Despite senolytic drugs appear to prevent, delay, or alleviate multiple age-related conditions and chronic diseases in experimental animals, they generally have short elimination half-lives and scarce targeting capability, especially because local administration of senolytics would be less beneficial than systemic one.[270]

A third new approach for the treatment of age-associated pathologies is the immune cell-mediated elimination of senescent cells, even though a better understanding of the interactions between senescent cells and the immune systems is required.[265] The discovery of distinct senescent cell antigens or ligands for immune monitoring would be of great interest for the clinical translation of this new technology.

The cell membrane-coating technology, which, as mentioned, relies most of its features on the selected source cells, could be a key player in senescence-related therapeutic approaches. Due to the promising features of cell membrane-derived nanovesicles, exploring the "nanoghost" strategy for the encapsulation and release of cargos (such as senolytic compounds) to specifically target senescent cells would be of great interest. So far, no biomimetic nanosystem has been developed to such application. Moreover, the exploitation of immune cells to such biomimetic technology could enhance the potential therapeutic advantages in a synergistic manner.

1.2.2.3. Immunotherapy

Immunotherapy has emerged as a central treatment approach for numerous diseases, capitalizing on our profound comprehension of the interactions between the immune system and various ailments. Immunotherapy involves the manipulation or fine-tuning of the body's immune function to align with the disease's underlying mechanisms. This approach encompasses the development of monoclonal antibodies, immune adjuvants, and vaccines, all of which hold great potential as therapeutic agents for combatting cancer and infections.[274]

Since RBC membrane coated NPs were first reported,[200] cell membrane coated-NPs research has experienced successful developments in many applications, including immunotherapy.

Autoimmune diseases caused by the failure of self-tolerance are among the leading causes of death in the world.[275] Conventional treatments for autoimmune diseases have historically involved the use of cytotoxic drugs, the administration of antibodies, and glucocorticoid agents. Nevertheless, these broad, non-specific immunosuppressive strategies frequently entail substantial risks and may even result in the development of more severe conditions. As an innovative therapeutic strategy, the employment of cell membrane-coated NPs has emerged as a potential immunotherapy approach to act as decoy for targeting the autoimmune disease. For instance, Copp and coworkers developed RBC membrane-coated PLGA NPs as alternative targets for anti-erythrocyte antibodies.[276] These biomimetic NPs did not cause the inhibition of either normal lymphocytes or immune effector cells, compared to traditional immunotherapy, and by selectively depleting disease-causing antibodies they could disrupt disease progression in a minimized toxic manner. In another study, Wei and coworkers used platelets membrane-coated NPs as successful platelet-bionic NPs to specifically remove anti-platelets antibodies.[277]

In the past few decades, tumor immunotherapy has earned growing significance for tumors treatment. While several clinical anti-tumor vaccines have shown success, challenges related to versatility and tumor-specificity still exist in their clinical applications.[278] Hence, numerous studies have concentrated on the development of biomimetic cell membrane-coated nanoparticles aimed at achieving effective anti-tumor immunotherapy.

Cell membrane delivery, together with either checkpoint blocking therapy or immune stimulation adjuvant, has been proved to promote antigen presentation and activate tumor-specific immune responses.[279] Fang et al. reported that melanoma cell membranes coated-PLGA NPs could deliver tumor-associated antigens to antigen-presenting cells and then promote anti-tumor immune responses. When used in combination with immune adjuvants, these biomimetic NPs significantly promote the maturation of antigen presenting cells, stimulate T cell immunity, and realize anti-tumor immunotherapy.[220]

In addition to cell membrane coating technology application to anti-tumor vaccines, several studies have been performed for the employment of immune cell membrane-coated NPs to target tumors, by inhibiting or enhancing proinflammatory effects, and produce anti-tumor immune effects.[280] The research of membrane coating technology in activating antitumor immunity have shown great potential in successful tumor treatments.

1.2.2.3.1. Vaccines

The combination of distinctive characteristics originating from diverse core materials and the overlay of cell membranes offers the cell membrane-coated nanoparticles approach significant potential for vaccine design.[275]

The biggest challenge of 2020 and beyond was to develop effective therapeutic or vaccine candidates for one of the deadliest pandemics in history, which caused more than 600 million cases and more than 6.5 million confirmed deaths. The role of nanomedicine against viruses has proved to be crucial, and nano-based approaches have attracted special attention for developing versatile nanosized diagnostics, therapeutics, and vaccine to face coronavirus disease 2019 (COVID-19).[281] A common approach in nanomedicine is to create nanocarriers aimed at enhancing the effectiveness of newly developed or repurposed therapeutic compounds, which can encompass antivirals, small molecules, and antigens.[282] In recent times, biomimetic approaches such as antigen or nucleic acid vaccination have yielded promising outcomes. Messenger RNA-encapsulating lipid NPs achieved particular success in COVID-19 pandemic (**Figure 1-12**).[283]

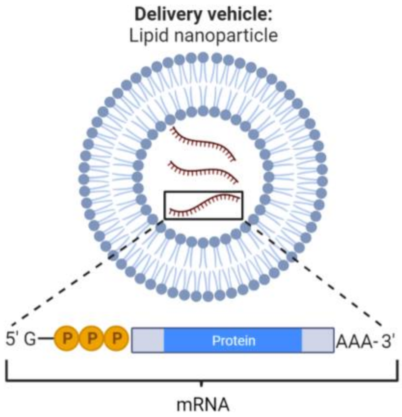

Figure 1-12 Schematic structure of BioNTech and Moderna COVID-19 vaccines, both mRNA-encapsulating lipid NPs.

However, other strategies have also been explored to bring novel insight in the fight against the pandemic. One of these strategies involves the use of engineered biomimetic nanosystems that mimic the biological functionalities of cellular components, an approach still underexplored for COVID-19 applications.

In addition to traditional vaccines, modern strategies incorporate novel nanotechnologies, like lipid nanoparticles loaded with messenger RNA (mRNA). Examples of these include Pfizer-BioNTech's BNT162b2 and Moderna's mRNA-1273. These vaccines deliver mRNA encoding antigens into the cell cytoplasm, resulting in the expression of SARS-CoV-2 (severe acute respiratory syndrome coronavirus 2) antigens. These antigens are then presented on the host cell's surface, making them recognizable to immune cells.[284]

The role of a cell membrane-derived surface is to serve as a biological coating that shields the internal contents from early clearance, degradation, or release. It also functions as a highly customizable interface to replicate and improve biological interactions. Cell membrane-based nanoparticles have already demonstrated promising results in therapeutic approaches against COVID-19.[285] For example, mesenchymal stem cell-derived exosomes can be a valuable tool for reducing lung infection and alleviate COVID-19-related symptoms.[286] So far, only host epithelial cell membrane-coated NPs,[287] hybrid cell membrane nanovesicles,[288] and leukocyte cell membrane vesicles[289] have been applied to COVID-19 management, particularly COVID-19 therapeutics.

1.2.2.4. Inflammation

Inflammation is considered to be related to many diseases, such as ischemic strokes, ischemic heart disease, rheumatoid arthritis, atherosclerosis, ulcerative colitis, etc.[290] Once inflammation occurs, immune cells are recruited to the inflamed tissue and, crossing the biological barriers around the disease region, manage to penetrate into the tissue. Other cells such as RBCs and stem cells also play key roles in disease prevention and tissue repair. Moreover, cancer has been identified as a form of chronic inflammation, involving the participation of a large pool of cell types.[290] Thus, targeting inflammation based on cell membrane biomimetic nanotechnology may provide an opportunity for targeted drug delivery.

For instance, acute pancreatitis (AP), characterized by severe abdominal pain, frequently leads to inflammation in nearby tissues and can even trigger life-threatening systemic inflammatory responses. The primary challenge in treating AP is the blood-pancreas barrier. Neutrophils are rapidly recruited and can be activated by cytokines to migrate to the site of inflammation. Leveraging the surface composition of neutrophils, researchers successfully created PEG-PLGA nanoparticles loaded with celastrol (an antioxidant and anti-inflammatory compound) and camouflaged them with neutrophil membranes to overcome the blood-pancreas barrier.[291]

Inspired by platelets function as circulating sentinels for vascular damage, platelet membrane-coated NPs have been designed for immune evasion, sub-endothelium adhesion, and pathogens interactions. This unique design is benefited by platelets targeting capability to the injury site and prevents activation of the complement system.[292]

1.2.2.4.1. Stroke

Ischemic stroke, as one of the most serious health diseases, occurs when blood clots or other particles block the blood vessels to the brain. It causes the injury of neurons due to the upregulated enormous release of toxic reactive oxygen species (ROS) after reperfusion.

To achieve specific targeting of ischemic sites and adequate circulation times, smart bioengineered drug delivery carriers were developed for ischemic stroke therapy. In one study, smart ROS-responsive NPs coated with RBC membrane inserted with a stroke-homing peptide were fabricated.[293] The resulting smart NPs exhibited improved homing functionalities and could also improve infarct volume in response to the surgical middle cerebral artery occlusion injury.

Tissue plasminogen activator (tPA) is a serine protease that catalyzes the conversion of plasminogen to plasmin, the major enzyme responsible for clot breakdown. Pharmacological thrombolysis with intravenously recombinant tPA (rtPA) is the gold standard treatment (approved by FDA in 1995) for patients with acute ischemic stroke (**Figure 1-13**). However, its use has some limitations, such as short half-life (about 5 minutes), low reperfusion rate, the risk of hemorrhagic transformation, and potential neurotoxic effects.[294] These drawbacks limit the rtPA therapeutic window to 4.5 hours after symptoms onset.[295] Nanomedical approaches which focus on targeting the drug to the arterial clot-region and induce a controlled drug release may increase the number of patients that can safely benefit from rtPA.[296]

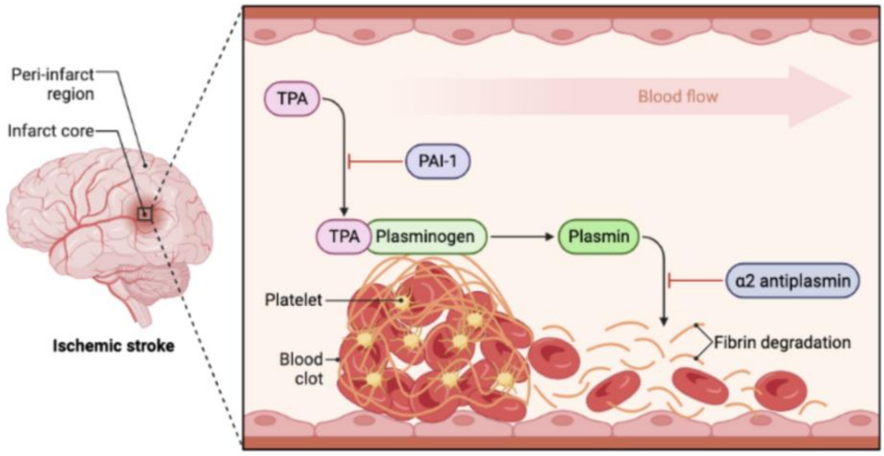

Figure 1-13 *Tissue plasminogen activator(tPA) activity at ischemic region in the brain.*

For this reason, trying to develop biomimetic nanosystems able to both preserve tPA activity and release the drug at the ischemic stroke site would be of great interest.

1.2.2.5. Gene therapy

One of the most innovative branches of nanomedicine is gene therapy, a technique that uses genetic material via a vector that facilitates the delivery of foreign genetic material into the host organ. Its main goal is the correction of a mutation or genetic defect using recombinant DNA technologies.[297]

The advancement of genome editing tools, including zinc-finger nucleases (ZFNs), transcription activator-like effector nucleases (TALENs), and clustered regularly interspaced short palindromic repeat (CRISPR)/CRISPR-associated (Cas) nucleases, has significantly enhanced genome manipulation.[298]

These programmable nucleases can efficiently create double-strand breaks (DSBs), which are typically repaired through nonhomologous end joining (NHEJ), an error-prone process that often leads to the disruption of the targeted gene.[299] Alternatively, genome editing tools can be employed for gene repair by enhancing the utilization of homologous recombination (HR) templates, such as single-stranded oligonucleotides or homology-based targeting vectors. (**Figure 1-14**).[299]

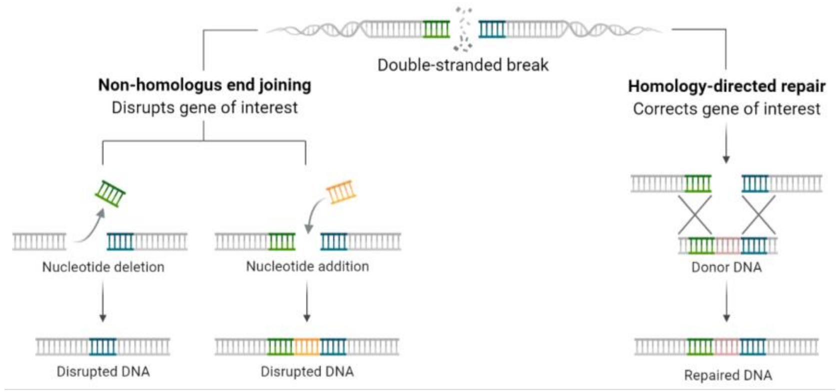

Figure 1-14 *DSBs possible repair processes. On the left: NHEJ; on the right: HR.*

However, beyond the biological barriers that restrict site-specific delivery, gene therapies using ENMs face an additional obstacle, namely the instability of genetic materials like mRNA, antisense oligonucleotides, and siRNA. In the case of plasmid DNA, they must also traverse the nuclear envelope. This instability is primarily due to endosomal compartmentalization, which exposes the genetic material to an enzyme-rich environment with low pH. Even if the genetic material successfully escapes the endosome, it remains vulnerable to degradation by cytoplasmic nucleases.[300] Regarding plasmid DNA, even if it manages to evade degradation by enzymes and nucleases within the intracellular compartment, it must still access the nucleus. The cell genome is encased by the nuclear envelope, which comprises an outer and inner membrane forming a continuous structure connected to the endoplasmic reticulum.[301] The inner and outer membranes are fused at nuclear pore complex sites, which serve to regulate the passage of macromolecules, allowing the transit of molecules with a molecular weight of approximately 40 kDa or smaller.[302]

While traditional nucleic acid therapies have historically utilized viral vectors for transfection purposes,[303] a parallel line of research has focused on the use of NP-based platforms for gene delivery, including liposomes,[304] magnetic NPs,[305] and gold NPs.[306]

About 50 years ago, scientists begin to hypothesize that genetic modification by exogenous DNA might be an effective treatment for genetic human diseases. This “gene therapy” strategy optimistically suggested that a durable and possibly curative clinical treatment would be achieved by a single medication. Although the journey from concept to clinical application has been challenging, gene therapy is now bringing new treatment options to multiple fields of medicine.[307]

Clinical trials for gene delivery vectors began in the early 1990s, primarily employing viral vectors like replication-defective retroviruses and adeno-associated viruses (AAVs). Although these vectors demonstrated promising outcomes in preclinical disease models, early trials revealed significant therapy-related side effects, notably inflammatory responses triggered by vector-mediated insertional activation of proto-oncogenes. Lentivirus vectors offered an improved ability to transfer genes to non-dividing cells. Viral vectors, however, exhibited substantial success in local gene delivery. For example, in vivo delivery of therapeutic AAV vectors to the retina, liver, and nervous system resulted in clinical improvements for patients with congenital blindness, hemophilia B, and spinal muscular atrophy, respectively. In 2017, the FDA granted approval for the first gene therapy products to treat B cell malignancies. Moreover, congenital blindness was addressed through chimeric antigen receptor (CAR)-T cell therapy using AAV vectors.[307]

The use of viral vectors has always been controversial. Even though viral vectors should not cause any harm to patients, the potential to trigger immunogenic responses and transgene mis-insertion was too risky not to search for other non-viral delivery systems. In recent years, polymers, lipids, inorganic NPs, or combinations of different types of nanocarriers have been investigated as possible non-viral vectors in gene therapy.[308]

Among non-viral gene therapy vectors, cationic polymers have been deeply studied because of their versatile chemical structure and potential high loading capacity. They are supposed to neutralize the negatively charged genetic material to form a complex (polyplex) and carry the payload to the targeted cells. Cationic polymer PEI[309] and cationic dendrimer PAMAM[310] are only a few examples of the most studied and used polymers for gene therapy.

Compared with other materials, lipids show many advantages, such as biodegradability and less toxicity and they can incorporate hydrophilic and hydrophobic substances. For example, the first FDA-approved small interfering RNA (siRNA) treatment (Onpattro) utilized a lipid-based vector.[311] Another promising lipid-based siRNA therapy (inclisiran) for hyperlipidemia treatment has been approved in the EU in December 2020.[312]

Since in gene therapy applications targets are generally nucleic acids, gene carriers should reach cell cytoplasm or nuclei without being entrapped in the endolysosomal internalization pathway.

In lipid-based vectors, the lipid composition is crucial for both preserving the cargo stability and activity and achieving the targeting purpose. Typical lipids in lipid-based carriers possess one positively charged head group. Commonly employed positively charged head groups include ammonium, imidazolium, pyridinium, lysine, and arginine, among others. DOTAP (1,2-dioleoyl-3-trimethylammonium-propane) represents the most prevalent cationic lipid structure utilized for nucleic acid and protein delivery, both in vitro and in vivo. The hydrophobic tails can consist of two saturated or unsaturated hydrocarbon chains or steroids. In lipid-based gene delivery systems, in addition to cationic lipids, "helper lipids" are frequently incorporated to improve transfection efficiency, stabilize particles, or enhance intracellular trafficking.[171] DOPE (1,2-dioleoyl-sn-glycero-3-phosphoethanolamine) is a frequently employed helper lipid, known for its cone-like molecular shape, which promotes membrane fusion and bilayer disruption. Additionally, cholesterol is another commonly used helper lipid, as it can enhance cell membrane fluidity and stabilize bilayer lipids in lipid-based vector formulations. This leads to enhanced efficacy and stability in these systems.[313]

1.2.2.5.1. Gene editing: CRISPR/Cas system

Unlike viral vectors, which primarily facilitate gene addition, genome editing approaches provide a precise method for not only adding genes but also deleting and correcting genes. Genome editing can be carried out on cells in vitro, or the editing tools can be introduced in vivo to perform genome editing directly within the organism.[307]

The field of genome editing underwent a significant transformation in 2012 with a groundbreaking discovery by Doudna and Charpentier (both Nobel Prize laureates in 2020). They demonstrated that a bacterial defense system, known as clustered regularly interspaced short palindromic repeat (CRISPR) and CRISPR-associated 9 (Cas9) nucleases, can be effectively customized to cleave DNA at specific locations of interest. This is achieved by designing a short guide RNA (sgRNA) that is complementary to the target site of interest.[314]

Clustered regularly interspaced short palindromic repeats (CRISPR) and CRISPR-associated proteins (Cas) are elements of the prokaryotic adaptive immune system, which serves as a defense mechanism protecting prokaryotes (such as bacteria and archaea) from viral infections.

Cas proteins, which are naturally found in bacteria and archaea, are categorized into Class 1 or Class 2 based on their homology and function. Among these, Cas9 is the most well-known and widely used Cas protein for genome editing. Specifically, Streptococcus pyogenes Cas9 (SpCas9) has been extensively employed for efficient genome editing in various species and cell types, including human cell lines, bacteria, and yeast.

The CRISPR/Cas9 system, as well as other Cas proteins, relies on two main components: the sgRNA (single-guide RNA) and the Cas nuclease. The sgRNA is a specific RNA sequence designed to recognize the target DNA region of interest and guide the Cas nuclease during the editing process. The sgRNA is composed of two parts: the crRNA (crispr RNA), a 17-20 nucleotide sequence that is complementary to the target DNA, and a tracrRNA that acts as a scaffold for binding the Cas nuclease. When selecting target sites for Cas9, the only requirement is the presence of a protospacer-adjacent motif (PAM) located immediately downstream of the target site.[298]

Additionally, in 2015, new members of the class 2 Cas proteins were discovered. One of these proteins is C2c2 (Class 2 candidate 2), also known as Cas13. Unlike other Cas proteins, C2c2 contains two higher eukaryotes and prokaryotes nucleotide-binding domains (HEPN), which are predicted to confer RNAse activity to the protein.[316] The discovery of Cas13 proteins that bind and cut RNA instead on DNA opened the door to a new world of possibilities for genome editing.[317]

All Cas13 family members are smaller than Cas9, with Cas13d being the smallest protein and making it suitable for molecular genetics.[318]

Cas13 proteins in bacteria serve as a defense mechanism to silence foreign RNA. Unlike Cas9 or Cas12, Cas13 specifically binds to and cleaves single-stranded RNA molecules. This unique property makes Cas13 particularly well-suited for RNA targeting and manipulation. (**Figure 1-15**). The gRNA associated with Cas13 typically comprises a conserved sequence of approximately 70 nucleotides. This conserved region has a hairpin-like structure that is recognized and bound by the Cas13 protein. Following the conserved region, there is a variable sequence of about 29 nucleotides that is designed to be complementary to the specific target RNA of interest. This variable sequence is customizable, allowing researchers to target different RNA molecules by designing gRNAs with the appropriate complementary sequence.

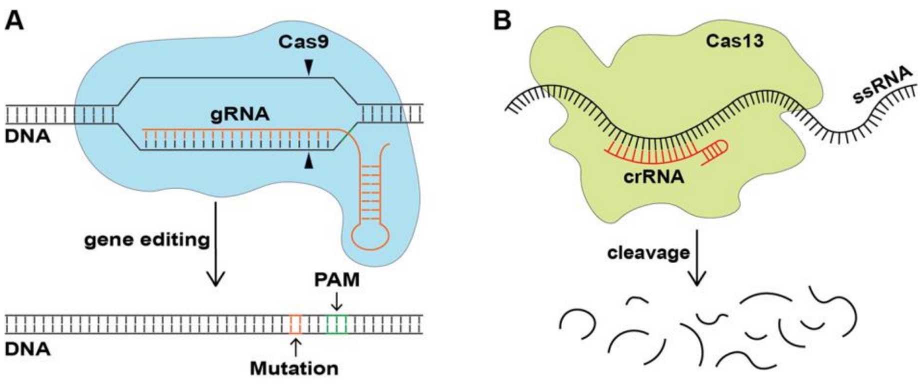

Figure 1-15 *Functional overview of CRISPR/Cas9 and CRISPR/Cas13 systems.*[318]

Cas13d proteins are present in at least 21 bacterial genomes.[315] These Cas13 proteins all contain two HEPN domains, but the size of the full-length protein can vary depending on the specific bacterial source from which they originate. As a result, they are subclassified as Cas13a, Cas13b, Cas13c, Cas13d, and so on, based on the bacterial origin and specific characteristics of each Cas13 protein variant.

CRISPR/CasX has been proved to be an extremely promising gene editing tool in many different applications, including the development of biotechnological products and the diagnosis and treatment of many diseases. Appropriate delivery methods should be developed for its purposes and, to further improve its targeting capability, fusogenic cell-derived nanovehicles may be considered to best exploit CRISPR/CasX functionalities.

1.3. OBJECTIVES

The main objective of this thesis is to design and exploit the biomimetic properties of cell membrane-derived nanovesicles for different biomedical applications. The biochemical surface features of these nanostructures (called cellsomes, or CSMs) have been deeply studied during the last decade, raising much attention on the possibility of mimicking the natural functions of the source cells to evade or tune the immune response, thus finding in CSMs an innovative biomimetic nanocarrier for molecules and drugs.

The other great advantage of CSMs is their tissue-specific targeting capabilities. Nanocarriers derived from specific cell lines, especially tumoral ones, are expected to enhance the interactions with their source cells, due to the characteristic biological surface pattern.

This work, divided into four main chapters, will try to represent the multifunctional applications array of tuneable engineered CSMs, their beneficial improvements in the nanomedicine field and their principal drawbacks mostly regarding the optimization of the synthesis method.

1.3.1. Chapter 1

The major objective of Chapter 1 is to develop standardized protocols for fabricating and characterizing a library of CSMs derived from different cell types. CSMs are synthetized and characterized from a physical, chemical, and biological perspective: their hydrodynamic size, colloidal stability and morphology have been investigated.

Here, preliminary results regarding the interactions of CSMs with the biological environment are also shown. In particular, CSMs homotypic targeting capabilities have been assessed to be one of the crucial properties of cancer cell membrane-derived nanovesicles. Moreover, the CSMs internalization process into different cell types has been investigated with the aim of identifying the endocytosis pathway through which CSMs undergo when exposed to cells.

Preliminary cargo encapsulation/release studies are then performed to assess CSMs ability to retain loaded cargos and to release them during time inside living cells. This particular feature is subsequently employed for the loading of cytotoxic molecules (such as doxorubicin) in order to investigate the toxicity pattern of senescent cell-derived CSMs, with the further idea of encapsulating more specific compounds (i.e. senotherapeutics).

In addition, the exploration of CSMs surface modification is performed through the expression of Spike-protein on cells plasma membrane in order to enhance CSMs intrinsic properties of active targeting.

Based on the results obtained in this first chapter, three different biomedical applications are further explored as follows.

1.3.2. Chapter 2

The main purpose of Chapter 2 is to produce CSMs derived from human platelets that are used as biomimetic nanocarriers for the treatment of ischemic stroke. This work involved in the PLATMED project, focuses on developing a non-toxic nanovehicle for tissue plasminogen activator (tPA), the current gold standard treatment for ischemic stroke therapy. Platelets are here used as source cells for the fabrication of CSMs with the aim of evading the immune system and targeting the whole nanoformulation to the inflammation site.

A major part of Chapter 2 highlights the experimental setting used to obtain, purify and storage reproducible samples which are then employed for both *in vitro* and *in vivo* experiments.

1.3.3. Chapter 3

Once explored the possibility of employing CSMs as biomimetic drug delivery systems, further modifications of CSMs surface composition are performed to enhance their capability of releasing the encapsulated cargo into the cells cytosol.

In Chapter 3, fusogenic CSMs (FCSMs) are fabricated, characterized, and used as biomimetic nanovehicles for gene therapy application. Here, CSMs not only can benefit from their biological natural source, but they also present a modified lipidic surface which favors the interaction and fusion with cells plasma membranes, thus avoiding the CSMs internalization mediated by endocytic pathways and therefore releasing the cargo directly inside the cytosol.

The widely studied CRISPR/Cas9 genome editing system is encapsulated into FCSMs and released inside GFP-reporter cells, where the nanoformulation acts as a knock-out system. Then, a similar genome editing system (CRISPR/Cas13d) is utilized for its ability to target and cut mRNA, whose application in this chapter is suppressing the expression of viral genes.

1.3.4. Chapter 4

Chapter 4 investigates the employment of CSMs and FCSMs as biomimetic coating for synthetic nanomaterials. Here, two distinct NPs (PSNPs and UiO-67 nanoMOF) are used as core in the fabrication of core-shell nanostructures for biomedical applications.

PSNPs are mostly used to understand the core-shell nanosystem behavior when interacting with the biological environment and to optimize the synthesis protocol. While UiO-67 nanoMOF, due to their unique porous structures and controlled released properties, are selected as potential drug delivery nanomaterials. The endocytosis mechanism regulating the internalization of the core-shell nanosystem (both for CSMs and for FCSMs) is studied through different experimental procedures, which include flow cytometry analysis, fluorescence microscopy imaging and several *in vitro* assays.

2. Materials and methods

2.1. SYNTHESIS OF CELL-DERIVED NANOVESICLES

Cellsomes (CSMs) synthesis was carried out following an optimized protocol described in the literature[319], with a procedure to obtain monodispersed vesicles of about 150-200 nm in size. Synthesized CSMs are derived from many different cell lines: human tumoral cell lines such as cervix epithelial carcinoma cells (HeLa cells) and adenocarcinomic human alveolar basal epithelial cells (A549 cells); human lung fibroblast MRC-5; human platelets; murine macrophage-like cells (RAW264.7); human epithelial kidney cells (HEK293); horse fibroblast (E. Derm). HeLa, A549, MRC-5, E. Derm, HEK293 and RAW264.7 were purchased from ATCC®, while Human Platelet Concentrate (#SER-PCEX) were purchased from Zen-bio©.

To prepare the CSMs, HeLa, A549, MRC-5, E. Derm, HEK293 and RAW264.7 were incubated in 175 cm^2 cell culture flasks in Dulbecco's Modified Eagle Medium (DMEM, high glucose (4.5 $g \cdot L^{-1}$) and pyruvate, GIBCO™ #41966052), supplemented with 10% heat inactivated fetal bovine serum (FBS, GIBCO™ #10270106) and Penicillin-Streptomycin (50 $U \cdot mL^{-1}$ - 50 $\mu g \cdot mL^{-1}$) (GIBCO™ #15140122) (complete DMEM or cDMEM) in a humidified chamber at 37 °C under 5% CO_2. Cells were grown in their preferred environment as they approached 70-80% surface coverage. Then, cells were harvested after trypsinization for 2 minutes with 2 mL of 0.25% Trypsin-EDTA (GIBCO™ #24200056). 10 mL of DMEM supplemented with 10% FBS was added to recover the cells and transferred to a 50 mL sterile tube. The cells were collected after centrifugation at 500 g for 5 minutes.

To induce senescence, A549 cells were subjected to bleomycin treatment.[320] In particular, $4 \cdot 10^6$ cells were plated in p150 Petri dish in cDMEM. Bleomycin sulfate (Sigma-Aldrich® #BP971) 20 µM was added directly to the medium. Cells were left in a humidified chamber at 37 °C under 5% CO_2 for 5 days, then collected after centrifugation at 500 g for 5 minutes.

Once purchased, platelets were aliquoted (about 10^6 cells each) and stored at 4 ºC until use. Each aliquot was used as the equivalent of a 175 cm^2 cell culture flask where the other cells were grown. The procedure to fabricate platelets-derived CSMs proceeded as follows.

The collected cells ($10\text{-}20 \cdot 10^6$ cells) were washed with precooled phosphate buffered saline (PBS, pH 7.4 Thermo Fisher #14190169) and centrifuged at 600 g for 5 minutes. The cell pellet was resuspended in 10 mL of hypotonic buffer (0.25x PBS) containing 1x Protease inhibitor cocktail (PIC, Sigma-Aldrich® #P2714-BTL) and incubated in an ice bath for 10 minutes. Then the cell lysis was carried out using a freeze-thaw method consisting of 4 cycles of freezing in liquid nitrogen for 1 minutes followed by thawing at 37 °C for 10 minutes. Finally, the solution was placed in a bath sonicator for 5 minutes. To purify the cell membrane fragments, the solution was subjected to several centrifugation steps. First the solution was centrifuged at 700 g for 10 minutes at 4 °C to discard the nuclei or whole cells. Then the cell membrane fragments remained in the supernatant were precipitated by centrifugation at 15,000 g for 30 minutes at 4 °C. To allow for self-assemblage of the membrane fragments into CSMs, a mechanical extrusion process was applied. The pellet was dispersed in 1 mL of 1x PBS or 20 mM of 2-(4-(2-hydroxyethyl)-1-piperazinyl)-ethanesulfonic acid (HEPES, Sigma-Aldrich® #H7006) buffer pH 7.4 or in 0.5 mL of 1 mM ammonium hydroxide pH 9 and subjected to 10 cycles of extrusion by using an Avanti® Mini extruder with 800 nm polycarbonate membrane.

2.2. FUNCTIONALIZATION AND SURFACE MODIFICATION

Fluorescently labeled CSMs were produced using fluorescent phospholipids that can be intercalated in the lipidic bilayer. In particular, 1,2-Dioleoyl-sn-glycero-3-phosphoethanolamine labeled with Atto 647N or Atto 488 (DOPE Atto 647N, Sigma-Aldrich® #42247; DOPE Atto 488 Sigma-Aldrich® #67335) (**Figure 2-1**) was added to the lipid bilayer of the CSM. 1 mL of obtained CSMs solution dispersed in 1x PBS was mixed with 2 µL of 1 mg·mL^{-1} of DOPE Atto 488 or DOPE Atto 647N (dissolved in dichloromethane:methanol 8:2 or dichloromethane, respectively) and sonicated for 10 minutes. The resulting fluorescent CSMs were extruded 10 times using an Avanti® Mini extruder (with a 800 nm polycarbonate membrane) and purified by ultrafiltration using Amicon® Ultra-0.5 Centrifugal Filter Devices (cutoff of 100 kDa, Millipore Sigma-Aldrich® #UFC510096) and washing the solution with 1x PBS or 20 mM HEPES at least 3 times.

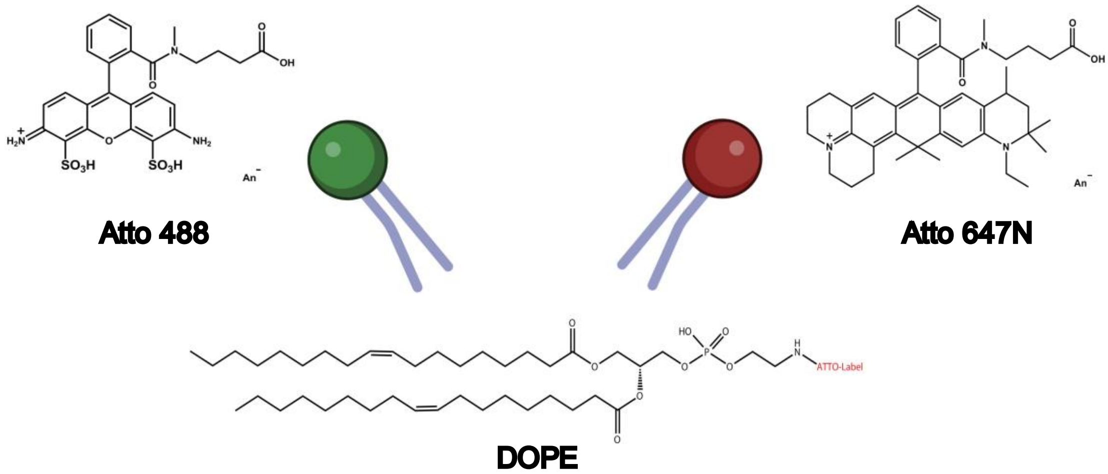

Figure 2-1 DOPE chemical structure with the two fluorophores Atto 488 and Atto 647N.

Fusogenic cellsomes (FCSMs) were prepared using a lipids mixture consisting of neutral lipids, positively charged lipids and aromatic/fluorescent compounds. The mixture of two lipids, 18:1 (Δ9-Cis) PE (DOPE) (Avanti® Polar Lipids #850725P) and 18:1 TAP (1,2-dioleoyl-3-trimethylammonium-propane, DOTAP) (Avanti® Polar Lipids #890890) (**Figure 2-2**) was used at a ratio of 1/1 (mol/mol). Precisely, 1 mL of non-fluorescent CSMs dispersed in 20 mM HEPES was mixed with 20 µL of DOPE Atto 647N or DOPE Atto 488 (1 mg·mL^{-1}), 10 µL of DOTAP (10 mg·mL^{-1}), and 9 µL DOPE (10 mg·mL^{-1}), trying to reduce the volume of organic solvents in the FCSMs aqueous dispersion at a maximum of 0.02 mL (5% v/v of the entire solution). The solution was sonicated for 10 minutes and extruded 10 times using an Avanti® Mini extruder with an 800 nm polycarbonate membrane and purified by ultrafiltration using Amicon® Ultra-0.5 Centrifugal Filter Devices (cutoff of 100 kDa) and washing the solution with 20 mM HEPES at least 3 times. The solution of DOPE Atto 647N-labeled FCSMs was resuspended in 100 µL 20 mM HEPES volume.

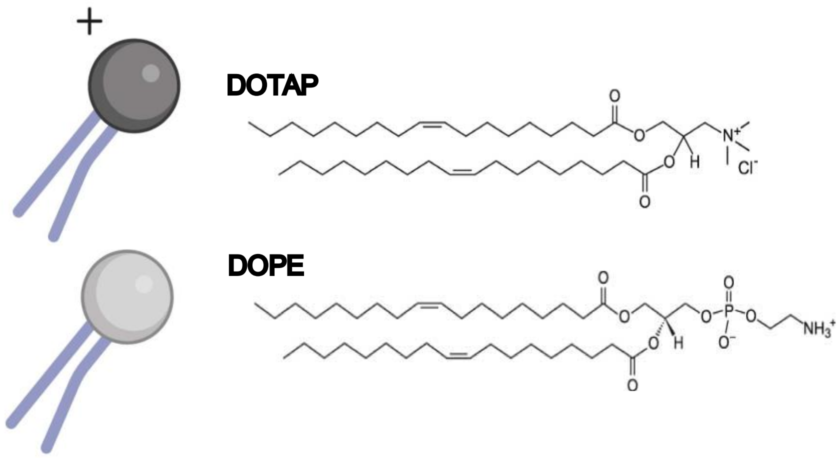

__Figure 2-2__ DOTAP and DOPE chemical structures.

SARS-CoV-2 Spike glycoprotein (S protein) expression was induced in HEK293 cells through plasmid transfection mediated by polyethyleneimine (PEI). In particular, $2.5 \cdot 10^6$ HEK293 cells were plated in a p60 dish and left 24 hours at 37 ºC 5% CO_2. Then, 5 µg of the plasmid of interest were added to the cells with 30 µL of 1 mg/mL polyethyleneimine (PEI) (Polysciences). After 24 hours, the medium was replaced with fresh cDMEM and the cells were left 48 hours at 37 ºC 5% CO_2. Two different plasmids were used to transfect HEK293 cells (**Figure 2-3**): pBOB-CAG-SARS-CoV2-Spike-HA (Addgene #141347), here named HA; pCMV14-3X-Flag-SARS-CoV-2-Spike (Addgene #145780), here named FLAG.

The resulting HEK293 cells expressing S protein on the surface were obtained from Collado's Lab (IDIS, Santiago de Compostela) and used to fabricate S protein derived CSMs (S-CSMs) as described in Section 2.1.

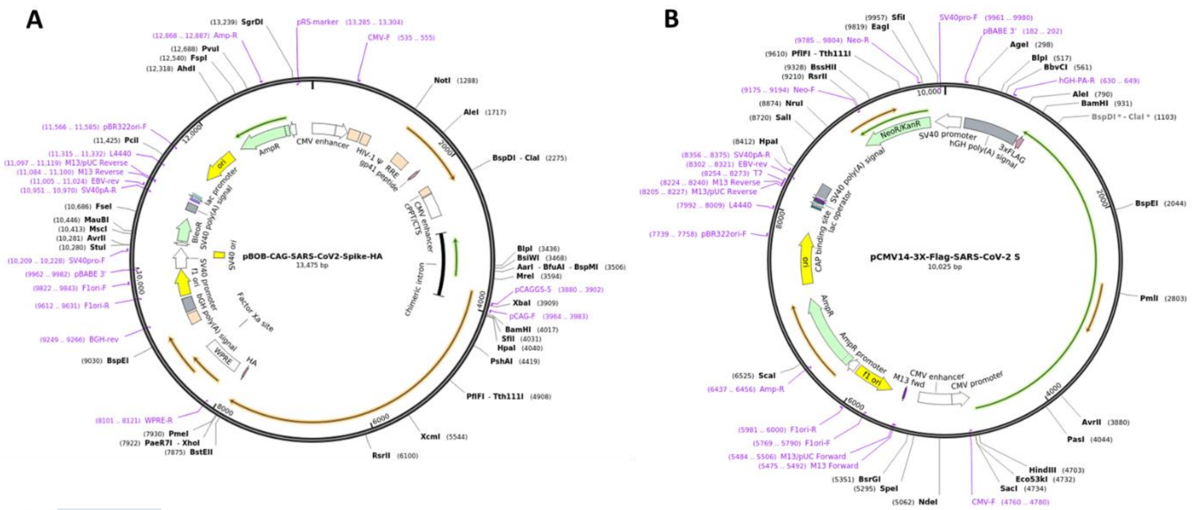

__Figure 2-3__ (A) HA and (B) FLAG plasmids used to transfect SARS-CoV-2 Spike glycoprotein in HEK293 cells.

2.3. CARGO LOADING: ENCAPSULATION AND PURIFICATION METHODS

2.3.1. Biomimetic coating of synthetic NPs

2.3.1.1. Polystyrene NPs (PSNPs)

To prepare CSM-coated NPs and FCSM-coated NPs, 1 mL of obtained A549 CSMs and FCSMs dispersed in 20 mM HEPES were mixed to polystyrene NPs (PSNPs) of either 100 nm or 200 nm diameter (Malvern Panalytical™ #NTA4093) at 4:1 molar ratio. After 15 minutes sonication, the mixture was extruded using an Avanti® Mini extruder with an 800 nm polycarbonate membrane. The resulting product was purified by centrifugation at 12,000 g for 10 minutes for 3 times and the collected PSNP@(F)CSM were re-suspended in 200 µL of 20 mM HEPES.

2.3.1.2. Metal-organic frameworks (MOFs)

UiO-67 MOFs at the nanometric range were fabricated following the procedure described by our group in the literature.[321] Briefly, zirconium oxychloride octahydrate ($ZrOCl_2 \cdot 8H_2O$), biphenyl dicarboxylic acid (H_2BPDC) and acetic acid (AA) were used as Zr source, ligand, and modulator, respectively, using a molar ratio of 1:2:220.

Rhodamine6G (Rho6G) and Cresyl Violet (CV) fluorophores were used as fluorescent cargos. Carboplatin (CaPt) was used as non-fluorescent drug cargo. UiO-67 were loaded by immersion of the NPs in a Rho6G/CV/CaPt aqueous solution for 3 days stirring at 80 ºC.[322] The post-synthesis loading is a highly efficient method that enables biomolecules loading in mild conditions.

To prepare CSM-coated and FCSM-coated MOFs, 1 mL of obtained A549 CSMs or FCSMs dispersed in 20 mM HEPES were slowly added to UiO-67 at 5:1 molar ratio while sonicating and the solution was left sonicating 15 minutes. Then, the mixture was extruded using an Avanti® Mini extruder with an 800 nm polycarbonate membrane and purified from the excess of empty (F)CSMs by a centrifugation step (10 minutes at 7,100 g). UiO-67@(F)CSM solution was finally resuspended in 20 mM HEPES.

2.3.2. Cargo encapsulation

2.3.2.1. Hoechst H 33258 (HOE)

0.05 mL of 1 mg·mL^{-1} Hoechst H 33258 (HOE) (Thermo Fisher Scientific™, #H3569) dissolved in methanol were added to 1 mL of CSMs dispersed in 1x PBS. The solution was sonicated 5 minutes and extruded 10 times using an Avanti® Mini extruder with an 800 nm polycarbonate membrane.

To purify the CSM(HOE) solution from the excess of non-encapsulated HOE, two different purification methods were used. In one case the solution was subjected to dialysis (Float-A-Lyzer G2, 1000 kDa cut-off) overnight. Otherwise, the solution was purified by size exclusion chromatography (using a PD-10 desalting column).

2.3.2.2. Doxorubicin (DOX)

0.5 mL of 1 mg·mL^{-1} doxorubicin (DOX) (Doxorubicin hydrochloride, Sigma-Aldrich®, #D1515-10MG) were added to 1 mL of CSMs derived from both proliferative and senescent A549 cells dispersed in 1 mM ammonium hydroxide. The solution was left stirring 1 hour at 37 ºC, then sonicated 10 minutes and extruded 10 times using an Avanti® Mini extruder with an 800 nm polycarbonate membrane.

The solution was purified from the excess of non-encapsulated DOX by size exclusion chromatography (using a PD-10 desalting column).

2.3.2.3. Recombinant tissue plasminogen activator (rtPA)

5 mg of commercially available recombinant tissue plasminogen activator (rtPA) (Actilyse®) were labeled with fluorescein isothiocyanate isomer I (FITC) by mixing 25 FITC/rtPA (mol/mol) in 1x PBS + L-Arg (3.5 mg·mL^{-1}). The reaction was left overnight at 4 ºC and then purified from the excess of FITC by size exclusion chromatography using a PD-10 desalting column and recollecting the fractions in 1 mL each.

Before rtPA-FITC encapsulation in CSMs, Bradford assay was used to quantify rtPA protein concentration of each fraction after the size exclusion purification technique (PD-10 column). Protein content was calculated by standard curve in **Figure 2-4** and in **Table 2-1**.

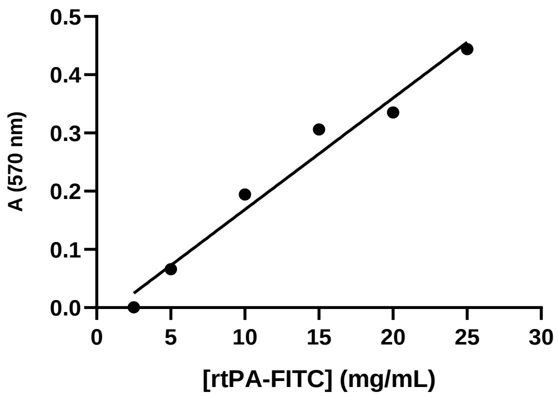

Figure 2-4 *Bradford assay calibration curve.*

Cal. curve	λ_A (nm)	Equation	R squared
rtPA-FITC	570	y = 0.0187x + 0.0144	0.9777

Table 2-1 *Absorbance measurements for the construction of Bradford assay calibration curve.*

0.4 mL of rtPA-FITC (fraction 2, 1 mg·mL^{-1}) was added to 0.5 mL of platelet-derived CSMs fluorescently labeled with DOPE Atto 647N. The solution was sonicated for 15 minutes, extruded 10 times using an Avanti® Mini extruder with an 800 nm polycarbonate membrane and purified from the excess of rtPA-FITC and DOPE Atto 647N by centrifugation (1 hour, 70,000 g, 4 ºC). CSM(rtPA) were finally resuspended in 1 mL of 1x PBS.

2.3.2.3.1. rtPA-FITC cargo activity

Tissue plasminogen activator chromogenic substrate (Sigma-Aldrich® #T2943) was used to determine rtPA-FITC activity once encapsulated in CSMs. 10 µL of 20 µg·mL^{-1} rtPA-FITC were diluted in 200 µL of 1x PBS + L-Arg (3.5 mg·mL^{-1}) and 48 µL of the chromogenic substrate were added subsequently. The measurement of absorbance was then determined with a plate reader (TECAN, Infinite® 200 PRO) at 405 nm during at least 12 hours (kinetics time point = 1 hour).

Since CSMs should prevent rtPA endogenous inactivation, rtPA activity was also tested in the presence of plasminogen activator inhibitor (PAI) (2 µL of PAI solution 0.25 mg·mL^{-1}).

2.3.2.4. Cas13d-gRNA complex

Cas13d protein obtained from the laboratory of Dr. M. A. Moreno (CABD, Sevilla) was labeled with sulfo-Cy3-maleimide (Lumiprobe®, #21380) according to the manufacturer's protocol. Briefly, Cas13d protein was dissolved in degassed 50 mM KCl 250 mM HEPES pH 7.5 and 100x molar excess of tris-carboxytheylphosphine (TCEP, Sigma-Aldrich®, #C4706) degassed reagent was added to reduce disulfide bonds. The solution was left 20 minutes at room temperature. Then, 20x molar excess of sulfo-Cy3-maleimide was added to the protein solution and left overnight at 4 ºC. The mixture was purified by ultrafiltration using Amicon® Ultra-0.5 Centrifugal Filter Devices (cutoff of 100 kDa) and washing the solution with 20 mM HEPES 3 times.

Fluorescently labeled Cas13d protein was added to single guide RNA (gRNA), obtained from the laboratory of Dr. M. A. Moreno (CABD, Sevilla), and left 5 minutes at 37 °C.

Cas13d*Cy3-gRNA complex was then added to 1 mL of A549 or E. Derm FCSMs (protein concentration: 0.05 mg·mL^{-1}), left 10 minutes at 37 °C and extruded using an Avanti® Mini extruder with an 800 nm polycarbonate membrane 10 times. The solution was then purified from the excess of non-encapsulated Cas13d-gRNA complex using Amicon® Ultra-0.5 Centrifugal Filter Devices (cutoff of 100 kDa).

2.3.2.5. Cas9-gRNA complex

Single guide RNA (sgRNA) sequence (Invitrogen™ TrueGuide™ Synthetic guide RNAs) was specifically designed *in silico* to target eGFP expressed in HEK-293 cells (293T-dEGFP), obtained from Collado's Lab (IDIS, Santiago de Compostela), by using the software provided by http://crispor.tefor.net/. The resulting synthetic sgRNA was designed as follows:

$$\mathrm{G*A*G*CUGGACGGCGACGUAAACGG}$$

According to manufacturer's procedure protocol for gene editing (including gene knockout), editing efficiency is highest with a 1:1 molar ratio of gRNA to Cas9 (Invitrogen™ TrueCut™ Cas9 Protein v2). Two different sample preparations were used (A and B).

Sample preparation A was composed as follows:

Reagent	Quantity
Opti-MEM™ I Medium	5 µL
Cas9 protein	50 ng (0.3 pmol)
gRNA	10 ng (0.3 pmol)
FCSM	20 µL

The solution was subjected to ultrasounds for 1 minute and incubated 15 minutes at room temperature. Then, the transfection complex A (10 µL of sample preparation A + 90 µL of cDMEM) was added to HEK293-GFP cells (volume/well).

Sample preparation B was composed as follows:

Reagent	Quantity
Opti-MEM™ I Medium	205 µL
Cas9 protein	250 ng (1.5 pmol)
gRNA	50 ng (1.5 pmol)
FCSM	80 µL

The solution was subjected to ultrasounds 1 minute, incubated 15 minutes at room temperature, extruded using an Avanti® Mini extruder with an 800 nm polycarbonate membrane 10 times and concentrated to 50 µL using Amicon® Ultra-0.5 Centrifugal Filter Devices (cutoff of 100 kDa). Then, the transfection complex B (10 µL of sample preparation B + 90 µL of cDMEM) was added to HEK293-GFP cells (volume/well).

2.4. CHARACTERIZATION OF CELL-DERIVED NANOVESICLES

2.4.1. Dynamic light scattering (DLS)

Dynamic light scattering (DLS) was used to characterize the colloidal properties of the (F)CSMs. All the samples were analyzed in 1x PBS or in 20 mM HEPES buffer by using a DLS Malvern Zetasizer Nano ZSP (Malvern Instrument Ktd) equipped with a 10 mW He-Ne laser operating at a wavelength of 633 nm laser and fixed scattering angle at 173º. All measurements were carried out at 37 ºC.

DLS was further used to characterize the monodispersity of CSMs solutions over time (24, 48, and 72 hours). CSMs were redispersed in different media to study their stability at different pH. The media evaluated were Dulbecco's Modified Eagle Medium (DMEM), phosphate buffered saline (PBS), 2-(N-morpholino)ethanesulfonic acid (MES), and Phagolysosomal Simulant Fluid (PSF), all of which further enriched with 10% FBS to better understand CSMs behavior in the different biological environments.

2.4.2. ζ potential

ζ potential of (F)CSMs re-dispersed in Milli-Q® water was measured with laser Doppler anemometry by Malvern Zetasizer Nano ZSP (Malvern Instrument Ktd.). ζ potential measurements reported are an average of three independent measurements.

2.4.3. Nanoparticle tracking analysis (NTA)

The principle of Nanoparticle Tracking Analysis (NTA) is based on the characteristic movement of NPs in solution according to the Brownian motion. The NPs trajectory in a defined volume is documented by a camera that captures the scatter light upon illumination of the NPs with a laser. Applying the Stokes-Einstein equation results in size determination for each tracked particle. Single particle count in relation with the cell volume enables particle concentration determination.

NTA was used to characterize the colloidal properties of the (F)CSMs and determine the (F)CSMs concentration in solution. All the samples were analyzed in 1x PBS or in 20 mM HEPES buffer by using a NanoSight NS300 (Malvern Instrument Ktd) equipped with a 405 nm laser. All measurements were carried out at 24 ºC. (F)CSMs were diluted 1:1,000 in Milli-Q® water (200 nm filtered) to a final volume of 1 mL and loaded in the measurement chamber with a flow rate of 50 $\mu L \cdot min^{-1}$. Flow mode measurements were obtained recording 3 videos of 60 s for each measurement. The NanoSight NS300 software was used to analyze the sample (10-100 particles/frame).

2.4.4. Quantification of protein content

The Bradford assay (PierceTM Coomassie Plus Assay Kit; ThermoFisher #23236) was used to determine the protein concentration. Following the manufacturer's instructions, 150 µL of diluted standard protein samples (standard bovine serum albumin, BSA stock 2 mg·mL^{-1}) in a working range of 1-25 µg·mL^{-1} and samples to be analyzed were mixed with 150 µL of Coomassie reagent in a 96 well microplate. The absorbance at 570 nm was read using a microplate reader (TECAN, Infinite® 200 PRO) and the protein content was calculated by the standard curve shown in **Figure 2-5** and **Table 2-2** and constructed by the linear regression.

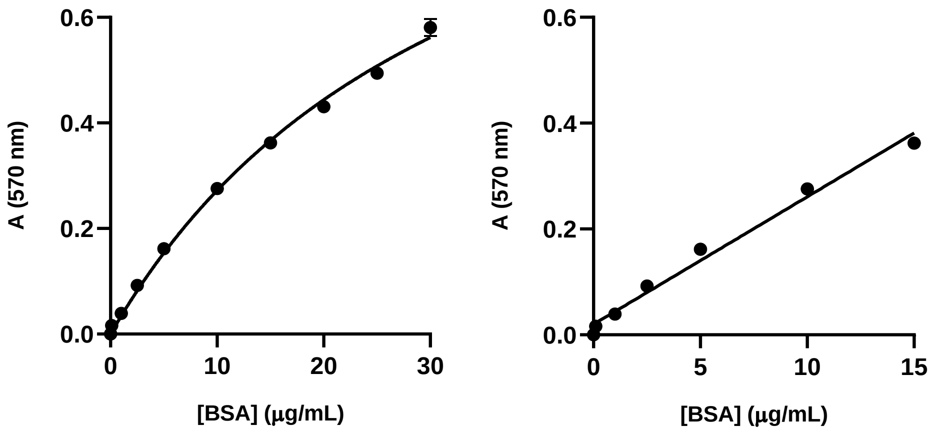

Figure 2-5 *BSA calibration curve.*

Cal. curve	λ_A (nm)	Equation	R squared
BSA	570	y = 0.02410x + 0.01981	0.9848

Table 2-2 *Absorbance measurements for the construction of Bradford assay calibration curve.*

2.4.5. Scanning transmission electron microscopy (STEM)

Scanning electron microscopy (SEM) and scanning transmission electron microscopy (STEM) analysis allowed the characterization of the structural properties of (F)CSMs. (F)CSMs solution was stained by using a 2% uranyl acetate solution. All images were obtained using a scanning transmission electron microscope ZEISS FESEM ULTRA Plus. The (F)CSMs were deposited from a dilute solution onto a 3-4 nm thick film of amorphous carbon supported on a 400-mesh copper grid (Ted Pella Inc., #01822-F). One drop (2 µL) of (F)CSMs suspension was deposited onto the grid, and the solvent was evaporated at room temperature.

2.4.6. Quantification of intercalated fluorescent lipids

The amount of fluorescent lipids intercalated in the lipidic bilayer of (F)CSMs was quantified by fluorescence analysis using a microplate reader (TECAN, Infinite® 200 PRO) equipped with monochromator-based optics and wavelength selection between 280 and 850 nm. The $\lambda_{ex}/\lambda_{em}$ ranges used for the different lipids are reported in **Table 2-3**. The lipids concentration in the solution was determined by interpolation of the measured fluorescence intensity from a previously constructed analytical calibration curve (**Table 2-3** and **Figure 2-6**).

Lipid	$\lambda_{ex}/\lambda_{em}$ (nm)	Equation	R squared
DOPE Atto 488	485/535	y = 1973x + 4.930	0.9996
DOPE Atto 647N	635/670	y = 43141x – 6.200	0.9935

Table 2-3 Fluorescence measurements for the construction of lipids calibration curves.

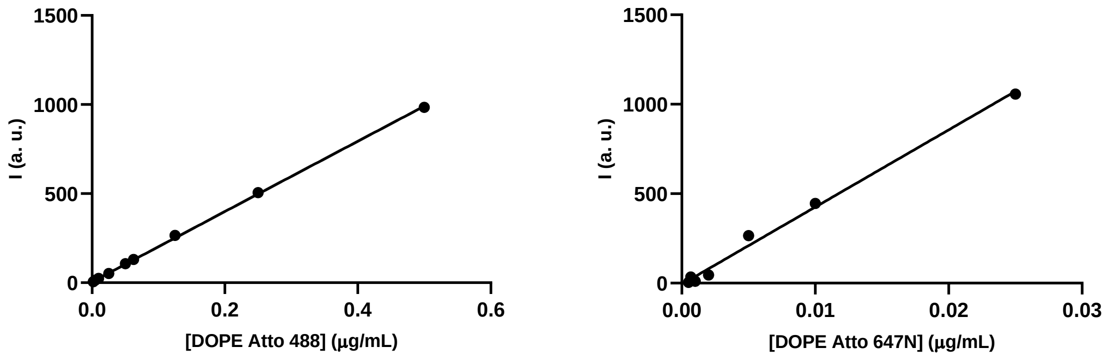

Figure 2-6 Calibration curves of the different lipids intercalated into (F)CSMs.

2.4.7. Quantification of encapsulated cargo

The amount of cargo molecules loaded into (F)CSMs was quantified by fluorescence or absorbance analysis using a microplate reader (TECAN, Infinite® 200 PRO) equipped with monochromator-based optics and wavelength selection between 280 and 850 nm or using a Horiba FluoroMax-3 spectrometer equipped with a 150-W xenon ozone-free lamp as excitation source and an R928P emission detector (180-850 nm). The λ_{abs} and $\lambda_{ex}/\lambda_{em}$ ranges used for the different molecules are reported in **Table 2-4**. The cargo concentration in the solution was determined by the interpolation of the measured absorbance or fluorescence intensity from a previously constructed analytical calibration curve (**Table 2-4** and **Figure 2-7**).

Cargo	$\lambda_{ex}/\lambda_{em}$ (nm)	λ_A (nm)	Equation	R squared
HOE	350/450	-	y = 578991x + 61557	0.9959
rtPA	485/535	-	y = 2855990x – 36.20	0.9990
Cas13d	545/580	-	y = 2174185x + 317.7	0.9989
DOX	-	480	y = 5.285x + 0.002692	0.9998

Table 2-4 *Fluorescence/absorbance measurements for the construction of cargos calibration curves.*

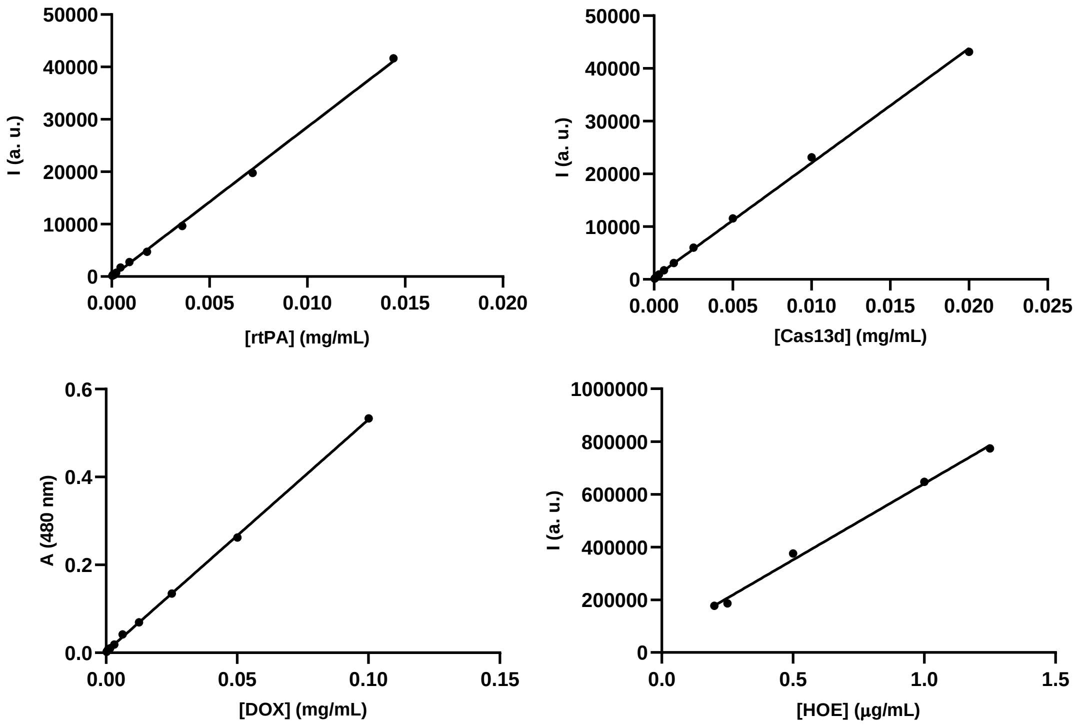

Figure 2-7 *Calibration curves of the different cargos loaded into (F)CSMs.*

Nevertheless, as shown in **Figure 2-8**, free HOE has its maximum of emission at around 500 nm (A), while encapsulated HOE's maximum of emission shifts to around 450 nm (B), where it should emit according to literature data: when bound to nucleic acids, HOE's fluorescence intensity is generally measured at 450 nm. Moreover, when bound to nucleic acids, its fluorescence intensity greatly increases.[323] Encapsulated HOE resulted to have a higher fluorescence intensity compared to free HOE, probably due to nucleic acids fragments remained in CSMs solution. Therefore, the quantification of encapsulated HOE through fluorescence measurements was impossible to achieve.

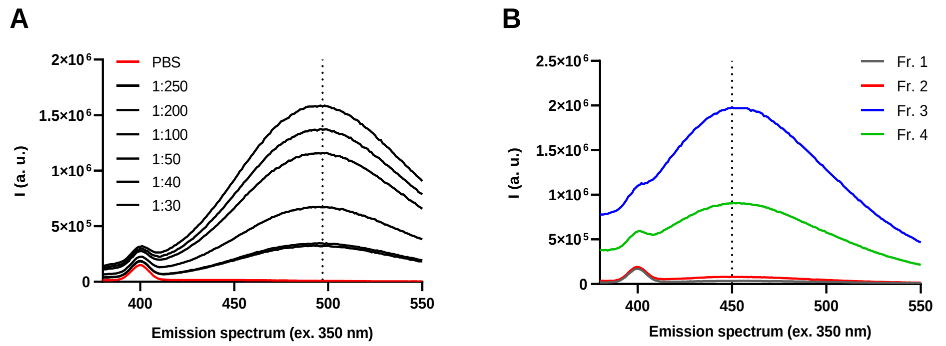

Figure 2-8 *Emission spectra of (A) free HOE at different concentrations and (B) CSM@HOE after purification with size exclusion chromatography (PD-10 column).*

The encapsulation efficiency (EE) was calculated by dividing the quantity of the cargo obtained from the encapsulation process by the initial quantity of cargo in the (F)CSMs solution:

$$EE\ (\%) = \frac{cargo_f\ (mg)}{cargo_i\ (mg)} \cdot 100$$

The concentration of PSNPs@(F)CSM and UiO-67@(F)CSM, was measured by NTA analysis and proved through fluorescence measurement by interpolation with the corresponding calibration curve.

2.4.8. Flow cytometry (FC)

Flow cytometry (FC) measurements were performed to detect the lipid intercalation into CSMs and to characterize the fluorescence signal from the cargo encapsulation and any specific surface markers in CSMs surface composition. The lower size-detection limit for light scattering of conventional flow cytometers is typically in the order of 200-500 nm. CSMs signal is discernible from the background by fluorescence intensity, forward and side light scattering detector. The forward and side scattering and fluorescence intensity of CSMs samples were measured with a Guava® easyCyte flow cytometer (Millipore®), using a blue laser emitting at 488 nm, a green laser emitting at 532 nm, and a red laser emitting at 642 nm as excitation sources. Background measurements in 1x PBS or in 20 mM HEPES buffer were performed before each measurement series and the corresponding threshold applied to remove the buffer signal. Forward (FSC) and side scattering (SSC) signals were recorded to gather information of the CSMs concentration and dispersion.

2.4.9. Storage and stability

(F)CSMs were either left at 4 ºC or subjected to lyophilization with a freeze dryer (Lyovapor™ L-300 Büchi) and subsequent resuspension in the designated buffer to study their stability in different storage conditions. In particular, the loaded cargo stability and activity were investigated before and after lyophilization and resuspension processes.

2.5. *IN VITRO* STUDIES

2.5.1. Cellular uptake

2.5.1.1. Flow cytometry (FC)

Before exposing to (F)CSMs, HeLa and A549 cells were seeded in 48-well plate at a density of 25,000 cells per well while the MRC-5, RAW264.7 and HEK cells were seeded at a density of 30,000 cells per well in 0.3 mL of cDMEM. After 24 hours, cells were washed with 1x PBS and the medium was replaced with freshly prepared CSMs dispersions of interest in cDMEM. Experiments were performed by exposing the cells to CSMs dispersions at $1 \cdot 10^5$ CSMs per cell at 37 °C and 5% CO_2 for 10 minutes, 1, 3 or 6 hours. After CSMs exposure, cells were washed with 0.5 mL 1x PBS per well. Then, cells were harvested after trypsinization for 2 minutes with 0.070 mL 0.25% Trypsin-EDTA. 0.15 mL of PBS was added to each well to recover the cells, which were then moved to a 96-well plate. Cell fluorescence intensity was measured using a Guava Millipore flow cytometer equipped with a 488 nm blue laser, a 532 nm green laser and a 642 nm red laser coupled with 525/30 nm, 583/26 nm, 620/50 nm, and 695/50 nm filters, depending on the CSMs fluorescence. Results are reported as the median of cell fluorescence intensity.

2.5.1.2. Inductively coupled plasma-optical emission spectrometry (ICP-OES)

Before exposing to UiO-67@(F)CSM, $1 \cdot 10^6$ A549 cells were seeded in T-75 flask in 10 mL of cDMEM. After 48 hours, cells were washed with 1x PBS and the medium was replaced with freshly prepared UiO-67@(F)CSM dispersions of interest in cDMEM. Experiments were performed by exposing the cells to different UiO-67 dispersions at 40 pM at 37 °C and 5% CO_2 for 1 hour. After CSMs exposure, cells were washed with 10 mL 1x PBS per T-75 flask. Then, cells were harvested after trypsinization for 2 minutes with 2 mL 0.25% Trypsin-EDTA by centrifuging them 5 minutes at 500 g. 0.1 mL of Milli-Q® water was added to each tube to resuspend the cells pellet.

A mixture of 3.6 mL of HCl 37% and 1.2 mL of HNO_3 65% was added to each tube, which was then subjected to an inorganic digestion protocol (up to 185 ºC) with a microwave digestion system (Anton Paar Multiwave GO Plus Microwave Digestion System). Subsequently, 0.5 mL of each digested sample was diluted in 5 mL of HCl 2% and Zr concentration was measured with inductively coupled plasma-optical emission spectrometry (Agilent 5800 ICP-OES).

The Zr concentrations (ppm) in the solutions were determined by interpolation of the measured optical emission intensities from previously constructed analytical calibration curves (**Figure 2-9**).

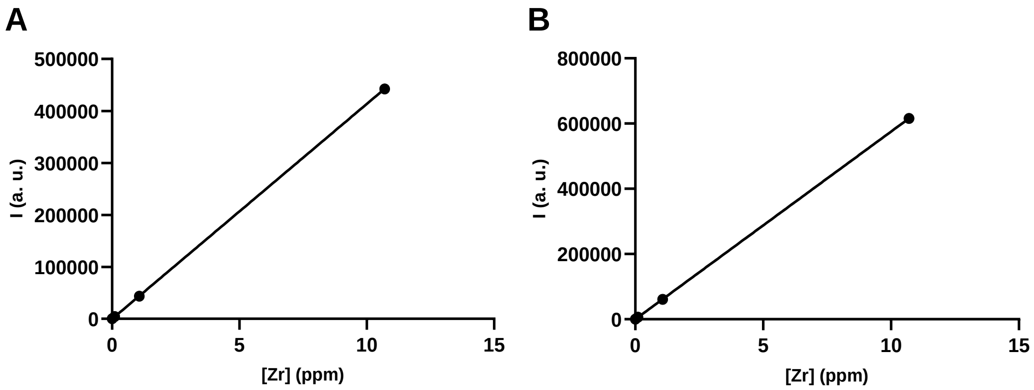

Figure 2-9 *Zr calibration curves measured at two different emission wavelengths: (A) 339.198 nm and (B) 343.823 nm.*

2.5.1.3. Fluorescence microscopy

To perform the confocal and epifluorescence imaging experiments with living cells, 25,000 A549 cells were seeded in 0.2 mL of cDMEM on µ-Slide 8 well-ibiTreat chambers (1 cm^2 per well, Ibidi, Germany, #80826). After 24 hours (F)CSMs were exposed to the cells by replacing the medium with freshly prepared (F)CSMs dispersions of interest in cDMEM. According to the incubation time, cells were washed once with 1x PBS in order to remove non-internalized particles. Cells were then washed twice with 1x PBS and 0.2 mL of HEPES supplemented media (DMEM without phenol red, 4.5 g·L-1 D-glucose and L-glutamine, 25 mM HEPES and without pyruvate, Gibco, #21063-029) was added to each Ibidi well.

For the fixation, cells were washed three times with 1x PBS and incubated with 3.6% formaldehyde solution (Sigma-Aldrich® #F8775) in PBS solution for 20 minutes at room temperature. Then, the formaldehyde solution was removed, and the cells were washed with 1x PBS before adding IBIDI Mounting Medium (Ibidi, #50001).

Fluorescence images of living and fixed cells were captured using a Thunder Leica® Microscope type DMI8 equipped with a Leica® DFC9000 camera. In the case of living cells, an OKO-lab incubator was used to keep cells at 37 °C during all the experiment. All the images were processed with ImageJ®.

Confocal images of living and fixed cells were captured on an Andor Dragonfly spinning disk confocal system mounted on a Nikon TiE microscope equipped with a Zyla 4.2 PLUS camera (Andor, Oxford Instruments). In the case of living cells, an OKO-lab incubator was used to keep cells at 37 °C during the experiment. Images were taken with different magnification objectives (20x, 60x, 100x). All the images were processed with ImageJ®.

2.5.2. Cellular toxicity

2.5.2.1. MTT assay

To study the number of viable cells after (F)CSMs exposure, 3-[4,5-dimethylthiazol-2-yl]-2,5-diphenyltetrazolium bromide (MTT) assay was performed. MTT is a colorimetric assay based on the reduction of the yellow tetrazolium salt to purple formazan crystals by metabolically active cells. A549 cells were seeded in 96-well plates, 7,500 cells per well in 100 µL of cell growth medium 24 hours before (F)CSMs exposure. The media was then removed and 100 µL of cell culture growth medium with the desired concentration of (F)CSMs were added. After the incubation time of (F)CSMs selected for each experiment, each well was rinsed once with 1x PBS and 110 µL of freshly prepared MTT solution diluted in cDMEM was added. After 3 hours at 37 °C and 5% CO_2, 85 µL of MTT solution were removed, 50 µL of DMSO were added to each well to dissolve the formazan crystals and the 96-well plate was left 10 minutes at 37 °C and 5% CO_2.

After the incubation time, absorbance was measured with a microplate reader (TECAN, Infinite® 200 PRO) at 540 nm. The absorbance value of each well provided by the instrument is an average of nine consecutive measurements in the same well.

Final absorbance value for control cells (Ac) (untreated), is an average of, at least, nine different well values. Final absorbance values for samples (As) are a mean of three independent well values. Cell viability value is calculated as follows:

$$Cell\ viability\ (\%) = \frac{As}{Ac} \cdot 100$$

2.5.2.2. Resazurin assay

Another way to study (F)CSMs toxicity is the resazurin assay. Cells were seeded in 96-well plates, 7,500 cells per well in 100 µL of cDMEM 24 hours before (F)CSMs exposure. The media was then removed and 100 µL of cell culture growth medium with the desired concentration of (F)CSMs were added. After the incubation time of (F)CS selected for each experiment, each well was rinsed once with 1x PBS and 110 µL of freshly prepared solution with 90% of cDMEM and 10% of Resazurin Sodium Salt (Sigma Aldrich®, #199303-1G) dissolved in Milli-Q® water (0.2 mg·mL^{-1}). Cells were incubated during 4 hours at 37 ºC and 5% CO_2 under dark conditions. Non-fluorescent resazurin (Almar blue) is oxidized by living cells into its fluorescent product resorufin. Therefore, in each well the fluorescence intensity can be considered proportional to the number of living cells.

After the incubation time, fluorescence was measured with a microplate reader (TECAN, Infinite® 200 PRO) under 560/20 nm excitation and collecting fluorescence intensities with a 610/20 nm filter. The fluorescence value of each well provided by the instrument is an average of nine consecutive measures in the same well.

Final fluorescence intensity value for control cells (Fc) (untreated), is an average of, at least, nine different well values. Final fluorescence intensity values for samples (Fs) are a mean of three independent well values. Cell viability value is calculated as follows:

$$Cell\ viability\ (\%) = \frac{Fs}{Fc} \cdot 100$$

2.5.3. Endocytic mechanism

For endocytosis studies, cells were seeded in 48-well plates in 0.3 mL of cDMEM at a density of 25,000 cells per well for the HeLa and A549 cells and of 30,000 cells per well for the MRC-5, RAW264.7, and HEK cells. After 24 hours the medium was replaced with the freshly prepared inhibitors solutions of interest in cDMEM at the concentrations reported in **Table 2-5**. Different endocytosis inhibitors were used for the endocytic mechanism study: nystatin (NYS) (Nystatin readymade solution, Sigma Aldrich®, #N9150), dynasore (DYN) (Dynasore hydrate, Sigma Aldrich®, #D7693), chloroquine (CQ) (Chloroquine diphosphate salt, Sigma Aldrich®, #C6628-25G), chlorpromazine (CP) (Chlorpromazine hydrochloride, Sigma Aldrich®, #C8138-5G), and methyl-β-cyclodextrin (MBCD) (Methyl-β-cyclodextrin, Sigma Aldrich®, #C4555-1G) (the chemical structures of all the endocytosis inhibitors are shown in **Figure 2-10**).

Inhibitor	Concentration	
	(mM)	(μg/mL)
Nystatin (NYS)	0.01	10
Dynasore (DYN)	0.08	25.78
Chloroquine (CQ)	0.1	32
Chlorpromazine (CP)	0.03	10
Methyl-β-cyclodextrin (MBCD)	5	6250

Table 2-5 *Inhibitors used to study CSMs endocytic pathway.*

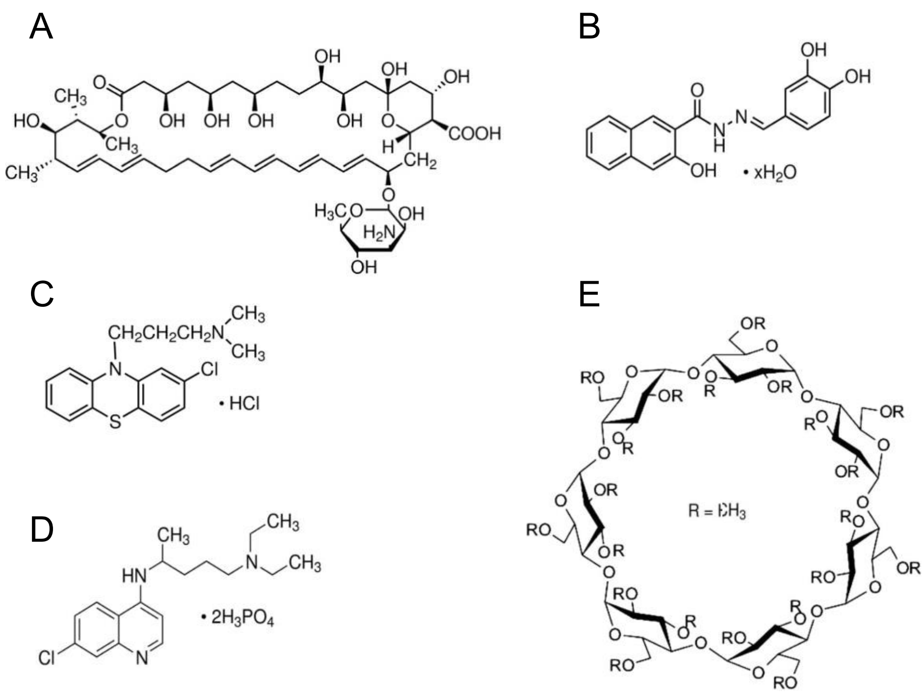

Figure 2-10 Chemical structures of endocytosis inhibitors. A: nystatin (NYS); B: dynasore (DYN); C: chlorpromazine (CP); D: chloroquine (CQ); E: methyl-β-cyclodextrin (MBCD).

After 30 minutes of treatment, the inhibitor solutions were replaced with the same solutions enriched with fluorescent CSMs at a concentration of $2 \cdot 10^{11}$ CSMs·mL^{-1} at 37 °C and 5% CO_2 for 2 hours. Then the cells were washed with 1 mL of PBS per well and harvested after trypsinization for 2 minutes with 0.075 mL of 0.25% Trypsin-EDTA. 0.15 mL of PBS were added to each well to recover the cells. The CSMs uptake under the different inhibitor conditions was evaluated by cell fluorescence intensity that was measured using a Guava Millipore flow cytometer equipped with a 488 nm blue laser and a 532 nm green laser coupled with 525/30 nm, 583/26 nm, 620/50 nm and 695/50 nm filters, depending on the CSMs fluorescence.

2.5.4. Cargo activity

2.5.4.1. Doxorubicin (DOX)

DOX has the ability to intercalate into the DNA helix and/or bind covalently to proteins involved in DNA replication and transcription, leading to cell death. For this reason, DOX activity in cells was measured with the toxicity assays described above (Sections 2.5.2.1 and 2.5.2.2).

2.5.4.2. Cas13d-gRNA complex activity

Before exposing to FCSMs, A549-GFP cells were seeded in 48-well plate at a density of 25,000 cells per well in 0.3 mL of cDMEM. After 24 hours, cells were washed with 1x PBS and the medium was replaced with freshly prepared FCSMs dispersions of interest in cDMEM. Experiments were performed by exposing cells to Cas13d-gRNA dispersions overnight at 1 µg per well. 48, 72 and 120 hours after FCSM(Cas13d-gRNA) exposure, cells were washed with 0.5 mL of 1x PBS per well. Then, cells were harvested after trypsinization for 2 minutes with 0.07 mL of 0.25% Trypsin-EDTA. 0.15 mL of PBS was added to each well to recover the cells, which were then moved to a 96-well plate. Cell fluorescence intensity was measured using a Guava Millipore flow cytometer equipped with a 488 nm blue laser coupled with 525/30 nm. Results are reported as the median of cell fluorescence intensity.

2.5.4.3. Cas9-gRNA complex activity

Before exposing to FCSMs, HEK293-GFP cells were seeded in 96-well plate at a density of 18,000 cells per well in 0.1 mL of cDMEM. After 24 hours, cells were washed with 1x PBS and the medium was replaced with freshly prepared FCSMs dispersions of interest in cDMEM following manufacturer's procedure protocol (see Section 2.3.2.4). Experiments were performed by exposing cells to Cas9-gRNA dispersions overnight at a ratio of 250 ng:50 ng (Cas9:gRNA) per well. 48 hours after FCSM(Cas9-gRNA) exposure, cells were washed with 0.05 mL of 1x PBS per well. Then, cells were harvested after trypsinization for 2 minutes with 0.03 mL of 0.25% Trypsin-EDTA. 0.12 mL of PBS was added to each well to dilute Trypsin-EDTA concentration. Cell fluorescence intensity was measured using a Guava Millipore flow cytometer equipped with a 488 nm blue laser coupled with 525/30 nm filter. Results are reported as the median of cell fluorescence intensity.

2.5.5. Statistical analysis

All data are presented as the mean and standard deviation (SD). Two-way ANOVA was used to test the differences between groups. Statistical significance was set at $p<0.05$. All statistical analysis were conducted using GraphPad Prism 8.0.1.

2.6. PRELIMINARY *IN VIVO* STUDIES

All the *in vivo* experiments have been performed in collaboration with Dr. F. Campos and Dr. C. Correa from LINC group (IDIS, Santiago de Compostela).

2.6.1. Animal procedures

Swiss male mice (Harlan Laboratories, Barcelona, Spain) with a weight between 25 to 30 g were used. Mice were kept in separate rooms under controlled conditions of temperature (22°C ± 1°C) and humidity (60% ± 5%) with a 12/12 hours light/dark cycle for a week prior to surgery and up to 7 days after surgery. They had access to food and water ad libitum.

All the procedures were performed under anesthesia. Anesthesia was induced by the inhalation of 5% sevoflurane in a nitrous oxide/oxygen mixture (70/30). Rectal temperature was monitored and maintained at 37°C ± 0.5°C by using a feedback-controlled heating system. At the end of the procedures, mice were sacrificed under deep anesthesia (8% sevoflurane).

Experimental protocols and animal handling were approved by the chief of the Servicio provincial de ganadería del departamento territorial da consellería de medio Rural e do Mar de la provincia de A Coruña being the main responsible Dr. Francisco Campos Pérez and under the procedure number 15011/2022/005, according to the Spanish and EU rules (86/609/CEE, 2003/65/CE, 2010/63/EU, RD 1201/2005 AND RD 53/2013).

2.6.2. Therapeutic effect

Thromboembolic stroke model was induced by injection in the middle cerebral artery (MCA) of mice.[324] Mice were placed in a stereotaxic frame, the skin between the right ear and eye was cut, the temporal muscle was retracted, and the temporal and parietal bones exposed. A small craniotomy was performed over the artery bifurcation, the meninges were cut using a 25 G needle (BD Microlance, Ref. 300600) and the MCA was exposed.

A micropipette (tip size: 20-40 µm), made with hematologic glass capillaries (World Precision Instruments, Inc. USA) using a puller (Sutter Instruments), was pneumatically filled with 1.5 µL of 1.5 U/µL thrombin (Murine Thrombin 0.05 mg MIIA. Stago-BNL). The micropipette was placed in a micromanipulator and 1 µL of thrombin solution was injected into the lumen of the artery bifurcation to induce the formation of a clot. The micropipette was removed 15 minutes later, when the clot was stabilized.

Cerebral blood flow (CBF) was monitored with a Periflux 5000 laser Doppler perfusion monitor (Perimed AB, Järfälla, Sweden) by placing the Doppler probe (MT B500-0L240, Straight Microtip, Perimed) in the parietal territory of the MCA. Basal CBF and throughout the experiment was measured. Artery occlusion was considered successful when the CBF downfall more than 60% relative to the basal.

After 30 minutes, the different treatments were administered intravenously into the tail vein. A small incision was made in the animal's tail. The skin was cut out and the tail vein was exposed. A 30 G needle (BD Microlance, Ref. 4656300) was used for every treatment administration; then the puncture was rapidly closed to prevent bleeding. In the animals whose treatment was administered as perfusion, the 30 G needle was put in a catheter (polythene tube, 0.28 mm internal diameter, 0.61 mm outside diameter, Smiths) and the rate of injection was controlled using an injection pump.

Animals' groups of treatment are shown in **Table 2-6**.

Group of treatment	Way of administration	Nº animals
Vehicle	Bolus	8
rtPA	1 mg/kg as bolus	8
CSM	Corresponding to the same number of CSM(rtPA) as bolus	8
CSM(rtPA)	1 mg/kg of loaded rtPA as bolus	8
Lyophilized CSM(rtPA)	1 mg/kg of loaded rtPA as bolus	8

Table 2-6 *Animals' groups of treatment for the study of rtPA therapeutic effect.*

2.6.3. Magnetic resonance imaging (MRI) analysis

MRI studies were conducted on a 9.4 T horizontal bore magnet (BrukerBioSpin, Ettligen, Germany) with 12 cm wide actively shielded gradient coils (440 mT/m). Radiofrequency transmission was achieved with a birdcage volume resonator; signal was detected using a two-element arrayed surface coil (RAPID Biomedical, Germany), positioned over the head of the animal, which was fixed with a teeth bar, earplugs and adhesive tape. Respiratory frequency and body temperature were monitored throughout the experiment. Transmission and reception coils were actively decoupled from each other. Gradient-echo pilot scans were performed at the beginning of each imaging session for accurate positioning of the animal inside the magnet bore.

2.6.3.1. T2-weighted sequence

The progression of ischemic lesions and infarct volumes were determined from T2-maps calculated from T2-weighted images. Ischemic lesion was determined by counting pixels with apparent T2-map values above a threshold in the ipsilateral brain hemisphere.

In healthy mice, the T2-map values of the brain are over 50 ms. In the ipsilateral ischemic hemisphere, hyperintensity on T2-map determined the analysis of the ischemic damage (T2 map values > 60 ms).

T2-weighted images were acquired using a multi-slice multi-echo (MSME) sequence with a 11 ms echo time (TE), 2.8 s repetition time (TR), 12 echoes with 11 ms echo spacing, FA of 180º, 2 averages, 50 KHz spectral bandwidth (SW), 16 slices of 0.5 mm, 19.2 × 19.2 mm^2 FOV with saturation bands to suppress signal outside this FOV, a matrix size of 256 × 256 (isotropic in-plane resolution of 75 µm/pixel × 75 µm/pixel) and implemented without fat suppression option. The acquisition time was 23 minutes.

2.6.3.2. T2*-weighted sequence

T2*-weighted images were acquired using a multi-gradient-echo sequence (MGE) with a 5 ms TE, 1.2 s TR, 8 echoes with 4.5 ms echo spacing, 100 KHz spectral bandwidth, FA of 20º, 16 slices of 0.55 mm, 2 averages, 19.2 × 19.2 mm^2 FOV with saturation bands to suppress signal outside this FOV, a matrix size of 256 × 256 (isotropic in-plane resolution of 75 µm/pixel × 75 µm/pixel) and implemented with fat suppression option. The acquisition time was 10 minutes.

2.6.4. Plasmatic activity

Pharmacokinetic activity of rtPA was analysed in healthy animals treated with (1) vehicle, (2) rtPA at 1 mg/kg as bolus, (3) CSM(rtPA) (1 mg/kg of rtPA) as bolus; (4) CSM(rtPA)/L (1 mg/kg of rtPA) as bolus. All treatments were administered as a final volume of 0.2 mL through the tail vein. For enzymatic analysis, blood samples were collected in a microtainer BD (Microtainer K2E Tubes. Ref: 365975, Franklin Lakes, NJ) from the carotid artery in basal conditions (before treatment administration) and 1, 5, 15 and 40 minutes after the treatment administration. Blood samples were processed to obtain plasma, which was subsequently assayed using a commercial kit (Sensolyte AMC tPA Activity Assay, Anaspec, France).

2.6.5. Tail bleeding assay

After anesthetizing the mice, different treatments were intravenously administered, and 20 mm of the tail was cut using a blade. Immediately, the tail was inserted in an Eppendorf with 1 mL of saline pre-heated to 37°C, where the blood was collected. The bleeding time and re-bleedings were controlled for 20 minutes.

Animals' groups of treatment are shown in **Table 2-7**.

Group of treatment	Way of administration	Nº animals
Vehicle	Bolus	5
rtPA	1 mg/kg as bolus	5
CSM(rtPA)	1 mg/kg of loaded rtPA as bolus	5

Table 2-7 *Animals' groups of treatment for the tail bleeding assay.*

2.6.6. Statistical analysis

All data are presented as the mean and standard error of the mean (SEM). Data was first examined to assess distribution using D'Agostino-Pearson omnibus normality test. One-way ANOVA was used to test the differences between groups. Statistical significance was set at $p<0.05$. The statistical analysis was conducted using GraphPad Prism 8.0.1.

3. Results and discussion

3.1. ENGINEERING BIOMIMETIC NANOVESICLES

Engineered nanomaterials (ENMs) have raised huge expectations in therapeutic and diagnostic applications and during the last 15 years nanomedicine has clearly made improvements in different therapeutic areas by enhancing the bioavailability of therapeutic agents and their sustained release at precise target tissues.[325]

In this regard, compared to other nanomaterials, liposomes and lipids-based nanomaterials show decreased toxicity, improved pharmacokinetics parameters (such as circulation time, biodistribution, controlled release, etc.) and enhanced stability, being in most cases the first choices nanoformulations approved to date.[326] These advantages are mainly due to the phospholipid bilayer that characterizes lipidic formulations. However, synthetic lipids-formulations may imply important drawbacks regarding bloodstream clearance and tissue targeting capabilities, which could impair the entire beneficial contribution of the phospholipid bilayer itself.

Cell membrane-derived nanovesicles (here called cellsomes or CSMs) represent a validate candidate not only for overcoming the principal limitations of common synthetic nanomaterials, but also to enhance liposomal formulations' main drawbacks. Cells plasma membrane defines the biological identity and behavior of cells and has many essential functions, including mediating cell interactions with the biological environment.[327] Translating cells membrane features to nanomaterials would allow the achievement of innovative biomimetic nanocarriers that could take advantage of the biological sources from which they are originated.

The cell membrane strategy provides several beneficial features when exploited for the fabrication of drug delivery systems. It allows the mediation between the nanocarrier and the biological milieu, favoring the NPs-cells interaction and the recognition as "self" by the immune system.

Moreover, cells plasma membrane possesses a unique biological pattern, not only composed by a distinctive phospholipidic bilayer, but also enriched with surface and transmembrane proteins, glycoproteins, receptors, ion channels, etc. that characterize each cell type. This attribute of individuality ends up in the intrinsic ability of cell membrane-derived nanosystems to interact preferentially with their source cells, called homotypic targeting.

On the other hand, the possibility of using cell plasma membrane as a smart approach for the biomimetic coating of synthetic nanomaterials (e.g., inorganic or polymeric NPs) permits the lowering of encapsulated drug doses and therefore the reduction of potential toxic side effects. In addition, the ideal core-shell strategy should be composed by an inner multifunctional drug carrier and a universal biomimetic coating able to enhance the interactions with the biological environment.

Cell membrane-derived nanocarriers have shown several benefits, such as reducing immune activation, prolonging blood circulation times, and enabling specific targeting of tumors. Most studies have demonstrated their biocompatibility and safety in mouse models. However, for successful clinical applications, standardized protocols for synthesis and characterization, and a deeper understanding of their behavior at the cellular level is required.

Standardization protocols are challenging due to the different requirements for various cell types, leading to heterogeneity in the produced nanocarriers. This requires well-defined characterization tools to analyze the surface composition and the biological efficacy. Identifying critical motifs responsible for targeting specific surface markers and cell receptors is crucial for designing efficient nanocarriers to target individual tissues. Ensuring the integrity and correct orientation of key membrane proteins on cell surface fragments are essential for maintaining targeting ability and long-term stability of the nanocarriers after assembly. The targeting ability may be affected by the loss of proteins or their functionality during cell membrane extraction, purification, or storage processes. Addressing these challenges will contribute to advancing the clinical potential of biomimetic nanocarriers for precise drug delivery.

This chapter provides a comprehensive description of the study and assessment of the synthetic protocol for obtaining CSMs from various cell lines. Additionally, the physicochemical properties of CSMs were thoroughly examined and their interactions with cells were explored.

3.1.1. Preparation and characterization of cell-derived nanovesicles from different cell lines

Here, CSMs derived from different cell lines (tumoral and non-tumoral cell lines, platelets, red blood cells, immune cells, etc.) were obtained following the protocol described in Section 2.1 (**Figure 3-1**). The synthetic optimized protocol is based on two physical disruption methods that have the capability to break down cell membranes. This process involves the application of different external forces, such as heat and pressure, to lyse the cells. The complete cell lysis occurs through two main steps: (i) an osmotic shock induced by a hypotonic buffer and (ii) a thermal lysis achieved by subjecting the cells to repeated freezing-thawing cycles. The hypotonic solution plays a crucial role in this process by providing the necessary osmotic pressure to cause cell swelling. When the concentration of salt surrounding the cell suddenly decreases, the cell membrane becomes permeable to water due to the osmosis effect. As a result, temporary openings are formed in the cell membrane, allowing the cellular components to be emptied from the cell.

Once collected, $10\text{-}20\cdot10^6$ cells were washed and resuspended in a hypotonic buffer to induce cells osmotic swelling and bursting. To preserve the biological identity of cells plasma membrane a protease inhibitor cocktail (PIC) was added to the solution and left 10 minutes at 4 ºC. Then a thermal shock (freeze-thaw method) was used to promote the cells lysis: the solution was subjected to 4 cycles of freezing in liquid nitrogen for 1 minutes and thawing at 37 °C for 10 minutes. Repeated cycles of freezing and thawing steps lyses cells through ice crystal formation inside the cell which helps in rupturing the cell membrane. Finally, a mechanical shock (ultrasounds) was applied to the solution for 5 minutes.

To purify the cell membrane fragments, the solution was then subjected to two different centrifugation steps. A first centrifugation step (700 g for 10 minutes) was used to discard the nuclei or the remained whole cells. The cell membrane fragments remained in the supernatant were subsequently precipitated by another centrifugation step (15,000 g for 30 minutes at 4 °C).

The purified cell membrane fragments precipitated were resuspended in physiological buffer (generally PBS or HEPES) and induced to self-assemble into nanovesicles through a mechanical extrusion process. It is worth noting here that the extrusion process was found to be a critical point to obtain highly monodispersed CSMs solutions. Increasing the number of extrusion steps would narrow the size distribution of the CSMs synthesized. The solution was subjected to 10 cycles of extrusion by using an Avanti® Mini extruder with 800 nm polycarbonate membrane.

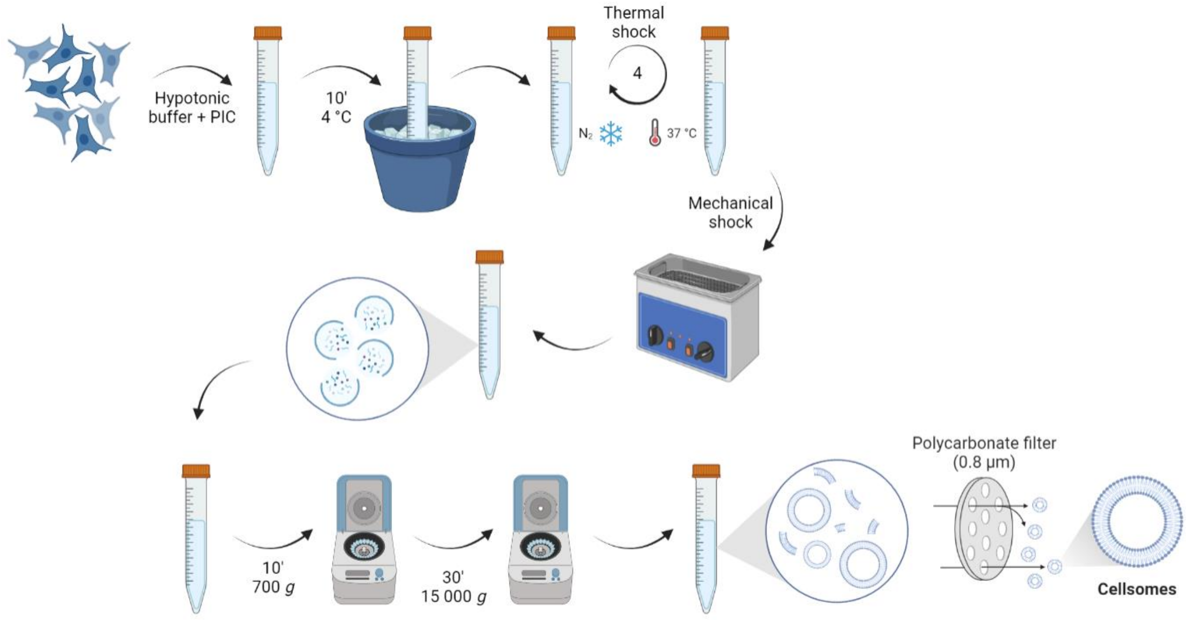

Figure 3-1 *Schematic CSMs synthesis main steps.*

Then, the cell-derived nanostructures produced should be fully characterized. A wide range of techniques are employed to assess their physicochemical features: Electron Microscopy (EM) for morphology determination, Dynamic Light Scattering (DLS) for hydrodynamic size and colloidal stability, Nanoparticles Tracking Analysis (NTA) for concentration and size distribution analysis. Moreover, proteomic techniques and immunofluorescence are applied to characterize the biological properties. To evaluate the biomimetic capabilities of the synthesized CSMs, *in vitro* cell studies were conducted.

3.1.1.1. Physicochemical characterization

In this first chapter, different cell lines were used as natural sources to fabricate CSMs, which were then characterized from a physicochemical perspective to highlight the universal feature of CSMs. In particular, RAW264.7 (a murine macrophage cell line) was used as a prototype cellular model for different characterization protocols.

DLS is a common and robust technique used to determine the hydrodynamic diameter of NPs and the quality and monodispersity of the size distribution indicated by the polydispersity index (PDI). DLS was used to characterize the colloidal properties of CSMs. Size distribution analysis of RAW264.7-CSMs (**Figure 3-2**) was performed by DLS measurements to obtain size distribution in intensity (A), in number (B), and in volume (C) values. Similar values of the hydrodynamic diameter (about 150-200 nm) for the three of them, intensity (I), volume (V) and number distributions (N), and low values of PDI (below 0.2) were obtained. These results show that only one size distribution is present in the CSMs sample solution and there were no agglomerates or aggregates.

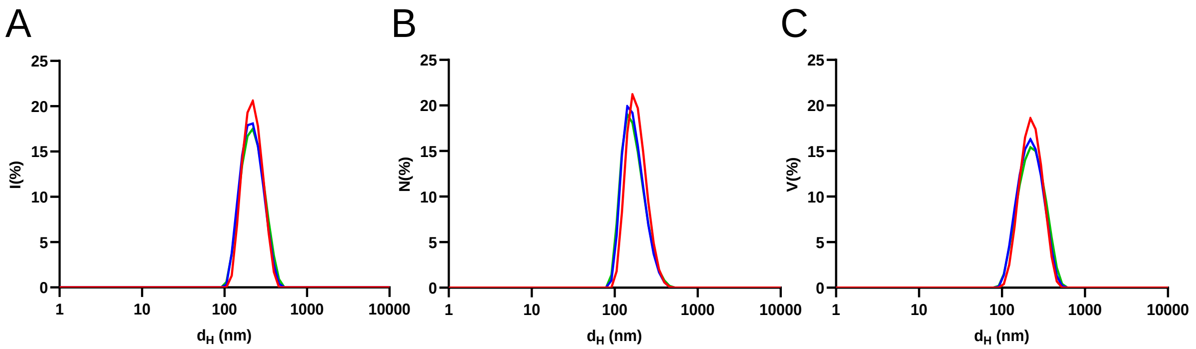

Figure 3-2 *Hydrodynamic diameter distribution analysis of RAW264.7-derived CSMs. DLS measurements were performed to obtain (A) intensity, (B) number, and (C) volume values.*

Then, DLS measurements were performed for CSMs derived from other cell lines (tumoral cell lines such as cervix epithelial carcinoma cells, HeLa cell, and adenocarcinoma human alveolar basal epithelial cells, A549 cells; healthy embryonic adrenal cell line, HEK cells; fibroblasts, MRC-5, platelets, red blood cells, and macrophages, RAW264.7 cells), which showed highly monodisperse size distribution and nearly constant hydrodynamic diameter for all the CSMs samples obtained from the different cell lines (**Table 3-1**), indicating that the synthesis protocol used to fabricate CSMs was optimized to generate monodisperse nanovesicles with the same diameter size.

Sample	Z-Average (nm)	PdI	$d_{H,I}$ (nm)	$d_{H,N}$ (nm)	$d_{H,V}$ (nm)
HeLa-CSM	196.1 ± 1.5	0.149 ± 0.044	221.4 ± 4.1	162.9 ± 4.6	230.5 ± 5.4
A549-CSM	256.4 ± 49.2	0.435 ± 0.113	144.5 ± 5.2	133.9 ± 4.0	142.7 ± 5.3
Platelets-CSM	254.7 ± 6.2	0.296 ± 0.053	238.8 ± 4.4	205.1 ± 4.2	250.4 ± 6.7
RAW264.7-CSM	211.5 ± 6.7	0.157 ± 0.023	225.4 ± 3.1	180.5 ± 7.9	235.1 ± 4.1
HEK293-CSM	255.0 ± 29.5	0.320 ± 0.010	255.0 ± 29.5	231.6 ± 3.1	291.9 ± 41.3
MRC-5-CSM	228.4 ± 12.2	0.211 ± 0.028	247.2 ± 12.5	193.1 ± 21.7	263.4 ± 20.9
RBC-CSM	166.3 ± 1.1	0.093 ± 0.028	180.3 ± 1.3	140.5 ± 5.9	179.4 ± 0.8

Table 3-1 *DLS analysis of CSMs derived from different cell lines.*

As mentioned, one of the most important and innovative feature of cell membrane-derived nanovesicles is their universality. Thanks to the optimization of each step of the synthesis process, CSMs derived from many different cell lines were fabricated. The physicochemical characterization indicates that, regardless of the source cell from which they derived, all of them showed similar particles size distribution.

NTA (**Figure 3-3** and **Table 3-2**) was used to further corroborate the colloidal properties of CSMs and determine their concentration in solution, a key parameter to establish and adapt the CSMs doses for *in vitro* and *in vivo* studies.

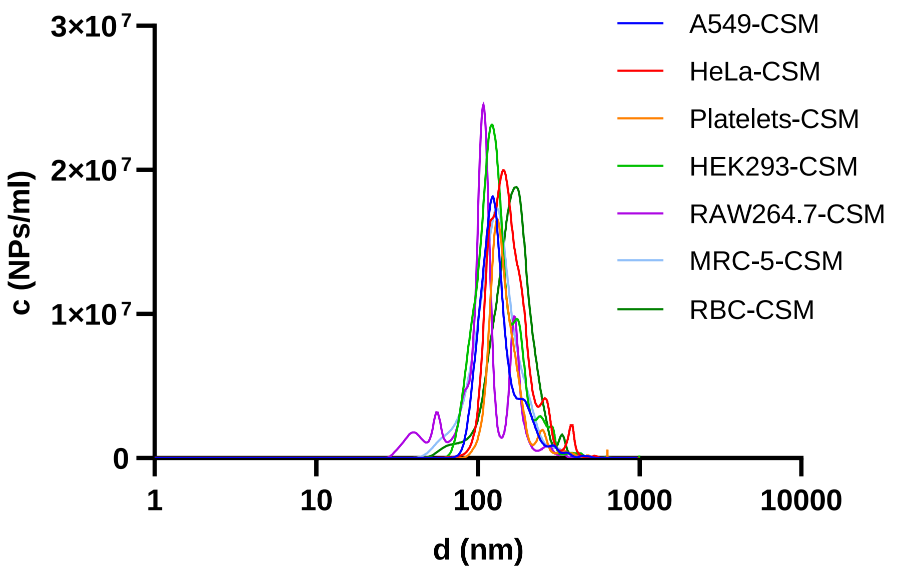

Figure 3-3 *NTA size distribution analysis of CSMs derived from different cell lines.*

Sample	d (mean) (nm)	d (mode) (nm)	c (NPs/mL)
HeLa-CSM	183.0 ± 4.6	137.7 ± 10.1	4.02E+11
A549-CSM	156.7 ± 4.9	119.9 ± 4.1	1.23E+12
Platelets-CSM	169.7 ± 2.0	134.1 ± 2.1	1.03E+12
RAW264.7-CSM	134.7 ± 2.5	108.4 ± 1.6	3.76E+10
HEK-293-CSM	157.4 ± 2.6	123.5 ± 5.2	3.76E+11
MRC-5-CSM	152 ± 0.7	122.2 ± 11	2.87 E+11
RBC-CSM	180.4 ± 3.9	170.0 ± 5.4	3.91E+11

Table 3-2 *NTA analysis data of CSMs derived from different cell lines.*

In addition, scanning transmission electron microscopy (SEM-STEM) images were acquired to corroborate the CSMs size and morphology. Here, negative staining with uranyl acetate was employed since uranyl ions combine in large quantities with phosphate and carboxyl groups of the cell surface, therefore allowing an adequate level of contrast in STEM imaging for biological samples.

As shown in **Figure 3-4**, CSMs, as phospholipidic-based nanovesicles, resemble liposomes morphology and structure.

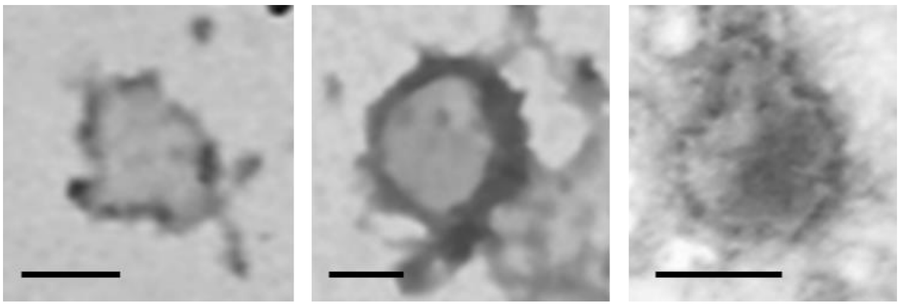

Figure 3-4 *STEM micrograph of CSMs. Scale bars: 100 nm.*

3.1.1.2. CSMs stability in different biological conditions

Nanomaterials for biological applications are expected to not sediment or aggregate. However, aggregation after changes in the ionic force or pH of the media can occur frequently for NPs dispersion. One of the main advantages of cell membrane-derived nanovesicles is their stability in physiological conditions.

To evaluate the polydispersity of the samples and assess their stability during time in different conditions, dynamic light scattering analysis were performed.

DLS analysis offers the possibility of measuring the correlation coefficient at different delay times. Correlation is a technique for extracting the time dependence of a signal in the presence of "noise". Typically, NPs mean size is indicated when the correlation function starts decaying. Moreover, DLS offers the possibility of measuring the random movement of a particle undergoing Brownian motion. In particular, for random Brownian motion, to which a monodisperse solution of NPs is subjected, the correlation curve should always decay. Increases in correlation at high delay times indicate non-random movements, such as sedimentation.

Here, RAW264.7 cells-derived CSMs were used as prototypical CSMs for stability studies in different biological settings (**Figure 3-5** and **Figure 3-6**). CSMs were diluted in buffers at different pH to mimic the biological conditions of the study.

Phosphate Buffer Saline (PBS) pH 7.4, 2-(N-morpholino)ethanesulfonic acid (MES) pH 6 and Phagolysosomal Simulant Fluid (PSF) pH 4.7 were chosen as biological conditions to which CSMs were subjected. As shown in **Figure 3-5**, at pH 7.4 (A) CSMs colloidal stability was not affected during time, while at pH 6 (B) and especially at pH 4.7 (C) CSMs correlation functions indicates a loss in samples monodispersity and the presence of possible sedimentation.

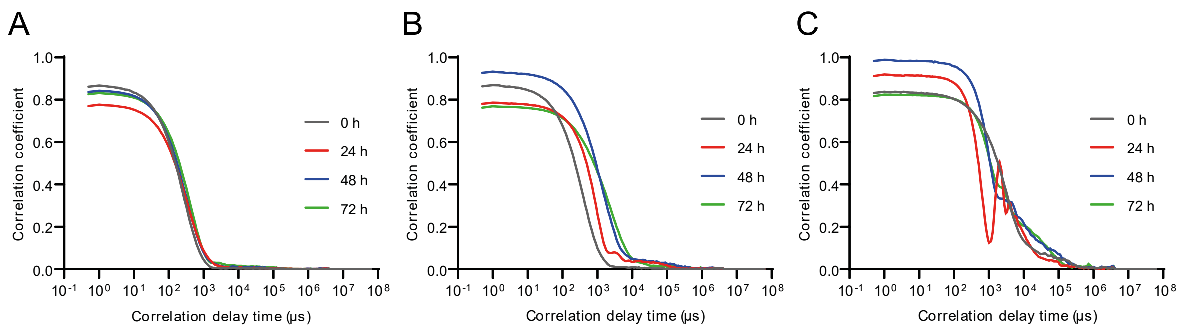

Figure 3-5 *Correlation functions of CSMs resuspended in (A) PBS pH 7.4, (B) MES pH 6, and (C) PSF pH 4.7 over time. DLS measurements were acquired right after CSMs resuspension in the different buffers and 24, 48, and 72 hours after the resuspension.*

To better understand CSMs behavior when interfacing the biological environment, Dulbecco's Modified Eagle's Medium (DMEM) was used. Moreover, all the biological conditions, including DMEM, were implemented with 10% fetal bovine serum (FBS). As illustrated in **Figure 3-6** and **Figure 3-7**, CSMs stability generally improved over time due to the presence of FBS. Nevertheless, at lower pH (4.7 and partially 6) CSMs solution was not completely monodispersed and traces of sedimentation were detected (**Figure 3-6** D). **Figure 3-7** represents CSMs size distribution over time at different pH.

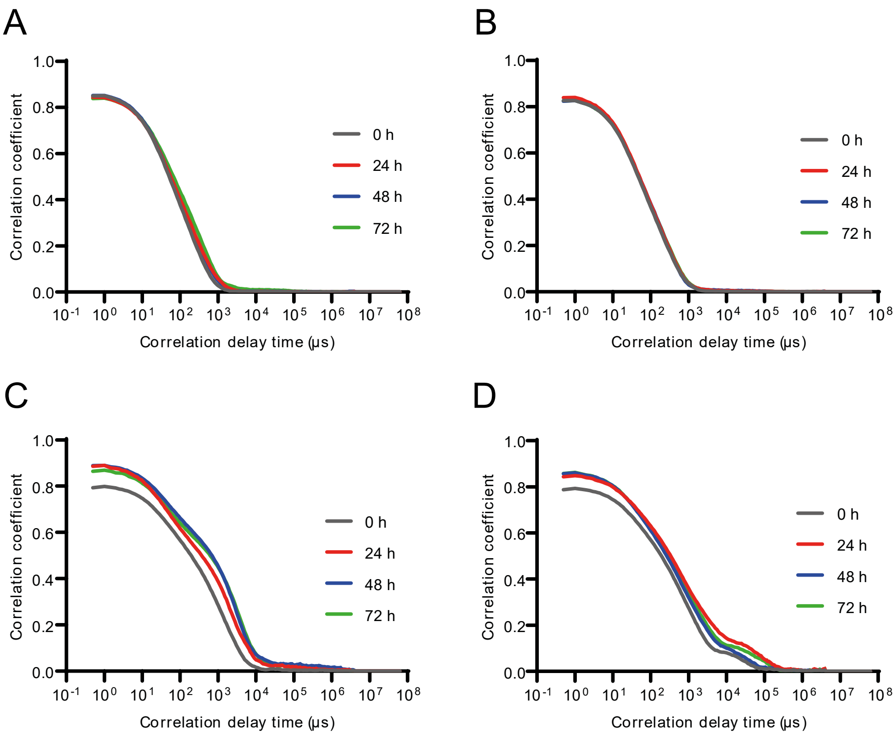

***Figure 3-6** Correlation functions of CSMs resuspended in (A) DMEM pH 7.4, (B) PBS pH 7.4, (C) MES pH 6, and (D) PSF pH 4.7 over time. 10% FBS was added to each buffer before CSMs resuspension. DLS measurements were acquired right after CSMs resuspension in the different buffers and 24, 48, and 72 hours after the resuspension.*

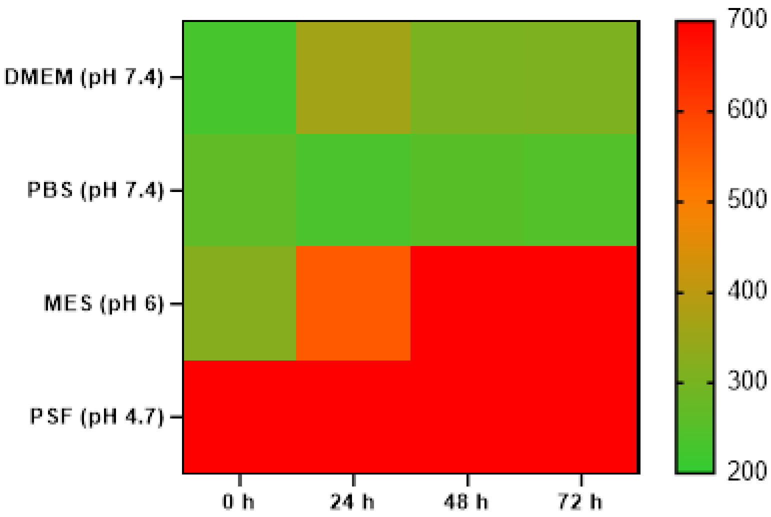

***Figure 3-7** Heatmap representation of CSMs size (nm) distribution at different pH during time.*

These results shown that the CSMs size and therefore their colloidal stability remained unaltered in physiological conditions (PBS buffer pH 7.4) as well as in complex media such as completed cell culture media (cDMEM). However, when the pH decreased below 6, the colloidal stability of the CSMs was compromised.

3.1.1.3. Biological characterization

As mentioned, cells plasma membrane, beyond the mere phospholipidic bilayer, possesses a unique biological pattern, characterized by different biological entities, mostly protein components. The protein content of CSMs samples was studied with Bradford assay, a colorimetric quantification of the total protein content determined by Coomassie dye-binding reaction. As shown in **Figure 3-8**, CSMs total protein content is directly correlated to the total number of cells used to prepare the sample.

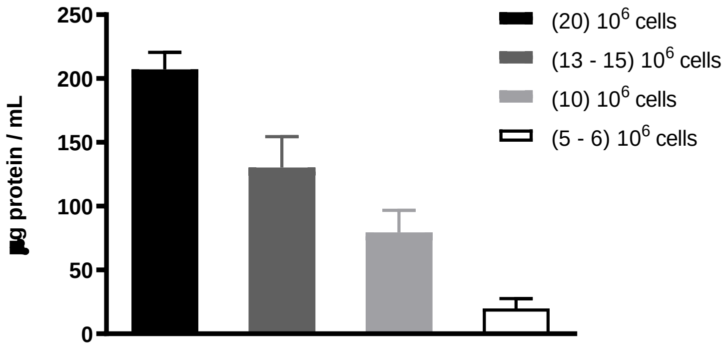

Figure 3-8 *Protein content of CSMs derived from different cells amounts.*

3.1.2. *In vitro* studies of cell-derived nanovesicles

Once optimized the synthesis protocol and assessed the principal physicochemical and biological aspects of the CSMs obtained, the viability of cells exposed to different concentration of CSMs was studied. 3-(4,5-dimethylthiazol-2-yl)-2,5-diphenyltetrazolium bromide (MTT) assay was used to estimate the toxicity of different doses of CSMs after 10 minutes, 1 hour, and 3 hours of exposure to A549 cells. MTT assay colorimetric evaluation of cellular metabolic activity provides a general idea of the cells viability when exposed to compounds or NPs.

As shown in **Figure 3-9**, cell viability was high and resulted partially affected at concentrations of 10^6 CSMs/cell. All the experiments of this thesis were performed at a maximum concentration of 10^5 CSMs/cell to preserve the cellular viability.

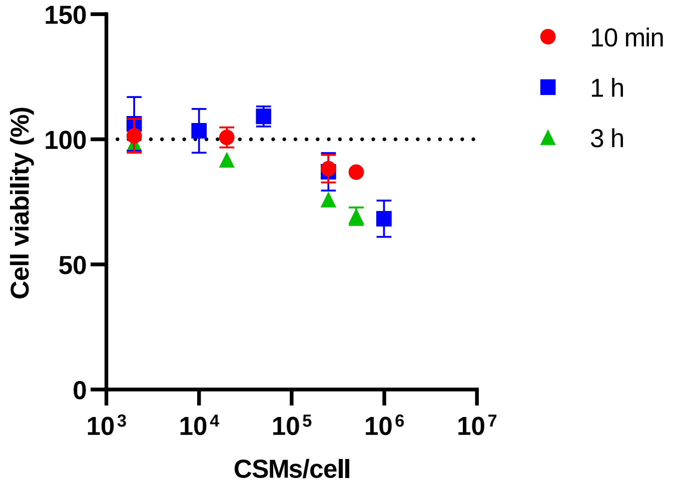

Figure 3-9 MTT assay of A549 cells exposed to different concentrations of CSMs at different time points.

Then, prior to investigate the interactions with cells, CSMs were fluorescently labeled by intercalating a fluorescent lipid into the lipidic bilayer (**Figure 3-10**). Following the procedure described in Section 2.2, 1,2-Dioleoyl-sn-glycero-3-phosphoethanolamine (DOPE) labeled with Atto 647N or Atto 488 was added to CSMs solution and the mixture was subjected to ultrasounds, which favor the dispersion of phospholipids through the aqueous environment and allow the phospholipids to spontaneously form the vesicles, which will include the exogenous lipid (DOPE) into the bilayer. To obtain a highly monodispersed solution, fluorescent CSMs were further subjected to a mechanical extrusion process using nanosized polycarbonate membranes. Then, they were purified from the non-intercalated DOPE by ultrafiltration. Finally, size distribution of fluorescent CSMs was analyzed by DLS and NTA, and the fluorescence signal was determined.

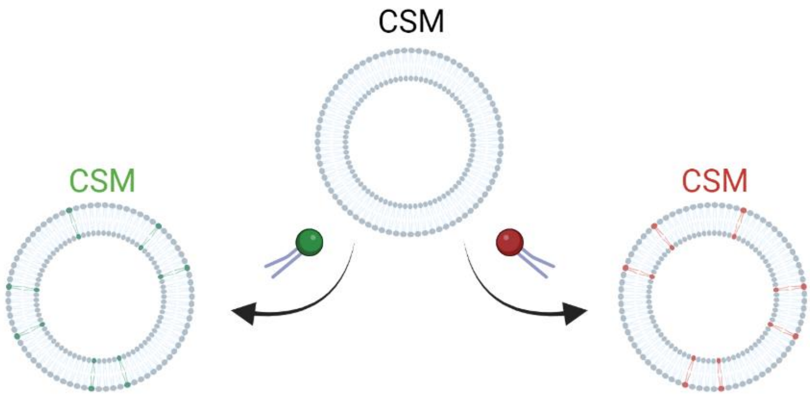

Figure 3-10 Schematic representation of CSMs fluorescent labeling with DOPE Atto 488 (on the left) or DOPE Atto 647N (on the right).

Either DOPE Atto 488 or DOPE Atto 647N was used to obtain fluorescently labeled CSMs in order to track the nanovesicles inside cells, both by fluorescence microscopy and using flow cytometry.

In **Figure 3-11**, the internalization of CSMs labeled with DOPE Atto 647N in cancer cells (A549 cells) is shown as an example of the CSMs internalization process. The dotted-like appearance of fluorescent CSMs inside cells suggests that the cellular uptake took place through an endocytosis mechanism, that will be later explored.

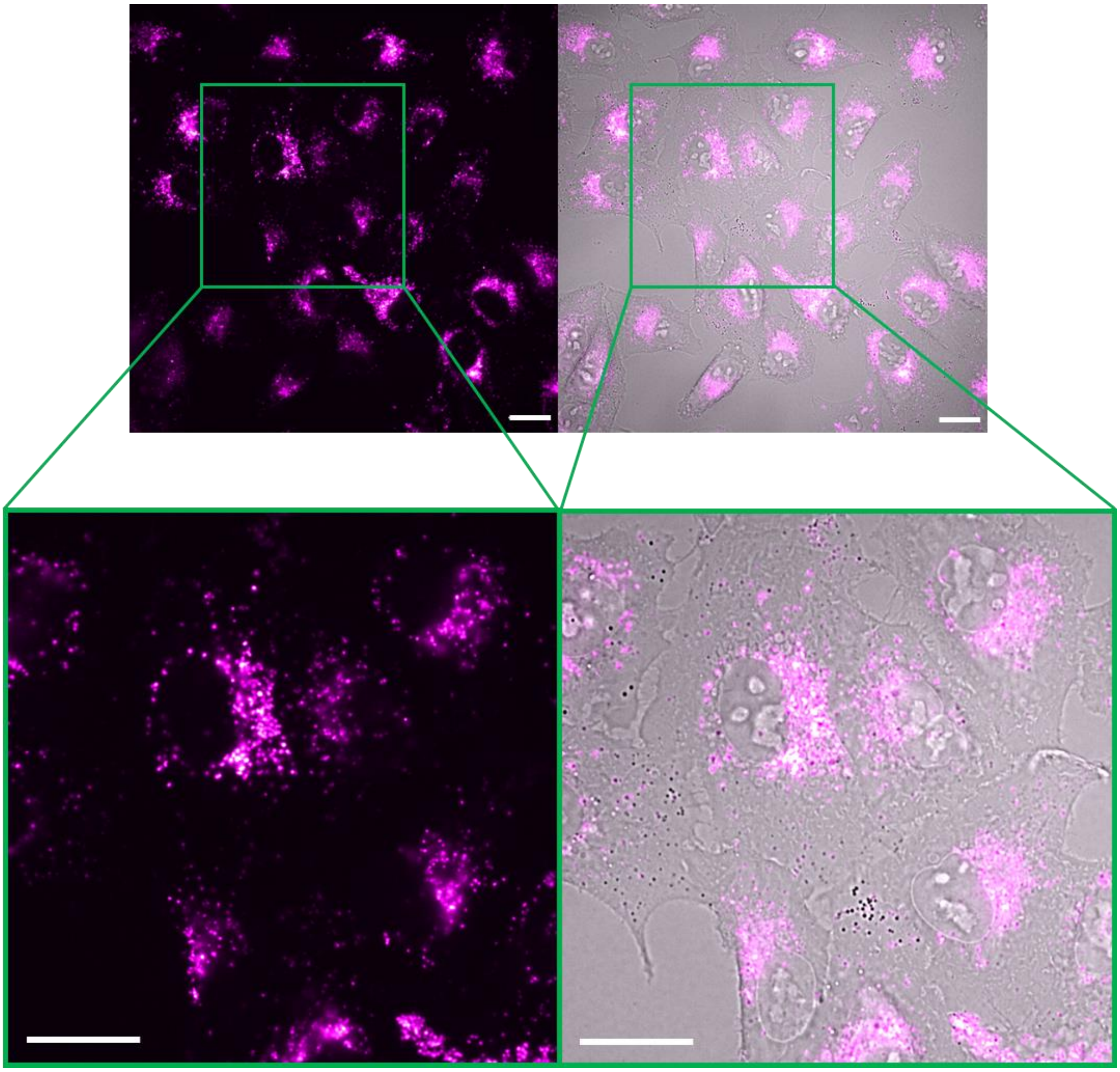

Figure 3-11 *Fluorescence microscopy images of A549-CSMs fluorescently labeled with DOPE Atto 647N internalized in A549 cells. Incubation time: 1 hour. Scale bars: 20 µm.*

Fluorescence microscopy time-lapse experiments will allow for studying the kinetics of CSM-cell interaction and uptake, as well as CSMs stability inside cells over extended time.

3.1.3. Homotypic targeting of specific cell types

One of the main advantages of cell-derived nanosystems is the intrinsic capability to preferentially interact with their source cells. This feature, called homotypic targeting, is due to the unique biological pattern that characterizes each cell plasma membrane, composed by a specific pool of surface and transmembrane proteins, glycoproteins, receptors, ion channels, etc. along with the distinctive phospholipidic bilayer. The homotypic targeting approach aims at directing the therapy effectiveness to specific cell populations in order to maximize the desired beneficial effects and minimize the damage to the surrounding healthy cells.

Here, the study of CSMs homotypic targeting capabilities was performed through flow cytometry to evaluate the interaction between fluorescently labeled CSMs and different cell lines (macrophages, embryonic kidney cells, and tumoral cells). CSMs derived from either tumoral or non-tumoral cells were synthesized and the interactions with the same type of cells were evaluated by flow cytometry after different time points (1, 3, and 6 hours) (**Figure 3-12**).

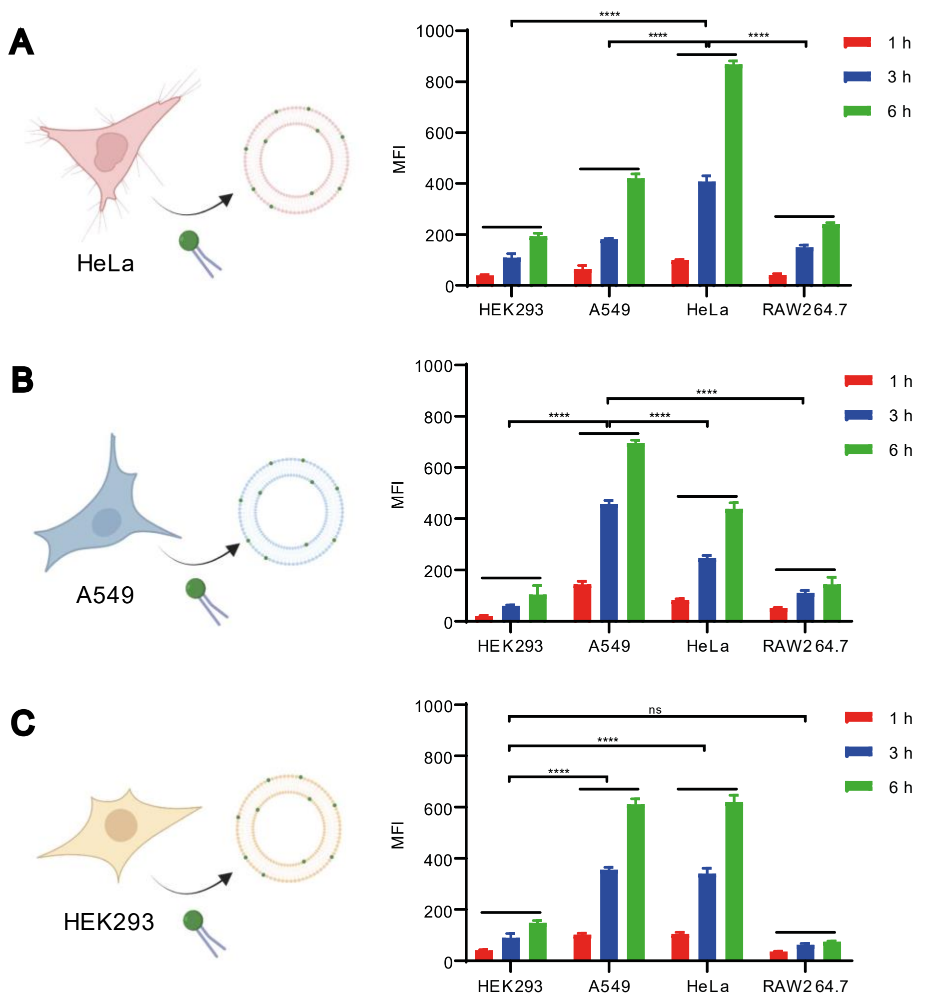

***Figure 3-12** Uptake experiments at different times of (A) HeLa, (B) A549, and (C) HEK293 -derived CSMs in different cell lines.*

As shown in **Figure 3-12**, CSMs internalization within the different cell lines generally occurred in a time-dependent manner. Understanding the kinetics undergoing CSMs cellular uptake may be important for designing effective drug delivery systems.

Moreover, CSMs derived from tumoral cells (HeLa and A549) were more prone to be internalized within their source cells, specifically by the same cell line from which the nanovesicles originated (**Figure 3-12** A and B). In addition, it is worth noting that, in the case of CSMs derived from HEK-293 (**Figure 3-12** C), no preference towards the originating line was observed, but the internalization appeared quite similar between the two tumoral cell lines (HeLa and A549). This could be attributed to the fact that tumoral cells, in general, exhibit a more active metabolism compared to non-tumoral cells. The heightened metabolic activity of tumoral cells, a phenomenon known as "Warburg effect", arises from their unique energy demands and adaptations to support rapid growth and proliferation.[328] Due to this elevated metabolic activity, tumoral cells tend to internalize a higher quantity of various substances compared to normal cells. This includes not only nutrients and signaling molecules, but also NPs or, as in this case, CSMs, which could be harnessed for targeted drug delivery, as tumoral cells are more receptive to uptake therapeutic agents.

Interestingly, macrophage-like cells (RAW264.7), when exposed to the different CSMs evaluated, did not display significant uptake, suggesting that CSMs may possess biomimetic stealth properties to evade detection or recognition by the immune system.

Overall, CSMs design was aimed at minimizing unwanted interactions that could lead to clearance or immune responses. This stealth property, achieved by using cells plasma membrane, may reduce the nanovesicles visibility to the immune system and enable them to effectively reach their target sites, such as tumoral cells. A more complete evaluation of CSMs homotypic targeting properties and their potential as drug delivery systems will be needed, including *in vivo* experiments.

3.1.4. Mechanism of endocytosis

One of the main concerns when investigating cells-NPs biological interactions is the efficiency of the internalization process. Among the main challenges associated with the use of NPs for biomedical applications, attaining successful cellular internalization remains pivotal. Once within the cells, NPs should evade the entrapment within endosomes and lysosomes to ensure efficient payload delivery. For this reason, understanding the endocytosis mechanisms used by NPs to enter the cells becomes crucial.

Endocytosis represents the most common internalization pathway used by NPs to enter the cells. Several endocytosis mechanisms have been recognized as potential NPs internalization pathways (**Figure 3-13**).

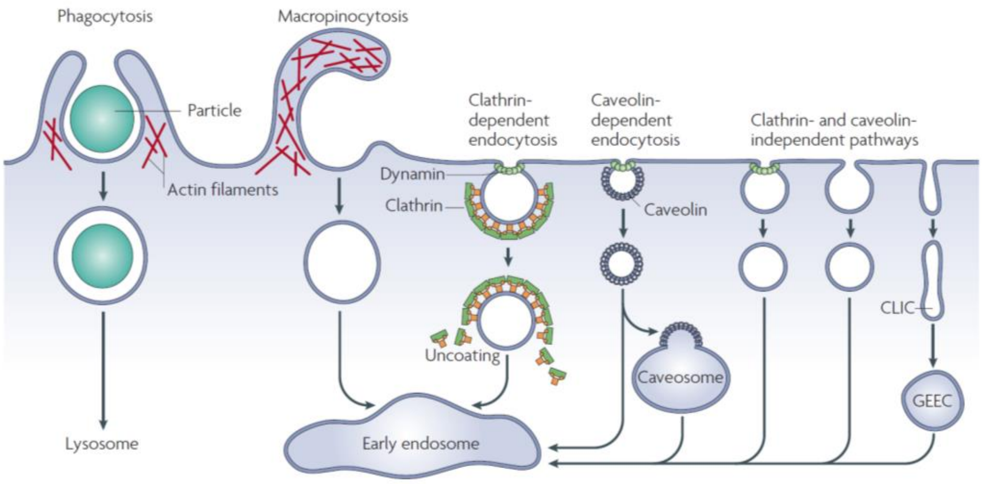

Figure 3-13 Main endocytosis pathways.[329]

To study the endocytosis mechanism used by CSMs to enter the cells, uptake experiments in presence of endocytosis inhibitors were performed (**Figure 3-14**). Each inhibitor was used to inhibit one single internalization pathway. Given that each cell type may utilize different endocytic pathways to internalize NPs and considering the uptake results showed in Section 3.1.3, tumoral cells (HeLa and A549) uptake of CSMs derived from HeLa, A549 and HEK293 cells was investigated with flow cytometry. HeLa and A549 cells were pre-treated with the specific inhibitor for 30 minutes before exposing them to CSMs solutions for 2 hours.

The endocytosis inhibitors used were: nystatin (NYS), a lipid raft inhibitor used to block caveolae-mediated endocytosis[330]; dynasore (DYN), a non-competitive inhibitor of dynamin, a GTPase that plays a key role both in clathrin-independent and in clathrin-dependent endocytosis (CIE and CDE, respectively)[331]; chloroquine (CQ), known to prevent lysosome acidification, thus impeding the fusion with the endocytic vesicles[332]; chlorpromazine (CP), a cationic amphiphilic drug which inhibits the function of AP2, one of the pivotal adaptor proteins in clathrin-mediated endocytosis[333]; methyl-β-cyclodextrin (MBCD), a cyclic oligomer of glucopyranoside used to determine whether endocytosis is dependent on the integrity of lipids rafts, due to its role in extracting the steroid out of the plasma membrane[334].

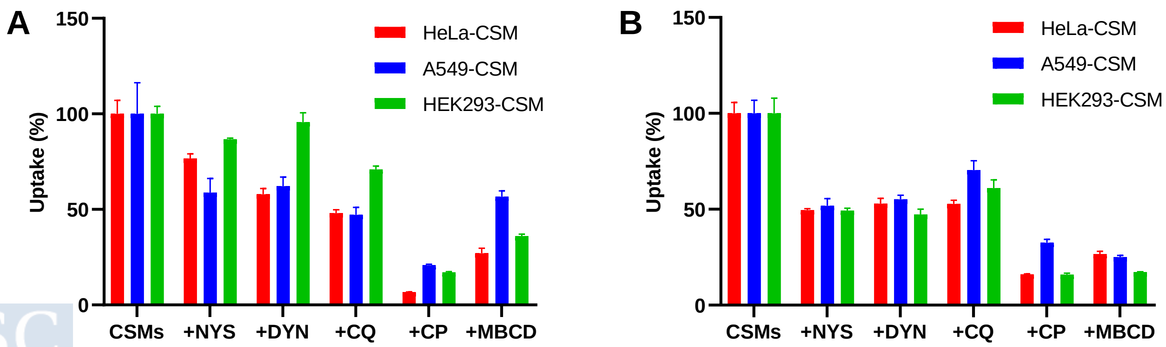

Figure 3-14 Uptake measurements of different CSMs type in (A) HeLa and (B) A549 cells by using different inhibitors.

Despite the cell type internalization dependance, the blocking tendency of all the endocytosis inhibitors was similar for all the samples, especially for the tumoral ones (**Figure 3-14**). In both tumoral cell lines, CP and MBCD were able to strongly inhibit the internalization of the CSMs derived from different cell types, suggesting that the uptake was mediated by both clathrin-dependent and lipid rafts-dependent endocytosis.

Nevertheless, further endocytosis studies will be needed to effectively assess the mechanisms undergoing CSMs cellular internalization and how to exploit them to achieve an efficient and safe delivery of the nanosystem within cells.

3.1.5. Functionalization and cargo loading

One of the main advantages of cell membrane-derived nanovesicles is the possibility of loading and retaining different types of cargos. The phospholipid bilayer is capable of retaining both hydrophilic and hydrophobic molecules, due to its amphiphilic nature, such as drugs, therapeutic agents, markers, or other bioactive substances. In addition, the lipidic composition itself represents an ideal biocompatible material, as it is originated from natural sources (cells). One of the primary objectives in designing biomimetic nanosystems is to fabricate advanced platforms for the transport, controlled release, and effective delivery of bioactive molecules within the target cells. This biomimetic strategy for cargo delivery inside cells has been deeply investigated during the last decade, bringing to light the possibility of designing the most suitable drug delivery system for different therapeutic applications.[335]

For these reasons, the process undergoing the encapsulation process and the optimization protocol to obtain bioactive molecules loaded into biomimetic nanovesicles need to be explored. Here, nanovesicles derived from HeLa plasma membrane were fabricated following the protocol described in Section 2.1. Then, a cell permeable nucleus staining, Hoechst H 33258 (HOE), was encapsulated into fluorescently labeled CSMs (CSM(HOE)) as described in Section 2.3.2.1 and illustrated in **Figure 3-15**.

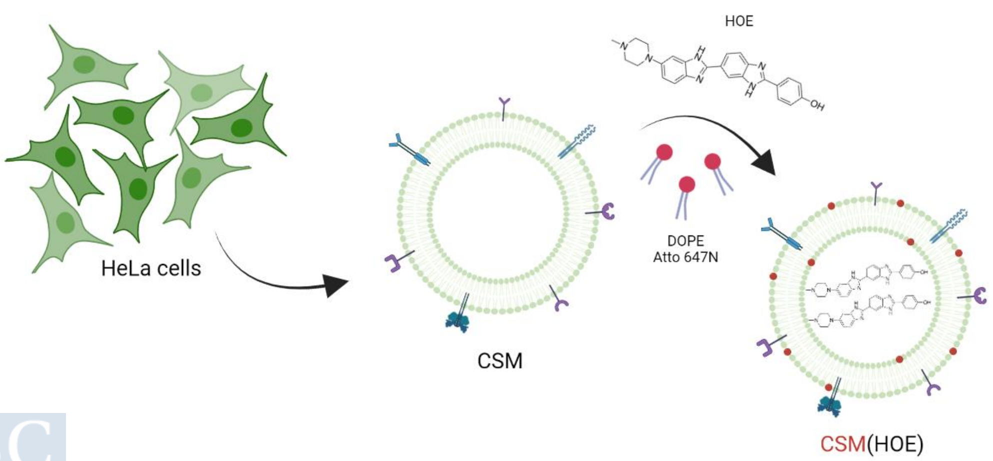

Figure 3-15 CSM(HOE) preparation and functionalization with DOPE Atto647N.

To purify CSM(HOE) solution from the excess of non-encapsulated HOE, two different purification methods were used. The solution was either purified through an overnight dialysis procedure, or it was passed through a size exclusion chromatography (SEC) column (PD-10).

Size distribution analysis of both purified samples was performed with NTA to assess that the two purification methods did not affect the stability of the nanosystem. As shown in **Figure 3-16** and **Table 3-3**, CSM(HOE) size distribution was maintained after both purification methods: the dialyzed sample and the first two fractions derived from SEC column (1 mL each) presented almost the same diameter size (about 200 nm).

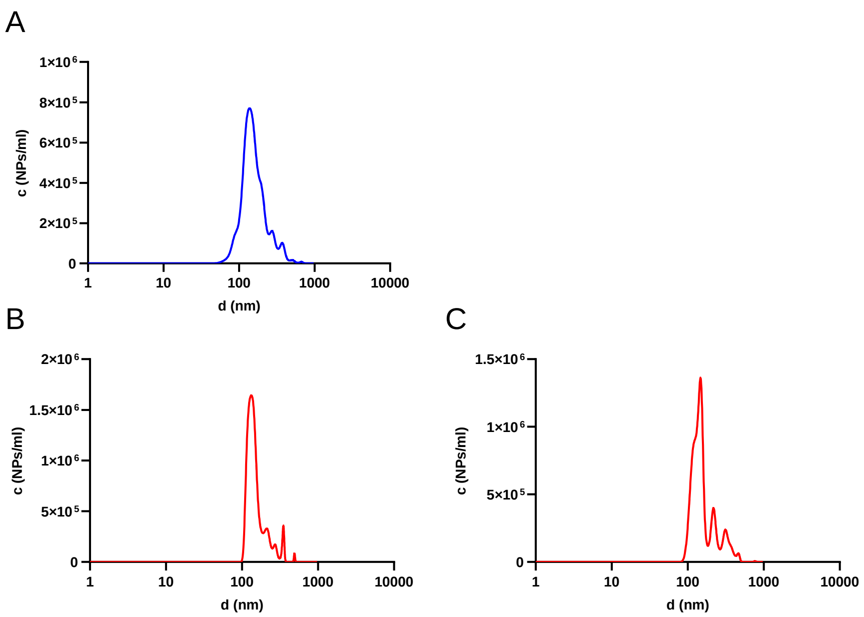

***Figure 3-16** Size distribution analysis of CSM(HOE). (A) shows the purified sample after dialysis, while (B) and (C) show fraction 1 and 2, respectively, of size exclusion chromatography (PD-10 column).*

Sample	d (mean) (nm)	d (mode) (nm)	c (NPs/mL)
CSM(HOE) post dialysis	200.6	138.0	9.31E+10
CSM(HOE) fr.1 SEC	181.2	132.8	1.14E+11
CSM(HOE) fr.2 SEC	203.5	147.4	1.09E+11

***Table 3-3** NTA analysis data of CSM(HOE) after purification (dialysis or SEC).*

However, NTA characterization does not offer much information about the efficiency of the purification method employed, thus confocal microscopy imaging was employed for this purpose.

HOE is a slightly fluorescent cell membrane permeable molecule which increases its fluorescence intensity when bound to nucleic acids, staining the whole cell nucleus. As shown in **Figure 3-17**, cells exposed to CSM(HOE) for 3 hours presented different nuclei staining according to the purification method used: when encapsulated into CSMs (in red) and purified through SEC (**Figure 3-17** C and D) the HOE could not reach the nucleus and bind to the DNA, while when purified by dialysis (**Figure 3-17** E) a slightly fluorescent nuclei staining was observed, indicating that the dialysis did not allow the complete elimination of free HOE, which, due to its cellular permeability, entered the cell and bound to the DNA. Since HOE and CSMs are very different compounds in size, SEC was probably the optimal purification method for this type of molecule.

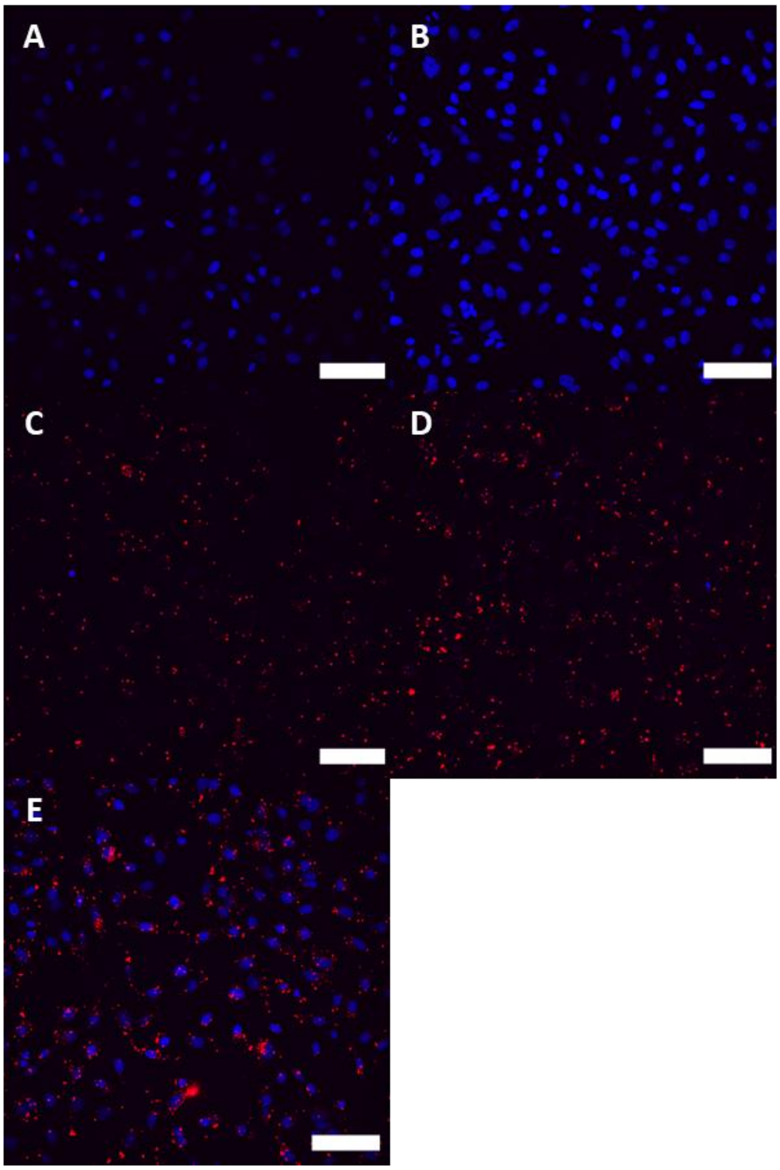

Figure 3-17 *Confocal images of HOE (in blue) internalization in HeLa cells. (A) and (B) show free HOE uptake (5 µg/mL and 10 µg/mL, respectively); (C) and (D) show CSM@HOE uptake after purification through SEC (fraction 1 and 2, respectively), (E) represents CSM@HOE uptake after purification through dialysis. CSMs have been functionalized with DOPE Atto 647N (in red) and all the samples were exposed to HeLa cells for 3 hours. Scale bars: 100 µm.*

Once established the most suitable purification method, confocal microscopy imaging was also employed to study the release of HOE from CSMs during time. A qualitative cargo release kinetics was investigated at different time points. As shown in **Figure 3-18**, after 3 hours of CSM(HOE) exposure, the cargo release inside cells was not observed, while after a longer exposure time (overnight), cells nuclei were stained by HOE.

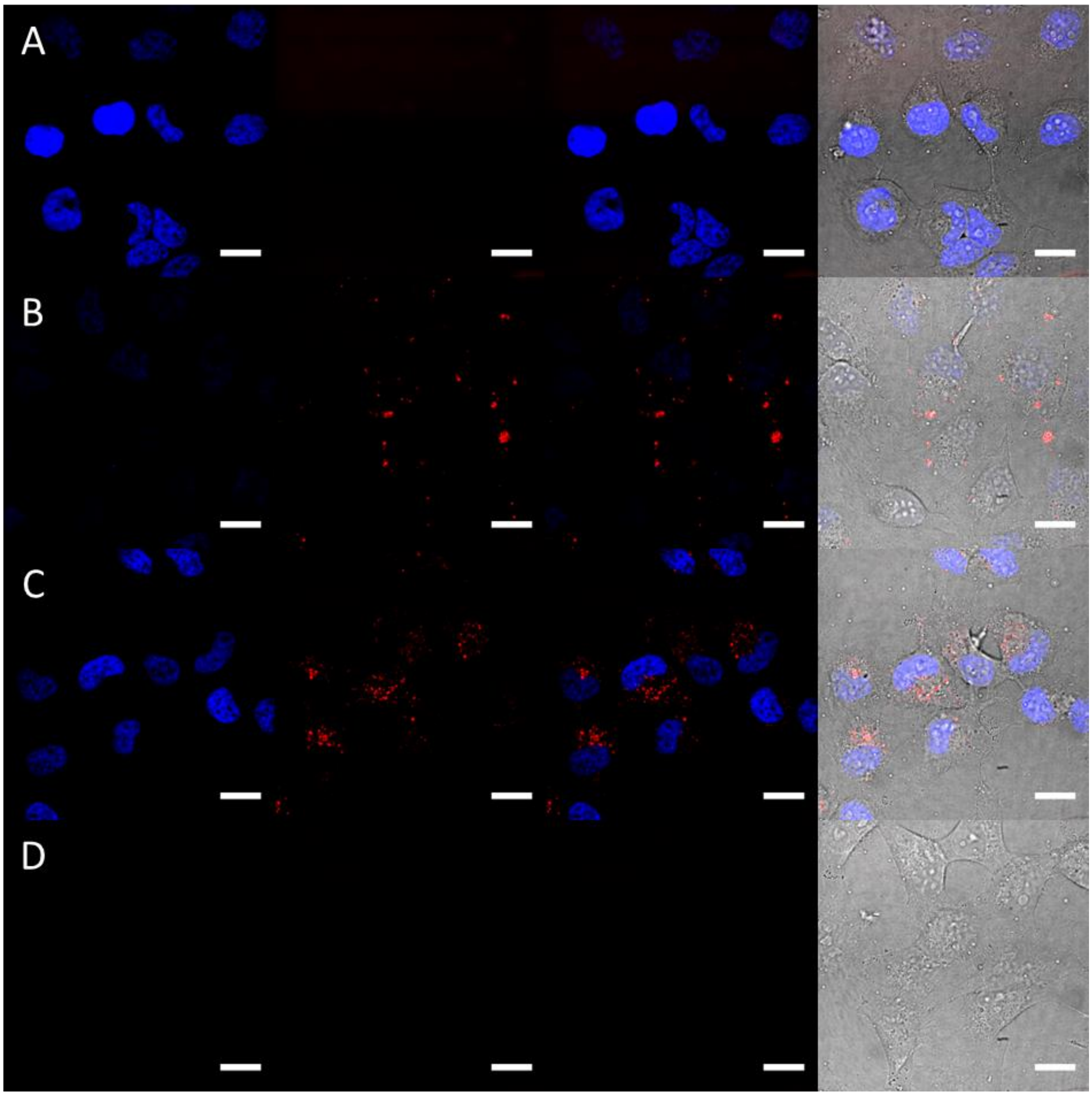

Figure 3-18 *Confocal images of HeLa cells incubated with (A) free HOE (3 hours), (B) CSM@HOE (3 hours), (C) CSM@HOE (overnight), (D) control. For each panel, from left to right, images show the fluorescence signal of HOE (in blue), CSMs functionalized with DOPE Atto 647N (in red), overlays of the two fluorescence signals (blue + red), and both merged with brightfield. Scale bars: 20 µm.*

As mentioned, HOE is a cell membrane permeable molecule which is most likely able to diffuse through CSMs phospholipid bilayer. Nevertheless, CSMs showed the capability of retaining HOE dye during time, suggesting that this biomimetic nanocarrier could be used as delivery system for similar types of molecules.

3.1.6. Biomimetic nanovesicles derived from senescent cells

Cellular senescence is defined as a stable state of growth arrest in which cells become unable to proliferate. It is a physiological mechanism that may also occur in response to several triggers, such as telomere dysfunction, DNA damage or oncogene activation.[336] Despite their state of growth arrest, senescent cells preserve an active metabolism, which, through several dynamic processes, causes pathophysiological transformations, such as the alteration of the paracrine signaling. The main effect of this so-called senescence-associated secretory phenotype (SASP) is the increased secretion of bioactive molecules, including growth factors, chemokines, proinflammatory cytokines (IL-6 and IL-8), etc.[263]

Cellular senescence has been proved to be one of the major causes of age-related diseases, such as neurodegenerative diseases, cardiovascular diseases, osteoporosis, pulmonary fibrosis, metabolic dysfunction, etc. Recent discoveries have brought to the theory that targeting cellular senescence may prevent, delay, or alleviate these pathologic conditions.[337]

Several therapeutic strategies aimed at targeting senescent cells have been proposed during the last few years.[338] The most studied senotherapeutic approaches include the selective removal of senescent cells, provoked by senolytic compounds, or the suppression of the SASP, conducted by senomorphics.[339] While other approaches are based on the activation of the immune system against senescent cells to stimulate their clearance or even the reprogramming of senescent cells to revert or bypass the state of senescence (**Figure 3-19**).

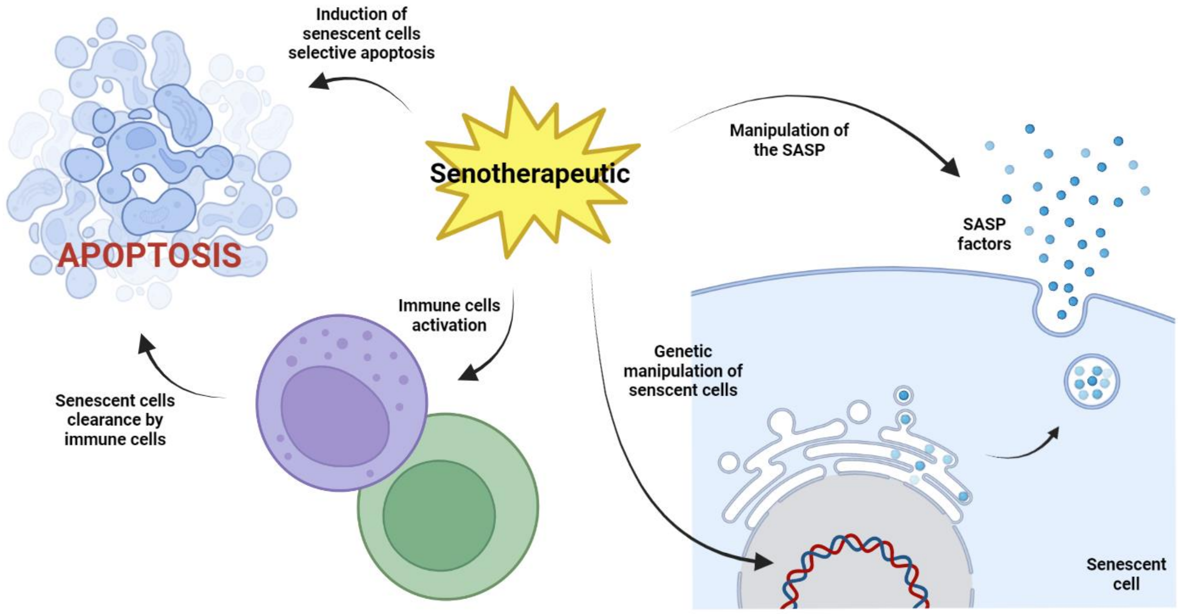

Figure 3-19 *Schematic representation of senotherapeutic potential approaches.*

In all of these approaches, one of the primary concerns is the delivery of the therapeutic compound to the senescent cell. The biomimetic feature of cell membrane-derived nanosystems may be exploited for this purpose.

Cell-membrane derived nanovesicles possess biomimetic features able to improve the targeting capabilities of NPs and molecules loaded into these nanosystems. Moreover, strategies involving the use of engineered nanocarriers might be useful to circumscribe the toxic profile of senolytic compounds, therefore enhancing the efficacy of the therapeutic treatment.

So far, biomedical research aiming at targeting not only cells or tissues but also a specific cell cycle step has not been widely explored. Some of the most used therapeutic approaches to promote senescent cells removal involve the targeting of pro-survival pathways, such as B-cell lymphoma-2 (BCL-2), p53 and phosphatidylinositol 3-kinases/ protein kinase B (PI3K/AKT) pathways. Nevertheless, due to the multifactorial heterogeneity of senescence biological environment, future perspectives would include more context-dependent approaches, such as personalized medicine approaches.[338]

In this perspective, cell membrane nanotechnology may be used as an innovative and useful tool for the treatment of age-related diseases, due to cell membranes remarkable versatility and biocompatibility.[199] Here, cell membrane-derived nanovesicles derived from both proliferative and senescent tumoral cells have been proposed as potential biomimetic nanocarriers for the treatment of age-related diseases. The original idea was to fabricate biomimetic nanosystems loaded with senolytic or senomorphic compounds in order to drive these drugs towards senescent cells or tissues.

3.1.6.1. Design and characterization of A549 Sen-CSMs and Pro-CSMs

Here, A549 cells were subjected to bleomycin treatment to obtain senescent A549 cells (SenA549) as described in Section 2.1. Senescent cells often exhibit a different morphology compared to healthy cells. During the process of cellular senescence, in fact, cells undergo structural changes that can affect their shape, size, and overall appearance. Senescent cells can become larger and more flattened, with a more irregular shape compared to young and vital cells. Additionally, they can accumulate aggregates of damaged cellular components and show alterations in their cytoskeleton and protein organization. These altered morphological features often reflect the activation of cellular signaling pathways involved in the senescence process and can serve as visual indicators of cellular age and their functional state.[340]

Fluorescence microscopy imaging was performed to assess the morphological changes of the obtained senescent cells (**Figure 3-20**). As shown, senescent cells appeared larger and displayed an irregular morphology (**Figure 3-20** B) compared to proliferative A549 cells (**Figure 3-20** A), indicating that the bleomycin treatment did induce cellular senescence.

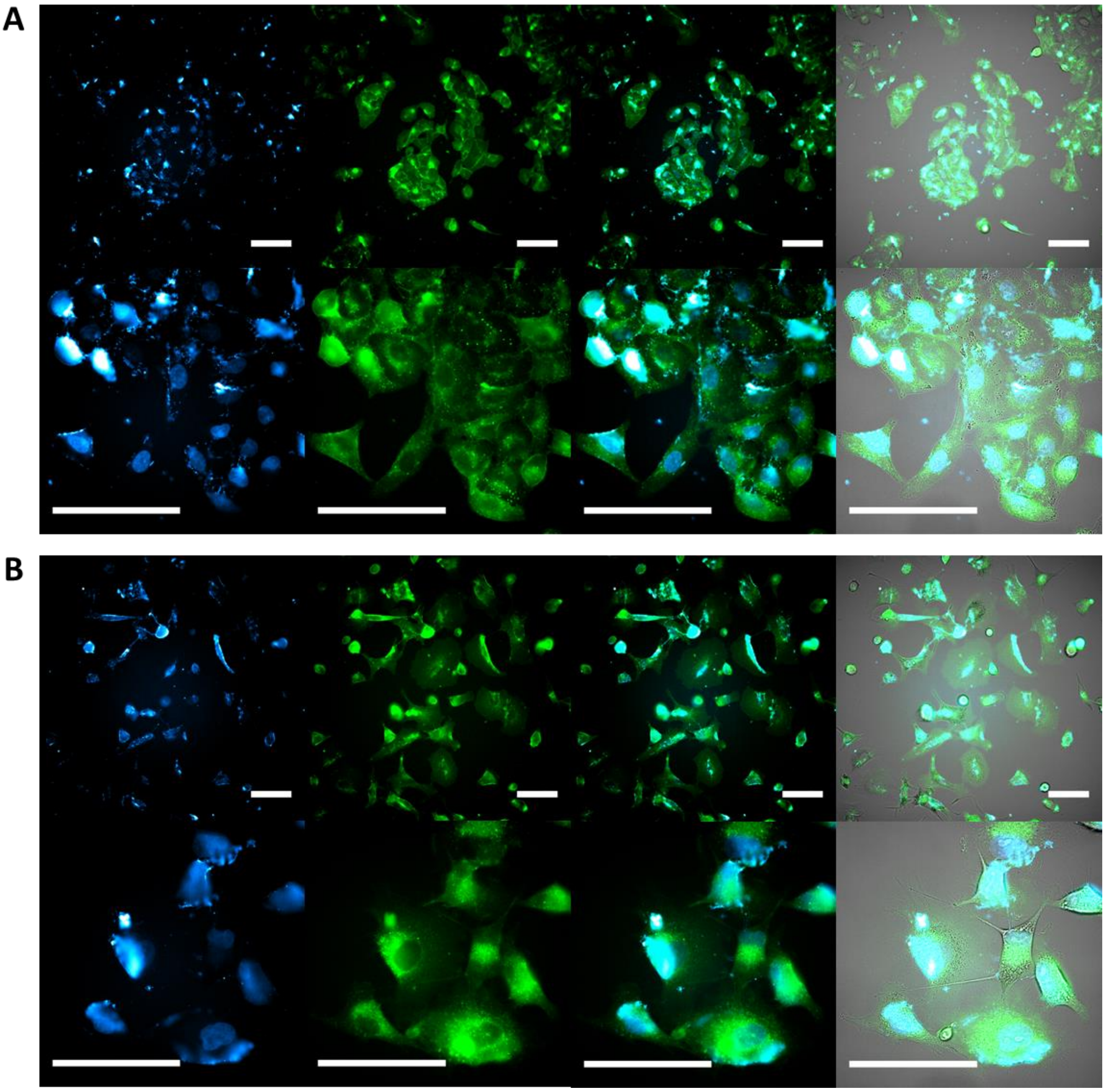

Figure 3-20 Fluorescence microscopy imaging of (A) proliferative A549 cells and (B) senescent A549 cells. For each panel, from left to right, images show the fluorescence signal of DAPI (in light blue), cell mask (in green), overlays of the two fluorescence signals (light blue + green), and both merged with brightfield. Scale bars: 100 µm.

Once obtained stably senescent A549 cells, both Sen- and Pro-derived nanovesicles were obtained following the protocol previously described (Section 2.1). Briefly, A549 cells (both proliferative and senescent) were induced to swallow in a hypotonic environment enriched with a proteases inhibitor cocktail (PIC) to preserve the surface properties of plasma membrane. The resulting disrupted cells were exposed to 4 cycles of freeze in N_2 and thaw at 37 ºC and subsequently subjected to mechanical disruption with ultrasounds. Plasma membranes fragments were extracted and recollected through differential centrifugal steps and extruded through polycarbonate membranes with nanosized pores in order to obtain self-assembled CSMs of about 150-200 nm in size.

Size distribution measurements (NTA analysis) of Pro-CSMs and Sen-CSMs are shown in **Figure 3-21** and **Table 3-4**.

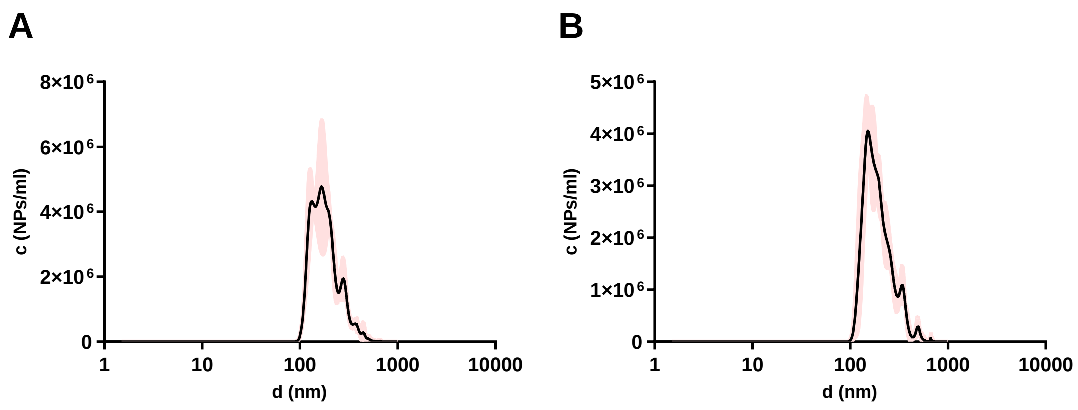

Figure 3-21 *Size distribution measurements (NTA) of (A) Pro-CSMs and (B) Sen-CSMs.*

Sample	d (mean) (nm)	d (mode) (nm)	c (NPs/mL)
Pro-CSMs	214.0 ± 2.5	158.0 ± 9.9	6.73E+11
Sen-CSMs	229.2 ± 3.2	158.7 ± 6.0	5.49E+11

Table 3-4 *NTA analysis of Pro-CSMs and Sen-CSMs.*

3.1.6.2. Uptake studies of A549 Sen-CSMs and Pro-CSMs

To study Pro-CSMs and Sen-CSMs uptake in different cell lines, both types of CSMs were fluorescently labeled with Atto 488 DOPE as described in Section 2.2. Uptake studies were performed as described in Section 2.5.1.1. Briefly, HEK293, HeLa, senescent and proliferative A549 cells were plated according to their growth rates. After 24 hours cells were exposed to fluorescently labeled Sen-CSMs and Pro-CSMs for 3 hours, after which cells were harvested, recollected, and measured with flow cytometry (FC).

As illustrated in **Figure 3-22**, the uptake of Pro-CSMs was higher in all the cell types tested compared to Sen-CSMs, probably due to the surface properties of tumoral proliferative cell plasma membrane, which typically shows a receptor array able to favor the interaction with cells.

Nevertheless, senescent A549 cells showed the highest uptake compared to the other cell lines. This is probably due to intrinsic senescent cellular dynamics that promote the internalization of different compounds and molecules in order to survive, given that senescent cells are non-dividing cells which are not supposed to go through apoptosis mechanisms.

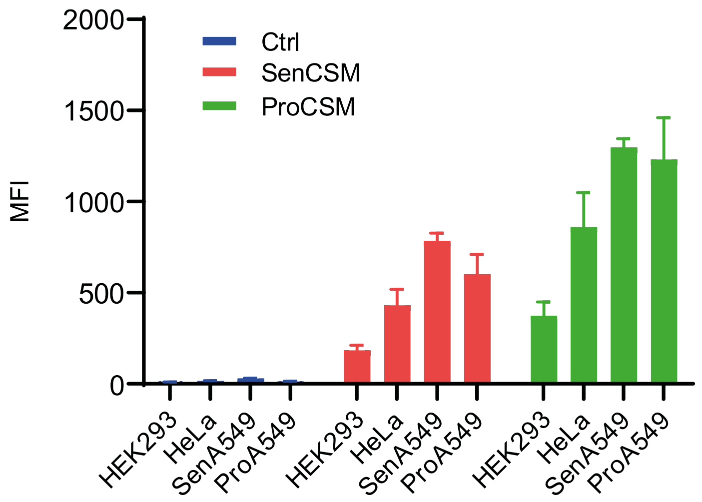

Figure 3-22 *Cells uptake of senescent and proliferative A549 derived nanovesicles. Flow citometry measurements were obtained 3 hours after samples incubations. Data are repesented as mean ± s.d. (n = 3).*

3.1.6.3. Toxicity studies of A549 Sen-CSMs and Pro-CSMs

Senescent cells are generally highly resistant to apoptosis, thus the main purpose of this project was to exploit cell membrane homotypic targeting capabilities towards senescent cells and at the same time senolytic compounds were meant to be loaded into cell-derived nanovesicles in order to inhibit pro-survival pathways. Some of the most common strategies to eliminate senescent cells by inhibiting pro-survival pathway is the deregulation of BCL-2 proteins. BCL-2 is a family of proteins localized in the mitochondria outer membrane, where it plays a key role in inhibiting the permeabilization and release of cytochrome c and ROS, fundamental signals in the apoptosis cascade. Navitoclax (ABT-263) is a specific inhibitor of BCL-2 family of proteins, which is able to selectively induce apoptosis in a variety of cells undergoing senescence.

Although senolytic drugs such as Navitoclax have been designed so far as the most suitable candidates for the treatment of age-related diseases as they selectively remove senescent cells, a first proof of concept trial was here performed to understand the principle regulating senescent cellular uptake dynamics. Doxorubicin (DOX), a senescence non-specific cytotoxic drug, was loaded into Pro- and Sen-CSMs as described in Section 2.3.2.1 and utilized to study cellular toxicity. The quantification of the encapsulated DOX is shown in **Table 3-5**.

Sample	**Cargo concentration**		
	µg/mL	**µM**	**EE (%)**
Pro-CSM(DOX)	31.8 ± 4.8	54.8 ± 8.3	6.3 ± 0.9
Sen-CSM(DOX)	32.0 ± 4.2	55.1 ± 7.2	6.4 ± 0.8

Table 3-5 *Characterization of cargo (DOX) encapsulation in Pro-CSMs and Sen-CSMs.*

Toxicity assay (MTT) was performed 24 and 48 hours after ProA549-CSMs and SenA549-CSMs exposure to senescent A549, proliferative A549, and HeLa cells (**Figure 3-23**). In general and according to the uptake results of Section 3.1.6.2, DOX loaded into ProA549-CSMs showed the highest cell viability decrease. Whereas, senescent A549 cells viability (**Figure 3-23** A and D) resulted affected mostly by free DOX, while DOX-loaded CSMs (both Pro and Sen) did not show great toxicity. This is a countertrend with the toxicity results of proliferative A549 cells and HeLa cells, which showed the opposite response: DOX loaded into CSMs was able to affect more cells viability than free DOX.

This unexpected result could be due to the endocytosis mechanisms governing molecules internalization inside the different cell lines considered. In this regard, further studies of the endocytosis mechanism of senescent cells will be needed.

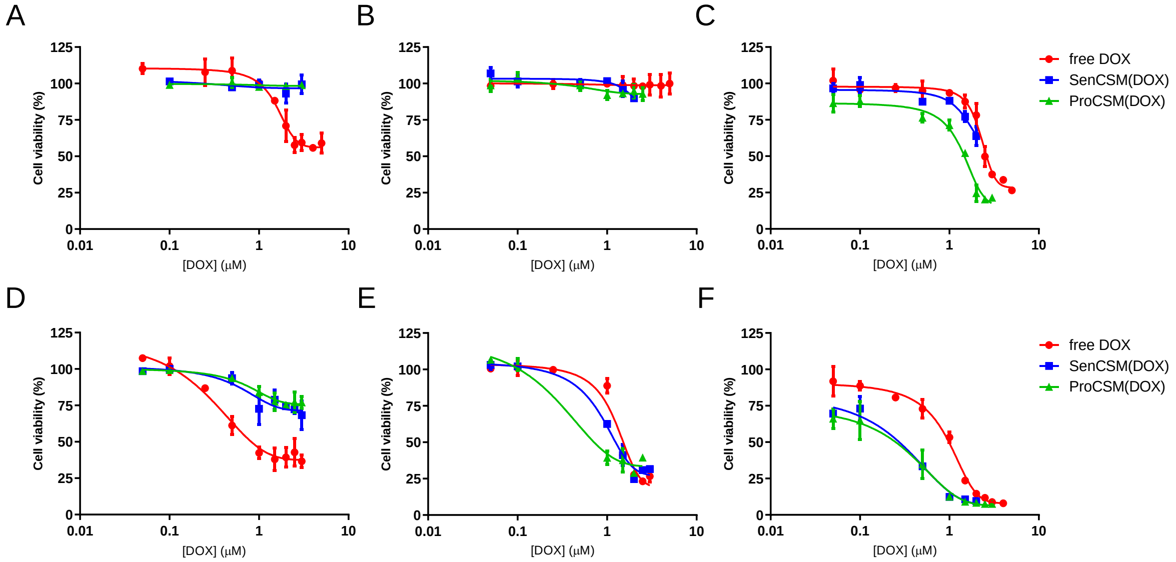

Figure 3-23 *MTT assay of CSM@DOX in (A and D) SenA549, (B and E) ProA549, and (C and F) HeLa cells, (A, B and C) 24 and (D, E and F) 48 hours after samples incubations. Data are shown as mean ± s.d. (n =3).*

3.1.7. Surface modification of biomimetic nanovesicles

Biomimetic nano-based approaches for antiviral therapeutics and vaccines have been deeply investigated, especially during the last three years due to the COVID-19 outbreak. According to the World Health Organization (WHO), the pandemic, caused by severe acute respiratory syndrome coronavirus 2 (SARS-CoV-2), has provoked more than 760,000,000 infections and more than 6,900,000 deaths[341], being the most contagious virus in its class (the same coronavirus class includes SARS (severe acute respiratory syndrome) and MERS (Middle East respiratory syndrome)), and one of the prior concerns for global public health.

The coronavirus life cycle is founded on the presence of four distinctive proteins, each of which has a precise and essential structural function (**Figure 3-24**). The membrane protein (M protein) preserves the viral membrane integrity; the envelope protein (E protein) plays a key role in helping the virus assembly and budding; the nucleocapsid protein (N protein) is the protein component of the helical nucleocapsid and binds to the genomic RNA participating in the modulation of viral transcription; the Spike glycoprotein (S protein) promotes the virus attachment to the host cell, provoking membrane fusion and therefore the virus entrance into the host cell.[342]

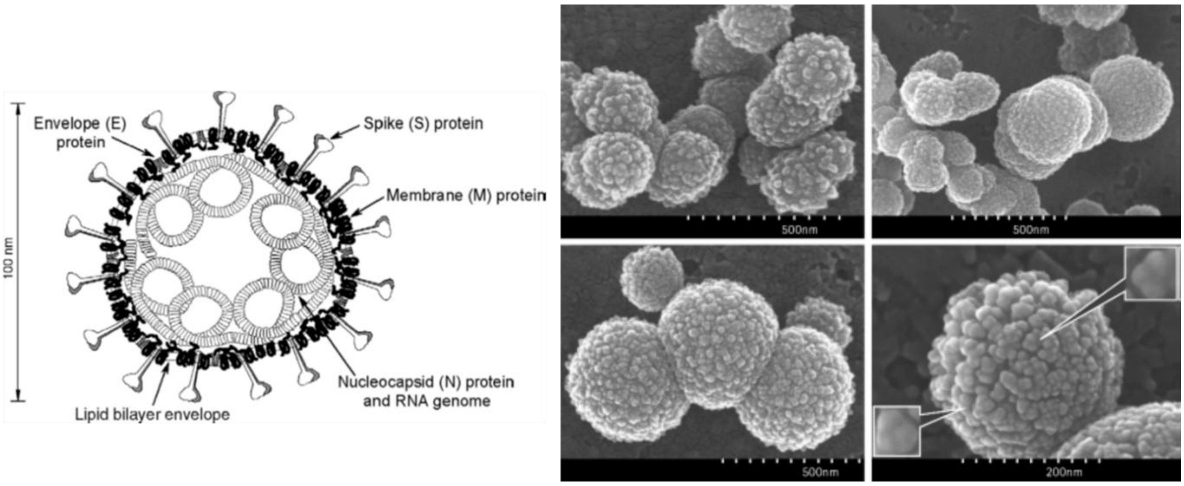

Figure 3-24 *Schematical structure (on the left[342]) and scanning electron microscopy (SEM) images (on the right[343]) of coronavirus.*

In order to mediate cells attachment and membrane fusion, SARS-CoV-2 S protein binds to the N-terminal region of angiotensin-converting enzyme 2 (ACE2) on the host cell surface.[344] This enzyme is a transmembrane zinc peptidase involved not only as substrate for SARS-CoV-2, but also in the regulation of the renin-angiotensin system and amino acids transport.[345] It is widely expressed in many organs and tissues, especially in the lungs and the cardiovascular system. SARS-CoV-2 infection reduces ACE2 expression in lung cells and this virus-induced ACE2 downregulation may be crucial for consequent pathologic disorders. Thus, ACE2 has been identified as one of the major modulators for the clinical implications of COVID-19 and the associated cardiovascular diseases.[346]

Due to the critical role of ACE2 in virus infection, it could also be exploited to improve the targeting abilities of SARS-CoV-2 antiviral therapeutics.

As mentioned, biomimetic cell membrane-based NPs exhibit unique properties when interfacing with the cellular milieu. One of the most advantageous features in fabricating functionally active nanosystems is the possibility to enhance the interaction with the biological environment and therefore to improve the internalization of the nanosystem inside cells. The employment of S protein and ACE2 in the fabrication of biomimetic NPs may be of great interest for the development of innovative antiviral therapeutics.

Here, cell membrane-derived nanovesicles derived from HEK293 cells expressing S protein were obtained following the protocol described in Section 2.1 (**Figure 3-25**).

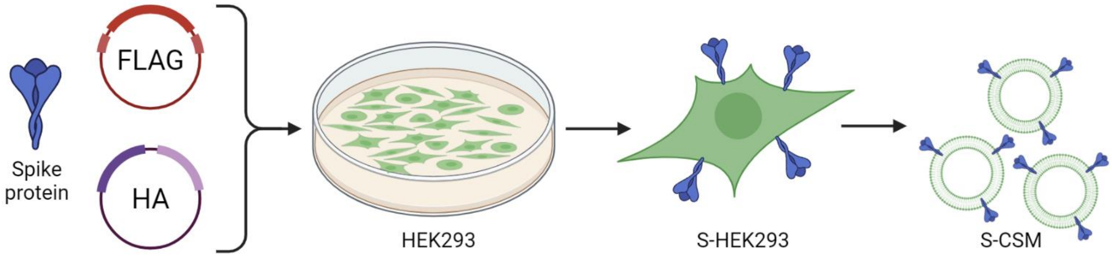

Figure 3-25 *Schematic synthesis method for the fabrication of Spike-CSMs (S-CSMs).*

The expression of S protein transfected in HEK293 cells was confirmed with confocal microscopy (**Figure 3-26**). Anti-Spike glycoprotein fluorescent antibodies (in red) were used to demonstrate the presence of the protein on the cell surface.

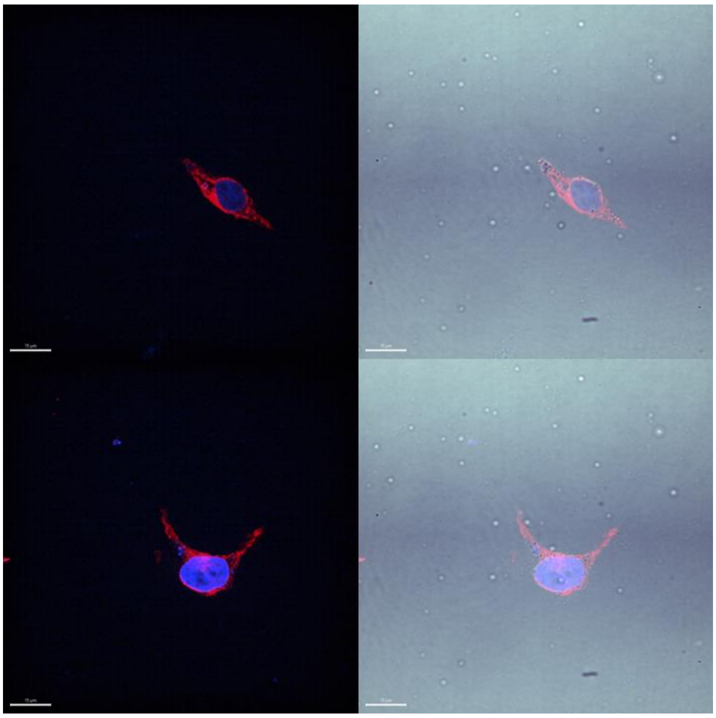

Figure 3-26 *Confocal microscopy images of HEK293 transfected to express Spike protein on the surface (anti-Spike Ab in red). Nuclei are stained with DAPI (in blue). Scale bars: 15 µm.*

Then, HEK293 expressing S-protein were used to fabricate Spike-cellsomes (S-CSMs). Size distribution analysis (NTA) of both S-CSMs derived from HEK293 transfected with plasmid FLAG and plasmid HA were performed and compared with CSMs derived from HEK293 not expressing S protein. As illustrated in **Figure 3-27** and **Table 3-6**, CSMs derived from all the cell lines mentioned showed the same size distribution, indicating that the expression of S-protein on HEK293 cells surface did not affect the stability of the nanovesicles.

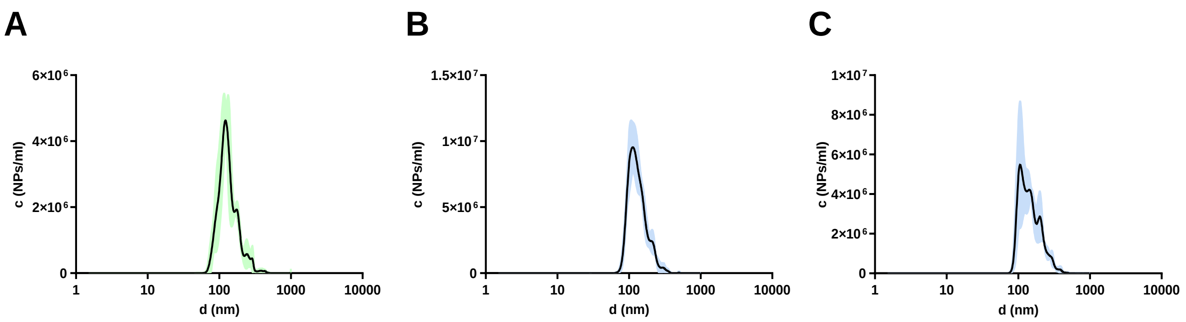

Figure 3-27 Size distribution analysis (NTA) of (A) HEK293-derived CSMs, (B) S-CSMs (FLAG), and (C) S-CSMs (HA).

Sample	d (mean) (nm)	d (mode) (nm)	c (NPs/mL)
HEK293-CSM	157.4 ± 2.6	123.5 ± 5.2	3.76E+11
S-CSM (FLAG)	150.0 ± 2.0	112.8 ± 3.9	8.33E+11
S-CSM (HA)	175.9 ± 4.7	117.2 ± 13.4	5.90E+11

Table 3-6 Size distribution analysis (NTA) of HEK293-CSMs and S-CSMs (FLAG and HA).

To further corroborate the presence of S-protein on S-CSMs surface, an anti-Spike glycoprotein fluorescent antibody was used for a flow cytometry analysis. As indicated in **Figure 3-28**, both S-CSMs derived from HEK293 transfected with plasmid FLAG and plasmid HA showed a fluorescence intensity increase when measured in presence of anti-Spike glycoprotein antibody. This qualitative result suggested that the S protein expression on the outer side of the lipid bilayer was maintained after CSMs fabrication procedure.

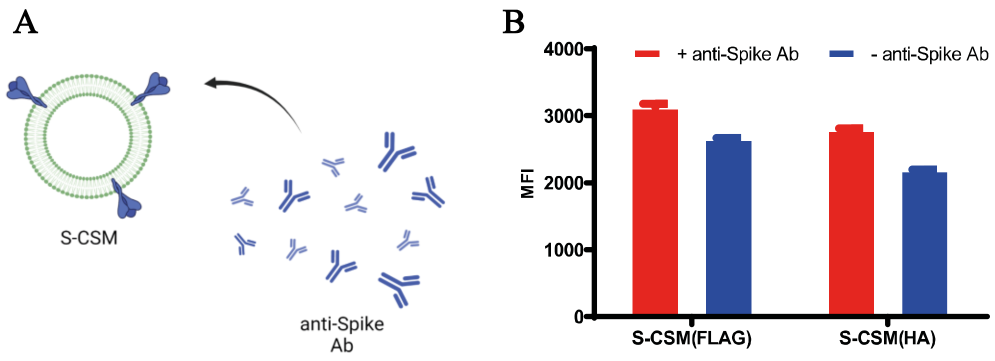

Figure 3-28 *(A) Schematic representation of the surface characterization of CSMs derived from transfected HEK293 measured with (B) flow cytometry.*

The presence of Spike glycoprotein on CSMs surface should improve the interaction with cells expressing ACE2 and therefore the internalization of the whole nanosystem.

Hence, once obtained and characterized the cell membrane-derived nanovesicles with Spike glycoprotein surface modification (S-CSMs), uptake studies in HEK293 and HEK293-ACE2 cells were performed with flow cytometry analysis.

In a first uptake experiment, both HEK293 and HEK293 cells expressing ACE2 were exposed to either S-CSMs derived from HEK293 transfected with plasmid FLAG or plasmid HA (named S-CSM(F) and S-CSM(H), respectively) for 3 hours. As shown in **Figure 3-29** A, the cellular internalization of both S-CSM(F) and S-CSM(H) was higher in HEK293-ACE2 compared to HEK293 non-expressing ACE2, indicating that the interaction between the S-protein and ACE2 promoted the internalization of the nanosystem.

Moreover, when compared to bare HEK293-CSMs, S-CSMs cellular internalization was higher in HEK293-ACE2, while HEK293 cells did not show any significant difference in the uptake of the two CSMs (**Figure 3-29** B), confirming that the surface modification of CSMs with the S-protein improved the interaction between the nanosystem and the cells expressing ACE2.

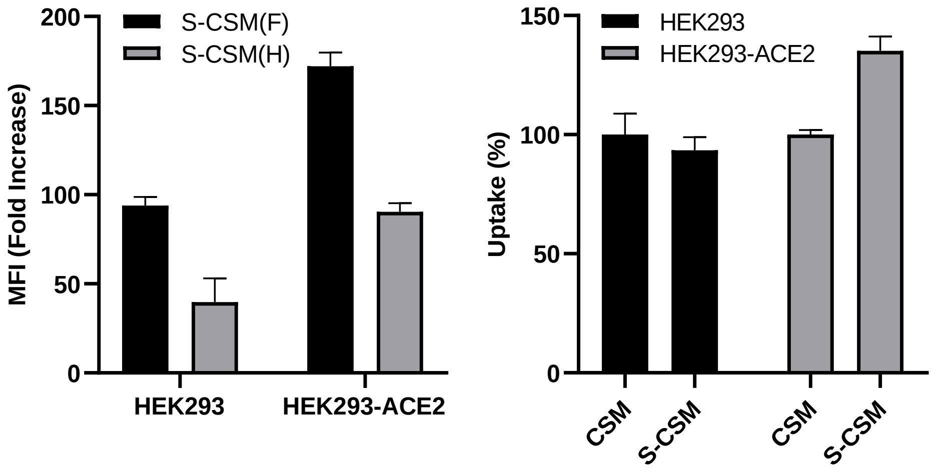

Figure 3-29 *Uptake analysis of HEK293 and transfected HEK293-Ace2 incubated with CSMs and S-CSMs for 3 hours.*

Taken together, these results may suggest that the surface modification strategy of cell membrane-derived nanosystem in combination with their intrinsic homotypic targeting capability could be an interesting and innovative approach for antiviral therapeutics.

Part of the results presented in the following chapter will be published in:

"Thrombolytic therapy based on lyophilized platelet-derived nanocarriers for ischemic stroke". *Journal of Nanobiotechnology*. (Submitted in **2023**)

Martina Migliavacca[1#], Clara Correa-Paz[2#], María Pérez-Mato[2], Patrick-Brian Bielawski[3], Issan Zhang[3], Pablo Hervella[2], Marina Rubio[4], Dusica Maysinger[3], Denis Vivien[4,5], Pablo del Pino[1], Beatriz Pelaz[1*], Ester Polo[1*], Francisco Campos[2*]

[1]*Center for Research in Biological Chemistry and Molecular Materials (CiQUS), University of Santiago de Compostela, 15705 Santiago de Compostela, Spain.* [2]*Clinical Neurosciences Research Laboratory (LINC), Health Research Institute of Santiago de Compostela (IDIS), 15706 Santiago de Compostela, Spain.* [3]*Department of Pharmacology and Therapeutics, McGill University, Montreal, QC, H3G 1Y6, Canada.* [4]*Normandie University, UNICAEN, INSERM UMR-S U1237, Physiopathology and Imaging of Neurological Disorders (PhIND), GIP Cyceron, Institute Blood and Brain @ Caen-Normandie (BB@C), 14000 Caen, France.* [5]*Department of Clinical Research, Caen Normandie University Hospital, Caen, France.*

Contributions: preparation, optimization, and characterization of the materials; writing – original draft.

Impact Factor: 10.2. Q1 in Nanoscience & Nanotechnology.

3.2. PLATELETS-DERIVED NANOVESICLES

Ischemic stroke is a cerebrovascular disease caused by the disruption of cerebral blood flow (CBF), which induces metabolic and cellular changes, leading to cell death and alteration of brain function.[347] Every year, approximately 15 million people experience a stroke episode worldwide. Of these, approximately 40% of cases result in death, while 33% are left with a permanent disability. Due to its global high impact, stroke is ranked as the second deadliest disease for individuals over 60 years of age, right after ischemic heart disease.[296]

The gold standard treatment for patients with acute ischemic stroke is the pharmacological thrombolysis with intravenous recombinant tissue plasminogen activator, (rtPA) a recombinant enzyme capable of degrading the fibrin network of the thrombus by converting the plasminogen into plasmin.

To date, rtPA remains the only thrombolytic drug for the treatment of acute ischemic stroke, which represents approximately 85% of all stroke cases.[348] However, one of the main drawbacks of rtPA is its poor stability and limited therapeutic window (only 4.5 hours after symptoms onset).[295] This limitation is mainly due to its short half-life (only 4 minutes) which implies an administration performed as an initial bolus followed by continuous infusion. In addition to rtPA's structural issues, it also leads to possible neurotoxic effects and the risk of hemorrhagic transformation.

Therefore, the need for the development of a carrier for a targeted and safe delivery of rtPA is impellent. Nanocarriers-based drug delivery systems have emerged as a promising technology to improve thrombolytic efficacy and safety of rtPA administration, as they can increase rtPA circulation time by protecting it from degradation and/or inactivation, reduce systemic side-effects (such as bleeding or hemorrhage), control the release within the therapeutic site, and potentially exploit external stimuli for the drug liberation. Despite these advantageous features of nanocarriers, they often lack *in vivo* efficacy, thus making them almost ineffective when compared to the gold standard treatment.

Within the group and in collaboration with Dr. F. Campos and Dr. C. Correa (LINC group, Santiago de Compostela), sonosensitive gelatin-modified polymeric nanocapsules (NCs) had already been developed as rtPA delivery nanocarriers.[347, 349] These polymeric NCs were optimized in terms of shell thickness to allow for ultrasound-induced release, thus preventing unspecific rtPA leaking or inactivation by plasminogen activator inhibitor-1 (PAI-1), the endogenous inhibitor of rtPA. The proposed strategy allowed to greatly extend rtPA half-life and activity in mice.[349]

To improve the stealthy properties and the targeting capabilities when circulating into the blood stream, biomimetic NPs or cell-derived nanosystems have recently been explored in the literature as nanocarriers for the treatment of ischemic stroke.[293] In a pioneering research study by Lv et al., a core-shell nanosystem composed of a dextran polymer modified with ROS-responsive boronic ester (core) and a red blood cell (RBC) membrane with stroke homing peptide inserted (shell) was able to prolong the *in vivo* circulation time and enhance the active targeting ability of the encapsulated molecule (a neuroprotective agent).[293]

Platelets are reported to escape clearance from the immune system and play a key role as multifunctional effectors of inflammatory responses. During an inflammatory response, inflammatory factors can activate platelets, which are recruited and accumulate at the inflammatory sites.[292] Furthermore, platelets and platelet membrane-based nanocarriers are especially promising for ischemic stroke therapies as they have thrombus targeting activity due to their content of immunoregulatory proteins, integrins, and glycoproteins, which interact with damaged vascular endothelial cells and fibrin. Moreover, the outer platelet membrane decrease NPs uptake by the mononuclear phagocyte system (MPS) potentially leading to a prolonged half-life of the encapsulated drug (e.g. rtPA).[350-352]

In order to exploit their capability to participate in inflammation, human platelets were used to fabricate cell-derived nanovesicles as drug delivery carriers. Then, commercially available rtPA (Actilyse®) was loaded into platelets-derived nanovesicles for the treatment of ischemic stroke (**Figure 3-30**).

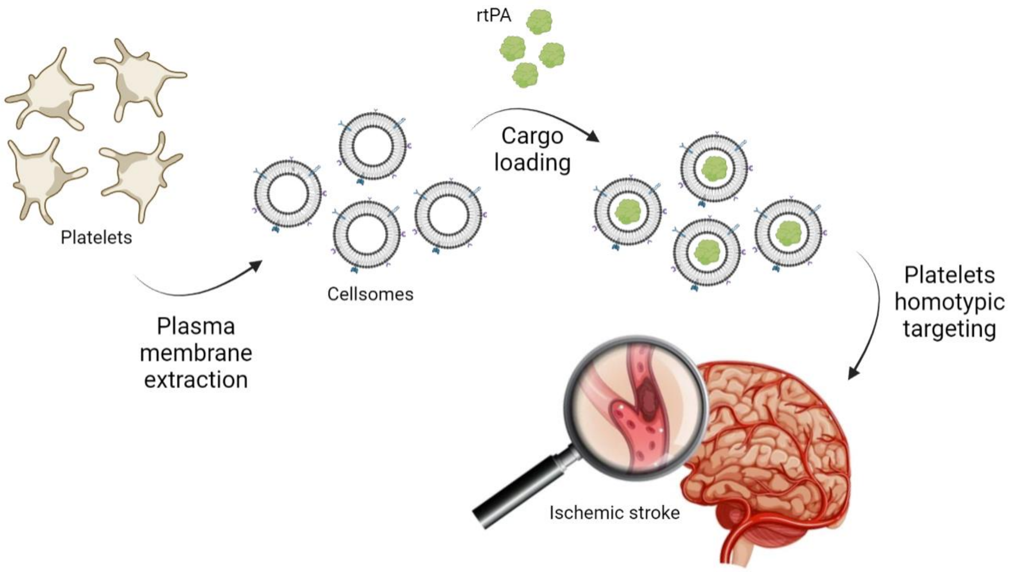

Figure 3-30 *Schematic representation of platelet-derived nanovesicles synthesis and use for ischemic stroke application.*

The studies and the results described in this chapter are part of the PLATMED Project (Biomimetic platelet-derived nanomedicines for the treatment of thromboembolic stroke AC20/0041, 2021-2023, ISC III- AES 2020 Euronanomed III, USC, IDIS, University Caen-Normandy, GIP Cyceron of France, and McGrill University of Canada). All *in vivo* studies have been carried out in collaboration with the LINC group (Dr. F. Campos and Dr. C. Correa-Paz, IDIS, Santiago de Compostela).

3.2.1. Design and characterization of platelets-derived nanovesicles

Platelets-derived CSMs were obtained following the protocol previously described (Section 2.1). Briefly, platelets were induced to swallow in a hypotonic environment enriched with a proteases inhibitor cocktail (PIC) to preserve the surface properties of plasma membrane. The resulting disrupted cells were exposed to 4 cycles of freeze in N_2 and thaw at 37 ºC and subsequently subjected to mechanical disruption with ultrasounds. Plasma membranes fragments were extracted and recollected through differential centrifugal steps and extruded through polycarbonate membranes with nanosized pores in order to obtain self-assembled platelets-CSMs of about 150-200 nm in size (**Figure 3-31**).

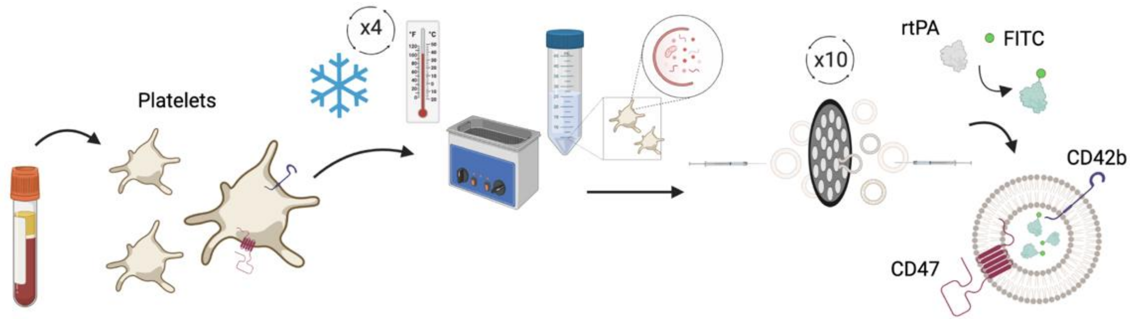

Figure 3-31 *Schematic representation of the experimental procedure used to obtain rtPA-loaded platelet-CSMs.*

The resulting platelets-CSMs were fluorescently labeled with DOPE Atto 647N by adding 5 µL of the fluorescent lipid resuspended in dichloromethane (1 mg·mL^{-1}). While commercially available rtPA (Actilyse®) labeled with fluorescein isothiocyanate (FITC) was loaded into fluorescent CSMs as described in Section 2.3.2.3.

To purify CSM(rtPA-FITC) from non-encapsulated rtPA-FITC and non-intercalated DOPE Atto 647N, two different purification methods were employed. Assumed that rtPA molecular weight is around 70 kDa, the solution was first filtered by ultrafiltration using Amicon® Ultra-0.5 Centrifugal Filter Devices (100 kDa cutoff). However, rtPA activity studies demonstrated that the purification method could be improved to eliminate the non-encapsulated drug. Hence, the purification method was optimized with a single semi-ultracentrifugation step. CSM(rtPA-FITC) were in fact purified from non-encapsulated rtPA-FITC and non-intercalated DOPE Atto 647N by centrifuging them 1 hour at 70,000 g at 4 ºC (**Figure 3-32**).

Once the purification method was optimized, the encapsulated rtPA-FITC was quantified by fluorescence intensity measurements. The cargo concentration was determined by interpolation of the measured fluorescence intensity in the analytical calibration curve. The loading efficiency (% LE) was determined as the mass of rtPA in purified CSM(rtPA) divided per the mass of total rtPA added, and an average of ~20 % LE was achieved for the CSM(rtPA) synthesized.

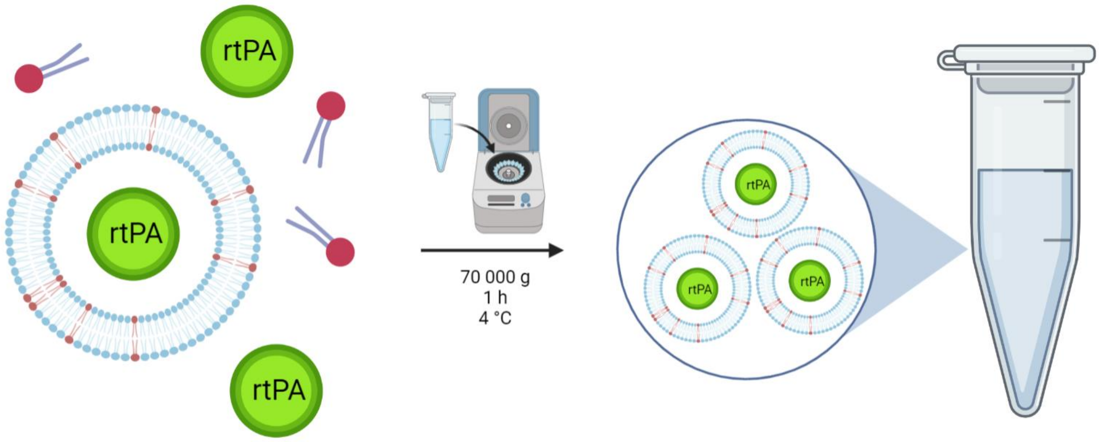

Figure 3-32 *Schematic representation of platelets-CSMs optimized purification method.*

The resulting physicochemical properties of fluorescent CSM(rtPA) were characterized with DLS and NTA to validate the colloidal size distribution and NPs concentration. Moreover, STEM micrographs were acquired to further corroborate size distribution analysis.

As shown in **Figure 3-33**, **Table 3-7**, and **Table 3-8**, size distribution measurements indicated that the obtained platelets-derived CSMs mean diameter was consistent with CSMs derived from other cell lines (described in the previous chapter) and it did not change after rtPA loading.

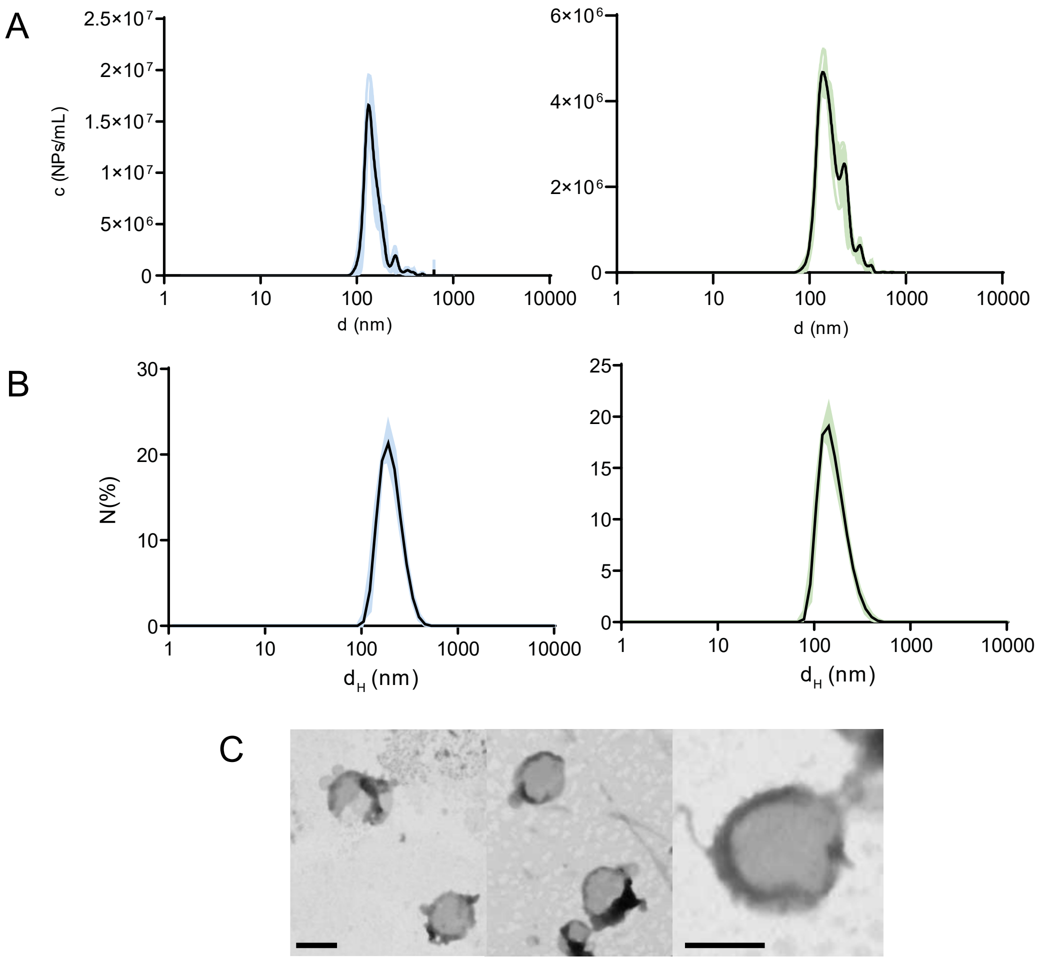

Figure 3-33 Size characterization of platelet-derived nanovesicles: (A) NTA size distribution before (on the left) and after (on the right) rtPA encapsulation; (B) DLS size number distribution before (on the left) and after (on the right) rtPA encapsulation. Data are shown as mean ± s.d. (n = 3). (C) STEM micrographs of platelet-derived nanovesicles before (on the left) and after (on the right) rtPA encapsulation stained with uranyl acetate (scale bars = 200 nm).

Sample	d (mean) (nm)	d (mode) (nm)	c (NPs/mL)
CSM	169.7 ± 2.0	134.1 ± 2.1	1.03E+12
CSM(rtPA)	196.7 ± 3.4	136.9 ± 3.1	5.47E+11

*Table 3-7 NTA analysis of platelets-derived CSMs before and after rtPA encapsulation. Data are illustrated in **Figure 3-33**.*

Sample	Z-Average (nm)	PdI	$d_{H,I}$ (nm)	$d_{H,N}$ (nm)	$d_{H,V}$ (nm)
CSM	254.7 ± 6.2	0.296 ± 0.053	238.8 ± 4.4	205.1 ± 4.2	250.4 ± 6.7
CSM(rtPA)	221.8 ± 3.5	0.305 ± 0.026	217.2 ± 12.0	163.2 ± 2.1	227.4 ± 16.0

*Table 3-8 DLS analysis of platelets-derived CSMs before and after rtPA encapsulation. Data are illustrated in **Figure 3-33**.*

Cells surface properties are a fundamental element for cell-derived nanovesicles, as they are supposed to offer biomimetic features, including homotypic targeting and immune escape capabilities.

Signal regulatory protein (SIRP) is an immunoglobulin (Ig) superfamily member expressed by different cell types that can function as an inhibitory receptor able to down-regulate phagocytosis. The ligand for SIRP is the cell-surface glycoprotein CD47, an integrin-associated protein virtually expressed by all cells, especially platelets.[353] CD47 is thought to be responsible for the prolonged circulation time of platelet-derived nanovesicles in the blood stream.

Glycoprotein Ib (GPIb) is a platelet surface membrane glycoprotein that functions as a receptor for von Willebrand factor (VWF). The binding of GPIb to VWF facilitates initial platelets adhesion to vascular subendothelium after vascular injury, and also initiates signaling events within the platelet that lead to enhanced platelet activation, thrombosis, and hemostasis.[354]

For these reasons, CD47 and CD42b/GPIbα were chosen as platelets surface markers. To corroborate their presence both in platelets and in platelets-derived CSMs, anti-CD47 and anti-CD42b/ GPIbα antibodies were used in a semi-quantitative flow cytometry analysis. As shown in **Figure 3-34**, both platelets and platelets-derived CSMs presented CD47 and CD42b/GPIbα surface receptors, indicating that these surface markers were successfully transferred to the CSM surface and that the self-assembled process of CSMs formation takes place with a right side-out membrane orientation.

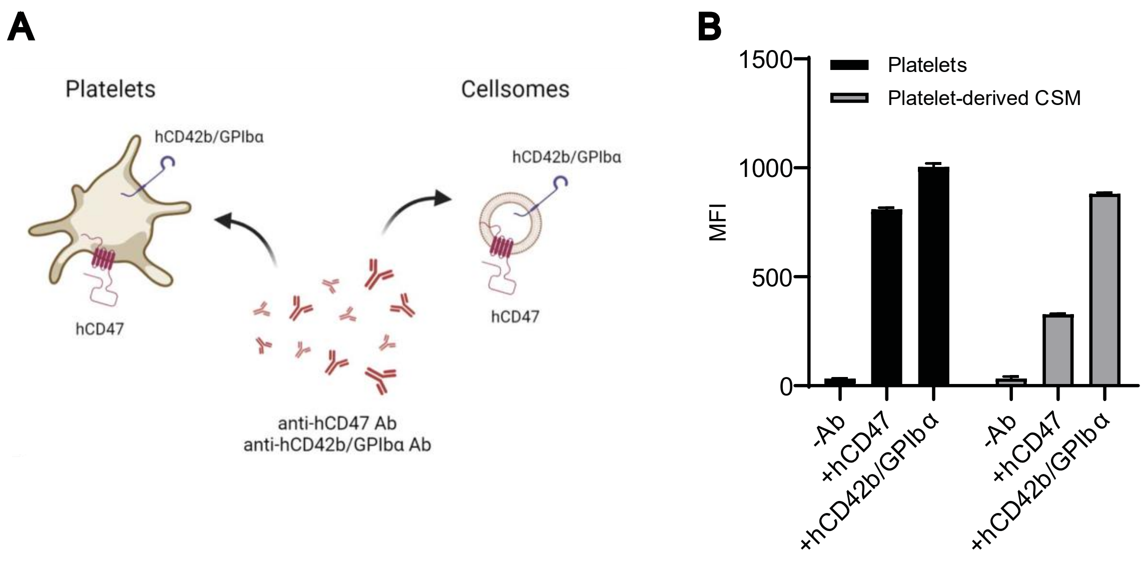

Figure 3-34 *Surface characterization of platelet-derived nanovesicles. (A) Schematic representation of platelets and platelet-derived nanovesicles surface proteins study. (B) Flow cytometry (FC) analysis of platelets and platelet-derived nanovesicles using anti-CD47 and anti-CD42b/GPIbα antibodies. Data are shown as mean ± s.d. (n = 3).*

3.2.2. rtPA activity

Because of the poor stability and the limited therapeutic window of rtPA, the major concern in fabricating platelets-derived CSMs loaded with rtPA was ensuring drug activity and stability during the synthesis and overtime (including once the CSM(rtPA) are dispersed in biological media). The need for stable and active CSM(rtPA) was given by the purpose of fabricating robust nanosystems able to preserve rtPA features even at room temperature.

Nevertheless, to enhance the possibility of long-term storage of the prepared samples, given the long-distance collaboration that characterized this project (different laboratories located in Spain, France, and Canada), a lyophilization process was optimized in order to storage and preserve physicochemical and biological properties of CSM(rtPA), opening the possibility to a more translational use of this nanosystem in clinical studies. For this purpose, all the colloidal stability characterization and rtPA activity evaluation were performed at different conditions (room temperature, 4 ºC and after the lyophilization process).

rtPA is a fibrinolytic serine protease known to convert plasminogen into plasmin, which then is able to degrade fibrin, the primary component of blood clots. To measure rtPA proteolytic activity once loaded into CSMs, a specific chromogenic substrate was used (a chromogenic peptide permeable to CSMs surface). This enzymatic activity results in the hydrolysis of the substrate and the subsequent release of free p-nitroaniline (pNA). Free pNA measurements were performed spectrophotometrically my monitoring the variation of absorbance (at 405 nm) in a kinetic cycle of 15-20 hours (ΔAbs/hour).

As mentioned above, rtPA activity assay was first performed to study and establish the most appropriate purification method. A comparison between the two purification methods was made: CSM(rtPA) purified by filtration and CSM(rtPA) purified by centrifugation were either stored at 4 ºC or subjected to lyophilization and later reconstituted to solution to measure rtPA activity. As shown in **Figure 3-35**, free tPA (in red) partially lost its activity during time due to the different storage conditions that may induce physicothermal changes. CSM(rtPA) purified by filtration (in blue) also tended to lose their activity, especially after lyophilization. This could be due to the purification method itself, which did not allow the complete elimination of the free rtPA in the solution, where therefore contained both rtPA encapsulated in CSMs and free rtPA. Consequently, the over-estimation of the total amount of rtPA in the solution might have produced a bias in the rtPA activity measurement, which in the end resulted low because of the high amount of free rtPA instead of CSMs-loaded rtPA. Moreover, it is worth noting that each handling procedure (such as filtration) may cause some loss in rtPA activity, which was the actual concern of this project. Whereas, CSM(rtPA) purified by centrifugation (in green) maintained their original activity, particularly after lyophilization, meaning that not only the purification method was able to eliminate all the free rtPA in the solution, but also the centrifugation itself resulted to be a safer process to handle delicate proteins, such as rtPA.

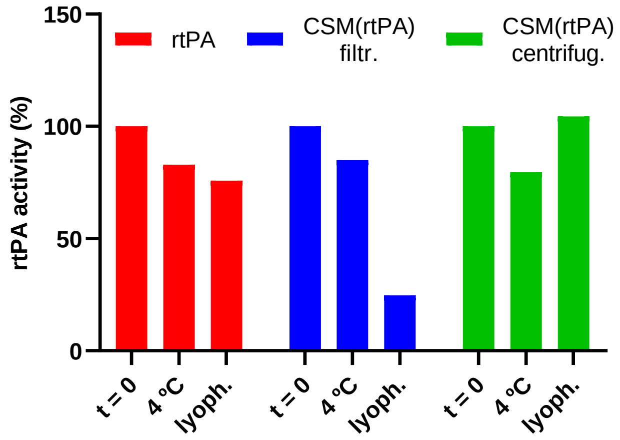

Figure 3-35 *Optimization of CSM(rtPA) purification method based on rtPA activity.*

Once established the most suitable purification method for CSM(rtPA), the same activity assay was performed in presence of plasminogen activator inhibitor 1 (PAI-1) (**Figure 3-36**), which is the principal inhibitor of tissue plasminogen activator and, therefore, of the whole fibrinolysis process.

As illustrated in **Figure 3-36** A, rtPA maintains its activity when loaded into CSMs, showing an extremely similar spectrophotometric kinetic profile compared to free rtPA. In the case of free rtPA the exponential phase was steeper, reaching the transitional and thus the plateau phases before compared to CSM(rtPA). This might be due to the chromogenic substrate relative accessibility: if the rtPA is free in the solution, it quickly reaches the chromogenic substrate and the free p-nitroaniline (pNA) is released, causing the rapid increase of the absorbance measurements; while the rtPA encapsulated in CSMs does not have the possibility of reaching the substrate fast, which needs to diffuse through the phospholipid bilayer before encountering the rtPA. Consequently, the two plateau curves reached the same values eventually, although following slightly different pathways.

Plasminogen activator inhibitor-1 (PAI-1) is the principal inhibitor of rtPA, which converts plasminogen into plasmin, thus inhibiting the whole fibrinolysis process. When loaded into CSMs, rtPA was not inhibited by PAI-1 (**Figure 3-36** B), as it was when free in the solution, indicating that the biomimetic nanocarrier was able to prevent its exposure to potential external inhibitors.

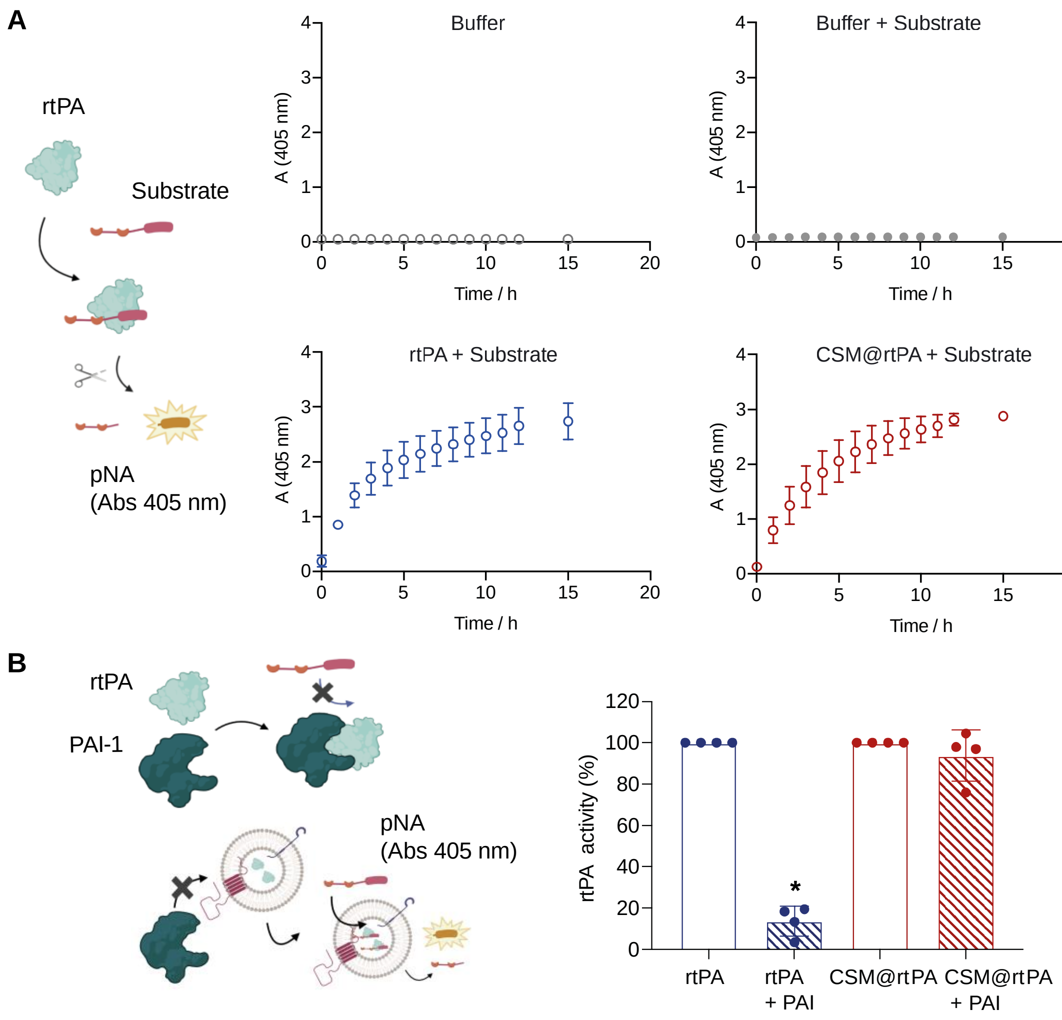

Figure 3-36 *rtPA activity studies (A) without and (B) with plasminogen activator inhibitor (PAI).*

3.2.3. Platelet-derived CSMs stability

As mentioned above, one of the main concerns in designing rtPA-loaded nanocarriers is the limited drug stability. To evaluate rtPA activity through time, CSM(rtPA) were exposed to different storage conditions and then re-characterized to determine the most suitable one. They were either left 72 hours at room temperature (**Figure 3-37**, **Table 3-9** and **Table 3-10**), or stored 48 hours at 4 ºC (**Figure 3-38**, **Table 3-11** and **Table 3-12**), or subjected to lyophilization and then reconstituted to solution (**Figure 3-39**, **Table 3-13** and **Table 3-14**).

The re-characterization consisted of NTA and DLS analysis, with a particular focus on the correlation coefficient measurements of the solutions before and after subjecting them to the specific storage condition. The correlation in DLS is a technique for extracting the time dependence of a signal in the presence of "noise", thus it indicates not only the polydispersity of the sample, but also Brownian motion-related events, such as sedimentation (see Section 3.1.1.2).

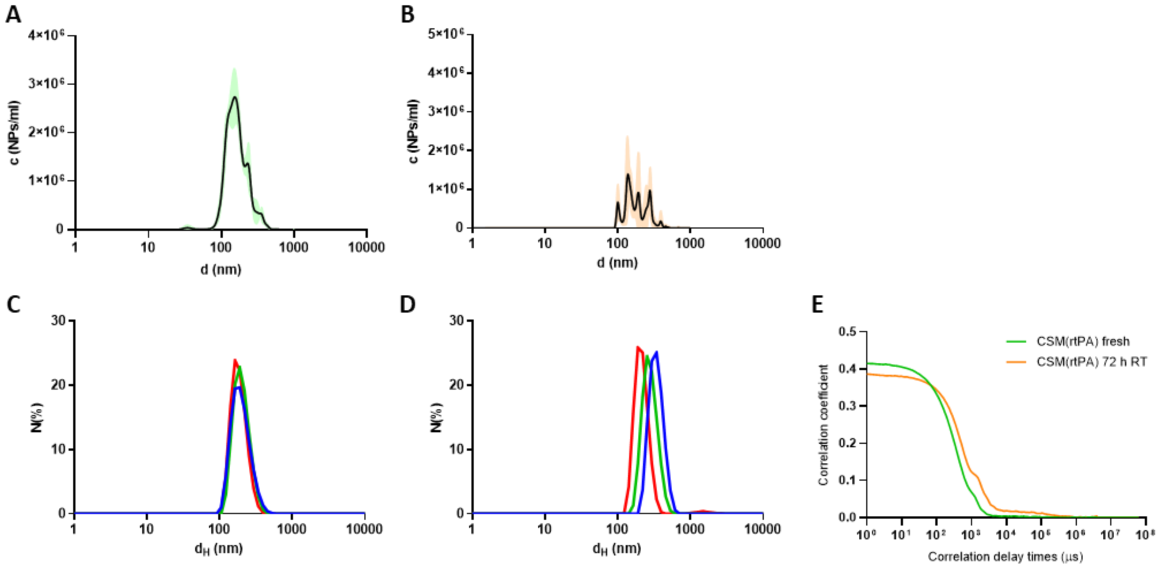

***Figure 3-37** (A and B) NTA and (C and D) DLS size distribution analysis of CSM(rtPA) (A and C) freshly prepared and (B and D) after 72 hours at room temperature. (E) shows the correlation coefficients of CSM(rtPA) freshly prepared and after 72 hours at room temperature.*

Sample	d (mean) (nm)	d (mode) (nm)	c (NPs/mL)
CSM(rtPA) fresh	194.0 ± 4.4	146.9 ± 13.1	3.50E+11
CSM(rtPA) 72 h RT	217.8 ± 8.9	185.1 ± 46.4	1.43E+11

***Table 3-9** NTA analysis of CSM(rtPA) freshly prepared and after 72 hours at room temperature.*

Sample	Z-Average (nm)	PdI	$d_{H,I}$ (nm)	$d_{H,N}$ (nm)	$d_{H,V}$ (nm)
CSM(rtPA) fresh	256.2 ± 12.0	0.384 ± 0.056	229.8 ± 15.2	198.2 ± 8.7	240.0 ± 19.4
CSM(rtPA) 72 h RT	456.8 ± 48.6	0.523 ± 0.087	302.1 ± 67.7	280.7 ± 64.8	4096 ± 1852

***Table 3-10** DLS analysis of CSM(rtPA) freshly prepared and after 72 hours at room temperature.*

As shown in **Figure 3-37**, **Table 3-9** and **Table 3-10**, when left 72 hours at room temperature, CSM(rtPA) tended to aggregate and therefore the solution lost its monodispersity. It is quite evident in all the size distribution analysis, but the DLS number distribution perfectly shows the aggregation tendency during time (being the red line the first measurement, and the blue line the last one). In addition, the correlation coefficient clearly indicates polydispersity and sample sedimentation once characterized after storing it 72 hours at room temperature.

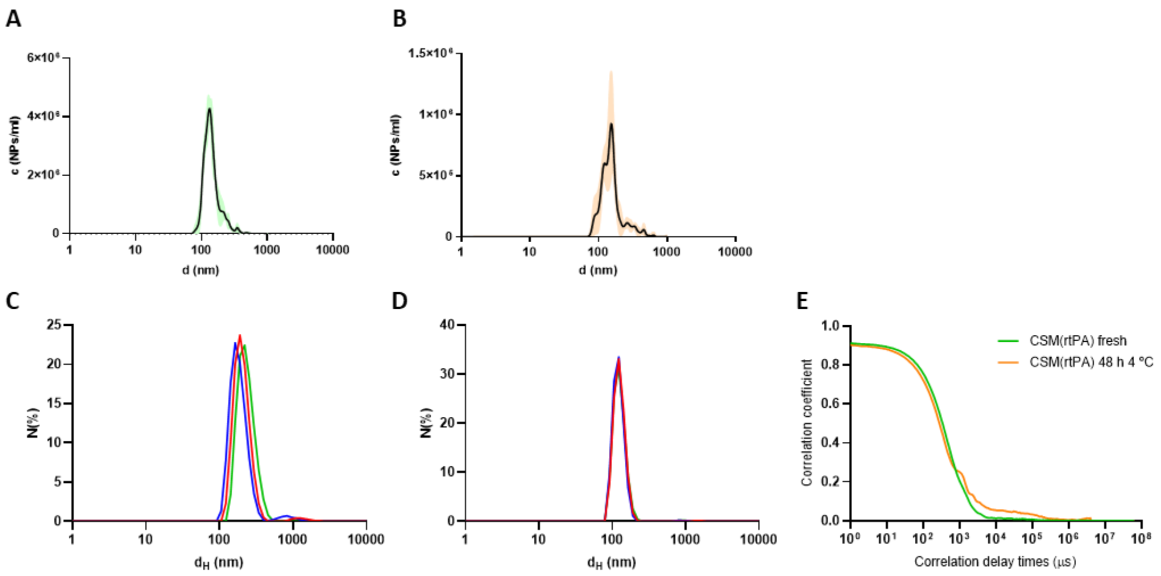

Figure 3-38 *(A and B) NTA and (C and D) DLS size distribution analysis of CSM(rtPA) (A and C) freshly prepared and (B and D) after 48 hours at 4 °C. (E) shows the correlation coefficients of CSM(rtPA) freshly prepared and after 48 hours at 4 °C.*

Sample	d (mean) (nm)	d (mode) (nm)	c (NPs/mL)
CSM(rtPA) fresh	165.9 ± 1.2	133.1 ± 3.6	3.15E+11
CSM(rtPA) 48 h 4 °C	201.7 ± 4.4	155.5 ± 3.0	8.12E+10

Table 3-11 *NTA analysis of CSM(rtPA) freshly prepared and after 48 hours at 4 °C.*

Sample	Z-Average (nm)	PdI	$d_{H,I}$ (nm)	$d_{H,N}$ (nm)	$d_{H,V}$ (nm)
CSM(rtPA) fresh	327.3 ± 23.4	0.430 ± 0.042	235.8 ± 27.8	207.8 ± 25.3	245.9 ± 32.8
CSM(rtPA) 48 h 4 °C	306.6 ± 18.8	0.447 ± 0.031	135.3 ± 3.5	124.4 ± 1.9	1256 ± 388.6

Table 3-12 *DLS analysis of CSM(rtPA) freshly prepared and after 48 hours at 4 °C.*

As shown in **Figure 3-38**, **Table 3-11** and **Table 3-12**, CSM(rtPA) solution left 48 hours at 4 ºC presented quite good monodispersity and no tendency to aggregation during time. Nonetheless, the correlation coefficient indicates that even so a small part of the solution tended to sediment (orange line).

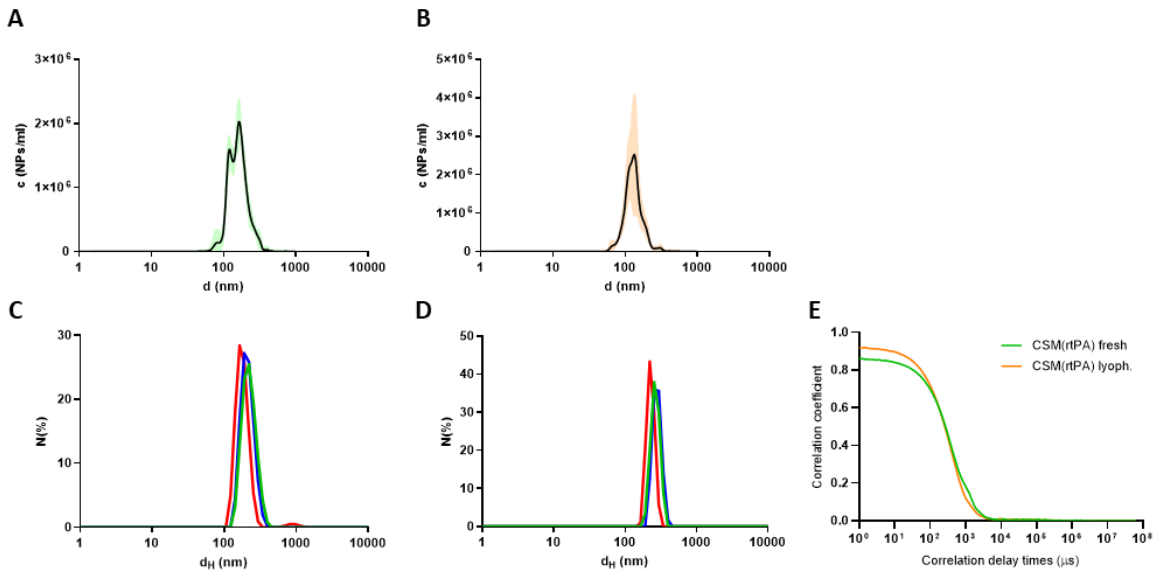

Figure 3-39 (A and B) NTA and (C and D) DLS size distribution analysis of CSM(rtPA) (A and C) freshly prepared and (B and D) after lyophilization. (E) shows the correlation coefficients of CSM(rtPA) freshly prepared and after lyophilization.

Sample	d (mean) (nm)	d (mode) (nm)	c (NPs/mL)
CSM(rtPA) before lyoph.	180.4 ± 1.2	166.0 ± 2.5	2.18E+11
CSM(rtPA) after lyoph.	151.2 ± 7.1	127.5 ± 7.2	1.93E+11

Table 3-13 NTA analysis of CSM(rtPA) freshly prepared and after lyophilization.

Sample	Z-Average (nm)	PdI	$d_{H,I}$ (nm)	$d_{H,N}$ (nm)	$d_{H,V}$ (nm)
CSM(rtPA) before lyoph.	341.2 ± 26.0	0.453 ± 0.005	221.8 ± 27.1	205.8 ± 23.7	227.2 ± 29.9
CSM(rtPA) after lyoph.	273.3 ± 9.7	0.365 ± 0.054	261.2 ± 28.0	258.0 ± 26.8	264.4 ± 29.0

Table 3-14 DLS analysis of CSM(rtPA) freshly prepared and after lyophilization.

Whereas, as shown in **Figure 3-39**, **Table 3-13** and **Table 3-14**, lyophilization process resulted to be the most suitable storage condition for CSM(rtPA). Size distribution analysis (both NTA and DLS) and correlation coefficient indicate that the sample, once reconstituted to solution, maintained its physicochemical properties and stability over time.

Moreover, to completely assess drug stability, rtPA activity assay was performed after leaving the CSM(rtPA) in different storage conditions: after 48 hours at 4 ºC and after lyophilization and reconstitution processes. As shown in **Figure 3-40**, rtPA loaded in platelet-derived nanovesicles and subjected to lyophilization maintained its activity, indicating that the biomimetic carrier is able to preserve both colloidal stability and drug activity after lyophilization, a process that could be potentially beneficial for rtPA storage during time.

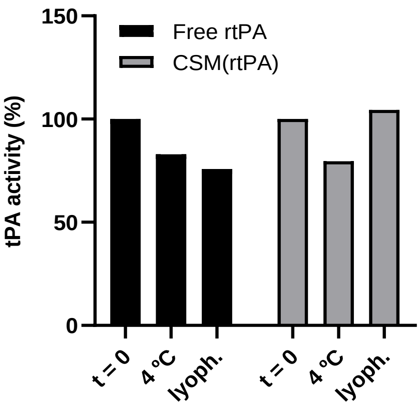

Figure 3-40 *rtPA activity in different storage conditions (t = 48 hours).*

3.2.4. Samples reproducibility

Once optimized all the synthesis steps and established the proper storage condition, *in vivo* experiments were performed to study the therapeutic effect of rtPA encapsulated in CSMs. However, since all the experiments, and especially *in vivo* studies (displayed in the next paragraph) require high reproducibility standards, one of the crucial concerns for the project was to obtain very similar batches of both CSM(rtPA) and empty CSMs, which were used as controls.

Here, size distribution studies and cargo encapsulation efficiency of most of the CSM(rtPA) (**Table 3-15**) and empty CSMs (**Table 3-16**) batches are presented. In each table, DLS and NTA analysis are shown as the mean of three measurements, while the amount of cargo loaded (in µg) and the percentage of encapsulation efficiency refer to calibration curves constructed *ad hoc* for each batch. Each calibration curve derives from each rtPA batch used, which was labeled with FITC, purified, and then used as standard for the fluorescence values of rtPA-FITC encapsulated in CSM(rtPA).

The last row of each table represents the mean and the standard deviation of the displayed values in each column. As shown, each batch of CSM(rtPA) (1 mL) included around 100 µg of rtPA-FITC (encapsulation efficiency of 20%), while size distribution analysis reported data consistent with all the CSMs described (150-200 nm in size).

Cargo (rtPA-FITC)		NTA			DLS		
µg	EE %	c (NPs/mL)	d (mean) (nm)	d (mode) (nm)	PdI	$d_{H,I}$ (nm)	$d_{H,N}$ (nm)
83	23	1.88E+11	179	123	0.279	195	171
77	21	1.52E+11	183	165	0.236	211	179
116	22	2.17E+11	174	136	0.409	213	190
131	25	1.30E+11	177	118	0.368	253	226
99	18	1.59E+11	169	119	0.260	237	192
100	19	2.38E+11	175	117	0.281	169	112
86	19	5.47E+11	197	137	0.272	267	207
110	19	7.21E+10	166	124	0.411	238	218
109	19	7.56E+10	162	126	0.490	236	217
129	22	5.78E+10	168	133	0.432	276	256
122	25	5.10E+10	168	135	0.485	252	239
168	25	1.01E+11	193	110	0.340	281	220
111 ± 25	**21 ± 3**	**1.48E+11 ± 5.93E+10**	**176 ± 11**	**129 ± 14**	**0.355 ± 0.090**	**236 ± 34**	**202 ± 38**

Table 3-15 *CSM(rtPA) characterization summary.*

Cargo (-)		NTA			DLS		
µg	EE %	c (NPs/mL)	d (mean) (nm)	d (mode) (nm)	PdI	$d_{H,I}$ (nm)	$d_{H,N}$ (nm)
-	-	1.24E+11	191	137	0.249	242	200
-	-	1.03E+11	200	138	0.329	297	152
-	-	1.01E+11	187	131	0.362	272	253
-	-	7.91E+10	198	162	0.302	242	196
-	-	1.26E+11	199	180	0.361	290	154
-	-	1.36E+11	194	132	0.290	225	166
-	-	4.78E+11	172	129	0.160	191	146
-	-	3.76E+11	173	139	0.230	183	133
-	-	3.43E+11	172	133	0.280	192	122
-	-	1.73E+11	174	144	0.383	182	139
-	-	9.46E+10	188	132	0.360	226	184
-	-	8.50E+10	160	108	0.364	205	172
-	**-**	**1.43E+11 ± 7.96E+10**	**184 ± 13**	**139 ± 18**	**0.306 ± 0.068**	**229 ± 41**	**168 ± 36**

Table 3-16 *Empty CSMs characterization summary.*

The preparation protocol, as well as the purification process and the storage conditions, were optimized with the aim of obtaining both empty CSMs and CSM(rtPA) batches that showed a great reproducibility in terms of size distribution and encapsulation efficiency (**Table 3-15** and **Table 3-16**). In particular, the lyophilization process allowed to storage and maintain both physicochemical and biological properties of CSM(rtPA), preserving the nanocarrier without altering the cargo's properties (such as rtPA activity, **Figure 3-40**), thus opening the possibility to a more translational use of this nanosystem in clinical studies.

3.2.5. Preliminary *in vivo* studies

Before assessing the actual therapeutic effect of platelets-derived CSM(rtPA) *in vivo*, rtPA plasmatic activity was studied by extracting blood samples before and 1, 5, 15, and 40 minutes after the administration of CSM(rtPA) in healthy animals (**Figure 3-41** A). When the vehicle was administered, rtPA plasmatic activity remained stable. Due to its short half-life when 1 mg/kg of rtPA was administered, plasma activity increased (6-fold), decreasing rapidly to a 3-fold increase after 15 minutes and achieving the basal activity 40 minutes after the administration. While in the case of CSM(rtPA), plasmatic activity increased 5 times respect to the basal timepoint. However, it remained elevated during all extractions, reaching a 3-fold increase in plasma activity at 40 minutes. Lyophilized CSM(rtPA) showed the same profile as the "fresh" CSM(rtPA), although its increase was not significant (**Figure 3-41** B).

Then, tail bleeding assay was performed to examine re-bleedings and the time of bleeding after the administration of the different treatments (**Figure 3-41** C). Bleeding time assay reflects the ability to control bleeding not only after relatively large vessels are injured, but also after the administration of compounds that are significantly involved in the coagulation cascade (**Figure 3-42**), as tissue plasminogen activator.

As illustrated in **Figure 3-41**, bleeding time was observed to increase after the treatment with free rtPA (14.16 minutes) compared to the vehicle group (4.49 minutes). Interestingly, the animals treated with CSM(rtPA) showed a bleeding time (5.10 minutes) comparable to the vehicle group, demonstrating that CSM(rtPA) decreased the risk of bleeding compared to free rtPA.

Re-bleeding is a phenomenon that is common when hemostatic action of platelets is partially inhibited.[355] In all the animals treated with rtPA re-bleeding occurred, while in none of the animals treated with the vehicle re-bleedings were observed. When CSM(rtPA) was administered, the percentage of animals in which re-bleeding occurred decreased to 40%, corroborating the evidence that the platelet-derived nanocarrier was able to decrease the risk of bleeding caused by rtPA.

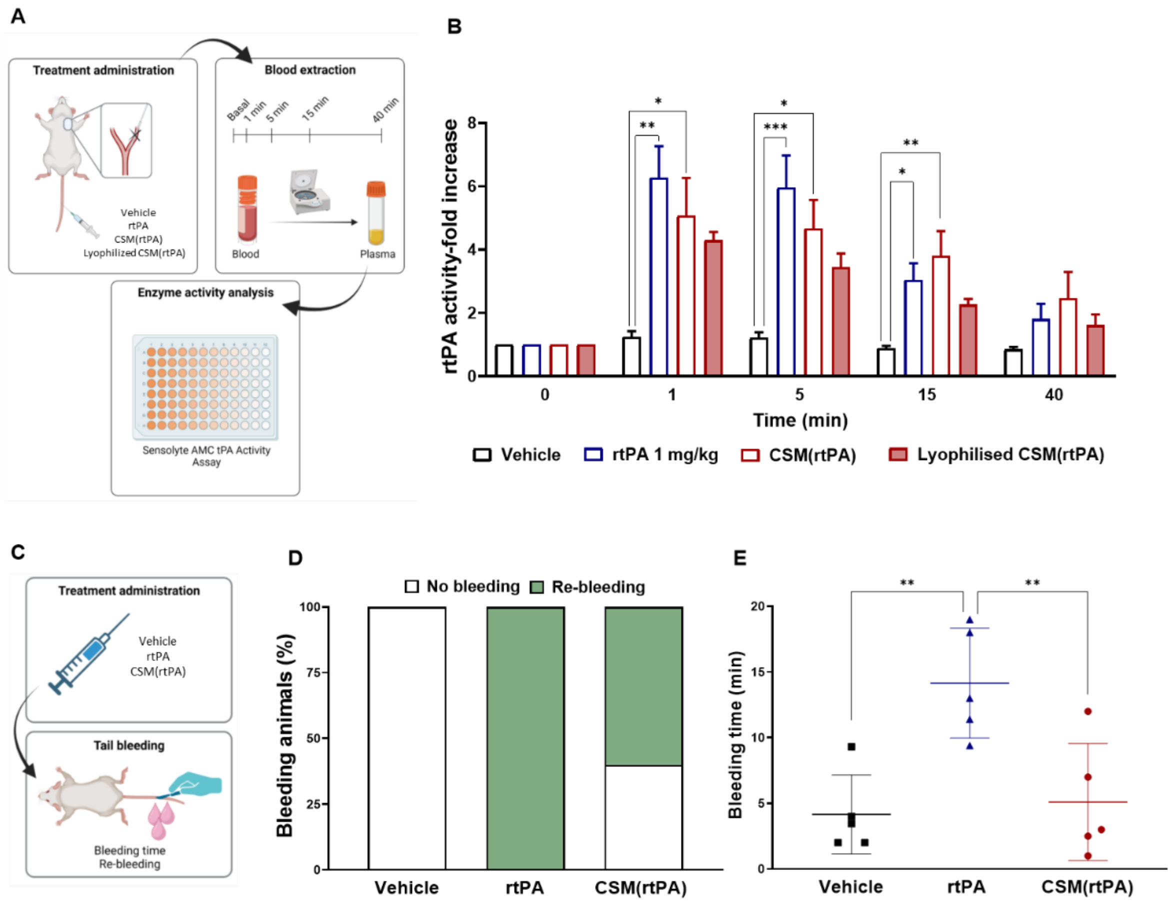

Figure 3-41 *(A and B) Plasmatic activity studied from extracted blood samples. (C, D, and E) Bleeding assays of CSM(rtPA) and non-encapsulated rtPA 20 minutes after treatment administration through jugular vein and subsequent tail docking (n = 5).Percentage of the animals in which re-bleeding occurred. Data represent mean ± s.d. (n = 5 per group of treatment).*

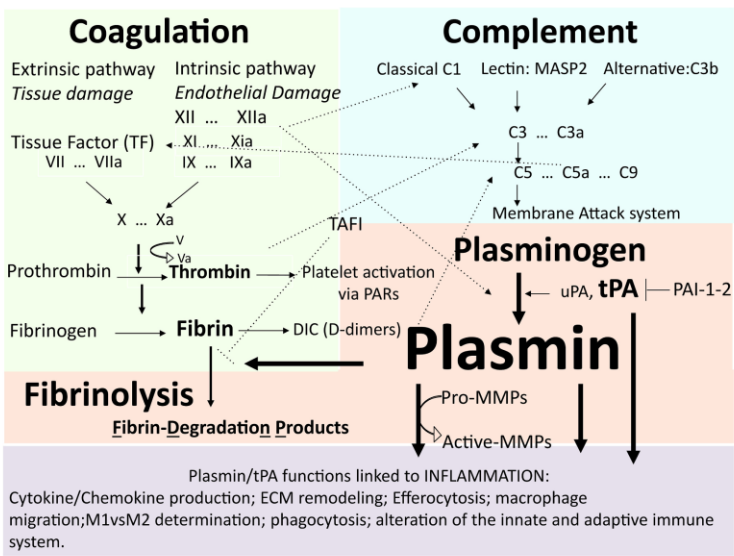

Figure 3-42 *Inflammatory response in fibrinolytic system, coagulation, and complement system crosstalk.*[356]

To study the therapeutic effect of platelets-derived CSM(rtPA) *in vivo*, a thromboembolic mouse model of stroke was induced by the occlusion of the middle cerebral artery (MCAo) with thrombin injection. During all the surgery, the CBF was registered using a Doppler to confirm clot generation. 30 minutes after thrombin injection, the different treatments were administered in the tail vein. To measure the infarct volume and study the presence of hemorrhages, 24 hours after the surgery MRI was performed.

As shown in **Figure 3-43**, rtPA treatment reduced the infarct volume compared to the vehicle group. When empty CSMs were administered, the infarct volume did not decrease the lesion, while in the case of CSMs loaded with rtPA, the reduction is similar to rtPA group.

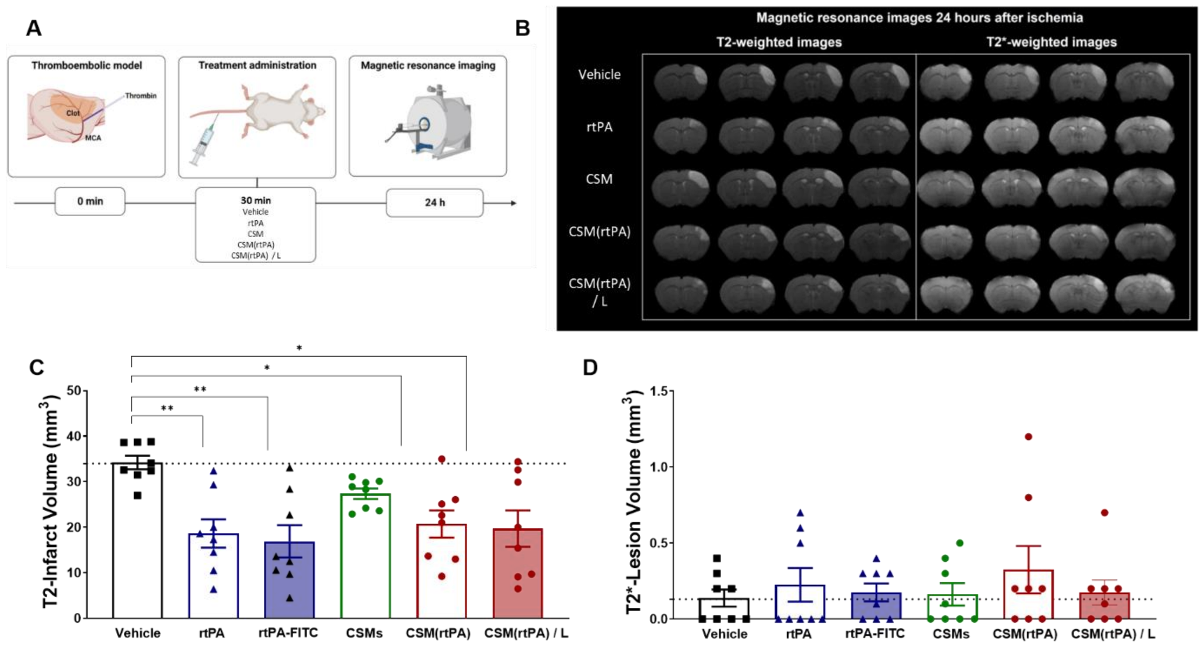

*Figure 3-43 (A) Representation of the therapeutic effect of rtPA in a thromboembolic stroke mouse model. (B) Ischemic lesion (white brain region) was determined by T2-weighted at 24 hours after the treatment administration. (C and D) The analysis of the infarct volume and the lesion volume were measured 24 hours after treatment administration. The dotted lines represent the median of the vehicle group. All data are represented as mean ± SEM (n = 8 per treatment group). In all data statistical analysis was assessed by the on-way ANOVA followed by post-hoc Tukey's test (*p<0.05; **p<0.01 compared with the vehicle group).*

Overall, these results suggest that the platelets-derived nanosystem here developed exhibited promising beneficial effects for the treatment of ischemic stroke. Given their innate ability to participate in inflammation, platelets were employed as source cells to fabricate CSMs, then used as nanocarrier for the delivery of rtPA enzyme, the gold standard treatment for ischemic stroke. Therapeutic evaluation of CSM(rtPA) showed that the encapsulated drug maintained its activity *in vivo*, enhancing both the plasmatic activity and the bleeding time in mice. Furthermore, the nanocarrier was optimized to protect the encapsulated rtPA enzyme, preserving its activity even after lyophilization process, thus opening the possibility to a more translational use of this nanosystem in clinical studies.

Part of the results presented in the following chapter has been published in:

“Fusogenic Cell-Derived nanocarriers for cytosolic delivery of cargo inside living cells”. *Journal of Colloid and Interface Science*, **2023**, *648*, 488-496.

Enrica Soprano, Martina Migliavacca, Miriam Lopez-Ferreiro, Beatriz Pelaz, Ester Polo*, Pablo del Pino*.

Centro Singular de Investigacion en Química Bioloxica e Materiais Moleculares (CiQUS), Universidade de Santiago de Compostela. Rúa Jenaro de la Fuente s/n, 15705, Santiago de Compostela, Spain.

Contributions: preparation and characterization of the materials; *in vitro* experiments; writing – original draft.

Impact Factor: 9.9. Q1 in Chemistry, Physical. No written permission from Elsevier is necessary. Copyright 2023. ISSN 0021-9797.

3.3. FUSOGENIC CELL-DERIVED NANOVESICLES FOR GENE EDITING

Gene editing is considered to be any modification on its own initiative that alters a sequence of genetic material in a cellular organism, either by adding, eliminating, or exchanging bases. In the perspective of treating diseases caused by alterations of DNA sequence, gene therapy could be a promising strategy for the treatment of monogenic disorders, which are caused by a mutation in a single gene.[357]

An innovative and efficient strategy for gene editing is targeting double strand breaks (DSBs) where the editing is aimed at delivering a template containing the desired mutation. With this purpose, several nucleases have been deeply studied during almost 40 years.[358] The first restriction enzymes identified in many microbial genomes were meganucleases, which were shown to be very efficient. Though, the two domains that characterize meganucleases' structure, the DNA-binding and the DNA-cleavage domains, are not easy to separate, representing a challenging factor in the enzyme engineering. This limitation, together with the complexity of the designing processes, makes meganucleases' application in genome editing limited and technically challenging.[359] Zinc-finger nucleases (ZFNs) were the first truly programmable nucleases with specific DNA sequence binding capacity. They are artificially engineered restriction enzymes for custom site-specific genome editing which, however, may cause genome fragmentation and instability due to potential off-target cleavages, ultimately causing toxicity to cells.[359] The other major discovery in the field of designer nucleases was transcription activator-like effector nucleases (TALENs), which resulted to be cheaper, safer, and more efficient compared to ZFNs. However, one of the main drawbacks of TALENs remains their large size, which may limit the possibility of intracellular delivery.[357, 359]

In this scenario, the discovery of the CRISPR/Cas system revolutionized the world of gene editing. CRISPR/Cas tool contains both the domain responsible for generating a cut in the target DNA and an RNA counterpart that acts as a guide (sgRNA) for the nuclease, allowing efficient, specific, fast, cheap, and easily programmable targeting and cutting of sequences.[357]

Many classes and types of Cas proteins have been identified and studied in the last few years (**Table 3-17**). So far, Cas9 remains the most explored, improved and optimized through different strategies for several applications.[357]

Class	Type	Example	Target
Class I	I	Cascade	DNA
	III	Cas10-Csm	
Class II	II	Cas9	
	V	Cas12	
	VI	Cas13	RNA

Table 3-17 *Classification of the different Cas proteins.*

Nevertheless, aiming at RNA-targeting applications, Cas9 cannot be considered a potential candidate not only because it just possesses DNA cleavage activity, but also due to its off-target effects, which are still a big concern for any bio-medical or therapeutic application.

RNA-targeting applications are increasingly generating interest among researchers since they can include the treatment of diseases related to G and A bases mutations using RNA editing, the rapid detection of various nucleic acids, the treatment of genetic diseases using RNA knockdown and the treatment of diseases related to incorrect mRNA splicing and high-throughput drug discovery.

In this regard, type VI CRISPR/Cas system brought a brand new feature to CRISPR tool due to its capability to target and edit RNA with great specificity. CRISPR/Cas13 system is mainly composed by two components: the programmable RNA-guided RNase Cas13 protein, and a guide RNA (gRNA) constituted by 24-30 nucleotides spacer region complementary to the target site of the single-stranded RNA (ssRNA).

The type VI Cas13 system is further sub-classified into four subtypes (a, b, c, and d) based on small different features, such as the presence of extra open reading frame (ORF) regions, associated accessory proteins, but mainly due to the significant divergence at the primary sequence except for the conserved two HEPN domains sequence (**Table 3-18**).

Cas13 subtype	**Structural composition***	**Functional region**	**Application**
Cas13a (1250 aa)	HEPN domains (center and C terminus), pre-crRNA processing, 3’ non-G PFS preference, DR present on 5’ end	ssRNA (spacer length 28-30 nt)	Virus resistance, RNA knockdown, disease diagnostics
Cas13b (1150 aa)	HEPN domains (N and C terminus), pre-crRNA processing, 5’ PFS preference of D, 3’ PFS NAN/NNA, DR present on 3’ end	ssRNA (spacer length 30 nt)	Virus resistance, RNA base editing, RNA knockdown
Cas13c (1120 aa)	HEPN domains (center and C terminus), pre-crRNA processing, no PFS preference, DR present on 5’ end	ssRNA (spacer length 28-30 nt)	RNA knockdown
Cas13d (930 aa)	HEPN domains (center and C terminus), pre-crRNA processing, no PFS preference, DR present on 5’ end	ssRNA (spacer length 23-30 nt)	Virus resistance, RNA knockdown, alternative splicing modulation

* HEPN: higher eukaryotes and prokaryotes nucleotide-binding domain; PFS: protospacer flanking region; DR: direct repeat.

Table 3-18 *Summary table of Cas13 protein subtypes.*[360]

The recently discovered Cas13d has shown several advantages over the other Cas13 variants such as its small size (only 930 aa) which makes it ideal and compatible for efficient delivery in mammalian systems through the loading into nanocarriers, such as viral vectors or NPs. Moreover, Cas13d has been found to have very limited or completely absent neurotoxic effects in mammalian systems. Thus, Cas13d represents an excellent choice for RNA-targeting applications.

Nevertheless, CRISPR/Cas systems require to be delivered to the intracellular space, directly to the cytoplasm (in case of Cas13d) or to the nucleus (in case of Cas9) in order to be functional and carry out their biological activity. Delivering the CRISPR/Cas complex to its target is nowadays a challenging task. Commonly, three main methods to overcome physical barriers such as the plasma membrane have been proposed since gene editing techniques have been explored. Viral vectors (such as retrovirus, adenovirus, and lentivirus) and physical delivery (such as microinjection and electroporation. among others) have been deeply described in literature.[361-362] However, as much as these approaches may be efficient they present many disadvantages. Physical methods can be employed only in *in vitro* or *ex vivo* systems, while viral vectors may be limited by immunogenicity and toxicity.[313] The third gene delivery method involves the use of nanovehicles, displaying several advantages as compared to the previous delivery approaches.

Different nanocarriers (lipid-based NPs, polymeric NPs, etc.) have also been explored for CRISPR/Cas delivery.[363] Though, drawbacks such as safety, the large size of Cas9, and potential off-target effects still need to be overcome by novel advanced nanocarriers formulations.

Within this work, modified cancer cell-derived CSMs were studied as potential nanocarriers for CRISPR/Cas intracellular delivery. In order to reach this aim, CSMs have been functionalized and modified with a combination of aromatic-labeled and cationic lipids to fabricate fusogenic nanocarriers. The introduction of this lipids combination, responsible for the fusogen-like properties of CSMs (fusogenic CSMs, or FCSMs), allowed the cargo delivery directly inside cells cytosol, circumventing lysosomal storage and reaching the intracellular target.[364]

As mentioned, CRISPR/Cas system need to be released into the cytosol and driven to the target site to perform gene editing at a specific DNA or RNA sequence (depending on the Cas protein type) guided by the single guide RNA (sgRNA). Here, two different CRISPR/Cas systems (Cas9 and Cas13d) have been selected as potential cargos to be loaded into fusogenic cell-derived nanovesicles to exploit both biomimetic features and fusogenic properties for gene editing applications.

The commercially available Cas9 protein was used to set the experimental knockdown conditions and to verify the functional role of the fusogenic nanosystem, able to release the loaded cargo directly inside the cytosol and therefore limiting the endolysosomal entrapment. Whereas Cas13d was utilized for its ability to target and cut mRNA, whose application in this chapter was suppressing the expression of viral genes. Cas13d protein was synthetized and delivered by the group of Dr. Miguel Angel Moreno Mateos (Andalusian Center of Developmental Biology (UPO/CSIC), Seville, Spain).[365]

Figure 3-44 illustrates a schematic representation of the theoretical roadmap of fusogenic cell-derived nanosystems loaded with the different CRISPR-Cas systems for different applications.

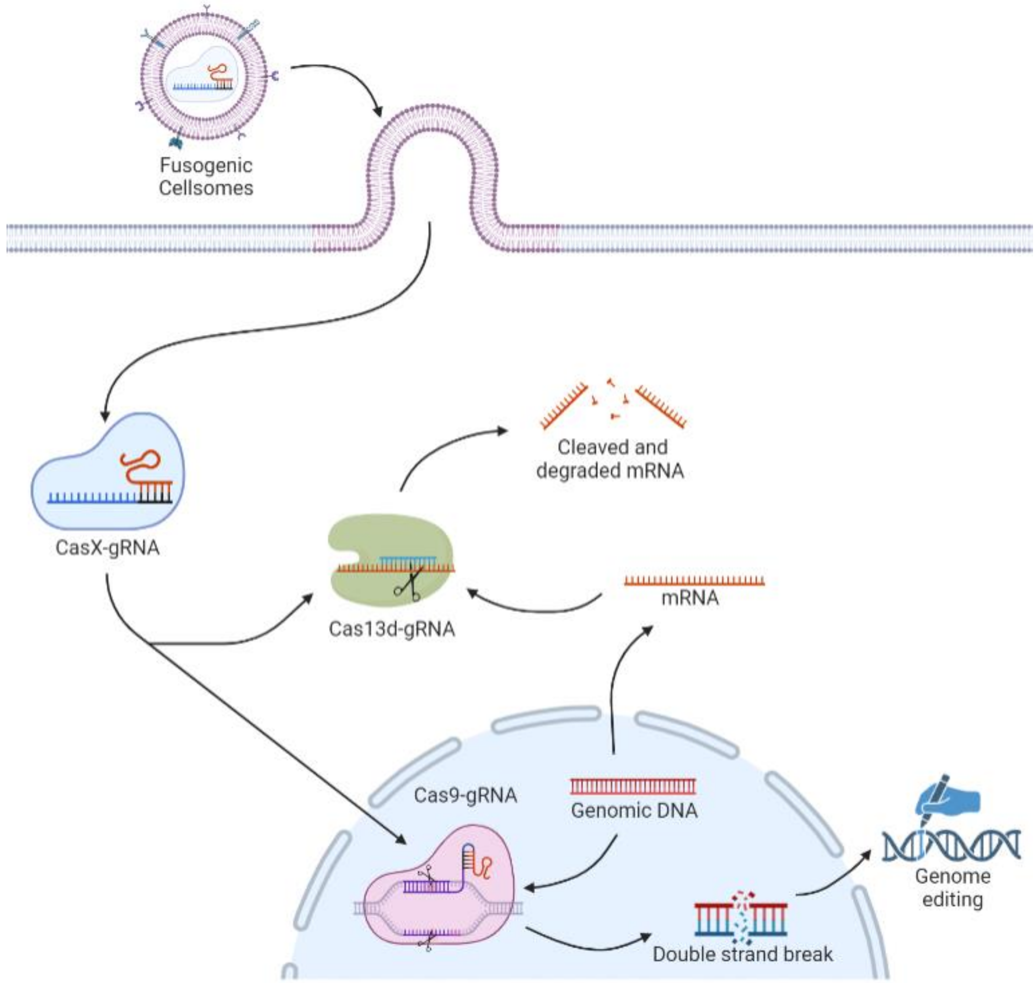

__Figure 3-44__ Schematic representation of fusogenic cell-derived nanovesicles for gene editing applications.

3.3.1. Delivery of CRISPR/Cas9

CRISPR-Cas9 system is a widely explored genome editing tool. Its high versatility is due to the possibility of engineering the (sgRNA) according to the target DNA sequence of interest.

Here, HEK-293 cells (293T-dEGFP) (obtained from the group of Dr. Manuel Collado, Health Research Institute of Santiago de Compostela, IDIS, Santiago de Compostela, Spain) were used as GFP-reporter systems in which eGFP was stably expressed to evaluate the nuclease activity of Cas9/sgRNA complex. To knock-out GFP expression, fusogenic cancer cells-derived nanovesicles were fabricated, loaded with Cas9-gRNA complex, and exposed to HEK-293-GFP. In cells, FCSMs released the cargo directly inside the cytosol, thus evading the endolysosomal entrapment mechanism. Once released, Cas9-gRNA reached the nucleus and exploited its DNase enzymatic function, therefore cutting the DNA sequence expressing GFP.

3.3.1.1. Design and characterization of FCSM(Cas9-gRNA)

A549 cells-derived nanovesicles were obtained following the protocol previously described (Section 2.1). Briefly, A549 cells were cultured according to the manufacturer's instructions. Once they reached 75-80% confluence, they were collected and induced to swallow in a hypotonic environment enriched with a proteases inhibitor cocktail (PIC) to preserve the surface properties of plasma membrane. The resulting disrupted cells were exposed to 4 cycles of freeze in N_2 and thaw at 37 ºC and subsequently subjected to mechanical disruption with ultrasounds. Plasma membranes fragments were extracted and recollected through differential centrifugal steps and extruded through polycarbonate membranes with nanosized pores in order to obtain self-assembled A549-CSMs of about 150-200 nm in size.

Fusogenic CSMs (FCSMs) were obtained following the procedure described in Section 2.2: a lipids mixture consisting of neutral lipid DOPE, positively charged lipid DOTAP and fluorescently labelled lipid DOPE Atto 647N was added to CSMs. These modifications were inspired by previous works conducted by Csiszár et al.[252, 366] where fusogenic liposomes were developed by using a specific synergistic combination of lipids. In particular, those liposomes acquired the fusogenic capability to favor the fusion with the cell plasma membrane thanks to the role of the cationic lipid (DOTAP), which presents an inverted conical shape, and the aromatic groups of the fluorescent lipid head (DOPE Atto 647N). Here, this strategy was aimed at modifying the composition of CSMs in order to develop fusogenic CSMs (FCSMs). This lipid engineering approach, together with the characteristic membrane biological pattern (proteins, glycoproteins, ions channels, receptors, etc.), allowed to obtain biomimetic nanocarriers with dual functionalities: the homotypic targeting capabilities derived from the source cells and the fusogenic properties, which allow to elude the endolysosomal entrapment that characterize most of the NPs internalization pathways (CSMs included).

The resulting solution (CSMs with the lipids mixture) was then subjected to sonication and extrusion through polycarbonate membranes to favor lipids intercalation in the lipidic bilayer of CSMs.

FCSMs were loaded with Cas9-gRNA as described in Section 2.3.2.5. Two different protocols were evaluated to load Cas9-gRNA complex into FCSMs. In one case (A) the solution was mixed, subjected to sonication, and left at room temperature for 15 minutes. While in the other case (B) the solution was additionally subjected to extrusion through polycarbonate membrane to favor the encapsulation into the nanocarrier and filtration to purify the sample from the cargo excess.

Both sample preparations (A and B) were characterized with NTA size distribution analysis (**Figure 3-45** and **Table 3-19**).

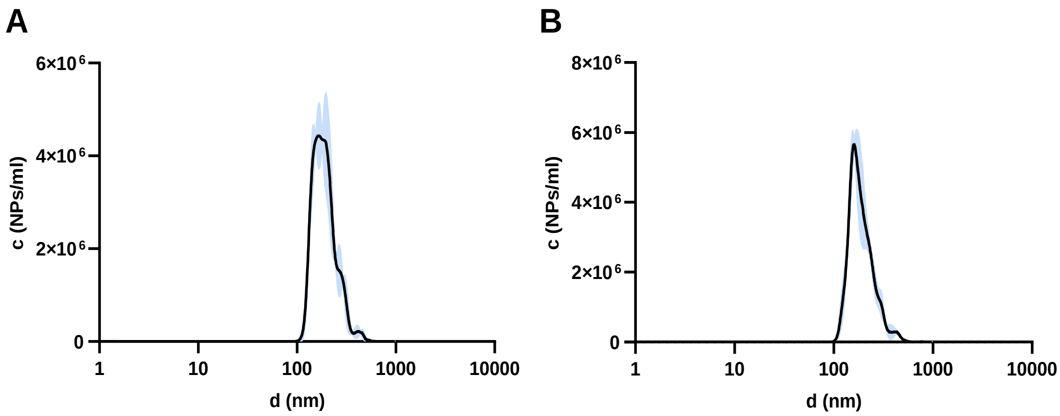

Figure 3-45 *Size distribution analysis (NTA) of FCSM(Cas9-gRNA) obtained with the two different preparation methods. (A) Sample preparation, (B) sample preparation B.*

Sample	d (mean) (nm)	d (mode) (nm)	c (NPs/mL)
FCSM(Cas9-gRNA) A	214.0 ± 1.6	189.5 ± 11.5	1.15E+12
FCSM(Cas9-gRNA) B	215.4 ± 1.6	162.0 ± 5.1	1.23E+12

Table 3-19 *Size distribution analysis (NTA) of FCSM(Cas9-gRNA) obtained with two different preparation methods.*

3.3.1.2. *In vitro* activity of FCSM(Cas9-gRNA)

FCSM(Cas9-sgRNA) complex was obtained by mixing the solutions as previously described (Section 2.3.2.5). The design of the optimal sgRNA used to target GFP gene in HEK-293 cells was made *in silico* as described in Section 2.3.2.5.

As mentioned, two different sample preparations were proposed: in one case (A) the mixed solutions were not purified, supposing that non-encapsulated Cas9-gRNA complex was unable to cross the plasma membrane and reach the target sequence inside the nucleus; while in the other case (B) FCSM(Cas9-gRNA) solution was additionally subjected to extrusion through polycarbonate membrane and filtrated to concentrate the sample and purify it from the cargo (Cas9-gRNA) excess.

Fluorescence microscopy studies were performed to demonstrate the fusogenic ability of FCSM (**Figure 3-46**). Atto 647N fluorescence signal (in magenta), used to label FCSMs, was clearly visible around cells, proving the interaction of FCSMs with cells plasma membranes after only 10 minutes incubation.

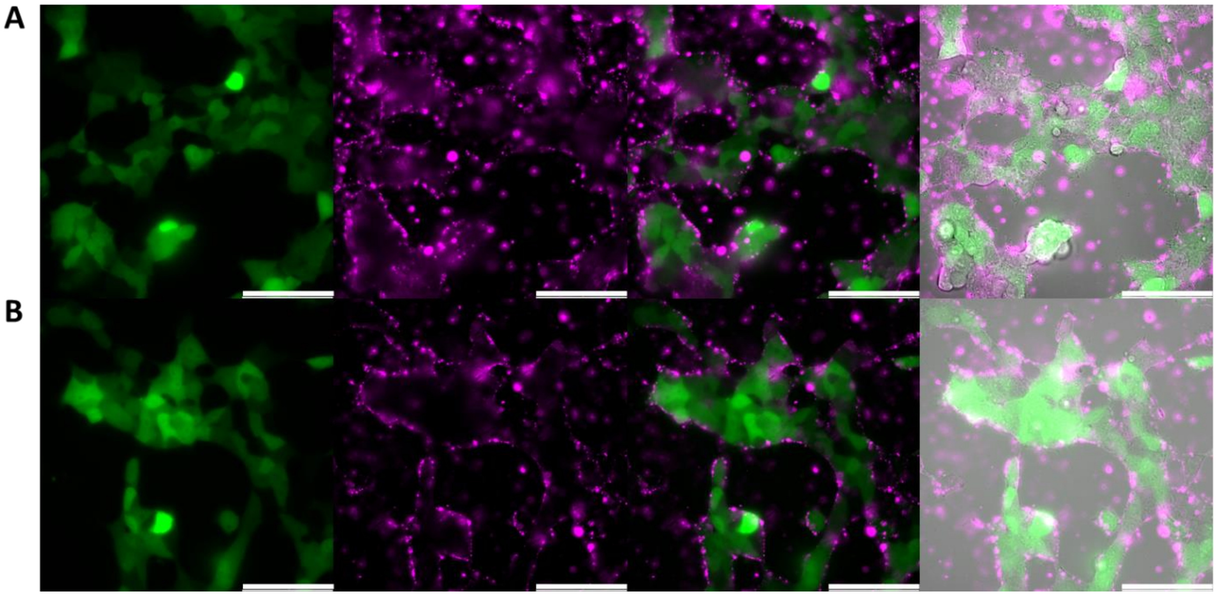

Figure 3-46 Fluorescence microscopy studies of FCSMs fusogenic properties. (A) shows sample preparation A, (B) shows sample preparation B, both incubated in HEK-293-GFP for 10 minutes. For each panel, from left to right, images show the fluorescence signal of GFP (in green), FCSMs (in magenta), overlays of the two fluorescence signals (green + magenta), and both merged with brightfield. Scale bars: 100 µm.

Since Cas9-gRNA was not fluorescently labeled, fluorescence microscopy analysis was used only to assess the fusogenic interactions between the nanocarrier and cells plasma membranes. However, to evaluate the knockout efficiency, HEK-293 cells expressing GFP were exposed overnight to the fusogenic nanosystem loaded with Cas9 protein and the designed sgRNA. After 48 hours, GFP fluorescence intensity was measured with flow cytometry.

As illustrated in **Figure 3-47**, GFP expression level decreased by more than 50% compared to untreated HEK-293-GFP (Ctrl) with both sample preparation methods (A and B), demonstrating that the fusogenic nanosystem allowed the cytosolic release of the cargo, which reached the nucleus, bound to the target DNA sequence and caused the knockout of GFP protein expression.

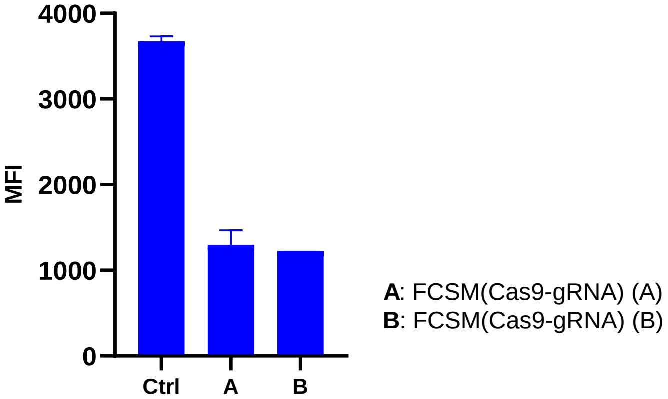

***Figure 3-47** FCSM(Cas9-gRNA) activity in HEK293-GFP cells measured with flow cytometry.*

Once evaluated the FCSMs ability as nanocarrier to allow the fast delivery of Cas9-gRNA complex into the intracellular target (nucleus), the project was directed at applying these nanocarriers in a more interesting and novel system. In collaboration with Dr. M. Moreno Mateos (UPO/CSIC, Seville, Spain), FCSMs able to deliver Cas13d in the intracellular environment were developed to target viral mRNA and therefore used as antiviral nanosystems.

3.3.2. Delivery of CRISPR/Cas13d

Due to the above-mentioned reasons, Cas13d has been shown to be a validate candidate for mRNA knockout, among other potential applications. Here, it was designated, along with specific gRNAs, for the targeting of selective mRNA. First, similar to CRISPR/Cas9 nanosystem, A549 cells stably expressing GFP protein were used as a model system to evaluate the efficacy of FCSMs in the delivery of Cas13-gRNA complex. Then the system was applied to reduce the viral mRNA expressed in E. Derm cell line after infection with torovirus.

3.3.2.1. Design and characterization of FCSM(Cas13d-gRNA)

In order to exploit the fusogenic features of biomimetic CSMs, two cell lines were chosen for the experimental setting of the *in vitro* system. A549 cell line was used to fabricate FCSMs loaded with Cas13d-gRNA complex to target GFP mRNA expressed by A549 cells. Following the same principle, another fibroblast cell type, E. Derm, was selected to obtain Cas13d-gRNA-loaded FCSMs as antiviral nanosystem.

A549 cells- and E. Derm-derived CSMs were obtained following the protocol previously described (Section 2.1). A549 and E. Derm cells were cultured according to the manufacturer's instructions. Once they reached 75-80% confluence, they were collected and induced to swallow in a hypotonic environment enriched with a proteases inhibitor cocktail (PIC) to preserve the surface properties of plasma membrane. The resulting disrupted cells were exposed to 4 cycles of freeze in N_2 and thaw at 37 ºC and subsequently subjected to mechanical disruption with ultrasounds. Plasma membranes fragments were extracted and recollected through differential centrifugal steps and extruded through polycarbonate membranes with nanosized pores in order to obtain self-assembled A549- and E. Derm- CSMs of about 150-200 nm in size.

A549- and E. Derm-FCSMs were obtained following the procedure described in Section 2.2: a lipids mixture consisting of neutral lipid DOPE, positively charged lipid DOTAP and fluorescently labelled lipid DOPE Atto 647N was added to CSMs. The resulting solution was then subjected to sonication and extrusion through polycarbonate membranes to favor lipids intercalation in the lipidic bilayer of CSMs.

Cas13d protein was labeled with sulfo-Cy3-maleimide as described in Section 2.3.2.4. To obtain the functional Cas13d-gRNA complex, fluorescently labeled Cas13d protein was added to gRNA and left 5 minutes at 37 °C. Two different gRNAs were chosen to demonstrate the specificity of the system: gRNA(Sj) (Sanjana) was used to target GFP mRNA in A549 cells, while gRNA(Tv) (Torovirus) was used to target viral mRNA in E. Derm infected with equine torovirus Berne virus (BEV).

Cas13d-gRNA complexes were then added to A549- and E. Derm-derived FCSMs and extruded through polycarbonate nanosized membranes to favor the encapsulation of the cargo into the nanosystems. The solution was then purified from the excess of non-encapsulated Cas13d-gRNA complexes with ultra-centrifugal filters devices.

In **Figure 3-48** and **Table 3-20** size distribution measurements (NTA) of FCSMs after Cas13d-gRNA loading are shown. In particular, A549 cells-derived FCSMs were loaded with Cas13d-gRNA(Sj), while E. Derm cells-derived FCSMs were loaded with Cas13d-gRNA (Tv). Moreover, **Table 3-21** shows the efficiency of cargo (Cas13d-gRNA) encapsulation in FCSMs.

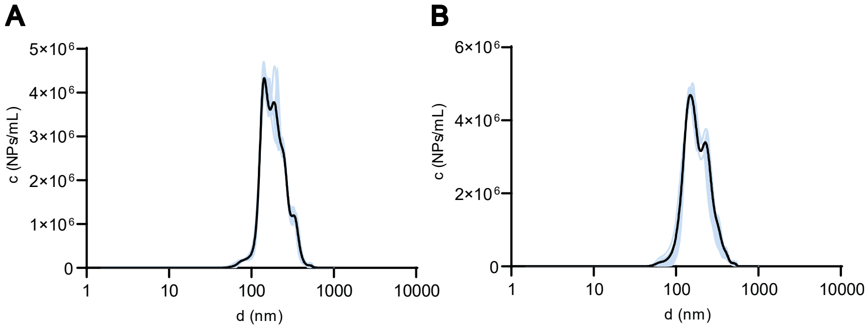

Figure 3-48 *Size distribution measurements (NTA) of (A) FCSM(Cas13d-Sj), and (B) FCSM(Cas13d-Tv).*

Sample	d (mean) (nm)	d (mode) (nm)	c (NPs/mL)
FCSM(Cas13d-Sj)	221.0 ± 1.1	160.0 ± 15.8	6.62E+11
FCSM(Cas13d-Tv)	216.0 ± 1.7	150.1 ± 4.8	7.31E+11

Table 3-20 *NTA analysis of FCSM(Cas13d-gRNA).*

Sample	Cargo concentration			
	µg/mL	**µg**	**nM***	**EE (%)**
FCSM(Cas13d-Sj)	76 ± 11	13 ± 1	758 ± 106	26 ± 2
FCSM(Cas13d-Tv)	63 ± 8	12 ± 1	630 ± 81	25 ± 3

*Considering that Cas13d (~900 aa) + gRNA (30 b) = ~100 kDa.

Table 3-21 *Characterization of cargo (Cas13d) encapsulation in FCSMs.*

The stability of Cas13d-gRNA complex is a primary concern for the design of functional fusogenic nanocarriers. To evaluate Cas13d-gRNA stability, FCSMs loaded with the transfection complex were subjected to lyophilization, stored at -20 ºC for a week, and then reconstituted to solution.

Size distribution measurements before and after (**Figure 3-49** and **Table 3-22**) lyophilization process demonstrated that the fusogenic nanosystems loaded with Cas13d-gRNA maintained their monodispersity and therefore the nanocarrier stability.

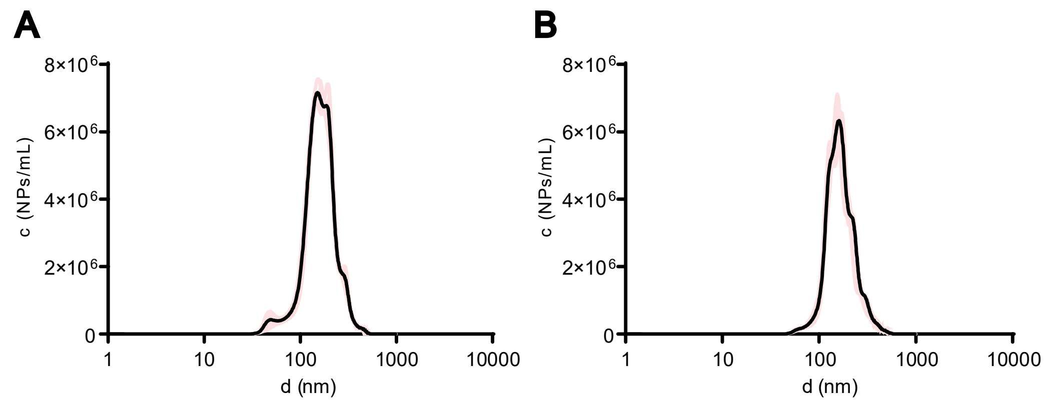

***Figure 3-49** Size distribution analysis (NTA) of FCSM(Cas13d-gRNA) (A) before and (B) after lyophilization.*

Sample	d (mean) (nm)	d (mode) (nm)	c (NPs/mL)
FCSM(Cas13d-gRNA) before lyoph.	192.2 ± 2.1	164.2 ± 16.2	9.97E+11
FCSM(Cas13d-gRNA) after lyoph.	198.1 ± 1.2	161.5 ± 6.3	7.91E+11

***Table 3-22** NTA analysis of FCSM(Cas13d-gRNA) before and after lyophilization.*

3.3.2.2. *In vitro* studies of FCSM(Cas13d-gRNA)

The main purpose of fusogenic cell-derived nanovesicles is the cytoplasmatic release of cargos that are not supposed to cross cell plasma membranes and whose target molecules are located inside cells (such as cytoplasm, nucleus, or specific organelles). In this view, the modification of CSMs lipid composition was aimed at gaining the fusogenic features able to promote the nanocarrier interactions with cell plasma membranes and allow the release of the loaded cargo inside cells, thus evading the entrapment into the endolysosomal system.

As mentioned above, Cas13d is an RNA endonuclease which, thanks to specific single guide RNAs, is able to bind and cut targeted mRNA, situated in cells cytoplasm. However, Cas13d is a protein which cannot cross cells plasma membrane by itself, thus requiring a carrier (FCSMs in this chapter) able to transport the protein inside cells.

Here, FCSMs were used as cytosolic nanocarriers to deliver Cas13d-gRNA complex inside cell cytoplasm, where the protein could bind and cut specific mRNAs.

First, a toxicity assay was performed to verify that Cas13d-gRNA complex did not affect cell viability. A549 and A549-GFP cell lines were exposed to both free Cas13d-gRNA and Cas13d-gRNA-loaded FCSMs overnight (the maximum incubation time used in all the experiments) and examined through resazurin assay. As shown in **Figure 3-50**, no cellular toxicity was detected at the maximum concentration used in all the other experiments (~50 pg/cell).

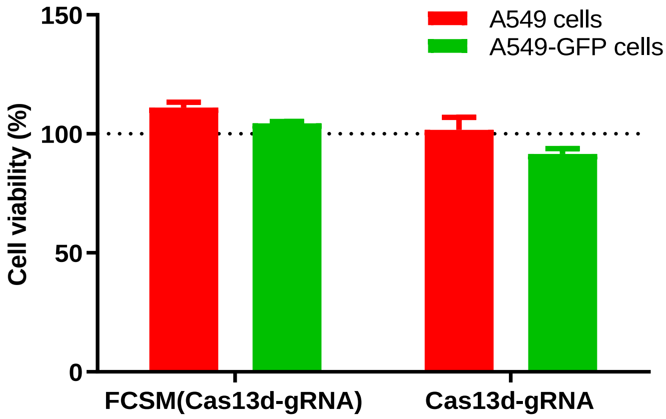

Figure 3-50 *Toxicity assay (resazurin) of FCSM(Cas13d-gRNA) and free Cas13d-gRNA complex in A549 and A549-GFP cells.*

Then, fluorescence microscopy analysis was performed to assess the fusogenic properties of the nanocarrier. An exhaustive study including both A549 and E. Derm cells exposed to either A549 cells-derived or E. Derm cells-derived FCSMs at different time points was conducted (**Figure 3-51**).

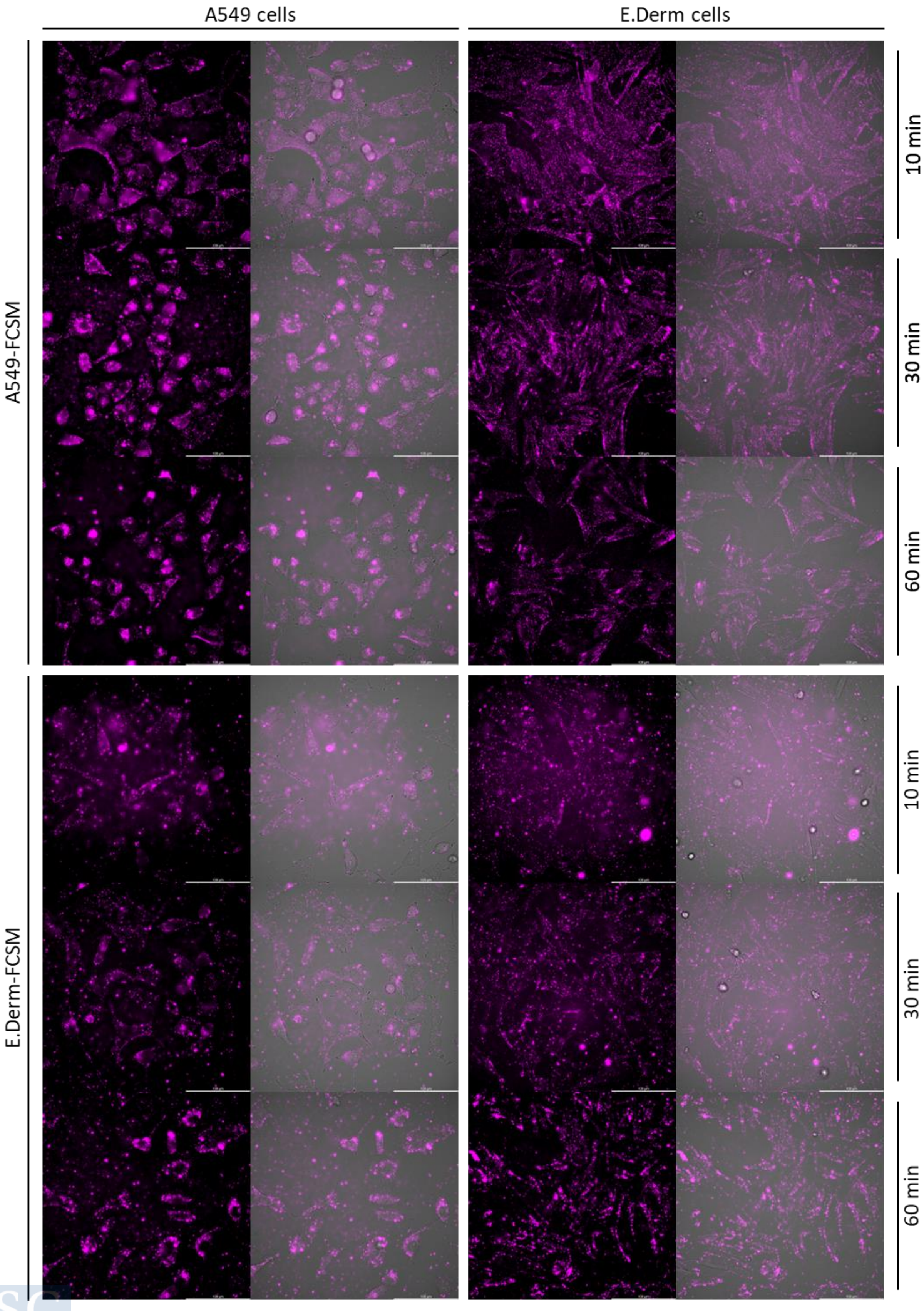

Figure 3-51 *Fluorescence microscopy study of FCSMs fusogenic properties. For each panel, from left to right, images show the fluorescence signal FCSMs (in magenta) and the overlay with brightfield. Scale bars: 100 µm.*

As shown in **Figure 3-51**, at shorter incubation times (10 minutes) the fusogenic properties of FCSMs were more evident: the fluorescence signal of DOPE Atto 647N (in magenta), in fact, is located in correspondence of cells plasma membranes. While the dotted-like fluorescence signal inside cells cytoplasm at longer incubation times (60 minutes) indicates an endo-lysosome internalization tendency. A549 cells-derived FCSMs better displayed their fusogenic features in both cell lines (A549 and E. Derm cells), probably due to the different cell surface protein pool, which, considered its tumoral origin, may favor the interaction between cells.

However, since the exact mechanism through which fusogenic nanocarriers fuse with the plasma membrane and release the cargo directly inside the cytosol is yet to be clarified, further studies regarding the mechanistic undergoing the whole process would be needed.

Nevertheless, although fusogenic properties were not entirely clear in all the cell lines and for all the FCSMs types, their capability to promote the interaction with cell plasma membrane and perhaps fuse with it to release a potential cargo inside the cytoplasm should remain unvaried.

As mentioned, Cas13d-gRNA complex is not able to cross the cell plasma membrane, neither for diffusion, nor through any endocytosis pathways. Therefore, it requires a carrier that not only allows the internalization inside cells, but also provides a direct passage to the cytoplasm, where the protein and its gRNA may bind and cut targeted mRNAs.

Here, A549 cells-derived FCSMs were loaded with Cas13d-gRNA labeled with Cy3 and exposed to both A549 and A549-GFP cells. To further corroborate the fusogenic properties of FCSMs and the intracellular delivery of the loaded cargo (Cy3-labeled Cas13d), confocal microscopy studies were performed.

Confocal microscopy imaging (**Figure 3-52**) shows that free Cas13d-gRNA was not able to enter neither in A549 nor in A549-GFP (**Figure 3-52** B and D, respectively), while the fusogenic cell-derived nanosystem permitted the internalization of Cas13d-gRNA complex in only 10 minutes of cells exposure to FCSMs (**Figure 3-52** A and C). In both cell lines, it is possible to notice that FCSMs (in magenta) seemed to surround the cell, overlaying with the plasma membrane, and suggesting the fast and efficient interaction with it, while the Cy3-labeled Cas13d (in orange) was both located inside the cytosol and colocalized with the FCSMs (**Figure 3-52** A and C). This may indicate that, after 10 minutes of cells exposure to FCSMs solution, part of the encapsulated cargo was able to reach the cytoplasm, while part of it still needed to be released from the nanocarrier.

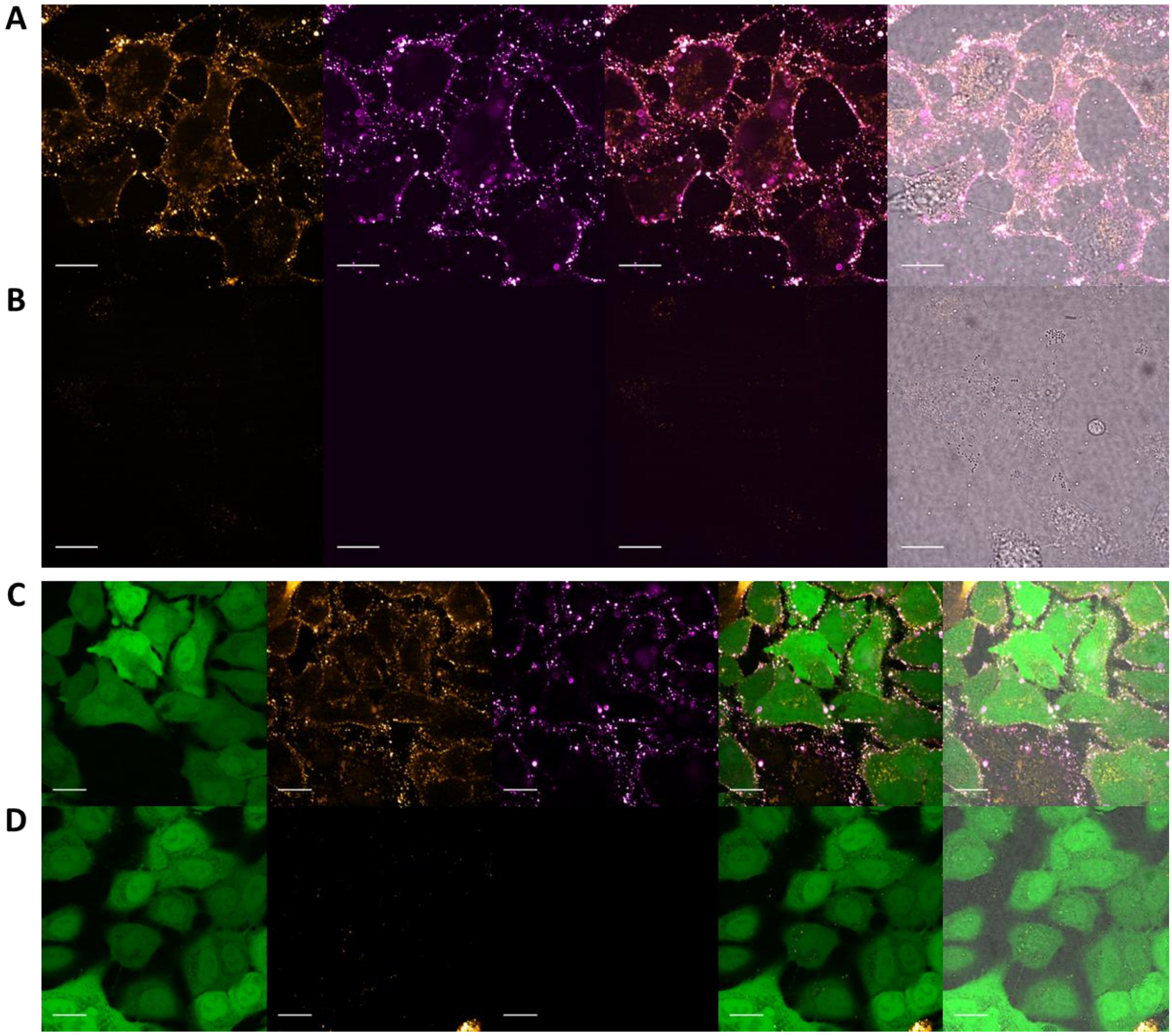

Figure 3-52 Confocal microscopy micrographs of (A and B) A549 and (C and D) A549-GFP cells exposed to (A and C) FCSM(Cas13d-gRNA) and (B and D) free Cas13d-gRNA. Samples were incubated for 10 minutes. For A and B panels, from left to right, images show the fluorescence signal of Cas13d (in orange), FCSMs (in magenta), overlays of the two fluorescence signals (orange + magenta), and both merged with brightfield. For C and D panels, from left to right, images show the fluorescence signal of GFP (in green), Cas13d (in orange), FCSMs (in magenta), overlays of the three fluorescence signals (green + orange + magenta), and all merged with brightfield. Scale bars = 20 µm.

To further assess and quantify not only Cas13d-gRNA uptake but also its knockdown activity in cells, flow cytometry experiments were performed. As shown in **Figure 3-53** B, Cy3 fluorescence signal, corresponding to Cas13d cellular uptake, increased in a time exposure-dependent manner, as expected. While GFP fluorescence signal began to decrease 48 hours after A549-GFP cells exposure to Cas13d-gRNA-loaded FCSMs, with a time exposure-dependent tendency (**Figure 3-53** A), demonstrating that Cas13d-gRNA complex was released directly inside the cytosol without being entrapped in the endolysosomal system.

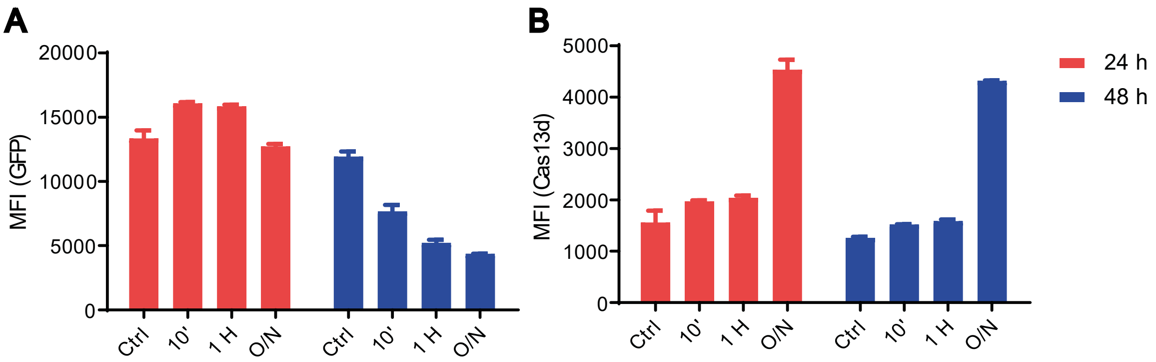

Figure 3-53 *Flow cytometry measurements of FCSM(Cas13d-gRNA) activity. A549-GFP cells were exposed to FCSM(Cas13d-gRNA) for 10 minutes, 1 hour and overnight, while Cas13d-gRNA complex activity was measured 24 and 48 hours after the incubations. (A) shows GFP fluorescence decrease after the internalization of FCSM(Cas13d-gRNA) (shown in (B)). Data are represented as mean ± s.d. (n = 2).*

Similarly, fluorescence microscopy imaging was used to evaluate qualitatively the activity of Cas13d-gRNA complex in A549-GFP cells. In addition, the specificity towards the mRNA expressing GFP protein in A549 cells was assessed by the use of two different gRNAs. The Sanjana gRNA (Sj) was used to target specifically GFP mRNA, while Torovirus gRNA (Tv) was used here as a control. As shown in **Figure 3-54**, GFP fluorescence intensity decreased after cells exposure to FCSMs loaded with Cas13d-Sj, but it maintained its intensity when cells were exposed to FCSM(Cas13d-Tv), demonstrating gRNA specificity towards its mRNA target.

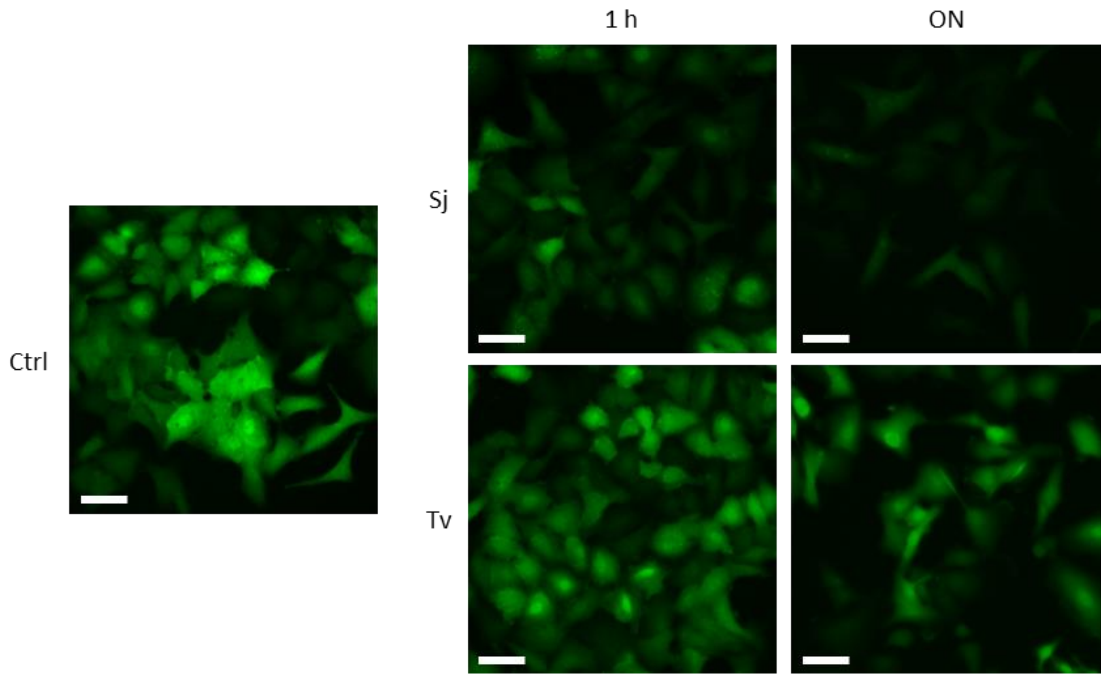

Figure 3-54 *Fluorescence microscopy images of A549-GFP cells 48 hours after the exposure (1 hours and overnight) to FCSM(Cas13d-gRNA). Two different gRNA were used (Sj and Tv). Scale bars = 50 µm.*

Flow cytometry and fluorescence imaging were also helpful to understand the cellular dynamics by which Cas13d-gRNA complex effectively reach GFP-mRNA and cut the target sequence. Nevertheless, further experiments were performed to optimize the sample preparation and to evaluate its stability.

Since non-encapsulated Cas13d-gRNA complex is not able to cross cell plasma membrane and because of each *in vitro* assay was performed normalizing the amount of Cas13d protein per cell, the purification method turned out to be a crucial step in FCSMs preparation. Two different purification methods were evaluated: in one case Cas13d-gRNA-loaded FCSMs were purified with filtration (sample A), while in the other case a single semi-ultracentrifugation step was used (sample B). In both cases (**Figure 3-55**) GFP fluorescence signal decreased, indicating that at least part of Cas13d-gRNA complex had been encapsulated efficiently. However, with a single semi-ultracentrifugation step the drop in GFP fluorescence intensity was higher than the sample purified by filtration, probably indicating that the centrifugation method allowed a more suitable purification from Cas13d-gRNA excess (after 48 hours).

Though, after longer times, 120 hours (in green), the drop of GFP fluorescence intensity was comparable between the two sample purification methods, suggesting that the amount of Cas13d need to knockdown GFP mRNA was sufficient even in the sample purified by filtration.

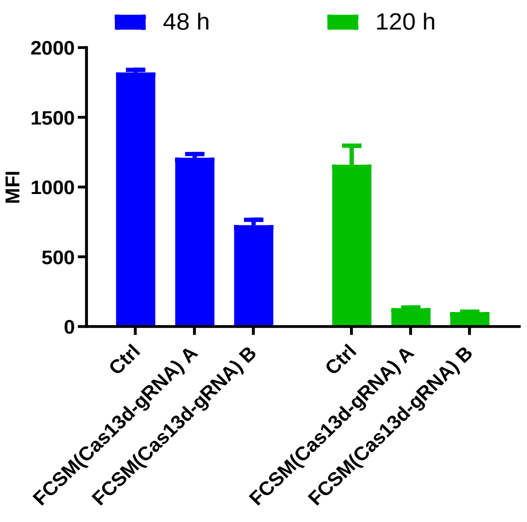

***Figure 3-55** Flow cytometry measurements of Cas13d-gRNA-loaded FCSM was used to evaluate different sample purification methods: FCSM(Cas13d-gRNA) were purified with filtration (sample A), or with a single semi-ultracentrifugation step (sample B). Data are shown as mean ± s.d. (n = 3).*

As mentioned before, the stability of Cas13d-gRNA complex is a major concern for the design of functional fusogenic nanovehicles. To assess Cas13d-gRNA stability, two different storage conditions were evaluated: in one case FCSM loaded with Cas13d-gRNA were stored at 4 ºC for two days (**Figure 3-56** A), while in the other case the sample was subjected to lyophilization (**Figure 3-56** B), stored at -20 ºC for two days, and subsequently reconstituted to solution.

As illustrated in **Figure 3-56**, in both storage conditions A549-GFP fluorescence intensity decreased, indicating that at least part of the biomimetic nanosystem remained stable and active. However, the samples subjected to lyophilization produced a higher decrease in GFP fluorescence signal, with both purification methods, suggesting that this storage condition might preserve Cas13d-gRNA complex more properly than storing it at 4 ºC.

Regarding the purification methods, flow cytometry analysis (illustrated in **Figure 3-56**) confirmed that the semi-ultracentrifugation allowed a more suitable purification of Cas13d-gRNA excess. Even lyophilized (**Figure 3-56** B), FCSM(Cas13d-gRNA) purified by centrifugation showed a knockdown activity comparable to fresh prepared samples (**Figure 3-55**).

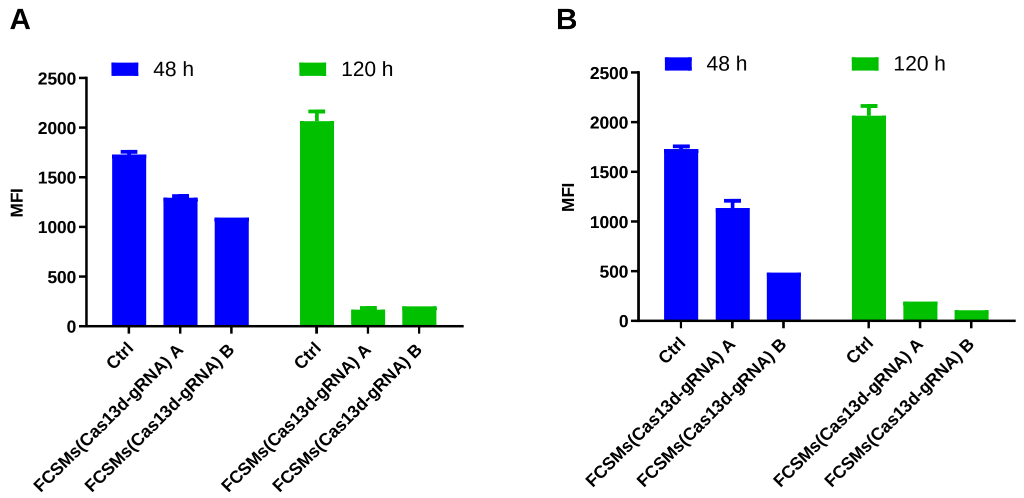

__Figure 3-56__ Cas13d-gRNA complex activity in different storage conditions: samples were (A) stored at 4 ºC or (B) lyophilized.

As mentioned above, the CRISPR/Cas13d family of enzymes targets and cuts RNA instead of DNA and they are capable of targeting viral mRNA. Since the appearance of SARS-CoV-2 and COVID-19 pandemic, there is growing interest in studying Cas13d-based systems to detect and treat diseases similar to COVID-19.

PAC-MAN (prophylactic antiviral CRISPR in human cells) (**Figure 3-57**) is a method developed in 2020 by Abbott et al.[367] that uses Cas13d targeted by properly designed gRNA to cleave not only SARS-CoV-2 viral genomic RNA, but also viral mRNA. Depending on the pool of gRNA sequences used, it is possible to suppress the expression of SARS-CoV-2 genes.

PAC-MAN method has the potential to become an important pan-coronavirus inhibition strategy, however it may be limited by the lack of an adequate delivery system. Therefore, FCSMs have been proposed here to overcome such limitation.

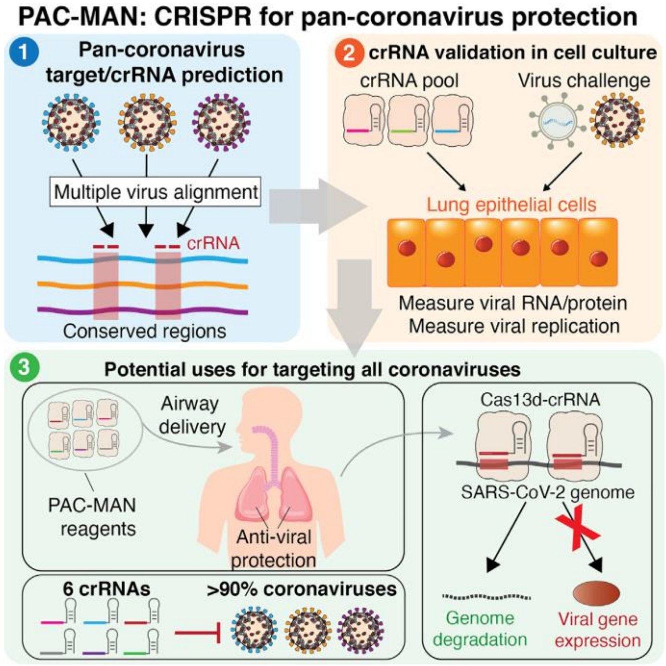

__Figure 3-57__ PAC-MAN method workflow.[367]

Toroviruses are enteric and respiratory viruses capable of infecting animals and humans. They are single stranded RNA-enveloped viruses that, together with coroviruses, belong to the *Coronaviridae* family. Equine torovirus (EToV) was the first torovirus identified in Berne (Switzerland) in 1972 and named Berne virus (BEV).[368] BEV shows many structural similarities with coronavirus (CoV) (**Figure 3-58**), such as the presence of Spike protein (S), distinctive of the virus family and considered the main mediator for viral entry into the host cells.

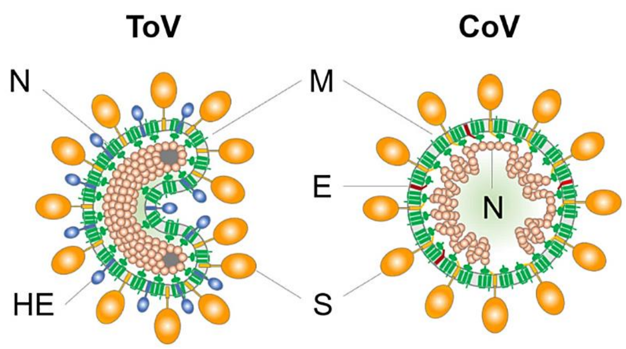

__Figure 3-58__ Torovirus (on the left) and Coronavirus (on the right) schematic structures. S: Spike protein; E: virus envelope; M: virus membrane; HE: haemagglutinin-esterase; N: nucleocapsid proteins.[369]

Due to the urgence in finding new and innovative treatments for human coronaviruses that cause the severe and acute respiratory syndromes (SARS-CoV) and because of its structural similarities with CoV, torovirus was used as an experimental prototype for the application of Cas13d as potential antiviral nanosystem.

Here, E. Derm were used as host cells infected with BEV and treated with FCSMs loaded with Cas13d-gRNA(Tv). While the empty nanosystem and the same nanosystem loaded with Cas13d and a different gRNA (Sj) were used as negative controls. These studies have been performed in collaboration with Dr. M. A. Moreno Mateos, Dr. I. Moreno Sánchez (CABD/CSIC, Seville, Spain), Dr. D. Rodríguez Aguirre, and Dr. L. Montoliu (CNB/CSIC, Madrid, Spain).

As shown in **Figure 3-59** A, the plaque forming units (PFU), which is a measure of the number of infectious virus particles, decreased by more than one order of magnitude when E. Derm cells were treated with Cas13d-gRNA(Tv)-loaded FCSMs. Whereas, the same nanosystem loaded with Cas13d-gRNA(Sj) did not affect the viral content.

Moreover, a western blot analysis of cells viral proteins (**Figure 3-59** B) was performed to corroborate the viral titration measurements. Overall, these results demonstrate that the fusogenic nanosystem was able to release Cas13d-gRNA complex in E. Derm cells, the specific gRNA(Tv) reaches its target viral mRNA and Cas13d cuts the single stranded nucleic acid.

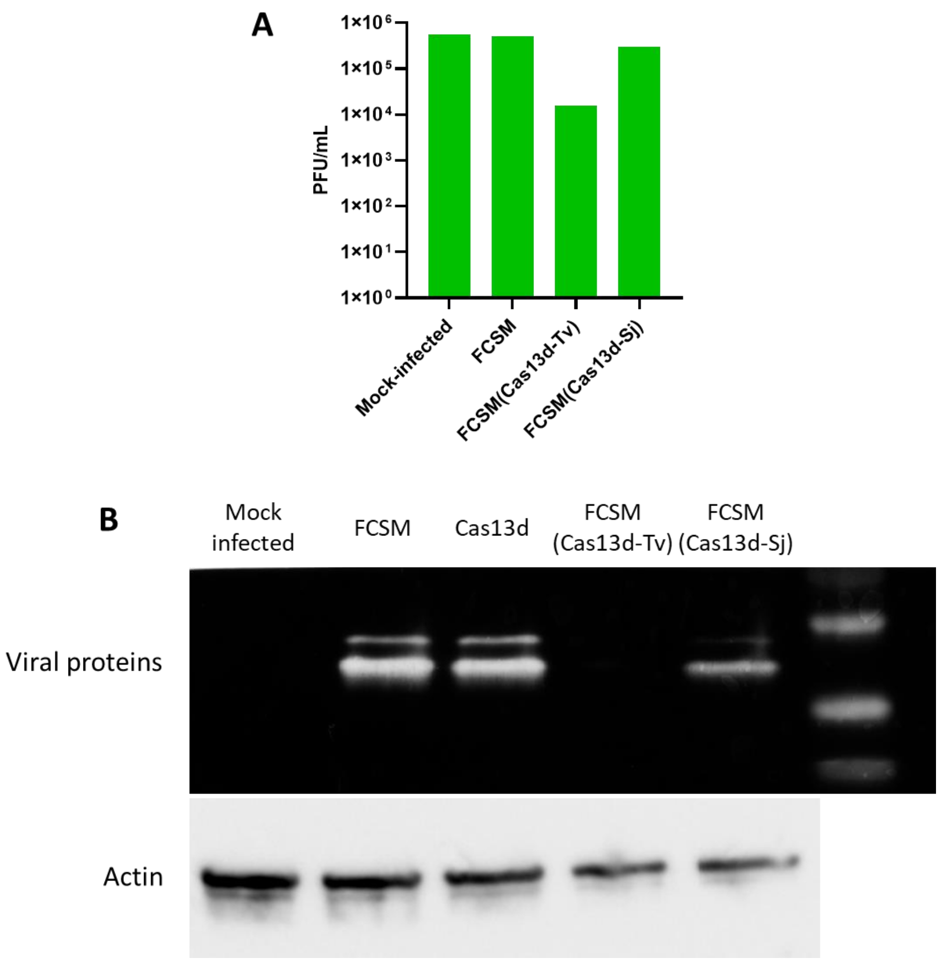

Figure 3-59 (A) Viral titration of supernatants' cells infected with BEV and treated with Cas13d-gRNA and (B) western blot analysis of cells viral proteins after the infection with BEV and the treatment with Cas13d-gRNA.

Taken together, these results suggest that the fusogenic lipid-engineered nanosystem here developed exhibited promising features as nanocarrier able to release the encapsulated cargo directly inside cells cytoplasm, thus managing to evade the entrapment into the endolysosomal system. Two different CRISPR/Cas systems were here utilized as functional cargos to be employed in gene editing applications. First, the commercially available and deeply studied Cas9 was successfully used to set the experimental knockout conditions and to verify the functional role of the fusogenic nanosystem. Then, Cas13d, a more recently discovered nuclease able to cut mRNA instead of DNA, was loaded into the fusogenic nanocarriers to be exploited as antiviral nanosystem.

Even though the fusogenic nanosystem here developed showed promising results *in vitro*, further studies would be needed to fully understand the mechanism undergoing the fusogenic features of the nanocarriers. Moreover, more complex systems, such as zebra fish or animals, would be of great help in assessing the actual potential of these nanosystems.

Part of the results presented in the following chapter has been published in:

"Fusogenic Cell-Derived nanocarriers for cytosolic delivery of cargo inside living cells". *Journal of Colloid and Interface Science*, **2023**, *648,* 488-496.

Enrica Soprano, Martina Migliavacca, Miriam Lopez-Ferreiro, Beatriz Pelaz, Ester Polo*, Pablo del Pino*.

Centro Singular de Investigacion en Química Bioloxica e Materiais Moleculares (CiQUS), Universidade de Santiago de Compostela. Rúa Jenaro de la Fuente s/n, 15705, Santiago de Compostela, Spain.

Contributions: preparation and characterization of the materials; *in vitro* experiments; writing – original draft.

Impact Factor: 9.9. Q1 in Chemistry, Physical. No written permission from Elsevier is necessary. Copyright 2023. ISSN 0021-9797.

3.4. BIOMIMETIC COATING OF NANOMATERIALS

Cell membrane-coated NPs have been widely studied as a biomimetic strategy to engineer therapeutic nanosystems consisting of a NP core coated with plasma membrane derived from different cell types (**Figure 3-60**).[335] By the so-called "nanoghost strategy", these smart nanosystems benefit both from the NP core tailored nanomaterial and from the cell membrane surface features, achieving the possibility to be applied in several diagnostic and therapeutic applications, especially in drug delivery. This biomimetic coating provides therefore an innovative platform that can mimic the natural functions of the source cell when interacting with the biological environment, preventing the formation of the protein corona that generally limit NPs blood circulation time.[280] In addition to the enhanced circulation time, the biomimetic coating provides specific targeting abilities that otherwise bare NPs could not achieve. Cells membrane-derived coating offer the possibility of self-recognition at the cellular level which can lead to effective NPs active targeting aimed at the cells or tissues developed from the same cell line.

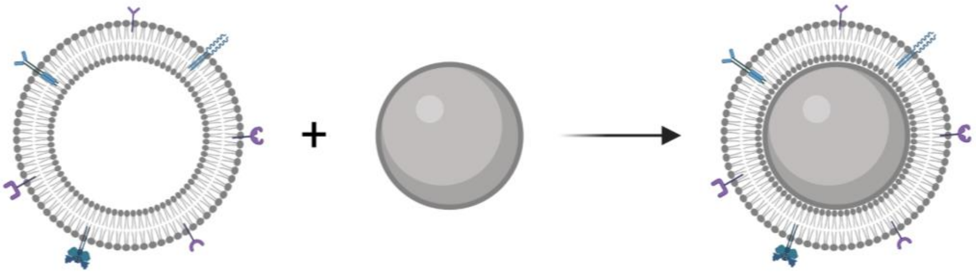

Figure 3-60 *Schematic representation of cell membrane-coated NPs.*

Here, biomimetic nanocarriers were applied to cloak different NPs in order to provide these synthetic nanomaterials with a new interface which enables the specific and effective targeting when interacting with the biological environment. Cell membrane-coated NPs were synthesized and used as biomimetic platform for drug delivery applications. Cell membrane coating was further modified to obtain fusogenic cell-derived nanovesicles able to release the loaded NPs directly inside the cytosol, thus evading the endolysosomal entrapment mechanism which is one of the main challenges in effective applications of nanomedicine.

NPs offer several advantages, such as fine control over size and morphology, and improved adsorption and desorption kinetics. Among the wide range of resources offered by nanomaterial science, two types of synthetic NPs were chosen as inner core of the biomimetic nanosystem fabricated: polystyrene NPs (PSNPs) and metal-organic frameworks (MOFs) NPs. Commercially available PSNPs were used both to optimize the experimental coating protocol and to evaluate the efficiency of the biomimetic coating. These functionalities were then applied to prepare cell-derived MOFs which were subsequently optimized and proposed as biomimetic platform for drug delivery applications.

3.4.1. Polystyrene nanoparticles (PSNPs)

Fluorescent polystyrene nanobeads of 100 and 200 nm (PSNPs) were coated either with CSMs or with FCSMs derived from human tumoral lung cells (A549 cells). PSNPs were used as a NP prototype to optimize the cell membrane-derived coating procedure and to understand the biological behavior of the biomimetic nanosystem when interacting with cells (**Figure 3-61**).

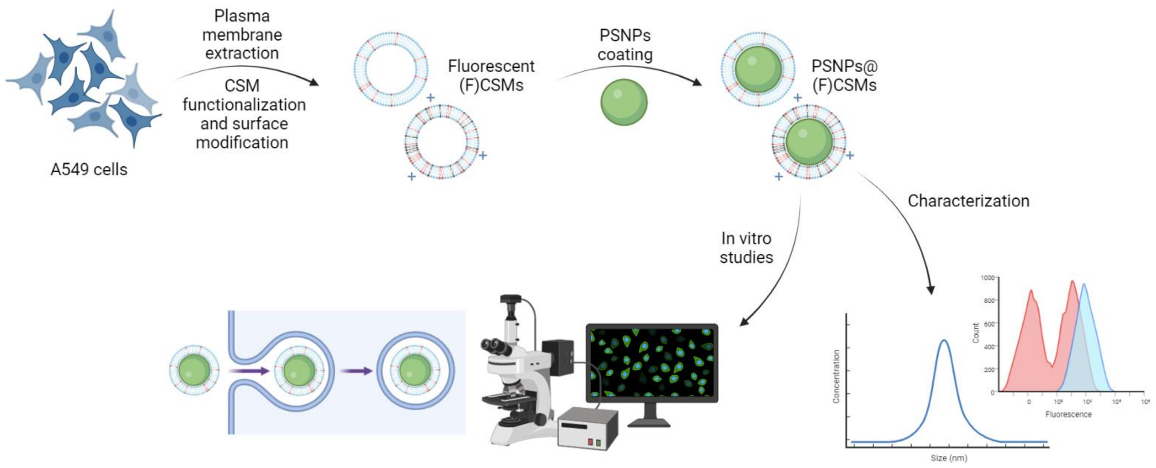

***Figure 3-61** PSNP@(F)CSM schematic experimental workflow.*

3.4.1.1. Design and optimization of PSNP@(F)CSM

A549 cells-derived nanovesicles were obtained following the protocol previously described (Section 2.1). Briefly, A549 cells were cultured according to the manufacturer's instructions. Once they reached 75-80% confluence, they were collected and induced to swallow in a hypotonic environment enriched with a proteases inhibitor cocktail (PIC) to preserve the surface properties of plasma membranes. The resulting disrupted cells were exposed to 4 cycles of freeze in N_2 and thaw at 37 ºC and subsequently subjected to mechanical disruption with ultrasounds. Plasma membranes fragments were extracted and recollected through differential centrifugal steps and extruded through polycarbonate membranes with nanosized pores in order to obtain self-assembled A549-CSMs of about 150-200 nm in size.

To obtain fluorescently labeled cell-derived nanovesicles, DOPE Atto 647N was added to the A549-CSMs solution as described in Section 2.2. While A549-FCSMs were obtained through the following procedure (described in Section 2.2): a lipids mixture consisting of neutral lipid DOPE, positively charged lipid DOTAP, and fluorescently labeled lipid DOPE Atto 647N was added to A549-CSMs. The resulting solutions (A549-CSMs and A549-FCSMs) were then subjected to sonication and extrusion through polycarbonate membranes to favor lipids intercalation in the lipidic bilayer of A549-(F)CSMs.

To evaluate the size and morphology of FCSMs, STEM micrographs were acquired. As shown in **Figure 3-62**, both CSMs and FCSMs, as phospholipidic-based nanovesicles, resemble liposomes morphology and structure. Due to the negative staining employed to acquire the images, both CSMs and FCSMs appeared dark, however it is still possible to identify the lipidic bilayer that characterizes the (F)CSMs structure.

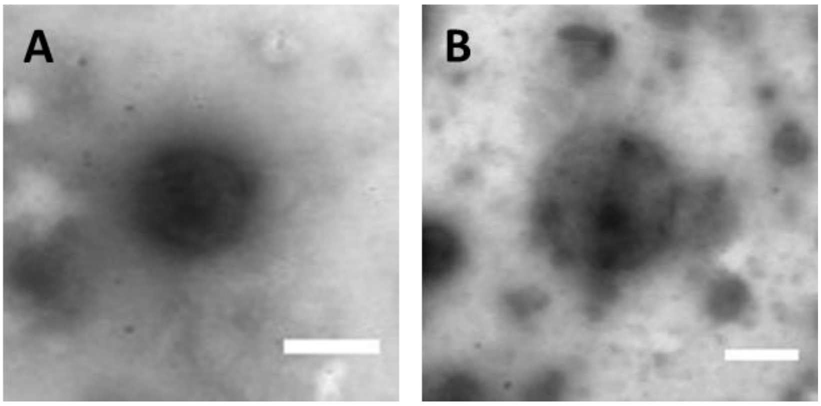

Figure 3-62 *STEM micrographs of (A) CSMs and (B) FCSMs. Scale bars = 200 nm.*

To prepare PSNP-coated CSMs (**Figure 3-63** A) and PSNP-coated FCSMs (**Figure 3-63** B), polystyrene nanobeads (PSNPs) of either 100 nm or 200 nm were added to the (F)CSMs solution as described in Section 2.3.1.1 and extruded through polycarbonate membranes to favor the coating of the PSNPs.

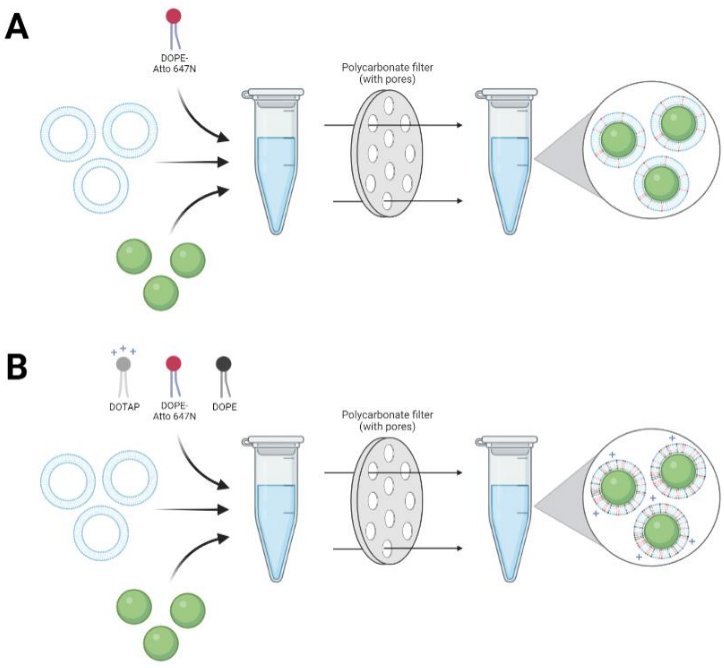

Figure 3-63 *Schematic representation of (A) PSNP@CSM and (B) PSNP@FCSM synthesis method.*

One key parameter for the coating optimization protocol was the ratio between PSNPs and (F)CSMs to efficiently fabricate biomimetic cloaked PSNPs. Each PSNP type (100 nm and 200 nm) coated with fusogenic or non-fusogenic A549-CSMs was obtained by mixing the cores and the plasma membrane coatings in two different ratios (1:1 and 1:4) considering that both of them presented similar diameter sizes (between 100 and 200 nm).

This protocol was designed to optimize the ratio between the two nanosystem components and, as shown in the following characterization steps, providing an excess of the coating component (1:4) favored the achievement of more monodisperse solutions. Moreover, since the purification method consists of centrifugation steps according to relative centrifugal force (RCF) of PSNPs, the excess of the (F)CSMs components should guarantee the coating of the whole PSNPs population, thus avoiding the presence of uncoated PSNPs in the solution. This purification step was also optimized. The solution of PSNP@(F)CSM was subjected to 7,100 g, which is a centrifugal force able to separate the two parts of the nanosystem. Providing an excess of the coating component and subjecting the whole nanosystem to extrusion through polycarbonate membranes should favor the elimination of the empty (F)CSMs, which should remain in the supernatant during the purification step. While the (F)CSMs-coated PSNPs should remain in the pellet, which was subsequently separated from the supernatant and resuspended in HEPES 20 mM pH 7.4.

Figure 3-64 and **Table 3-23** show size distribution analysis (NTA) of PSNPs (100 nm)-coated (F)CSMs with the two ratios protocols (1:1 and 1:4).

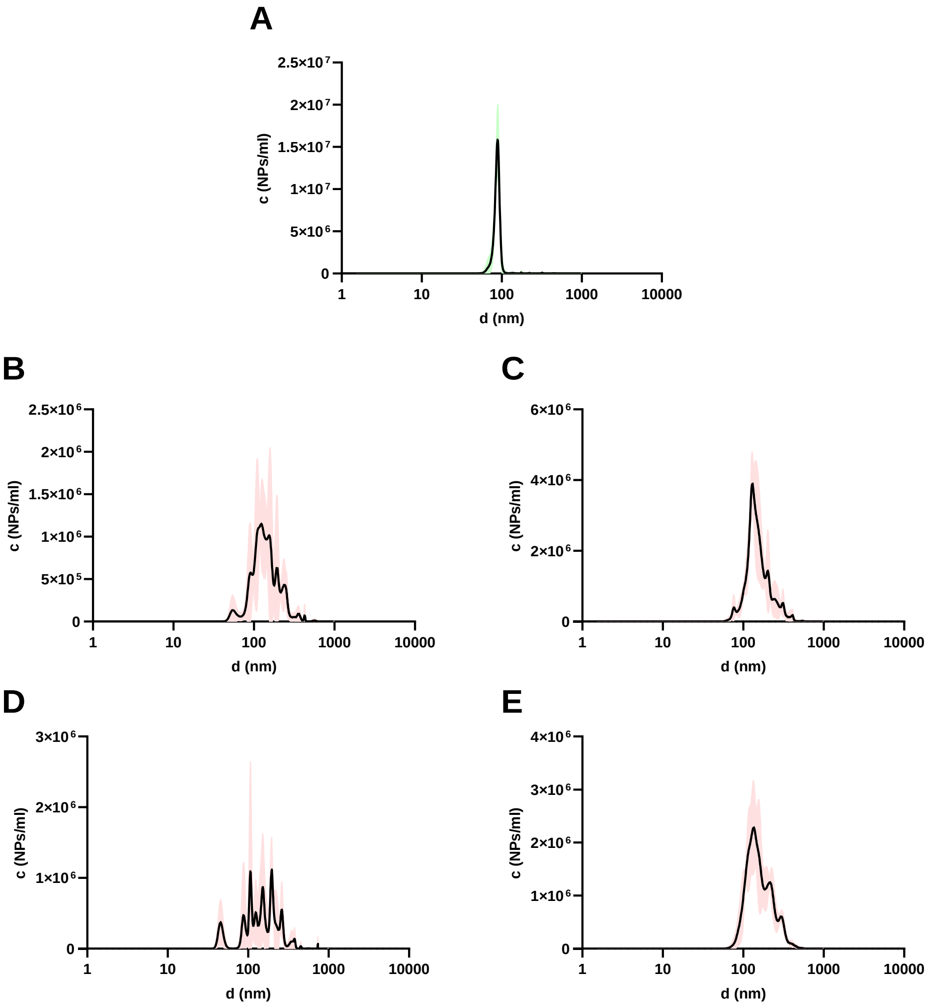

Figure 3-64 Size distribution analysis (NTA) of (A) PSNP100, (B) PSNP100@CSM 1:1, (C) PSNP100@CSM 1:4, (D) PSNP100@FCSM 1:1, and (E) PSNP100@FCSM 1:4.

Sample	d (mean) (nm)	d (mode) (nm)	c (NPs/mL)
PSNP100	90.0 ± 1.4	88.6 ± 0.3	4.74E+11
PSNP100@CSM 1:1	173.0 ± 6.4	139.8 ± 9.9	2.66E+10
PSNP100@CSM 1:4	182.5 ± 2.3	137.7 ± 6.3	6.54E+10
PSNP200@FCSM 1:1	190.8 ± 5.0	150.1 ± 1.36	2.16E+10
PSNP200@FCSM 1:4	193.1 ± 2.1	160.2 ± 16.9	5.72E+10

*Table 3-23 NTA analysis of PSNP100 with and without (F)CSMs coating depicted in **Figure 3-64**.*

Figure 3-65 and **Table 3-24** show size distribution analysis (NTA) of PSNPs (200 nm)-coated (F)CSMs with the two ratios protocols (1:1 and 1:4).

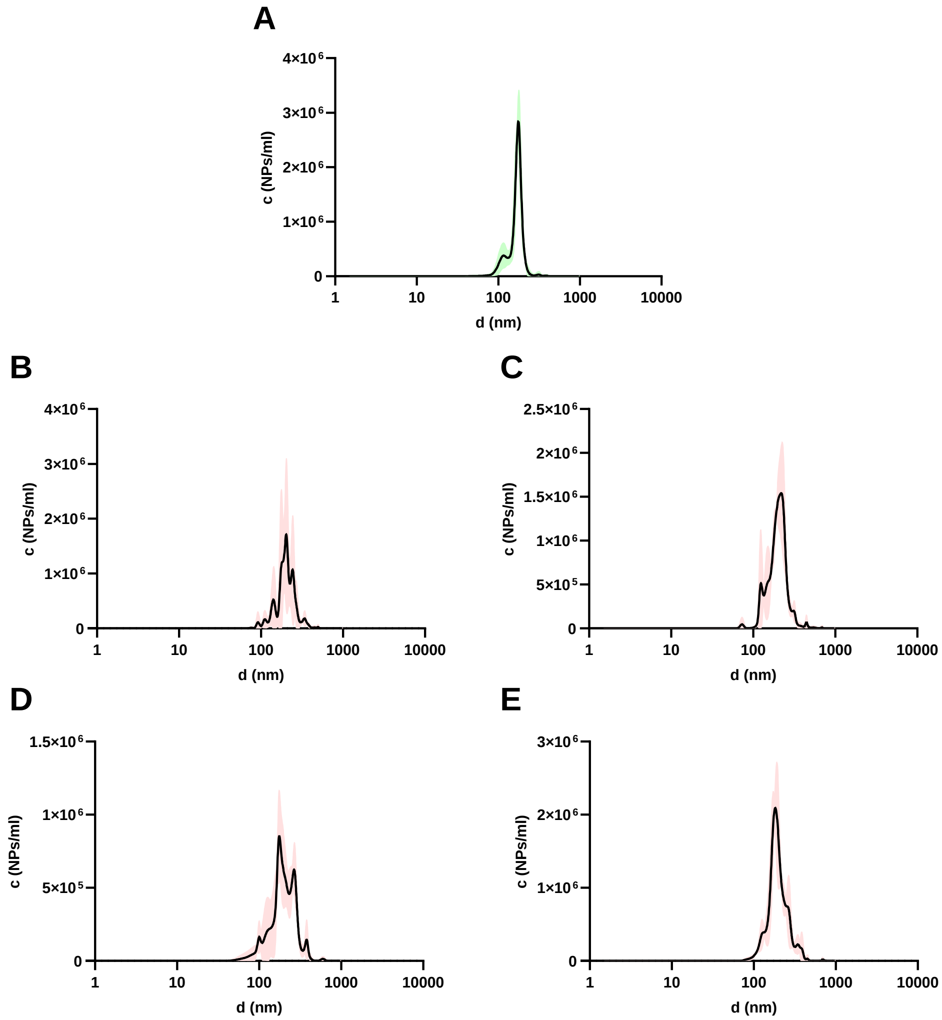

Figure 3-65 Size distribution analysis (NTA) of (A) PSNP200, (B) PSNP200@CSM 1:1, (C) PSNP200@CSM 1:4, (D) PSNP200@FCSM 1:1, and (E) PSNP200@FCSM 1:4.

Sample	d (mean) (nm)	d (mode) (nm)	c (NPs/mL)
PSNP200	173.6 ± 1.7	174.5 ± 3.1	1.28E+13
PSNP200@CSM 1:1	219.7 ± 4.7	192.3 ± 8.2	2.94E+10
PSNP200@CSM 1:4	219.1 ± 3.3	214.9 ± 8.7	3.22E+10
PSNP200@FCSM 1:1	230.5 ± 6.7	176.9 ± 6.2	2.14E+10
PSNP200@FCSM 1:4	219.9 ± 4.0	181.3 ± 5.6	3.98E+10

*Table 3-24 NTA analysis of PSNP200 with and without (F)CSMs coating depicted in **Figure 3-65**.*

As mentioned above, NTA analysis was used as a useful tool to investigate the polydispersity of the PSNP@(F)CSM solutions fabricated with the two different core-shell ratios.

The coating of PSNPs with (F)CSMs in a 1:1 (core:coating) ratio would imply that each NP should be coated by one single (F)CSM. Nevertheless, due to the 1:1 coating ratio employed during the protocol, the amount of coating materials to cloak the entire PSNPs population was not sufficient, generating aggregates in the solution and, therefore, polydispersity. This is quite well demonstrated in **Figure 3-64**, where the polydispersity of the nanosystem obtained with a 1:1 ratio between the core and the shell is shown (**Figure 3-64** B and **Figure 3-64** D). In addition, since the PSNPs and the (F)CSMs were relatively different in size (100 and 200 nm, respectively), the polydispersity of the solution due to the 1:1 ratio was even more evident compared to the results shown in **Figure 3-65**, where the PSNPs and the (F)CSMs were more similar in size (both around 200 nm). Therefore, an excess of (F)CSMs was provided (ratio 1:4) in order to favor the biomimetic coating of all the PSNPs in the dispersion (**Figure 3-64** C, **Figure 3-64** E, **Figure 3-65** C, and **Figure 3-65** E), thus obtaining monodisperse solutions of PSNPs coated with (F)CSMs.

To further investigate the population of PSNPs coated with (F)CSMs, flow cytometry (FC) analysis was conducted benefiting from the different fluorescent molecules (thus different emission wavelengths) used to label both the core and the coating (**Figure 3-67**). As mentioned, (F)CSMs were labelled with DOPE Atto 647N, while PSNPs were commercially available as fluorescent NPs where the fluorescent dye (FITC, green emitting) was loaded inside the NP core and not bound to the surface.

Flow cytometry is generally used to evaluate populations of cells. In this case the cytometer experimental settings were adjusted to measure small-sized populations. The analysis conducted with flow cytometry was used to evaluate the coating of PSNPs of both 200 nm (PSNP200) and 100 nm in size (PSNP100).

Although the whole population analysis was clearer for PSNP200, with both NPs sizes the coating process resulted to be successful. As shown, by using 1:4 (core:coating) mixing ratio (**Figure 3-66** D and **Figure 3-66** G), almost the entire NPs population shifted to the right part of the plot, indicating an increase in the red fluorescence signal (Atto 647N, red-emitting lipid). While with the 1:1 coating mixing ratio (**Figure 3-66** C) more than half of the NPs population still remained in the left part of the plot, suggesting that the coating efficiency was lower. However, no detectable green fluorescence signal shift was observed. This may be due to the poor green fluorescence intensity of PSNP100. The NPs diameter size in fact is proportional to their inner pores size and, therefore, to the quantity of fluorescent dye incapsulated into them.

The effect of the coating in PSNPs population was more evident with 200 nm PSNPs. As shown, by using the 1:4 (core:coating) mixing ratio, more than 95% of obtained PSNP@CSM (**Figure 3-67** D) and 85% of PSNP@FCSM (**Figure 3-67** G) populations exhibited fluorescence signals derived from both the PSNPs (green-emitting loaded dye) and the Atto 647N DOPE (red-emitting lipid) used to label the biomimetic coating. While with the 1:1 (core:coating) mixing ratio, the PSNP@CSM (**Figure 3-67** C) and PSNP@FCSM (**Figure 3-67** F) populations exhibiting the two different fluorescence signals were only around 40% and 50%, respectively.

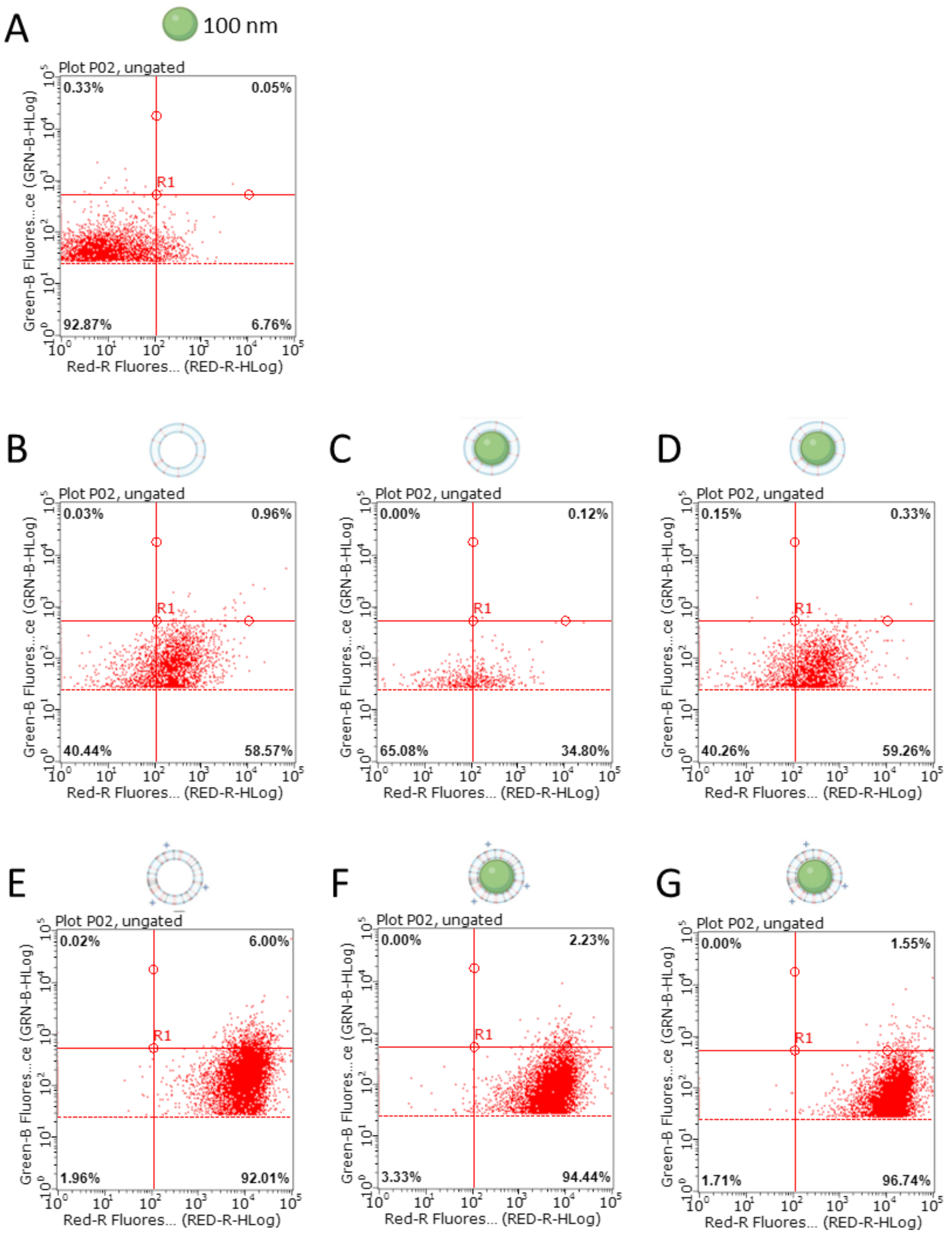

Figure 3-66 *Optimization of PSNP@(F)CSM encapsulation method. The analysis was conducted with flow cytometry to investigate the different NPs population through fluorescence intensities. NPs population investigated were (A) PS100, (B) CSMs, (E) FCSMs), (C) PS100@CSM obtained mixing the NPs 1:1, (D) PS100@CSM obtained mixing the NPs 1:4, (F) PS100@FCSM obtained mixing the NPs 1:1, and (G) PS100@FCSM obtained mixing the NPs 1:4.*

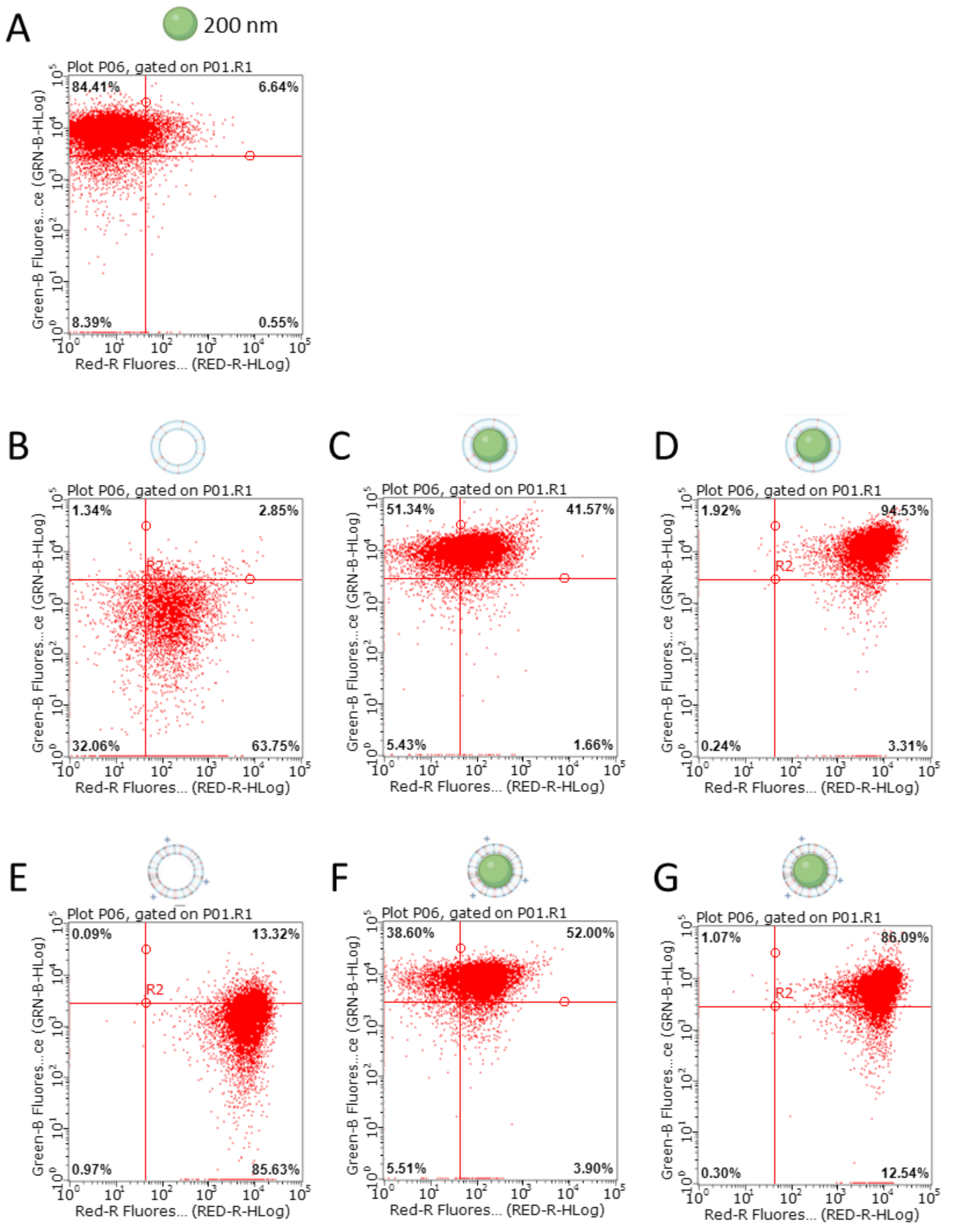

Figure 3-67 *Optimization of PSNP@(F)CSM encapsulation method. The analysis was conducted with flow cytometry to investigate the different NPs population through fluorescence intensities. NPs population investigated were (A) PS200, (B) CSMs, (E) FCSMs, (C) PS200@CSM obtained mixing the NPs 1:1, (D) PS200@CSM obtained mixing the NPs 1:4, (F) PS200@FCSM obtained mixing the NPs 1:1, and (G) PS200@FCSM obtained mixing the NPs 1:4.*

3.4.1.2. *In vitro* studies of PSNPs coated with (F)CSMs

Once optimized the synthetic protocol for biomimetic cloaked PSNPs, the effect of the CSMs coating on the interaction of PSNPs with different cell lines was evaluated. The aim was to study the homotypic targeting capabilities of CSMs-coated PSNPs and the differences in the uptake mechanisms.

First, the uptake of PSNPs and CSMs was evaluated in three different cell lines (HeLa, A549, and HEK-293) to estimate the most appropriate concentration later used in further uptake experiments. As shown in **Figure 3-68**, the uptake of CSMs was higher compared to PSNPs, probably due to the intrinsic targeting abilities of cell-derived nanovesicles which should favor the NP-cell interaction and consequently the NPs internalization.[370] This targeting effect is especially evident in tumoral cells (HeLa and A549) due to the surface protein pool preserved from the source cells, which enhances the recognition, interaction, and internalization of molecules, including NPs, into tumoral cells.

The uptake study shown in **Figure 3-68** also allowed to understand the NPs internalization trends. All the cell lines were exposed either to fluorescent PSNPs or to fluorescent CSMs at different concentrations (nº NPs/cell) for three hours, then subjected to trypsinization and measured by flow cytometry. The NPs internalization trend was approximatively the same for all the cell lines evaluated, reaching an uptake plateau at a certain concentration, which, considering both PSNPs and CSMs, was established at around $1 \cdot 10^5$ NPs/cell.

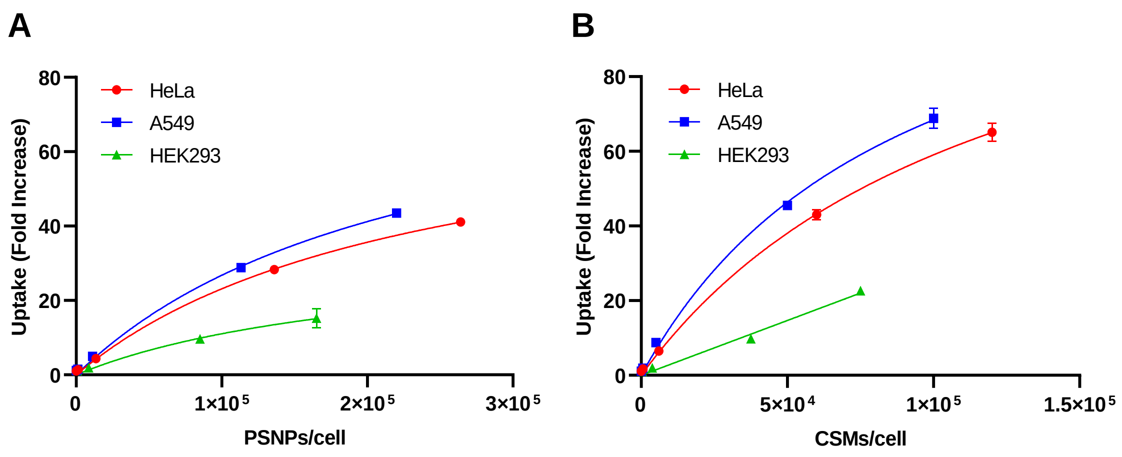

Figure 3-68 Uptake experiments of (A) PSNPs and (B) A549-derived CSMs at different concentrations (NPs/cell) evaluated in HeLa, A549, and HEK-293 cells after 3 hours incubation.

To further investigate the internalization pathway used by both PSNPs and CSMs to enter the cells, uptake experiments in presence of endocytosis inhibitors were performed. As mentioned above (Section 3.1.4), each endocytosis inhibitor is able to inhibit one single internalization pathway.

To perform the uptake experiments in presence of different inhibitors, HeLa cells were used as prototypical tumoral cells to fabricate cell-derived nanovesicles, later used as biomimetic coating for other types of NPs. HeLa and A549 cells were pre-treated with the specific inhibitor for 30 minutes before exposing them to the NPs solutions for 2 hours.

Some NPs may escape the endocytic route repressed by a specific inhibitor and be internalized through a different pathway. As shown in **Figure 3-69**, PSNPs represent the prototypical NPs capable of evading the inhibition of a specific pathway and entering the cells mediated by another endocytic route (pointed out in **Figure 3-69** B).

Other types of NPs, such as the ones that present on their surface certain biological entities (i.e., proteins, receptors, etc.), result more dependent on specific endocytic pathways. Despite their cell type dependence, CSMs internalization (shown in **Figure 3-69** A), due to their cell-derived surface features, was affected by specific endocytosis inhibitors, especially chlorpromazine (CP) and methyl-β-cyclodextrin (MBCD). CP is a cationic amphiphilic drug which inhibits the function of AP2, one of the pivotal adaptor proteins in clathrin-mediated endocytosis[333], while MBCD is a cyclic oligomer of glucopyranoside used to determine whether endocytosis is dependent on the integrity of lipids rafts, due to its role in extracting the steroid out of the plasma membrane.[334]

Regarding the core-shell nanosystem composed by PSNPs coated by CSMs, flow cytometry analysis of the two different fluorescent dyes (orange-emitting PSNPs and green-emitting CSMs) was performed (**Figure 3-69** C). Both the graphs show that in presence of CP the cellular internalization of CSMs-coated PSNPs decreased compared to the other endocytosis inhibitors. Overall, PSNP@CSM uptake pattern resembled the one of the coating itself, being more emphasized in the graph of the CSMs fluorescence (**Figure 3-69** C, on the left). This could be due to a possible incomplete coating of the PSNP, which, showing an even small bare part, managed to escape the endocytic route inhibited by the specific inhibitor, and, consequently, entered the cells (PSNPs fluorescence, **Figure 3-69** C, on the right). However, in presence of CP, PSNP@CSM uptake was reduced (confirmed by both the fluorescence intensities measured by flow cytometry), indicating that CSMs, used both as empty nanovesicles and as biomimetic coating for synthetic NPs, were internalized by cells through a clathrin-mediated endocytosis pathway.

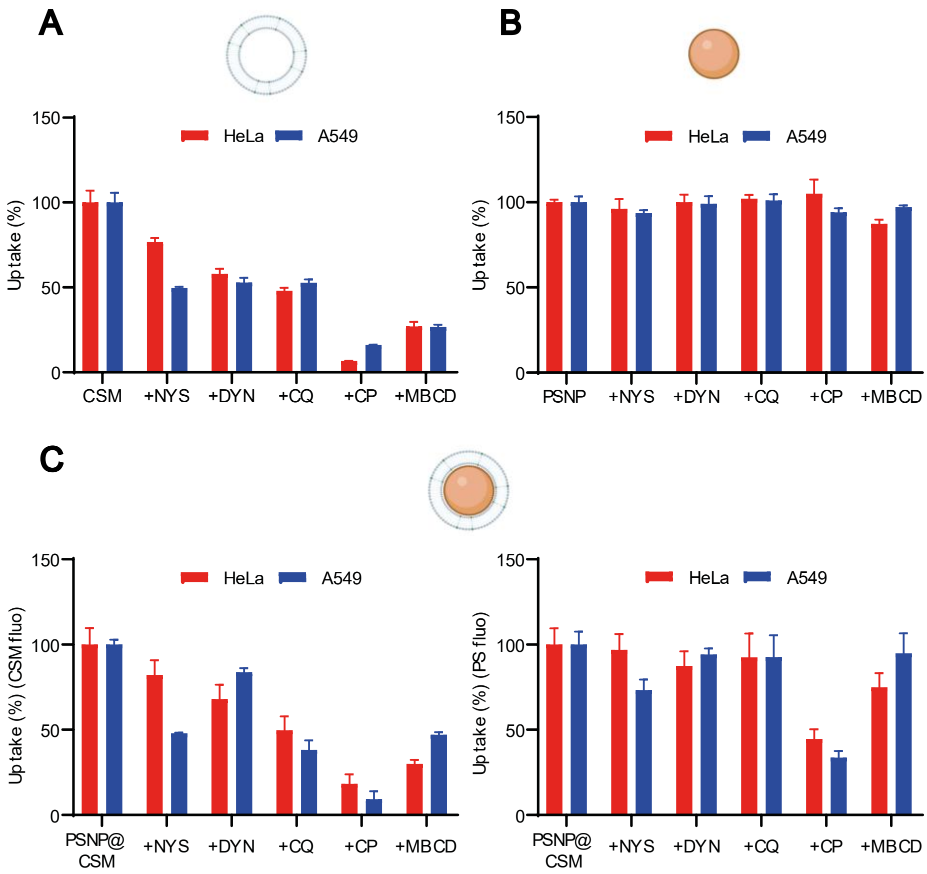

Figure 3-69 *HeLa and A549 cells uptake experiments of (A) CSMs, (B) PSNPs, and (C) PSNP@CSM in presence of different endocytosis inhibitors.*

Interestingly, dynasore (DYN) did not seem to affect neither the internalization of CSMs nor the one of PSNPs. DYN is a non-competitive inhibitor of dynamin, a GTPase that plays a key role both in clathrin-independent and in clathrin-dependent endocytosis (CIE and CDE, respectively)[331] (**Figure 3-70**). Since CSMs cellular uptake followed a clathrin-mediated endocytosis pathway, the internalization should be partly or totally affected by dynamin inhibition.

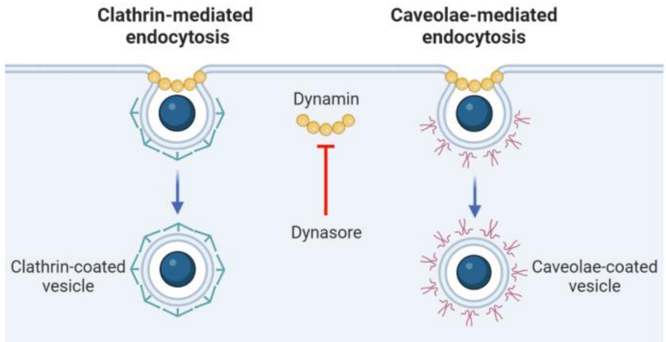

Figure 3-70 *Schematic representation of dynamin role in CDE and CIE.*

Nevertheless, this biomimetic prototypical nanosystem (PSNP@CSM) was fabricated and investigated to mimic more complex potential nanotherapeutics. Sometimes, in fact, the entrapment in the endolysosomal compartments, regardless of the internalization pathway followed, may limit the release of the NP or the loaded cargo in the cytosol, thus preventing the nanosystem potential beneficial effects over cytosolic or nucleic targets.

In order to enhance the NPs release inside cell cytoplasm, CSMs coating was engineered with a specific lipids mixture, which allowed the fusion of CSMs phospholipid bilayer with cell plasma membranes, therefore releasing the PSNPs directly inside the cytosol.

Fusogenic CSMs (FCSMs) were obtained as described in Section 2.2. Briefly, a lipids mixture composed by neutral lipid DOPE, cationic lipid DOTAP and fluorescent neutral DOPE Atto 647N was added to CSMs solution before the PSNPs (100 nm) coating process. Then, the solution was subjected to ultrasounds and extrusion through polycarbonate membranes to favor the intercalation in CSMs lipidic bilayer.

To assess the viability of cells exposed to (F)CSMs and to demonstrate the safety of these nanocarriers, MTT assay was performed at different concentrations of (F)CSMs per cell (**Figure 3-71**). Different time points (10 minutes, 3 hours, and 24 hours) were selected to evaluate the potential toxic effect of FCSMs fast interaction with cell plasma membrane.

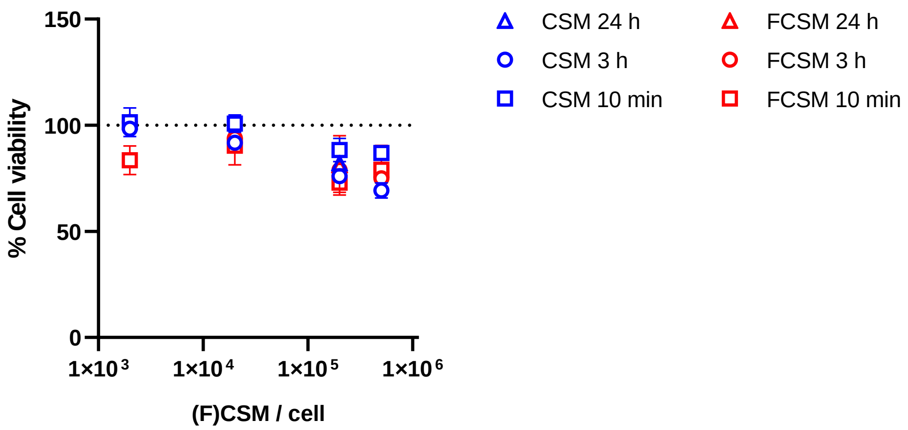

Figure 3-71 *Viability of A549 cells exposed to different of concentrations of (F)CSMs at different incubation times.*

As shown in **Figure 3-71**, no significant toxicity was detected even after long incubation times (24 hours), indicating that the biomimetic nanovesicles, regardless of the lipids modification, resulted to be non-toxic candidates, whether if used as nanovesicles or as coating for other types of NPs, when interacting with the biological environment. Thus, they might be employed in biomedical applications (such as drug delivery), without affecting the cell viability.

Furthermore, fluorescence microscopy analysis of PSNP@FCSM was performed to evaluate their fusogenic activity when interacting with cells. A549 cells were exposed to PSNP@(F)CSM for 1 hour, then washed and observed with a fluorescence microscope (Section 2.5.1.3).

As shown in **Figure 3-72**, the internalization of PSNPs was higher when coated with FCSMs (**Figure 3-72** B) compared to CSMs coating (**Figure 3-72** A). Moreover, green fluorescence intensity (PSNPs) appeared diffused in the case of FCSMs coating (**Figure 3-72** B) compared to dotted-like fluorescence signal of CSMs-coated PSNPs (**Figure 3-72** A) typical of the endolysosomal internalization, suggesting that the fusogenic coating allowed the release of PSNPs directly into cell cytosol.

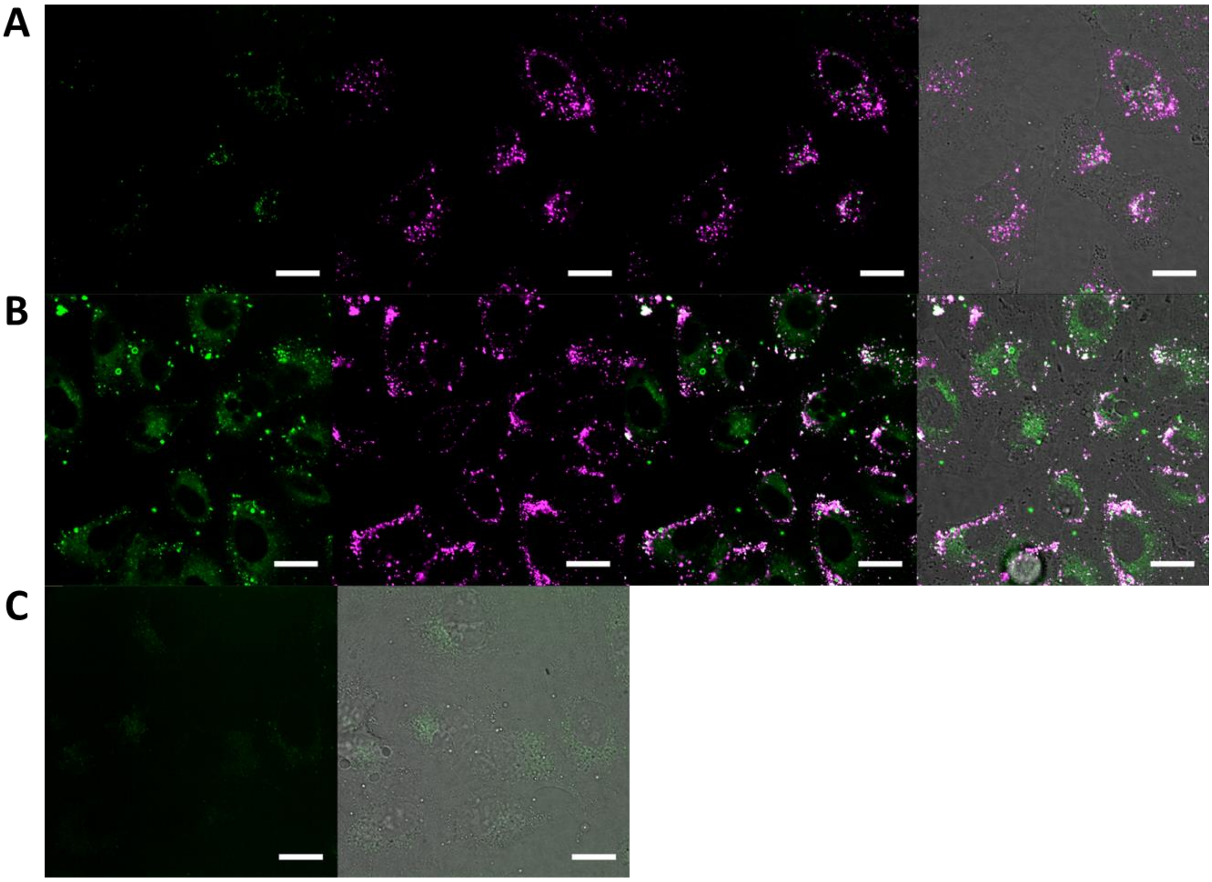

Figure 3-72 *Fluorescence microscopy images of A549 cells incubated with (A) PSNP@CSM, (B) PSNP@FCSM, and (C) with no NPs (control). For each panel, from left to right, images show the fluorescence signal of PSNPs (in green), (F)CSMs (in magenta), overlays of the two fluorescence signals (green + magenta), and both merged with brightfield. Scale bars: 20 µm.*

The fusion-like internalization of FCSMs, driven by the modification of the surface membrane lipidic composition, is presumably an extremely fast process. The biological interactions between the two lipidic bilayers (cells plasma membrane and FCSMs) resulted to be improved even at very short exposure times. A549 cells were exposed to high concentrations of PSNP@FCSM for 2 minutes. Then, the same fluorescence microscopy analysis was performed.

As shown in **Figure 3-73**, after only 2 minutes of exposure, PSNPs (in green) managed to enter the cells. Moreover, the diffused fluorescence signal indicates that the PSNPs were likely inside the cytoplasm, while the FCSMs fluorescence signal (in magenta) remained at the borders of the cells, suggesting the interaction and, probably, the fusion with the plasma membrane (**Figure 3-73** C).

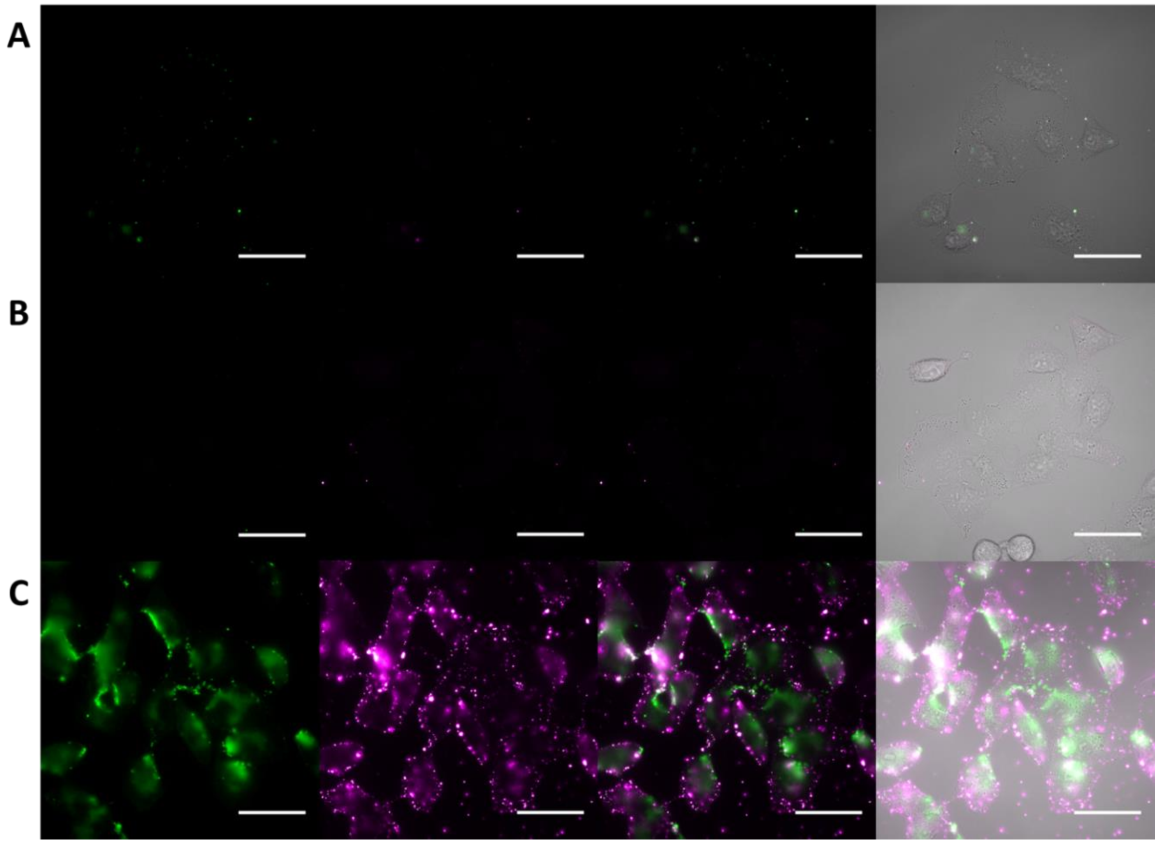

Figure 3-73 *Fluorescence microscopy images of A549 cells incubated with (A) PSNPs, (B) PSNP@CSM, and (C) with PSNP@FCSM. For each panel, from left to right, images show the fluorescence signal of PSNPs (in green), (F)CSMs (in magenta), overlays of the two fluorescence signals (green + magenta), and both merged with brightfield. Scale bars: 50 µm.*

To better visualize the internalization of the PSNP@FCSM into cells and, therefore, to understand the mechanism through which the fusogenic coating allows the interaction with the plasma membrane, a fluorescence microscopy 3D analysis of a portion of cells exposed to PSNP@FCSM was performed.

As shown in **Figure 3-74**, the Atto 647N fluorescence signal (FCSMs, in magenta) encircles the cells, indicating a fast (only 2 minutes of exposure) interaction with cells. While the FITC fluorescence signal (PSNPs, in green) reaches the inner part of the cells, appearing diffused compared to the dotted-like signal of FCSMs, suggesting a cytosolic internalization of the NPs.

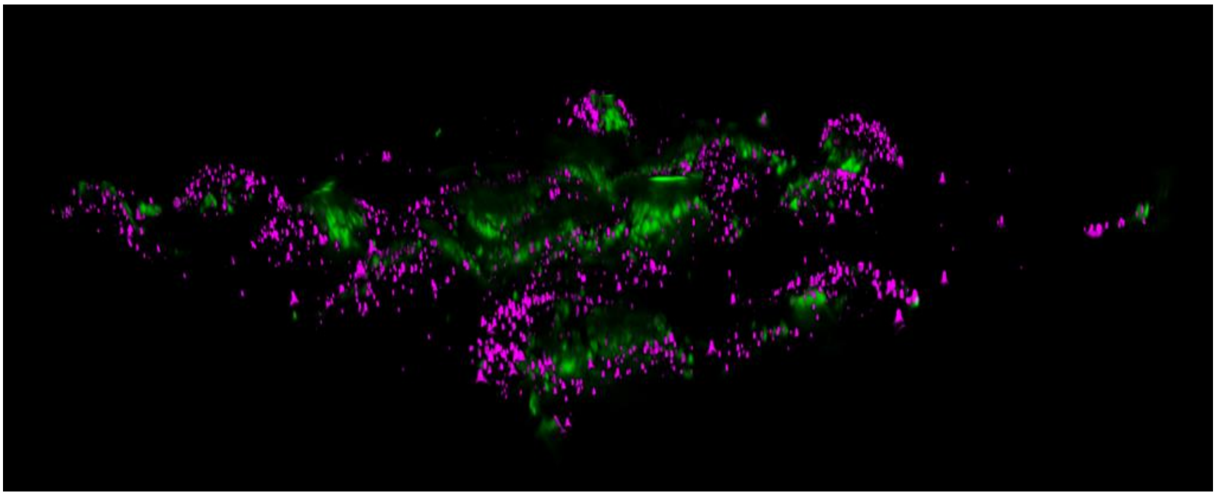

Figure 3-74 *Fluorescence microscopy 3D representation (Z-stack) of A549 cells exposed to PSNP@FCSM for 2 minutes.*

Taken together, these results demonstrate that the specific lipids mixture employed to engineer the biomimetic coating allowed the fabrication of fusogenic coated-NPs able to be internalized by cells without being entrapped into the endolysosomal system and, thus, being promising nanocarriers for the delivery of intracellular targeting cargos.

3.4.2. Metal-organic frameworks (MOFs)

In the second part of this chapter, porous metal-organic frameworks (MOFs) were selected as inner core of the biomimetic nanosystem, given their great suitability as potential nanotherapeutics. Recent efforts, in fact, have focused on the possibility of tuning their pore size and functionalizing the building blocks with chemical groups, obtaining highly monodispersed formulations which exhibit precise control over morphology, controlled cargo delivery, sensing capacity, and biocatalytic activity.[139]

Among MOFs family, Zr-based MOFs are extremely chemically stable, and they present bigger pore sizes compared to other types of MOFs, conferring them the capability of encapsulating larger quantities of different types of cargo. In the BioNanoTools group, the production of different MOFs at the nano-size range has been achieved,[321, 371] including UiO-67 nanoMOF of about 100 nm in size. Here, UiO-67 loaded with a fluorescently labeled cargo was used as a model system to study the coating process with (F)CSMs.

Following the procedure elaborated for prototypical PSNPs, UiO-67 were coated with CSMs derived from A549 cells to evaluate the biomimetic coating ability to enhance the cellular internalization of the nanoMOFs. Moreover, CSMs were further modified to obtain a cell-derived coating able to fuse with cells plasma membrane (FCSMs) and release the MOFs, in this case the Zr-based UiO-67, directly inside the cytoplasm, as shown in **Figure 3-75**. Thus, this biomimetic core-shell nanosystem was able not only to exploit the homotypic targeting capabilities of cell-derived coating, but also to evade the endolysosomal entrapment that typically characterize NPs internalization inside cells.

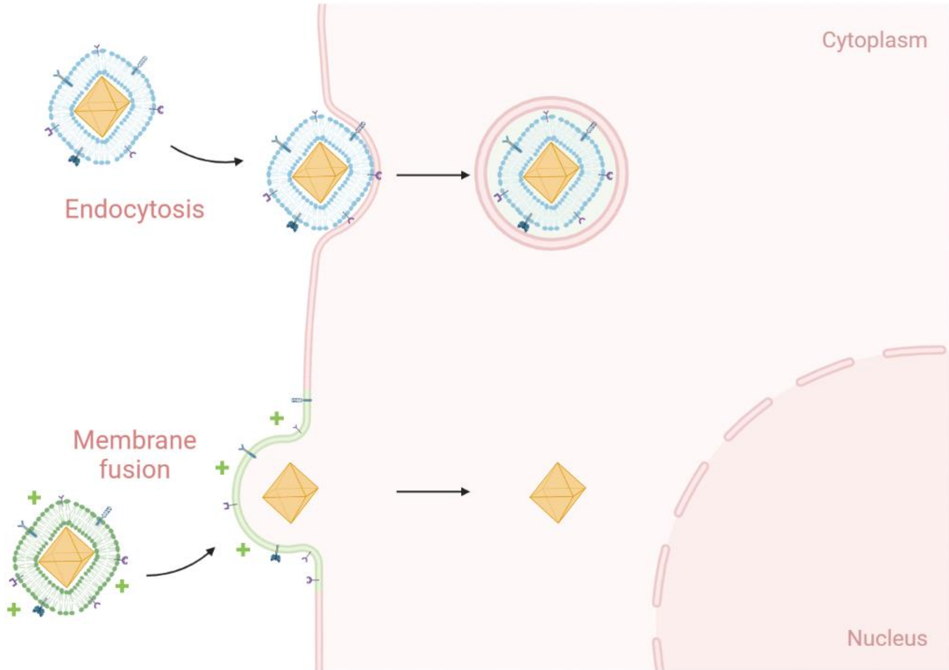

Figure 3-75 *Schematic representation of UiO-67@(F)CSM main experimental objective.*

As mentioned above, MOFs represent a promising candidate for drug delivery applications due to their unique porous structures and controlled released properties. In particular, UiO-67 MOFs show exceptional thermal, chemical, and mechanical stability, they present high surface areas and pores volumes, as well as low densities. For these reasons, combined with its good biocompatibility, UiO-67 was selected as potential drug delivery nanomaterial among others. Different fluorescent cargos, such as Rhodamine 6G or Cresyl Violet, or drugs, such as Carboplatin, were used to evaluate either the internalization or the toxicity profile when loaded into UiO-67.

To improve their targeting features, UiO-67 were coated with A549 cell membrane-derived nanovesicles, which were further modified to enhance the MOF release inside cell cytoplasm.

3.4.2.1. Design and characterization of biomimetic coated-UiO-67

A549 cells-derived nanovesicles were obtained following the protocol previously described (Section 2.1). Briefly, A549 cells were cultured according to the manufacturer's instructions. Once they reached 75-80% confluence, they were collected and induced to swallow in a hypotonic environment enriched with a proteases inhibitor cocktail (PIC) to preserve plasma membrane surface properties. The resulting disrupted cells were exposed to 4 cycles of freeze in N_2 and thaw at 37 ºC and subsequently subjected to mechanical disruption with ultrasounds. Plasma membranes fragments were extracted and recollected through differential centrifugal steps and extruded through polycarbonate membranes with nanosized pores in order to obtain self-assembled A549-CSMs of about 150-200 nm in size.

To obtain fluorescently labeled cell-derived nanovesicles, DOPE Atto 647N or DOPE Atto 488 was added to the CSMs solution as described in Section 2.2. While fusogenic A549-FCSMs were obtained through the following procedure (described in Section 2.2): a lipids mixture consisting of neutral lipid DOPE, positively charged lipid DOTAP, and fluorescently labeled lipid DOPE Atto 647N or DOPE Atto 488 was added to CSMs. Both the resulting solutions (CSMs and FCSMs) were then subjected to sonication and extrusion through polycarbonate membranes to favor lipids intercalation in (F)CSMs lipidic bilayer.

One of the main advantages of UiO-67 is their cargo loading versatility. According to the experimental need, UiO-67 were loaded either with Rhodamine 6G (Rho) or with Cresyl Violet (CV) (**Figure 3-76**). In particular, to perform DLS analysis and flow cytometry coating characterization, UiO-67 were loaded with Rho in combination with DOPE Atto 647N for (F)CSMs labeling, while CV was employed as cargo loaded in UiO-67 in combination with DOPE Atto 647N ((F)CSMs) for NTA analysis, toxicity assays, and flow cytometry uptake experiments, and in combination with DOPE Atto 488 ((F)CSMs) for fluorescence microscopy. Empty UiO-67 were used for SEM/STEM characterization and for ICP measurements. Moreover, preliminary results of Carboplatin (CaPt) delivery and cytotoxicity in tumoral cells were obtained by encapsulating the drug inside UiO-67 and performing the (F)CSMs coating.

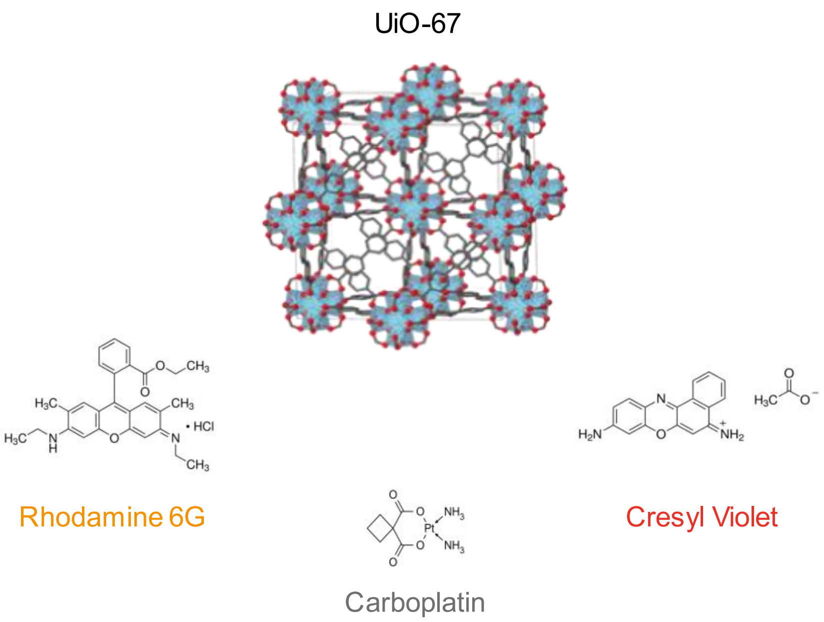

Figure 3-76 UiO-67 NPs chemical representation and Rhodamine 6G (Rho) and Cresyl Violet (CV) fluorophores chemical structures.

To prepare UiO-67-coated CSMs (**Figure 3-77** A) and UiO-67-coated FCSMs (**Figure 3-77** B), UiO-67 of about 100 nm (empty or loaded with Rho/CV) were added to the (F)CSMs solution as described in Section 2.3.1.1 and extruded through polycarbonate membranes to favor the MOF coating. The ratio of UiO-67:(F)CSMs was optimized following an experimental procedure similar to PSNPs (above in this chapter) and was assessed as 1:5 (core:coating) mixing ratio as the most suitable.

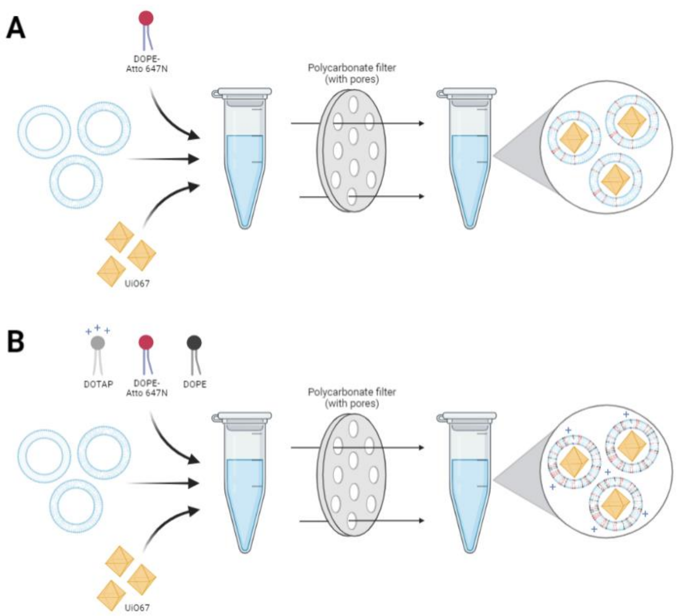

Figure 3-77 Schematic representation of (A) UiO-67@CSM and (B) UiO-67@FCSM synthesis method.

Size distribution analysis (DLS) of UiO-67(Rho), CSMs, FCSMs, UiO-67(Rho)@CSM, and UiO-67(Rho)@FCSM are reported in **Figure 3-78** and **Table 3-25**.

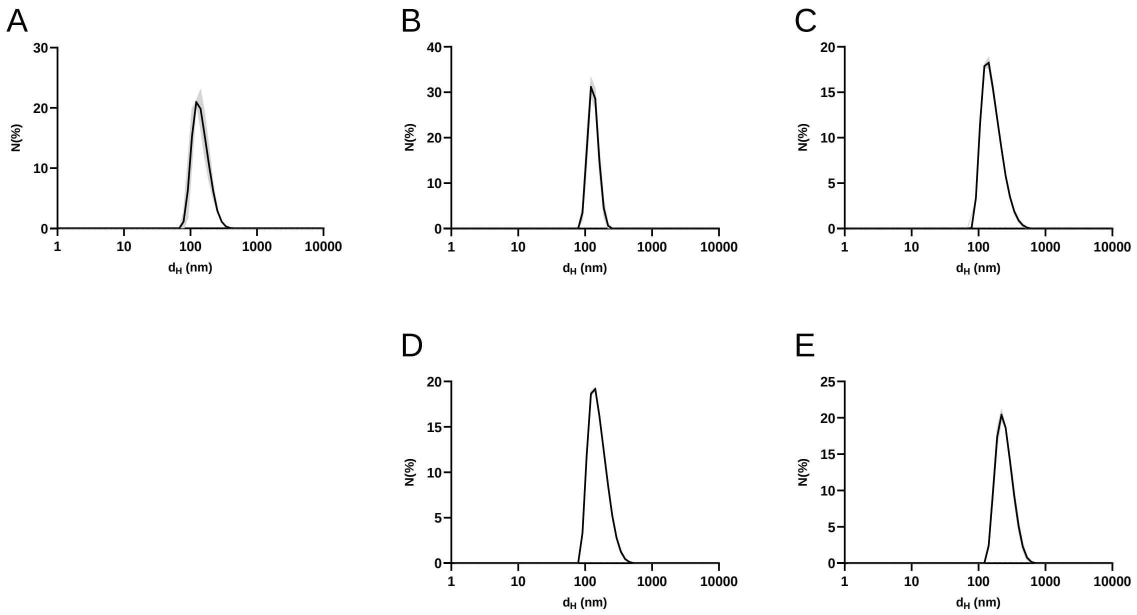

Figure 3-78 Size distribution measurements (DLS) of (A) UiO-67(Rho), (B) CSMs, (C) FCSMs, (D) UiO-67(Rho)@CSM, and (E) UiO-67(Rho)@FCSM.

Sample	Z-Average (nm)	PdI	$d_{H,I}$ (nm)	$d_{H,N}$ (nm)	$d_{H,V}$ (nm)
UiO-67(Rho)	175.9 ± 25	0.119 ± 0.02	191.6 ± 4.3	147.5 ± 8.3	188.7 ± 2.9
CSM	256.4 ± 49.2	0.435 ± 0.11	144.7 ± 5.2	133.9 ± 4.0	142.7 ± 5.3
FCSM	219.0 ± 7.0	0.205 ± 0.15	233.7 ± 8.2	168.2 ± 1.4	251.2 ± 12.3
UiO-67(Rho) @CSM	195.6 ± 6.1	0.111 ± 0.04	214.0 ± 5.0	162.8 ± 1.7	222.5 ± 7.1
UiO-67(Rho) @FCSM	296.2 ± 16.0	0.253 ± 0.04	295.8 ± 10.8	253.5 ± 7.0	320.1 ± 14.0

*Table 3-25 DLS analysis UiO-67(Rho) with and without (F)CSMs coating. Data are illustrated in **Figure 3-78**.*

Likewise, size distribution measurements (NTA) of UiO-67(CV), CSMs, FCSMs, UiO-67(CV)@CSM, and UiO-67(CV)@FCSM are reported in **Figure 3-79** and **Table 3-26**.

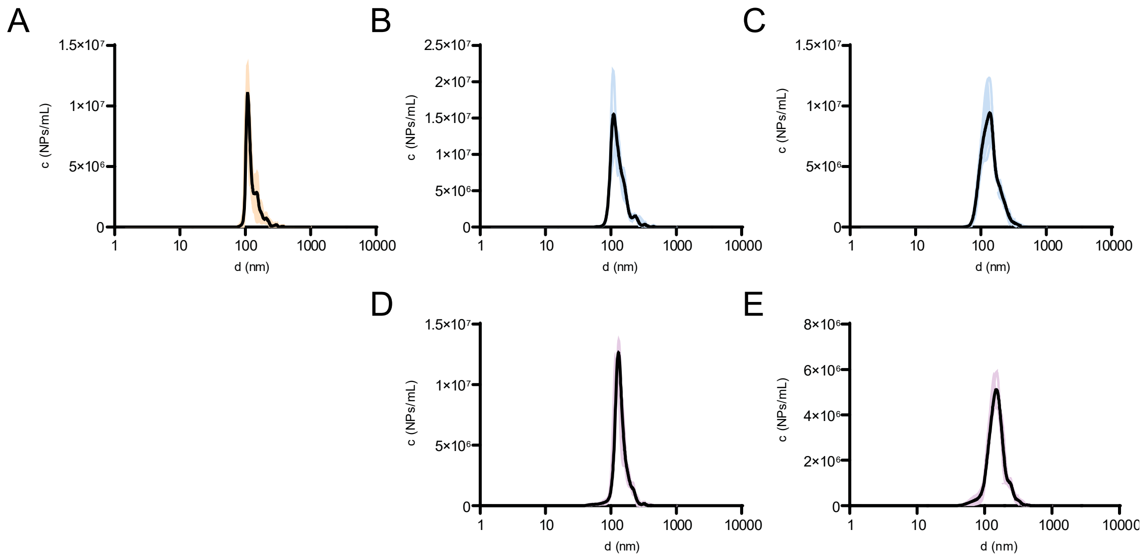

Figure 3-79 *Size distribution measurements (NTA) of (A) UiO-67(CV), (B) CSMs, (C) FCSMs, (D) UiO-67(CV)@CSM, and (E) UiO-67(CV)@FCSM.*

Sample	d (mean) (nm)	d (mode) (nm)	c (NPs/mL)
UiO-67(CV)	139.3 ± 0.5	109.9 ± 1.6	1.58E+12
CSM	148.0 ± 2.8	115.9 ± 5.1	9.83E+11
FCSM	160.7 ± 2.1	138.7 ± 5.0	9.15E+11
UiO-67(CV)@CSM	151.1 ± 0.2	130.0 ± 1.5	6.85E+11
UiO-67(CV)@FCSM	170.0 ± 3.4	148.6 ± 2.3	4.77E+11

Table 3-26 *NTA analysis of UiO-67(CV) with and without (F)CSMs coating depicted in* ***Figure 3-79****.*

The core-shell nanosystem composed by MOF inner core and cell-derived biomimetic coating (UiO-67@CSM and UiO-67@FCSM) was also characterized with electron microscopy (**Figure 3-80**) to further corroborate the presence of the coating around the NPs and their size. Scanning electron microscopy (SEM) was used to characterize bare UiO-67 since this technique provides information of the NP surface and composition (**Figure 3-80** A). Whereas, scanning transmission electron microscopy (STEM) was used to evaluate UiO-67 coating and how this could affect the NPs surface composition.

The organic matter (basically lipids and proteins) that characterizes the cell-derived coating is not a conductive material, thus, under the electron beam exposure, it is usually torn due to the mechanical forces produced from charging.[372] For this reason, when using STEM, the coating appeared bright around the UiO-67 NPs, as shown in **Figure 3-80** B (UiO-67@CSM) and C (UiO-67@FCSM).

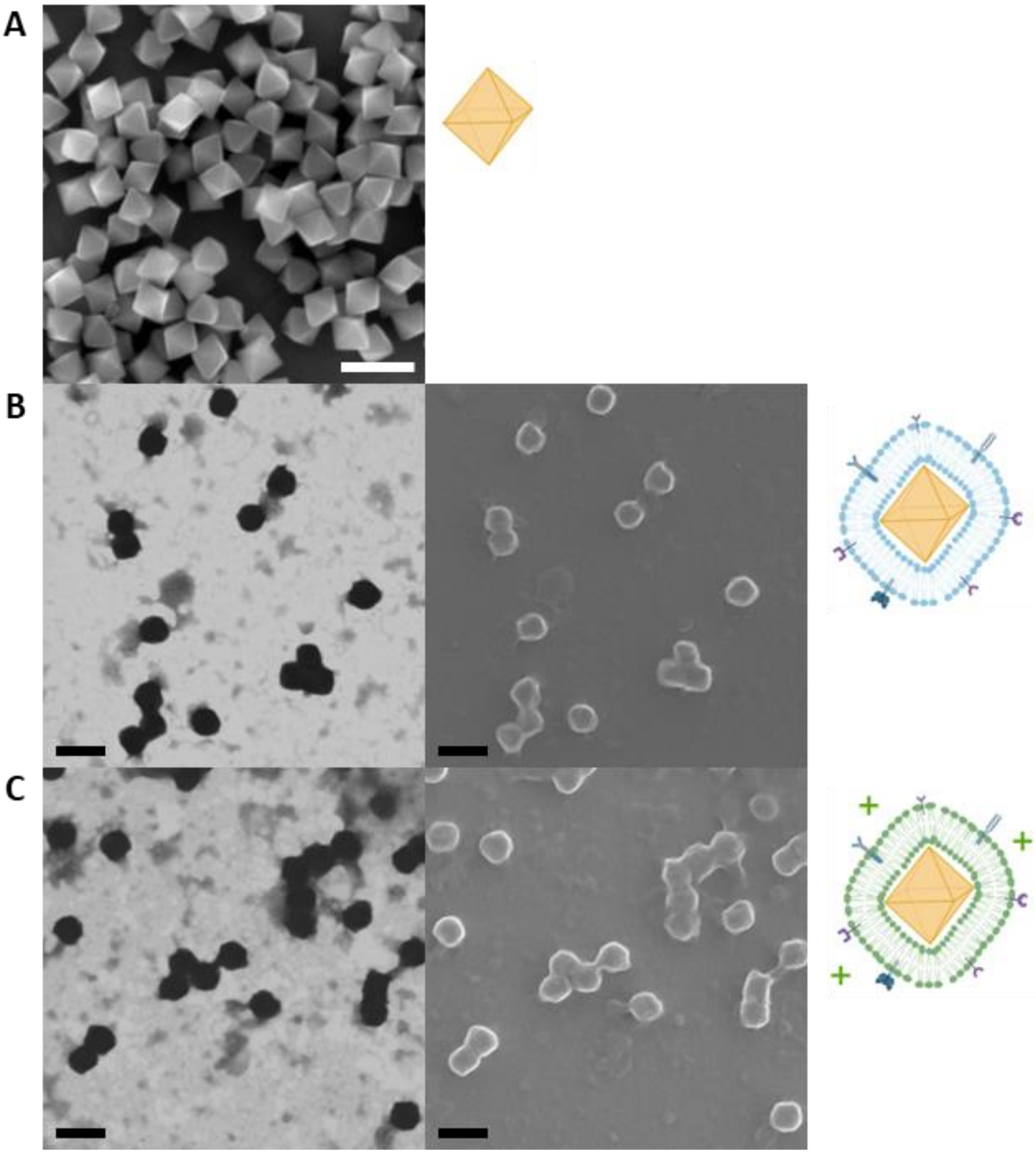

Figure 3-80 *SEM/STEM micrographs of (A) bare UiO-67, (B) UiO-67@CSM, and (C) UiO-67@FCSM. Scale bars = 200 nm.*

Once characterized the (F)CSMs-coated MOFs from a physicochemical perspective, NPs populations were examined with flow cytometry. As shown in **Figure 3-81**, the majority of coated UiO-67(Rho) exhibited fluorescence signals derived from both the Rho encapsulated in UiO-67 pores and the Atto 647N used to label the cell-derived coating, therefore demonstrating that UiO-67 were successfully coated with (F)CSMs.

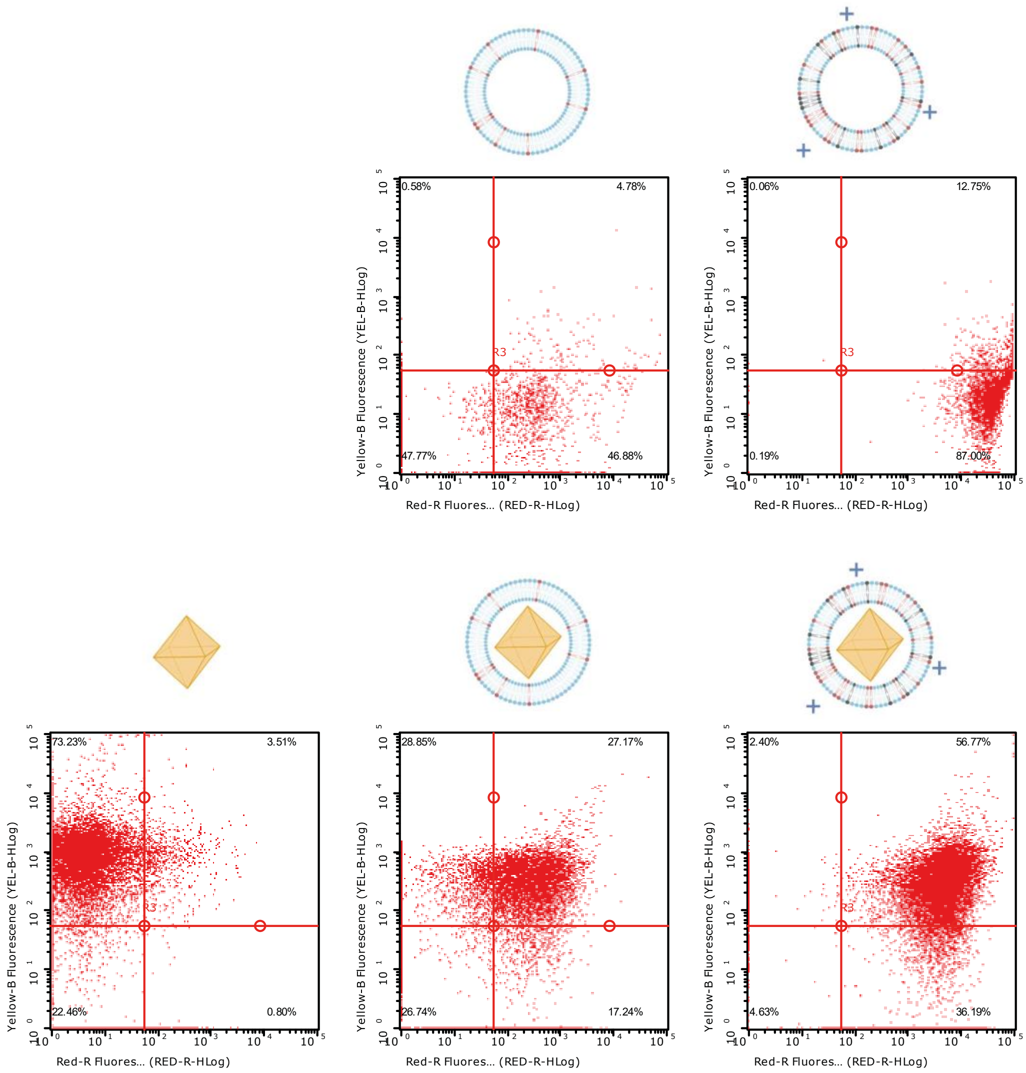

Figure 3-81 *UiO-67@(F)CSM NPs population analysis using flow cytometry.*

3.4.2.2. *In vitro* studies of UiO-67 coated with (F)CSMs

To understand the interaction of (F)CSMs coating with cells and how it can promote the internalization of UiO-67, different uptake experiments were conducted. UiO-67 were loaded with Cresyl Violet (CV), which is a basophilic dye traditionally used as staining method for nervous tissues. To highlight the nuclei heterochromatin, CV binds avidly to nucleic acids, thus resulting toxic at high concentrations.

For this reason, preliminary *in vitro* toxicity tests were performed to establish viable times and concentrations (**Figure 3-82**).

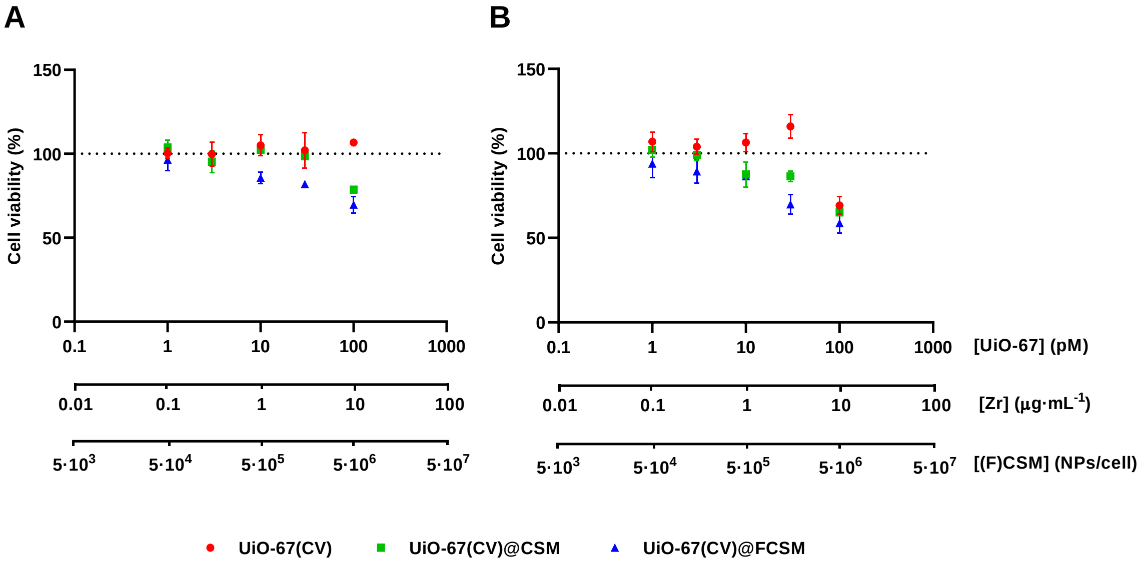

Figure 3-82 *Toxicity analysis of UiO-67(CV) (in red), UiO-67(CV)@CSM (in green), and UiO-67(CV)@FCSM (in blue) incubated in A549 cells for (A) 1 hour and (B) 3 hours.*

As shown in **Figure 3-82**, when loaded into UiO-67@(F)CSM, CV resulted to affect cell viability more than when loaded into bare UiO-67 and in a time-dependent manner (**Figure 3-82** A vs B). This can be due to the presence of the biomimetic coating itself, which facilitates the internalization of the entire nanosystem compared to the same nanosystem without the coating. Moreover, at short incubation times (**Figure 3-82** A), the toxicity caused by CV is even more evident, as a result of the fusogenic activity of (F)CSMs, which favor the uptake of the NPs in a receptor-mediated endocytosis-independent way.

Based on the toxicity assays performed, 1 hour was selected as the maximum time point to highlight the fusogenic behavior of FCSMs and 40 pM was set as the maximum concentration to study UiO-67 uptake, which corresponded to about $3.5 \cdot 10^{10}$ NPs·mL^{-1} ($3.5 \cdot 10^{5}$ NPs/cell).

Then, to assess the biomimetic features provided by the cell membrane-coating around UiO-67 nanoMOFs and to investigate their beneficial attributes in NPs internalization in cells, flow cytometry, ICP-OES, and fluorescence microscopy analysis were performed.

A549 cells were cultured and exposed to fluorescent (F)CSMs-coated UiO-67(CV) as described in Section 2.5.1. After 10 minutes and 1 hour, cells were harvested, recollected, and CV fluorescence was measured with flow cytometry. As illustrated in **Figure 3-83** A, NPs uptake in A549 cells was higher when exposed to UiO-67(CV)-coated nanosystems, indicating that the biomimetic coating favors the internalization the NPs inside cells. Moreover, when the coating was modified to obtain fusogenic CSMs, the uptake resulted even doubled after only 10 minutes incubation.

Whereas, for the uptake experiments measured with ICP-OES, the UiO-67 NPs used did not present any fluorescent dye, since the instrument can detect chemical elements, such as Zr-based MOFs. As shown in **Figure 3-83** B, UiO-67 internalization in A549 cells was higher when they presented the biomimetic coating. In addition, lipids modification of the biomimetic coating increased the uptake by 7 times compared to bare UiO-67 after 1 hour incubation.

Taken together, these results suggest that the biomimetic coating promotes the internalization of UiO-67 NPs and that the fusogenic ability of the proposed biomimetic modified coating is an extremely fast endocytic process, due to the lipids composition used to fabricate it.

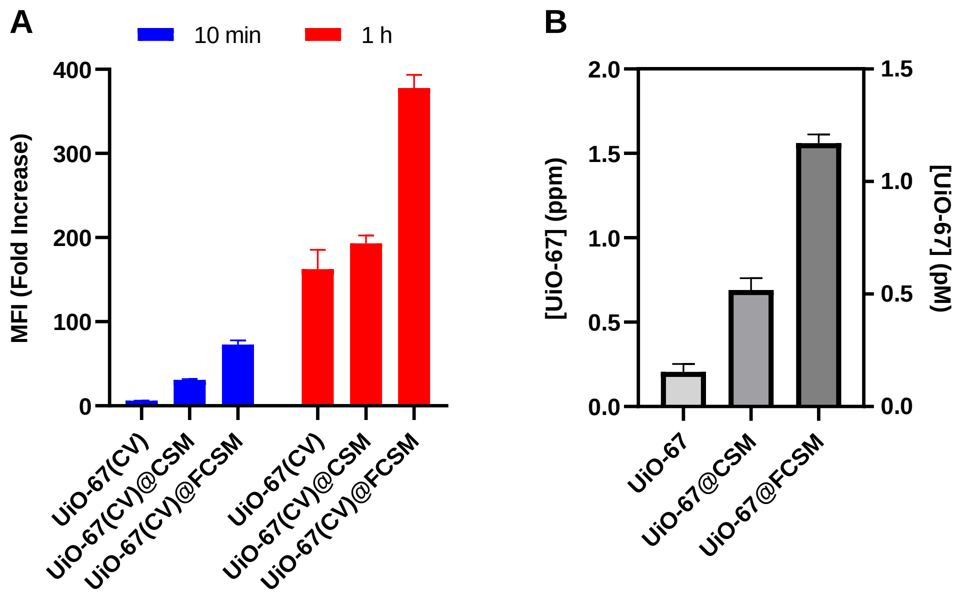

***Figure 3-83** UiO-67@(F)CSM uptake in A549 cells measured with (A) flow cytometry and (B) ICP-OES.*

Fluorescence microscopy analysis were performed to further investigate UiO-67(CV) uptake in A549 cells and how the biomimetic coating could affect the internalization pathway (**Figure 3-84** and **Figure 3-85**). Bare UiO-67(CV) showed very low fluorescent signal compared to UiO-67(CV) coated with (F)CSMs. Moreover, the two fluorescent signals spatially overlapped in the case of UiO-67(CV)@CSM, suggesting the co-localization of the two fluorophores (CV and Atto 488) which might indicate an endosome-mediated internalization pathway. While this co-localization was not observed in the case of UiO-67(CV)@FCSM, denoting a totally different internalization pathway, probably triggered by the fusion of the biomimetic nanosystem with the cell plasma membranes and the subsequent release of the UiO-67(CV) inside the cytoplasm.

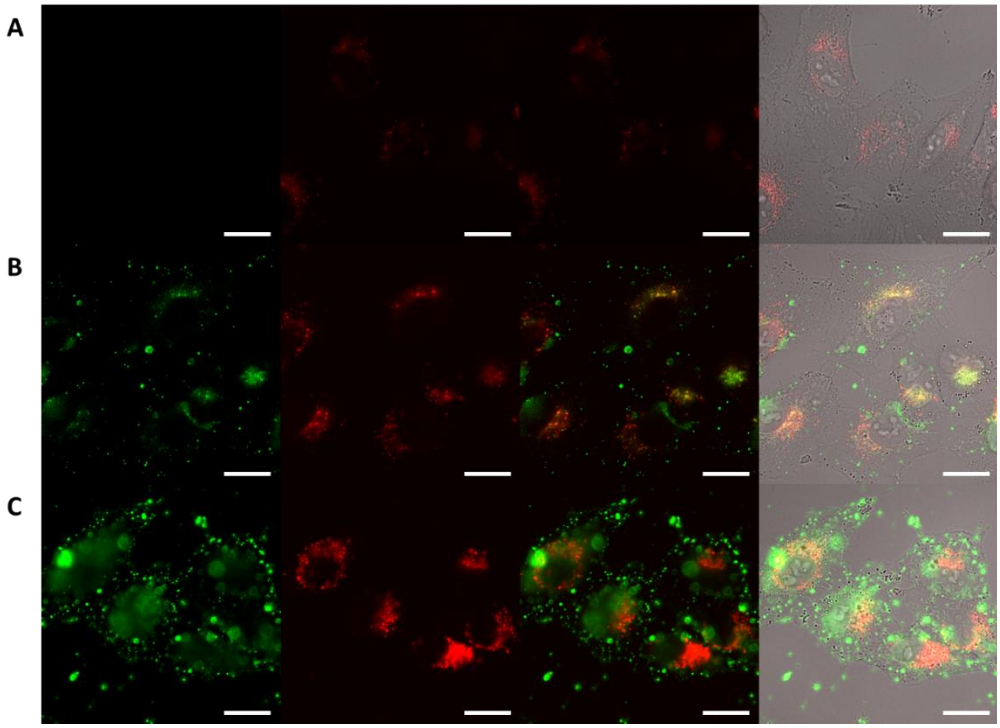

Figure 3-84 Fluorescence microscopy images of A549 cells incubated with (A) UiO-67(CV), (B) UiO-67(CV)@CSM, and (C) UiO-67(CV)@FCSM for 10 minutes. For each panel, from left to right, images show the fluorescence signal of (F)CSMs (in green), UiO-67(CV) (in red), overlays of the two fluorescence signals (green + red), and both merged with brightfield. Scale bars = 20 µm.

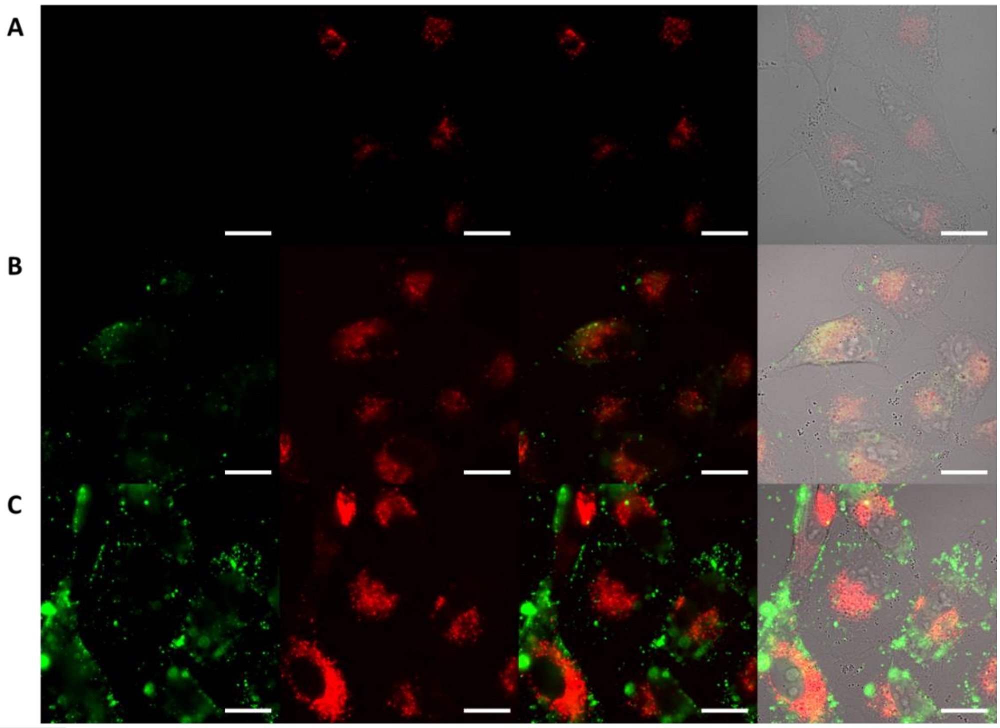

Figure 3-85 Fluorescence microscopy images of A549 cells incubated with (A) UiO-67(CV), (B) UiO-67(CV)@CSM, and (C) UiO-67(CV)@FCSM for 1 hour. For each panel, from left to right, images show the fluorescence signal of (F)CSMs (in green), UiO-67(CV) (in red), overlays of the two fluorescence signals (green + red), and both merged with brightfield. Scale bars = 20 µm.

As mentioned, the internalization driven by the fusogenic activity of the lipid-engineered coating is likely an extremely fast process. To better understand the process undergoing the internalization pathway promoted by the fusogenic coating, A549 cells were exposed to high concentrations of UiO-67(CV)@FCSM for 2 minutes and fluorescence microscopy 3D analysis of a portion of cells was performed.

As shown in **Figure 3-86**, the Atto 647N fluorescence signal (FCSMs, in magenta) surrounds the cells, indicating a fast (only 2 minutes of exposure) interaction with cell plasma membrane and probably the fusion with it. While the CV fluorescence signal (UiO-67, here in cyan) reaches the inner part of the cells, suggesting a cytosolic internalization of the NPs.

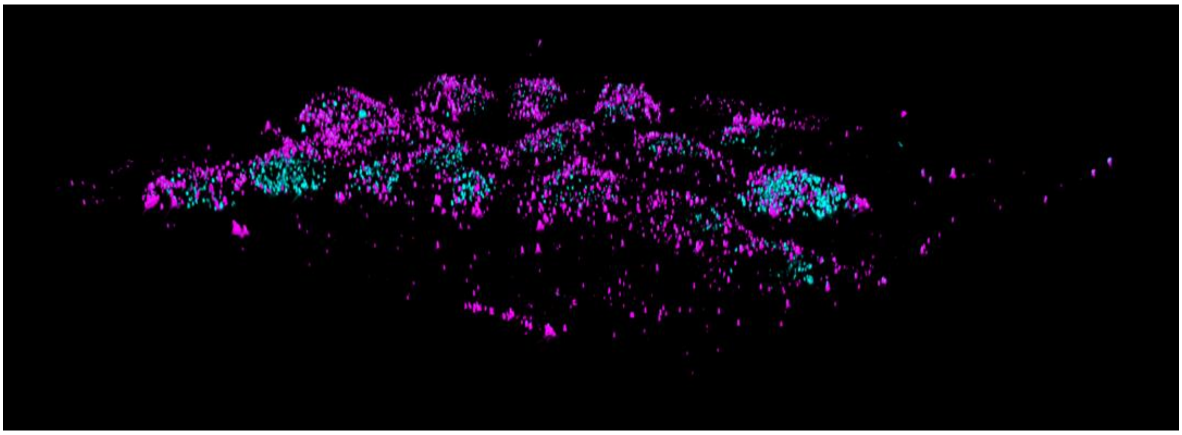

Figure 3-86 *Fluorescence microscopy 3D representation (Z-stack) of A549 cells exposed to UiO-67@FCSM for 2 minutes.*

Overall, these results indicate that the fusogen-like engineering approach employed to modify the biomimetic coating enables the fast and efficient release of cargos, including NPs, inside the cell cytoplasm, avoiding the endolysosomal entrapment and, thus, representing a valid strategy for drug delivery applications.

3.4.2.3. Engineered cloaked UiO-67 for intracellular drug delivery

Therefore, carboplatin (CaPt), a chemotherapeutic used for the treatment of several forms of cancer (ovarian cancer, lung cancer, brain cancer, and neuroblastoma, among others), was used as molecule loaded into UiO-67 pores and evaluated *in vitro* as potential drug delivered by fusogenic biomimetic coated-MOFs.

First, CaPt was loaded into UiO-67 nanoMOFs following the procedure described in Section 2.3.1.2. To prepare (F)CSMs-coated UiO-67(CaPt), the synthesis method utilized throughout this chapter was employed. Nevertheless, the UiO-67(CaPt)@(F)CSM solution, and especially the fusogenic coated MOFs, visibly began to aggregate right after the core-coating mixture was prepared (**Figure 3-87**). This could be due to the interaction between the lipids and the CaPt that partially remained attached to the UiO-67 surface.

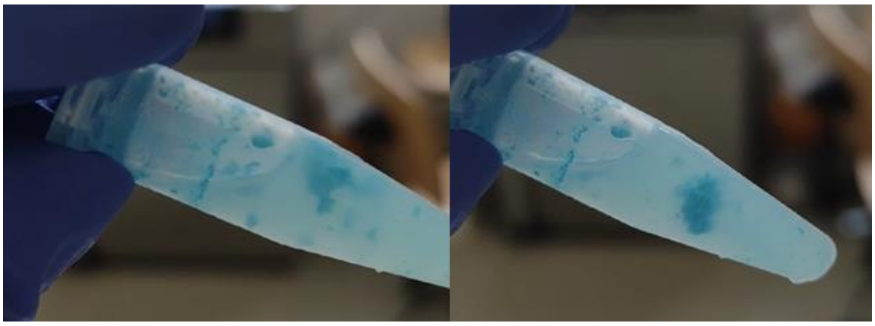

Figure 3-87 Pictures of aggregated UiO-67(CaPt)@FCSM prepared following the synthesis method utilized throughout this chapter.

Therefore, a slightly different preparation method was employed. Once prepared A549-derived CSMs, the previously obtained CaPt-loaded UiO-67 was slowly added to the solution with a 1:5 (core:coating) mixing ratio and the suspension was subjected to ultrasound for 15 minutes. Then, either the fluorescently labeled DOPE Atto 647N or the lipids mixture of neutral lipid DOPE, positively charged lipid DOTAP, and fluorescently labeled DOPE Atto 647N was added to the UiO-67@CSM solution, sonicated and extruded through polycarbonate membranes to favor lipids intercalation in (F)CSMs lipidic bilayer (**Figure 3-88**).

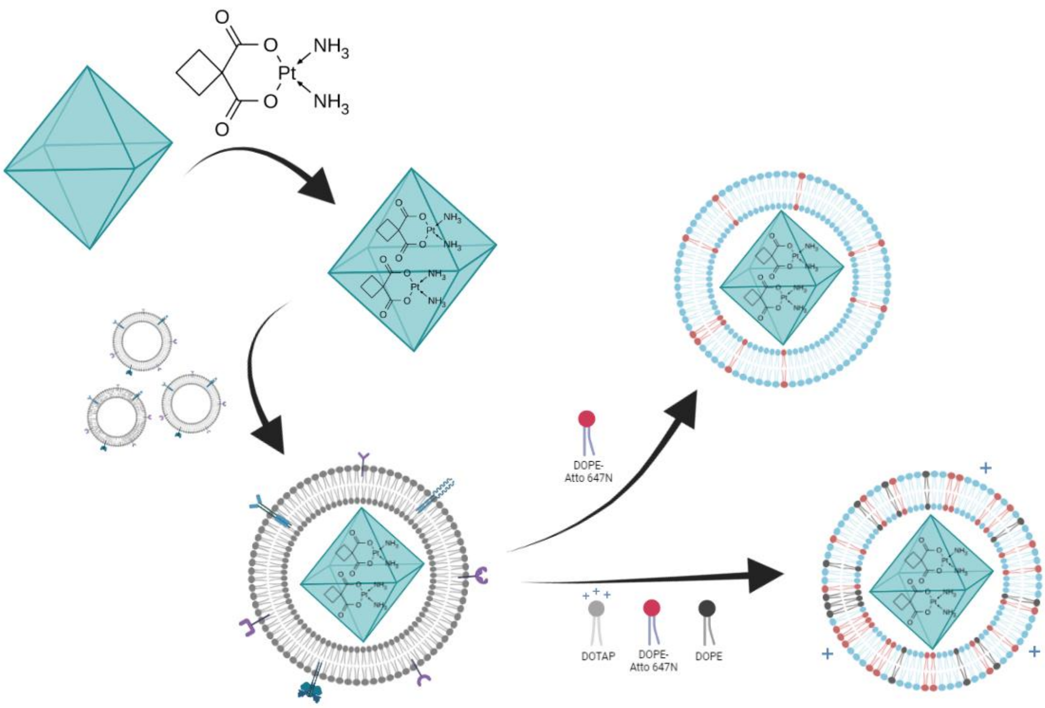

Figure 3-88 Schematic representation of UiO-67(CaPt)@(F)CSM synthesis method.

Size distribution measurements (NTA) of CSMs, UiO-67(CaPt), UiO-67(CaPt)@CSM, and UiO-67(CaPt)@FCSM are reported in **Figure 3-89** and **Table 3-27**.

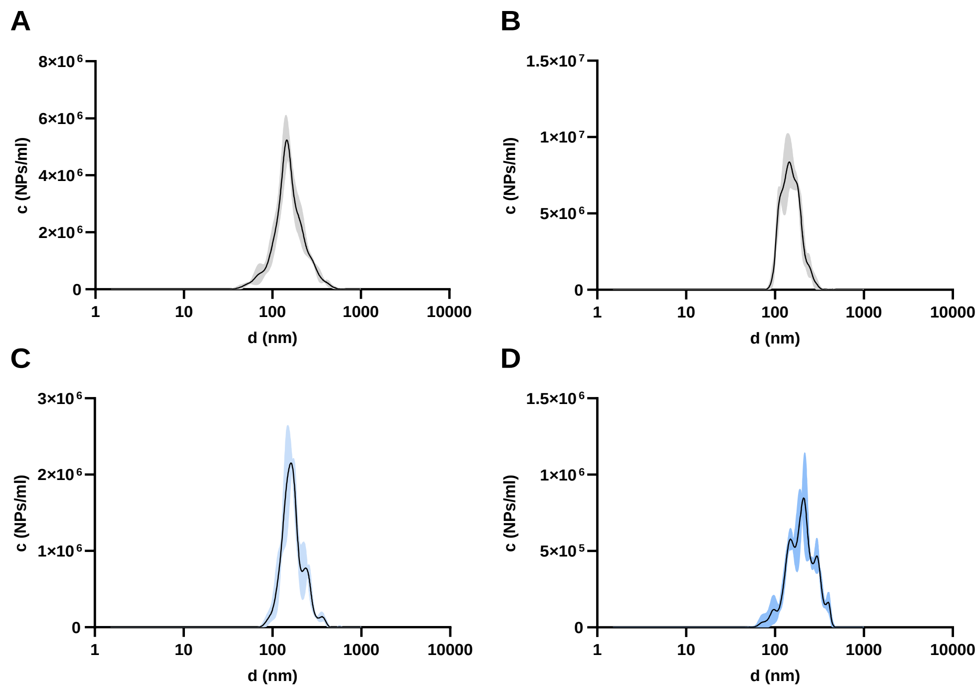

__Figure 3-89__ Size distribution measurements (NTA) of (A) CSMs, (B) UiO-67(CaPt), (C) UiO-67(CaPt)@CSM, and (D) UiO-67(CaPt)@FCSM.

Sample	d (mean) (nm)	d (mode) (nm)	c (NPs/mL)
CSM	193.4 ± 2.3	146.2 ± 2.7	6.04E+11
UiO-67(CaPt)	165.8 ± 0.6	152.4 ± 10.1	4.18E+12
UiO-67(CaPt)@CSM	192.3 ± 1.8	161.3 ± 7.1	2.17E+11
UiO-67(CaPt)@FCSM	235.3 ± 2.1	202.0 ± 7.3	1.33E+11

__Table 3-27__ NTA analysis of UiO-67(CaPt) with and without (F)CSMs coating depicted in __Figure 3-89__.

To assess the coating efficiency of the obtained UiO-67(CaPt)@(F)CSM, ζ potential measurements of all the samples were performed. As shown in **Figure 3-90** and **Table 3-28**, UiO-67(CaPt) show a positive surface charge (~ 9 mV), while when coated with either CSMs or FCSMs, they show a negative ζ potential (around – 23 mV), which correspond to the ζ potential of the empty (F)CSMs. A negative surface charge was predictable since cell plasma membrane is generally negatively charged[373] and the shift in the ζ potential of UiO-67(CaPt) towards a negative value when coated with the cell membrane-derived coating confirms that the CaPt-loaded MOFs were successfully coated with the cell-membrane cloaking approach used.

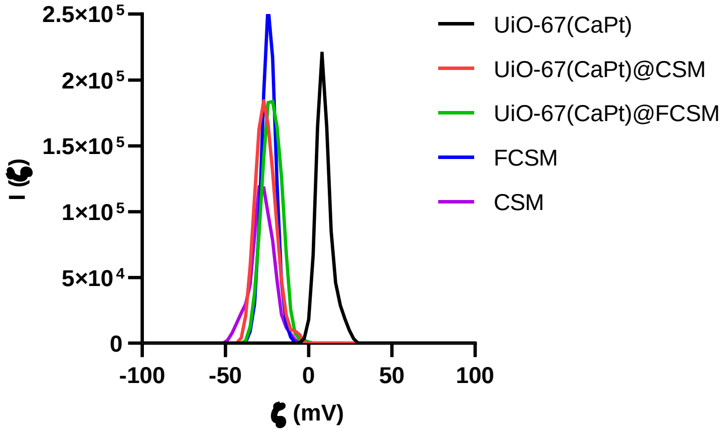

Figure 3-90 *ζ potential measurements of UiO-67@(F)CSM.*

Sample	ζ (mV)
UiO-67(CaPt)	+ 9.38 ± 0.20
CSM	- 23.57 ± 0.97
FCSM	- 23.27 ± 1.21
UiO-67(CaPt)@CSM	- 25.83 ± 1.17
UiO-67(CaPt)@FCSM	- 26.93 ± 1.16

Table 3-28 *ζ potential measurements of UiO-67@(F)CSM.*

Once prepared and characterized, UiO-67(CaPt)@(F)CSM were employed in preliminary *in vitro* toxicity assays to understand the behavior of the cell membrane-cloaked MOF and, in the future, to optimize the system for actual drug delivery applications.

The aim was to fabricate biomimetic coated-MOFs engineered to reach the intracellular milieu by overcoming the endolysosomal entrapment. For this reason, the fusogen-like approach proposed throughout this thesis was employed to modify the lipids composition of the cell membrane-derived coating to promote the interaction and the fusion of the nanosystem with cells plasma membrane.

As mentioned, UiO-67 represent an excellent choice for a core-shell nanostructured system because of its unique porous structures, which allow the loading of large quantities of cargo, and controlled released properties, critical in drug delivery applications.

Toxicity *in vitro* assays (MTT) were performed to evaluate the efficiency of the core-shell nanosystem loaded with the chemotherapeutic CaPt (**Figure 3-91**). Here, A549 cells, a human lung cancer cell line, were used both as source cells for the biomimetic coating fabrication and for the toxicity assays performed. This choice was made based on the exceptional homotypic targeting capabilities of A549-derived nanovesicles, already assessed during this thesis.

Two different time points were set to evaluate the toxicity of UiO-67(CaPt)@(F)CSM: a short exposure time (10 minutes), assuming that the fusogen-like approach is a quite fast process, and 24 hours, considering the release kinetics of the loaded drug from the UiO-67 pores. Thus, after the short incubation time, A549 cells were washed and fresh cDMEM was added to allow the release of the cargo. After 24 hours, cells were washed and MTT assay was performed.

As shown in **Figure 3-91**, free CaPt and CaPt-loaded UiO-67 present a similar toxicity profile at both incubation times, while in the case of the core-shell nanosystems (UiO-67(CaPt)@(F)CSM) the cell viability decreased at lower concentrations, indicating that the internalization of the drug was higher.

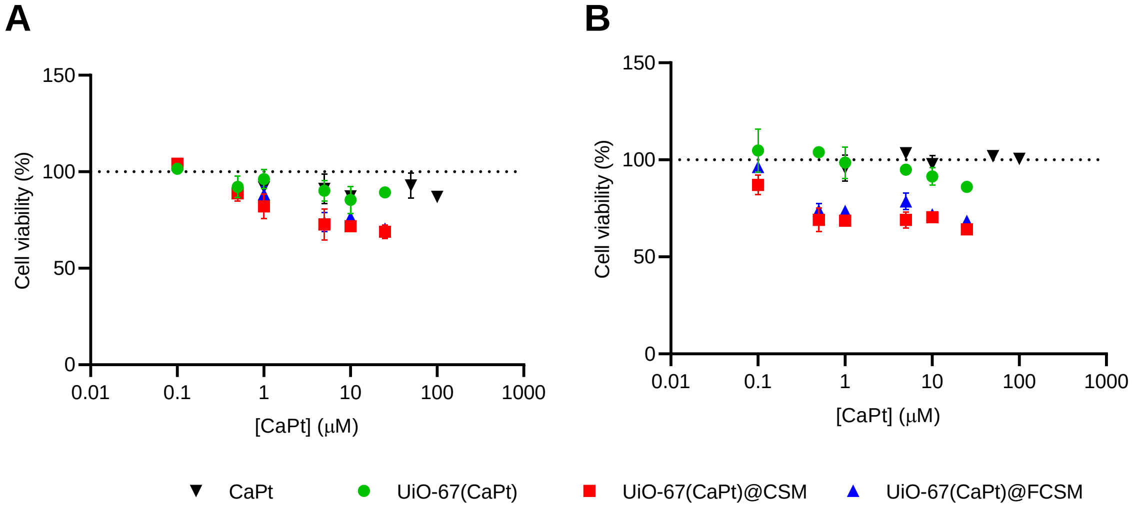

Figure 3-91 *Toxicity analysis of free CaPt (in black), UiO-67(CaPt) (in green), UiO-67(CaPt)@CSM (in red), and UiO-67(CaPt)@FCSM (in blue) incubated in A549 cells for (A) 10 minutes and (B) 24 hours.*

However, no significant difference between the two coating nanosystems was observed at these experimental conditions. Despite the promising results obtained from the characterization evaluation and the *in vitro* toxicity assays, further experiments and engineering modifications will be needed to evaluate the capabilities of the nanocarriers.

4. Conclusions

The experimental results presented in this doctoral thesis shed light on the multifaceted potential of cell membrane-derived nanovesicles (cellsomes, or CSMs) in diverse biomedical applications. The exploration of CSMs biomimetic properties has demonstrated their capacity as innovative nanocarriers for molecules and drugs, as well as advanced biomimetic coating for other types of NPs, capitalizing on their tissue-specific targeting capabilities and their ability to evade the immune response. The use of natural sources, such as cells, to fabricate CSMs has been proved to be a pivotal advantage in this endeavor. The phospholipid bilayer is capable of retaining both hydrophilic and hydrophobic molecules, due to its amphiphilic nature. In addition, the lipidic composition itself represents an ideal biocompatible material, as it is originated from natural sources (cells). Moreover, the natural surface pattern of living cells, preserved in CSMs synthesis process, is the true regulator in all the nano-bio interactions. By harnessing the innate biological properties of cell plasma membrane, CSMs offer a versatile platform for delivering cargos with enhanced efficiency and precision.

A diverse range of cell types, both healthy and tumoral cell lines, were strategically chosen as the source of cell membranes, leading to the development of a huge collection of different biomimetic nanovesicles. These CSMs exhibit several key properties, such as inherent self-recognition through homotypic targeting, the ability to avoid early detection by the immune cells, and the capacity to circumvent common challenges associated with NPs interaction with cells.

Specifically, Chapter 1 provided a solid foundation by comprehensively characterizing CSMs and establishing their unique homotypic targeting and internalization attributes. Here, different engineering approaches have been developed to better understand the potential of these cell membrane-derived nanovesicles in biomedical applications and how they can be optimized for this purpose.

Leveraging CSMs natural properties, Chapter 2 demonstrated the transformative potential of platelet-derived nanovesicles for ischemic stroke therapy. Moreover, it emphasized the critical aspect of optimizing the storage conditions of nanoformulations. This optimization is essential in order to develop a robust and effective treatment strategy for ischemic stroke, harnessing the unique attributes of CSMs to protect and preserve current standard treatments such as recombinant tPA during time, thus contributing to maximize the therapeutic impact of CSMs in the context of ischemic stroke and presenting a paradigm shift in treatment strategies.

In Chapter 3, the introduction of fusogenic CSMs (FCSMs) showcased the benefits of engineering cell membrane components to facilitate efficient intracellular cargo release for gene therapy applications. Here, CRISPR/Cas system was used as a pivotal tool in advancing gene editing possibilities. This strategic approach, which combined the CRISPR/Cas complex and the fusogenic capabilities of the engineered biomimetic nanovesicles, laid the foundation for unlocking new dimensions in gene editing applications by employing two different types of Cas proteins (Cas9 and Cas13d). Specifically, the Cas9 system was utilized as a model to pave the way for the development of nanovesicles equipped with Cas13d, opening doors for innovative gene editing approaches in antiviral strategies. This chapter presents a comprehensive exploration into the intricate integration of these advanced gene editing tools within the realm of fusogenic biomimetic nanocarriers, setting the stage for precise and targeted genetic interventions in disease management.

Chapter 4 embraced a comprehensive perspective, exploring the application of both CSMs and FCSMs as biocompatible coatings for synthetic NPs, encompassing two distinct types of NPs (polystyrene NPs and metal-organic frameworks) to unlock their full potential. The initial application of PSNPs served as a model, paving the way for the subsequent development of coatings for MOFs NPs, thereby capitalizing on the distinct advantages offered by these advanced nanomaterials. The optimization of the coating protocol was conducted with precision to attain core-shell nanostructures that embody both biomimetic properties and fusogenic abilities, thus enhancing their capacity for targeted cellular interactions and intracellular cargo delivery. Ultimately, these MOFs with tailored coatings were employed to achieve cytoplasmic release of carboplatin, offering a glimpse into the potential of this strategy for controlled drug delivery. It is important to note that these findings mark the preliminary stages of research, highlighting the exciting prospects that lie ahead for leveraging cell membrane-coated MOFs in the field of biomedical applications.

Overall, this comprehensive study highlights the versatility and promise of CSMs as a novel platform for addressing key challenges in modern medicine, ranging from targeted drug delivery to gene therapy. The successful attainment of the outlined objectives paves the way for further research and development in the expanding field of nanomedicine, offering a pathway towards more effective and personalized biomedical interventions.

References

1. Bayda, S.; Adeel, M.; Tuccinardi, T.; Cordani, M.; Rizzolio, F., The History of Nanoscience and Nanotechnology: From Chemical-Physical Applications to Nanomedicine. *Molecules* **2019,** *25* (1).

2. Chavda, V. P., Nanotherapeutics and Nanobiotechnology. In *Applications of Targeted Nano Drugs and Delivery Systems*, 2019; pp 1-13.

3. Feynman, R. P., There's plenty of room at the bottom. *JMEMS* **1992,** *1* (1).

4. Bharathala, S.; Sharma, P., Biomedical Applications of Nanoparticles. In *Nanotechnology in Modern Animal Biotechnology*, 2019; pp 113-132.

5. https://www.nano.gov.

6. Talebian, S.; Rodrigues, T.; das Neves, J.; Sarmento, B.; Langer, R.; Conde, J., Facts and Figures on Materials Science and Nanotechnology Progress and Investment. *ACS Nano* **2021,** *15* (10), 15940-15952.

7. Prasad, M.; Lambe, U. P.; Brar, B.; Shah, I.; J, M.; Ranjan, K.; Rao, R.; Kumar, S.; Mahant, S.; Khurana, S. K.; Iqbal, H. M. N.; Dhama, K.; Misri, J.; Prasad, G., Nanotherapeutics: An insight into healthcare and multi-dimensional applications in medical sector of the modern world. *Biomed Pharmacother* **2018,** *97*, 1521-1537.

8. Domingues, C.; Santos, A.; Alvarez-Lorenzo, C.; Concheiro, A.; Jarak, I.; Veiga, F.; Barbosa, I.; Dourado, M.; Figueiras, A., Where Is Nano Today and Where Is It Headed? A Review of Nanomedicine and the Dilemma of Nanotoxicology. *ACS Nano* **2022**.

9. Wagner, V.; Dullaart, A.; Bock, A.-K.; Zweck, A., The emerging nanomedicine landscape. *Nat Biotechnol* **2006,** *24* (10), 1211-1217.

10. Zhang, C.; Yan, L.; Wang, X.; Zhu, S.; Chen, C.; Gu, Z.; Zhao, Y., Progress, challenges, and future of nanomedicine. *Nano Today* **2020,** *35*.

11. Rizzo, L. Y.; Theek, B.; Storm, G.; Kiessling, F.; Lammers, T., Recent progress in nanomedicine: therapeutic, diagnostic and theranostic applications. *Curr Opin Biotechnol* **2013,** *24* (6), 1159-66.

12. Kunjachan, S.; Ehling, J.; Storm, G.; Kiessling, F.; Lammers, T., Noninvasive Imaging of Nanomedicines and Nanotheranostics: Principles, Progress, and Prospects. *Chem Rev* **2015,** *115* (19), 10907-37.

13. Pallotta, A.; Clarot, I.; Sobocinski, J.; Fattal, E.; Boudier, A., Nanotechnologies for Medical Devices: Potentialities and Risks. *ACS Appl Bio Mater* **2019,** *2* (1), 1-13.

14. Bobo, D.; Robinson, K. J.; Islam, J.; Thurecht, K. J.; Corrie, S. R., Nanoparticle-Based Medicines: A Review of FDA-Approved Materials and Clinical Trials to Date. *Pharm Res* **2016,** *33* (10), 2373-87.

15. Chen, H.; Gu, Z.; An, H.; Chen, C.; Chen, J.; Cui, R.; Chen, S.; Chen, W.; Chen, X.; Chen, X.; Chen, Z.; Ding, B.; Dong, Q.; Fan, Q.; Fu, T.; Hou, D.; Jiang, Q.; Ke, H.; Jiang, X.; Liu, G.; Li, S.; Li, T.; Liu, Z.; Nie, G.; Ovais, M.; Pang, D.; Qiu, N.; Shen, Y.; Tian, H.; Wang, C.; Wang, H.; Wang, Z.; Xu, H.; Xu, J.-F.; Yang, X.; Zhu, S.; Zheng, X.; Zhang, X.; Zhao, Y.; Tan, W.; Zhang, X.; Zhao, Y., Precise nanomedicine for intelligent therapy of cancer. *Science China Chemistry* **2018,** *61* (12), 1503-1552.

16. Li, C.; Wang, J.; Wang, Y.; Gao, H.; Wei, G.; Huang, Y.; Yu, H.; Gan, Y.; Wang, Y.; Mei, L.; Chen, H.; Hu, H.; Zhang, Z.; Jin, Y., Recent progress in drug delivery. *Acta Pharm Sin B* **2019,** *9* (6), 1145-1162.

17. Adepu, S.; Ramakrishna, S., Controlled Drug Delivery Systems: Current Status and Future Directions. *Molecules* **2021,** *26* (19).

18. Hardenia, A.; Maheshwari, N.; Hardenia, S. S.; Dwivedi, S. K.; Maheshwari, R.; Tekade, R. K., Scientific Rationale for Designing Controlled Drug Delivery Systems. In *Basic Fundamentals of Drug Delivery*, 2019; pp 1-28.

19. Albalawi, F.; Hussein, M. Z.; Fakurazi, S.; Masarudin, M. J., Engineered Nanomaterials: The Challenges and Opportunities for Nanomedicines. *Int J Nanomedicine* **2021,** *16*, 161-184.

20. Feliu, N.; Fadeel, B., Nanotoxicology: no small matter. *Nanoscale* **2010,** *2* (12), 2514-20.

21. Nystrom, A. M.; Fadeel, B., Safety assessment of nanomaterials: implications for nanomedicine. *J Control Release* **2012,** *161* (2), 403-8.

22. Rocks, L.; Dawson, K. A., The interaction between nanoparticles and biological barriers. *European Journal of Nanomedicine* **2014,** *6* (3).

23. Schneider, M.; Stracke, F.; Hansen, S.; Schaefer, U. F., Nanoparticles and their interactions with the dermal barrier. *Dermatoendocrinol* **2009,** *1* (4), 197-206.

24. Kreyling, W. G.; Hirn, S.; Möller, W.; Schleh, C.; Wenk, A.; Celik, G.; Lipka, J.; Schäffler, M.; Haberl, N.; Johnston, B. D.; Sperling, R.; Schmid, G.; Simon, U.; Parak, W. J.; Semmler-Behnke, M., Air-Blood Barrier Translocation of Tracheally Instilled Gold Nanoparticles Inversely Depends on Particle Size. *ACS Nano* **2014,** *8* (1), 222-233.

25. Alexis, F.; Pridgen, E.; Molnar, L. K.; Farokhzad, O. C., Factors Affecting the Clearance and Biodistribution of Polymeric Nanoparticles. *Mol. Pharm.* **2008,** *5* (4), 505-515.

26. Wohlfart, S.; Gelperina, S.; Kreuter, J., Transport of drugs across the blood-brain barrier by nanoparticles. *J Control Release* **2012,** *161* (2), 264-73.

27. Yoshida, S.; Hiyoshi, K.; Ichinose, T.; Takano, H.; Oshio, S.; Sugawara, I.; Takeda, K.; Shibamoto, T., Effect of nanoparticles on the male reproductive system of mice. *Int J of Andrology* **2008,** *32*, 337-342.

28. Herda, L. M.; Polo, E.; Kelly, P. M.; Rocks, L.; Hudecz, D.; Dawson, K. A., Designing the future of nanomedicine: current barriers to targeted brain therapeutics. *European Journal of Nanomedicine* **2014,** *6* (3).

29. Verma, A.; Stellacci, F., Effect of surface properties on nanoparticle-cell interactions. *Small* **2010,** *6* (1), 12-21.

30. Nel, A. E.; Madler, L.; Velegol, D.; Xia, T.; Hoek, E. M.; Somasundaran, P.; Klaessig, F.; Castranova, V.; Thompson, M., Understanding biophysicochemical interactions at the nano-bio interface. *Nat Mater* **2009,** *8* (7), 543-57.

31. Meng, H.; Leong, W.; Leong, K. W.; Chen, C.; Zhao, Y., Walking the line: The fate of nanomaterials at biological barriers. *Biomaterials* **2018,** *174*, 41-53.

32. Lademann, J.; Richter, H.; Teichmann, A.; Otberg, N.; Blume-Peytavi, U.; Luengo, J.; Weiss, B.; Schaefer, U. F.; Lehr, C. M.; Wepf, R.; Sterry, W., Nanoparticles--an efficient carrier for drug delivery into the hair follicles. *Eur J Pharm Biopharm* **2007,** *66* (2), 159-64.

33. Powell, J. J.; Faria, N.; Thomas-McKay, E.; Pele, L. C., Origin and fate of dietary nanoparticles and microparticles in the gastrointestinal tract. *J Autoimmun* **2010,** *34* (3), J226-33.

34. Turner, J. R., Intestinal mucosal barrier function in health and disease. *Nat Rev Immunol* **2009,** *9* (11), 799-809.

35. Kreyling, W. G.; Semmler-Behnke, M.; Takenaka, S.; Möller, W., Differences in the Biokinetics of Inhaled Nano- versus Micrometer-Sized Particles. *Acc. Chem. Res.* **2013,** *46* (3), 714-722.

36. Wang, X.; Duch, M. C.; Mansukhani, N.; Ji, Z.; Liao, Y. P.; Wang, M.; Zhang, H.; Sun, B.; Chang, C. H.; Li, R.; Lin, S.; Meng, H.; Xia, T.; Hersam, M. C.; Nel, A. E., Use of a pro-fibrogenic mechanism-based predictive toxicological approach for tiered testing and decision analysis of carbonaceous nanomaterials. *ACS Nano* **2015,** *9* (3), 3032-43.

37. Pietroiusti, A.; Campagnolo, L.; Fadeel, B., Interactions of engineered nanoparticles with organs protected by internal biological barriers. *Small* **2013,** *9* (9-10), 1557-72.

38. Choi, H. S.; Ashitate, Y.; Lee, J. H.; Kim, S. H.; Matsui, A.; Insin, N.; Bawendi, M. G.; Semmler-Behnke, M.; Frangioni, J. V.; Tsuda, A., Rapid translocation of nanoparticles from the lung airspaces to the body. *Nat Biotechnol* **2010,** *28* (12), 1300-3.

39. Mc Carthy, D. J.; Malhotra, M.; O'Mahony, A. M.; Cryan, J. F.; O'Driscoll, C. M., Nanoparticles and the blood-brain barrier: advancing from in-vitro models towards therapeutic significance. *Pharm Res* **2015,** *32* (4), 1161-85.

40. Pardridge, W. M.; Eisenberg, J.; Yang, J., Human blood-brain barrier transferrin receptor. *Metabolism* **1987,** *36* (9), 892-895.

41. Olivier, J.-C., Drug Transport to Brain with Targeted Nanoparticles. *ASENT* **2005,** *2*, 108-119.

42. Wiley, D. T.; Webster, P.; Gale, A.; Davis, M. E., Transcytosis and brain uptake of transferrin-containing nanoparticles by tuning avidity to transferrin receptor. *Proc Natl Acad Sci U S A* **2013,** *110* (21), 8662-7.

43. Oberdorster, G.; Sharp, Z.; Atudorei, V.; Elder, A.; Gelein, R.; Kreyling, W.; Cox, C., Translocation of inhaled ultrafine particles to the brain. *Inhal Toxicol* **2004,** *16* (6-7), 437-45.

44. Ma, X.; Yang, X.; Wang, Y.; Liu, J.; Jin, S.; Li, S.; Liang, X.-J., Gold nanoparticles cause size-dependent inhibition of embryonic development during murine pregnancy. *Nano Research* **2018,** *11* (6), 3419-3433.

45. Izhaky, D.; Pecht, I., What else can the immune system recognize? *Proc. Natl. Acad. Sci. USA* **1998,** *95*, 11509-11510.

46. Boraschi, D.; Italiani, P.; Palomba, R.; Decuzzi, P.; Duschl, A.; Fadeel, B.; Moghimi, S. M., Nanoparticles and innate immunity: new perspectives on host defence. *Semin Immunol* **2017,** *34*, 33-51.

47. Meng, H.; Xue, M.; Xia, T.; Ji, Z.; Tarn, D. Y.; Zink, J. I.; Nel, A. E., Use of Size and a Copolymer Design Feature To Improve the Biodistribution and the Enhanced Permeability and Retention Effect of Doxorubicin- Loaded Mesoporous Silica Nanoparticles in a Murine Xenograft Tumor Model. *ACS Nano* **2011,** *5* (5), 4131-4144.

48. Lundqvist, M.; Stigler, J.; Elia, G.; Lynch, I.; Cedervall, T.; Dawson, K. A., Nanoparticle size and surface properties determine the protein corona with possible implications for biological impacts. *Proc Natl Acad Sci U S A* **2008,** *105* (38), 14265-14270.

49. Casals, E.; Pfaller, T.; Duschl, A.; OOstingh, G. J.; Puntes, V., Time evolution of the nanoparticle protein corona. *ACS Nano* **2010,** *4* (7), 3623-3632.

50. Monopoli, M. P.; Pitek, A. S.; Lynch, I.; Dawson, K. A., Formation and characterization of the nanoparticle-protein corona. *Methods Mol Biol* **2013,** *1025*, 137-55.

51. Mahon, E.; Salvati, A.; Baldelli Bombelli, F.; Lynch, I.; Dawson, K. A., Designing the nanoparticle-biomolecule interface for "targeting and therapeutic delivery". *J Control Release* **2012,** *161* (2), 164-74.

52. Bigini, P.; Gobbi, M.; Bonati, M.; Clavenna, A.; Zucchetti, M.; Garattini, S.; Pasut, G., The role and impact of polyethylene glycol on anaphylactic reactions to COVID-19 nano-vaccines. *Nat Nanotechnol* **2021,** *16* (11), 1164-1175.

53. Chen, B. M.; Cheng, T. L.; Roffler, S. R., Polyethylene Glycol Immunogenicity: Theoretical, Clinical, and Practical Aspects of Anti-Polyethylene Glycol Antibodies. *ACS Nano* **2021,** *15* (9), 14022-14048.

54. Swierczewska, M.; Han, H. S.; Kim, K.; Park, J. H.; Lee, S., Polysaccharide-based nanoparticles for theranostic nanomedicine. *Adv Drug Deliv Rev* **2016,** *99* (Pt A), 70-84.

55. Liu, Z.; Jiao, Y.; Wang, Y.; Zhou, C.; Zhang, Z., Polysaccharides-based nanoparticles as drug delivery systems. *Adv Drug Deliv Rev* **2008,** *60* (15), 1650-62.

56. Smith, B. R.; Ghosn, E. E.; Rallapalli, H.; Prescher, J. A.; Larson, T.; Herzenberg, L. A.; Gambhir, S. S., Selective uptake of single-walled carbon nanotubes by circulating monocytes for enhanced tumour delivery. *Nat Nanotechnol* **2014,** *9* (6), 481-7.

57. Smith, D. M.; Simon, J. K.; Baker, J. R., Jr., Applications of nanotechnology for immunology. *Nat Rev Immunol* **2013,** *13* (8), 592-605.

58. Rodriguez, P. L.; Harada, T.; Christian, D. A.; Pantano, D. A.; Tsai, R. K.; Discher, D. E., Minimal “Self” Peptides That Inhibit Phagocytic Clearance and Enhance Delivery of Nanoparticles. *Science* **2013,** *339*.

59. Paatero, I.; Casals, E.; Niemi, R.; Ozliseli, E.; Rosenholm, J. M.; Sahlgren, C., Analyses in zebrafish embryos reveal that nanotoxicity profiles are dependent on surface-functionalization controlled penetrance of biological membranes. *Sci Rep* **2017,** *7* (1), 8423.

60. Monopoli, M. P.; Walczyk, D.; Campbell, A.; Elia, G.; Lynch, I.; Bombelli, F. B.; Dawson, K. A., Physical-chemical aspects of protein corona: relevance to in vitro and in vivo biological impacts of nanoparticles. *J Am Chem Soc* **2011,** *133* (8), 2525-34.

61. Corbo, C.; Molinaro, R.; Parodi, A.; Toledano Furman, N. E.; Salvatore, F.; Tasciotti, E., The impact of nanoparticle protein corona on cytotoxicity, immunotoxicity and target drug delivery. *Nanomedicine (Lond)* **2015**.

62. Arvizo, R. R.; Miranda, O. R.; Moyano, D. F.; Walden, C. A.; Giri, K.; Bhattacharya, R.; Robertson, J. D.; Rotello, V. M.; Reid, J. M.; Mukherjee, P., Modulating pharmacokinetics, tumor uptake and biodistribution by engineered nanoparticles. *PLoS One* **2011,** *6* (9), e24374.

63. Yao, C.; Wang, P.; Zhou, L.; Wang, R.; Li, X.; Zhao, D.; Zhang, F., Highly biocompatible zwitterionic phospholipids coated upconversion nanoparticles for efficient bioimaging. *Anal Chem* **2014,** *86* (19), 9749-57.

64. Hong, S.; Bielinska, A. U.; Mecke, A.; Keszler, B.; Beals, J. L.; Shi, X.; Balogh, L.; Orr, B. G.; Baker, J. R., Jr.; Banaszak Holl, M. M., Interaction of Poly(amidoamine) Dendrimers with Supported Lipid Bilayers and Cells: Hole Formation and the Relation to Transport. *Bioconjug Chem* **2004,** *15* (4), 774-782.

65. Kirchner, C.; Liedl, T.; Kudera, S.; Pellegrino, T.; Muñoz Javier, A.; Gaub, H. E.; Stölzle, S.; Fertig, N.; Parak, W. J., Cytotoxicity of Colloidal CdSe and CdSe/ZnS Nanoparticles. *Nano Lett.* **2005,** *5* (2), 331-338.

66. Roiter, Y.; Ornatska, M.; Rammohan, A. R.; Balakrishnan, J.; Heine, D. R.; Minko, S., Interaction of Nanoparticles with Lipid Membrane. *Nano Lett.* **2008,** *8* (3), 941-944.

67. Matsumura, Y.; Maeda, H., A New Concept for Macromolecular Therapeutics in Cancer Chemotherapy: Mechanism of Tumoritropic Accumulation of Proteins and the Antitumor Agent Smancs. *Cancer Res* **1986,** *46* (12), 6387-6392.

68. Torchilin, V., Tumor delivery of macromolecular drugs based on the EPR effect. *Adv Drug Deliv Rev* **2011,** *63* (3), 131-5.

69. Sindhwani, S.; Syed, A. M.; Ngai, J.; Kingston, B. R.; Maiorino, L.; Rothschild, J.; MacMillan, P.; Zhang, Y.; Rajesh, N. U.; Hoang, T.; Wu, J. L. Y.; Wilhelm, S.; Zilman, A.; Gadde, S.; Sulaiman, A.; Ouyang, B.; Lin,

Z.; Wang, L.; Egeblad, M.; Chan, W. C. W., The entry of nanoparticles into solid tumours. *Nat Mater* **2020,** *19* (5), 566-575.

70. Korsmeyer, R., Critical questions in development of targeted nanoparticle therapeutics. *Regen Biomater* **2016,** *3* (2), 143-7.

71. Huang, D.; Sun, L.; Huang, L.; Chen, Y., Nanodrug Delivery Systems Modulate Tumor Vessels to Increase the Enhanced Permeability and Retention Effect. *J Pers Med* **2021,** *11* (2).

72. Liu, X.; Lin, P.; Perrett, I.; Lin, J.; Liao, Y. P.; Chang, C. H.; Jiang, J.; Wu, N.; Donahue, T.; Wainberg, Z.; Nel, A. E.; Meng, H., Tumor-penetrating peptide enhances transcytosis of silicasome-based chemotherapy for pancreatic cancer. *J Clin Invest* **2017,** *127* (5), 2007-2018.

73. Liu, X.; Jiang, J.; Ji, Y.; Lu, J.; Chan, R.; Meng, H., Targeted drug delivery using iRGD peptide for solid cancer treatment. *Mol Syst Des Eng* **2017,** *2* (4), 370-379.

74. Liu, X.; Jiang, J.; Nel, A. E.; Meng, H., Major effect of transcytosis on nano drug delivery to pancreatic cancer. *Mol Cell Oncol* **2017,** *4* (4), e1335273.

75. Wilhelm, S.; Tavares, A. J.; SDai, Q.; Ohta, S.; Audet, J.; Dvorak, H. F.; Chan, W. C. W., Analysis of nanoparticle delivery to tumours. *Nat Rev Mater* **2016,** *1*, 1-12.

76. McNeil, S. E., Evaluation of nanomedicines: stick to the basics. *Nat Rev Mater* **2016,** *1*.

77. Bazak, R.; Houri, M.; El Achy, S.; Kamel, S.; Refaat, T., Cancer active targeting by nanoparticles: a comprehensive review of literature. *J Cancer Res Clin Oncol* **2015,** *141* (5), 769-84.

78. Dinauer, N.; Balthasar, S.; Weber, C.; Kreuter, J.; Langer, K.; von Briesen, H., Selective targeting of antibody-conjugated nanoparticles to leukemic cells and primary T-lymphocytes. *Biomaterials* **2005,** *26* (29), 5898-906.

79. Sinha, R.; Kim, G. J.; Nie, S.; Shin, D. M., Nanotechnology in cancer therapeutics: bioconjugated nanoparticles for drug delivery. *Mol Cancer Ther* **2006,** *5* (8), 1909-17.

80. Sapra, P.; Allen, T. M., Ligand-targeted liposomal anticancer drugs. *Progress in Lipid Research* **2003,** *42* (5), 439-462.

81. Dreaden, E. C.; Mwakwari, S. C.; Sodji, Q., H.; Oyelere, A. K.; El-Sayed, M. A., Tamoxifen-Poly(ethylene glycol)-Thiol Gold Nanoparticle Conjugates: Enhanced Potency and Selective Delivery for Breast Cancer Treatment. *Bioconjug Chem* **2009,** *20*, 2247-2253.

82. Chawla, J. S.; Amiji, M. M., Cellular Uptake and Concentrations of Tamoxifen Upon Administration in Poly(-caprolactone) Nanoparticles. *AAPS PharmSci* **2003,** *5* (3), 1-7.

83. Yang, P.; Sun, X.; Chiu, J.; Sun, H.; He, Q., Transferrin-Mediated Gold Nanoparticle Cellular Uptake. *Bioconjug Chem* **2005,** *16*, 494-496.

84. Parker, N.; Turk, M. J.; Westrick, E.; Lewis, J. D.; Low, P. S.; Leamon, C. P., Folate receptor expression in carcinomas and normal tissues determined by a quantitative radioligand binding assay. *Anal Biochem* **2005,** *338* (2), 284-93.

85. Dixit, V.; Van der Bossche, J.; Sherman, D. M.; Thompson, D. H.; Andres, R. P., Synthesis and Grafting of Thioctic Acid-PEG-Folate Conjugates onto Au Nanoparticles for Selective Targeting of Folate Receptor-Positive Tumor Cells. *Bioconjug Chem* **2006,** *17*, 603-609.

86. Attia, M. F.; Anton, N.; Wallyn, J.; Omran, Z.; Vandamme, T. F., An overview of active and passive targeting strategies to improve the nanocarriers efficiency to tumour sites. *J Pharm Pharmacol* **2019,** *71* (8), 1185-1198.

87. Meng, H.; Xia, T.; George, S.; Nel, A. E., A Predictive Toxicological Paradigm for the Safety Assessment of Nanomaterials. *ACS Nano* **2009,** *3* (7), 1620-1627.

88. Blanco, E.; Shen, H.; Ferrari, M., Principles of nanoparticle design for overcoming biological barriers to drug delivery. *Nat Biotechnol* **2015,** *33* (9), 941-51.

89. Lee, Y.; Fukushima, S.; Bae, Y.; Hiki, S.; Ishii, T.; Kataoka, K., A Protein Nanocarrier from Charge-Conversion Polymer in Response to Endosomal pH. *J. Am. Chem. Soc.* **2007,** *129* (17), 5362-5363.

90. Yuan, Y. Y.; Mao, C. Q.; Du, X. J.; Du, J. Z.; Wang, F.; Wang, J., Surface charge switchable nanoparticles based on zwitterionic polymer for enhanced drug delivery to tumor. *Adv Mater* **2012,** *24* (40), 5476-80.

91. Conner, S. D.; Schmid, L., Regulated portals of entry into the cell. *Nature* **2003,** *422*, 37-44.

92. Watson, P.; Jones, A. T.; Stephens, D. J., Intracellular trafficking pathways and drug delivery: fluorescence imaging of living and fixed cells. *Adv Drug Deliv Rev* **2005,** *57* (1), 43-61.

93. Xu, P.; Gullotti, E.; Tong, L.; Highley, C. B.; Errabelli, D. R.; Hasan, T.; Cheng, J.; Kohane, D. S.; Yeo, Y., Intracellular Drug Delivery by Poly(lactic-co-glycolic acid) Nanoparticles, Revisited. *Mol. Pharm.* **2008,** *6* (1), 190-201.

94. Swanson, J. A.; Watts, C., Macropinocytosis. *Trends Cell Biol.* **1995,** *5*, 424-428.

95. Patel, L. N.; Zaro, J. L.; Shen, W. C., Cell penetrating peptides: intracellular pathways and pharmaceutical perspectives. *Pharm Res* **2007,** *24* (11), 1977-92.

96. Walsh, M.; Tangney, M.; O'Neill, M. J.; Larkin, J. O.; Soden, D. M.; McKenna, S. L.; Darcy, R.; O'Sullivan, G. C.; O'Driscoll, C. M., Evaluation of Cellular Uptake and Gene Transfer Efficiency of Pegylated Poly-L-lysine Compacted DNA: Implications for Cancer Gene Therapy. *Mol. Pharm.* **2006,** *3* (6), 644-653.

97. Bao, G.; Bao, X. R., Shedding light on the dynamics of endocytosis and viral budding. *Proc Natl Acad Sci U S A* **2005,** *102* (29), 9997-9998.

98. Pelkmans, L.; Helenius, A., Endocytosis Via Caveolae. *Traffic* **2002,** *3*, 311-320.

99. Ehrlich, M.; Boll, W.; Van Oijen, A.; Hariharan, R.; Chandran, K.; Nibert, M. L.; Kirchhausen, T., Endocytosis by random initiation and stabilization of clathrin-coated pits. *Cell* **2004,** *118* (5), 591-605.

100. Wang, Z.; Tiruppathi, C.; Minshall, R. D.; Malik, A. B., Size and Dynamics of Caveolae Studied Using Nanoparticles in Living Endothelial Cells. *ACS Nano* **2009,** *3* (12), 4110-4116.

101. Le Roy, C.; Wrana, J. L., Clathrin- and non-clathrin-mediated endocytic regulation of cell signalling. *Nat Rev Mol Cell Biol* **2005,** *6* (2), 112-26.

102. Gould, G. W.; Lippincott-Schwartz, J., New roles for endosomes: from vesicular carriers to multi-purpose platforms. *Nat Rev Mol Cell Biol* **2009,** *10*, 287-292.

103. Luo, D.; Saltzman, W. M., Synthetic DNA delivery systems. *nat Biotechnol* **2000,** *18*, 33-37.

104. Sahay, G.; Alakhova, D. Y.; Kabanov, A. V., Endocytosis of nanomedicines. *J Control Release* **2010,** *145* (3), 182-95.

105. Simons, K.; Ikonen, E., Functional rafts in cell membranes. *Nature* **1997,** *387*, 569-572.

106. Levental, I.; Levental, K. R.; Heberle, F. A., Lipid Rafts: Controversies Resolved, Mysteries Remain. *Trends Cell Biol* **2020,** *30* (5), 341-353.

107. Diaz-Rohrer, B.; Levental, K. R.; Levental, I., Rafting through traffic: Membrane domains in cellular logistics. *Biochim Biophys Acta* **2014,** *1838* (12), 3003-3013.

108. Parton, R. G.; Simons, K., The multiple faces of caveolae. *Nat Rev Mol Cell Biol* **2007,** *8* (3), 185-94.

109. Verkade, P.; Harder, T.; Lafont, F.; Simons, K., Induction of Caveolae in the Apical Plasma Membrane of Madin-Darby Canine Kidney Cells. *Int. J. Cell Biol.* **1999,** *148* (4), 727-739.

110. Romer, W.; Berland, L.; Chambon, V.; Gaus, K.; Windschiegl, B.; Tenza, D.; Aly, M. R.; Fraisier, V.; Florent, J. C.; Perrais, D.; Lamaze, C.; Raposo, G.; Steinem, C.; Sens, P.; Bassereau, P.; Johannes, L., Shiga toxin induces tubular membrane invaginations for its uptake into cells. *Nature* **2007,** *450* (7170), 670-5.

111. Nativo, P.; Prior, I. A.; Brust, M., Uptake and Intracellular Fate of Surface- Modified Gold Nanoparticles. *ACS Nano* **2008,** *2* (8), 1639-1644.

112. Azevedo, C.; Macedo, M. H.; Sarmento, B., Strategies for the enhanced intracellular delivery of nanomaterials. *Drug Discov Today* **2018,** *23* (5), 944-959.

113. Martens, T. F.; Remaut, K.; Demeester, J.; De Smedt, S. C.; Braeckmans, K., Intracellular delivery of nanomaterials: How to catch endosomal escape in the act. *Nano Today* **2014,** *9* (3), 344-364.

114. Chou, L. Y.; Ming, K.; Chan, W. C., Strategies for the intracellular delivery of nanoparticles. *Chem Soc Rev* **2011,** *40* (1), 233-45.

115. Smith, S. A.; Selby, L. I.; Johnston, A. P. R.; Such, G. K., The Endosomal Escape of Nanoparticles: Toward More Efficient Cellular Delivery. *Bioconjug Chem* **2019,** *30* (2), 263-272.

116. Vermeulen, L. M. P.; De Smedt, S. C.; Remaut, K.; Braeckmans, K., The proton sponge hypothesis: Fable or fact? *Eur J Pharm Biopharm* **2018,** *129*, 184-190.

117. Selby, L. I.; Cortez-Jugo, C. M.; Such, G. K.; Johnston, A. P. R., Nanoescapology: progress toward understanding the endosomal escape of polymeric nanoparticles. *Wiley Interdiscip Rev Nanomed Nanobiotechnol* **2017,** *9* (5).

118. Manganiello, M. J.; Cheng, C.; Convertine, A. J.; Bryers, J. D.; Stayton, P. S., Diblock copolymers with tunable pH transitions for gene delivery. *Biomaterials* **2012,** *33* (7), 2301-9.

119. Dimitrov, D. S., Virus entry: molecular mechanisms and biomedical applications. *Nat Rev Microbiol* **2004,** *2* (2), 109-22.

120. Akita, H.; Kudo, A.; Minoura, A.; Yamaguti, M.; Khalil, I. A.; Moriguchi, R.; Masuda, T.; Danev, R.; Nagayama, K.; Kogure, K.; Harashima, H., Multi-layered nanoparticles for penetrating the endosome and nuclear membrane via a step-wise membrane fusion process. *Biomaterials* **2009,** *30* (15), 2940-9.

121. Kou, L.; Bhutia, Y. D.; Yao, Q.; He, Z.; Sun, J.; Ganapathy, V., Transporter-Guided Delivery of Nanoparticles to Improve Drug Permeation across Cellular Barriers and Drug Exposure to Selective Cell Types. *Front Pharmacol* **2018,** *9*, 27.

122. Farjadian, F.; Ghasemi, A.; Gohari, O.; Roointan, A.; Karimi, M.; Hamblin, M. R., Nanopharmaceuticals and nanomedicines currently on the market: challenges and opportunities. *Nanomedicine (Lond)* **2018**.

123. Mitragotri, S.; Lammers, T.; Bae, Y. H.; Schwendeman, S.; De Smedt, S.; Leroux, J. C.; Peer, D.; Kwon, I. C.; Harashima, H.; Kikuchi, A.; Oh, Y. K.; Torchilin, V.; Hennink, W.; Hanes, J.; Park, K., Drug Delivery Research for the Future: Expanding the Nano Horizons and Beyond. *J Control Release* **2017,** *246*, 183-184.

124. Hua, S.; de Matos, M. B. C.; Metselaar, J. M.; Storm, G., Current Trends and Challenges in the Clinical Translation of Nanoparticulate Nanomedicines: Pathways for Translational Development and Commercialization. *Front Pharmacol* **2018,** *9*, 790.

125. Mitchell, M. J.; Billingsley, M. M.; Haley, R. M.; Wechsler, M. E.; Peppas, N. A.; Langer, R., Engineering precision nanoparticles for drug delivery. *Nat Rev Drug Discov* **2021,** *20* (2), 101-124.

126. Strambeanu, N.; Demetrovici, L.; Dragos, D.; Lungu, M., Nanoparticles: Definition, Classification and General Physical Properties. In *Nanoparticles' Promises and Risks*, 2015; pp 3-8.

127. Luther, D. C.; Huang, R.; Jeon, T.; Zhang, X.; Lee, Y. W.; Nagaraj, H.; Rotello, V. M., Delivery of drugs, proteins, and nucleic acids using inorganic nanoparticles. *Adv Drug Deliv Rev* **2020,** *156*, 188-213.

128. Yang, W.; Liang, H.; Ma, S.; Wang, D.; Huang, J., Gold nanoparticle based photothermal therapy: Development and application for effective cancer treatment. *Sustainable Materials and Technologies* **2019,** *22*.

129. Wang, J.; Potocny, A. M.; Rosenthal, J.; Day, E. S., Gold Nanoshell-Linear Tetrapyrrole Conjugates for Near Infrared-Activated Dual Photodynamic and Photothermal Therapies. *ACS Omega* **2020,** *5* (1), 926-940.

130. Arias, L. S.; Pessan, J. P.; Vieira, A. P. M.; Lima, T. M. T.; Delbem, A. C. B.; Monteiro, D. R., Iron Oxide Nanoparticles for Biomedical Applications: A Perspective on Synthesis, Drugs, Antimicrobial Activity, and Toxicity. *Antibiotics (Basel)* **2018,** *7* (2).

131. Xu, C.; Nam, J.; Hong, H.; Xu, Y.; Moon, J. J., Positron Emission Tomography-Guided Photodynamic Therapy with Biodegradable Mesoporous Silica Nanoparticles for Personalized Cancer Immunotherapy. *ACS Nano* **2019,** *13* (10), 12148-12161.

132. Huang, K.-W.; Hsu, F.-F.; Qiu, J. T.; Chern, G.-J.; Lee, Y.-A.; Chang, C.-C.; Huang, Y.-T.; Sung, Y.-C.; Chiang, C.-C.; Huang, R.-L.; Lin, C.-C.; Dihn, T. K.; Huang, H.-C.; Shih, Y.-C.; Alson, D.; Lin, C.-Y.; Lin, Y.-C.; Chang, P.-C.; Lin, S.-Y.; Chen, Y., Highly efficient and tumor-selective nanoparticles for dual-targeted immunogene therapy against cancer. *Sci. Adv.* **2020,** *6*, 1-13.

133. Zhang, Y.; Meng, S.; Ding, J.; Peng, Q.; Yu, Y., Transition metal-coordinated graphitic carbon nitride dots as a sensitive and facile fluorescent probe for beta-amyloid peptide detection. *Analyst* **2019,** *144* (2), 504-511.

134. Wagner, A. M.; Knipe, J. M.; Orive, G.; Peppas, N. A., Quantum dots in biomedical applications. *Acta Biomater* **2019,** *94*, 44-63.

135. Manshian, B. B.; Jimenez, J.; Himmelreich, U.; Soenen, S. J., Personalized medicine and follow-up of therapeutic delivery through exploitation of quantum dot toxicity. *Biomaterials* **2017,** *127*, 1-12.

136. Stock, N.; Biswas, S., Synthesis of metal-organic frameworks (MOFs): routes to various MOF topologies, morphologies, and composites. *Chem Rev* **2012,** *112* (2), 933-69.

137. Furukawa, H.; Ko, N.; Bok Go, Y.; Aratani, N.; Beom Choi, S.; Choi, E.; Özgur Yazaydin, A.; Snurr, R. Q.; O'Keeffe, M.; Kim, J.; Yaghi, O. M., Ultrahigh Porosity in Metal-Organic Frameworks. *Science* **2010,** *329* (5990), 424-428.

138. Horcajada, P.; Gref, R.; Baati, T.; Allan, P. K.; Maurin, G.; Couvreur, P.; Ferey, G.; Morris, R. E.; Serre, C., Metal-organic frameworks in biomedicine. *Chem Rev* **2012,** *112* (2), 1232-68.

139. Giménez-Marqués, M.; Hidalgo, T.; Serre, C.; Horcajada, P., Nanostructured metal–organic frameworks and their bio-related applications. *Coordination Chemistry Reviews* **2016,** *307*, 342-360.

140. Howarth, A. J.; Peters, A. W.; Vermeulen, N. A.; Wang, T. C.; Hupp, J. T.; Farha, O. K., Best Practices for the Synthesis, Activation, and Characterization of Metal–Organic Frameworks. *Chemistry of Materials* **2016,** *29* (1), 26-39.

141. Valcourt, D. M.; Dang, M. N.; Scully, M. A.; Day, E. S., Nanoparticle-Mediated Co-Delivery of Notch-1 Antibodies and ABT-737 as a Potent Treatment Strategy for Triple-Negative Breast Cancer. *ACS Nano* **2020,** *14* (3), 3378-3388.

142. Strand, M. S.; Krasnick, B. A.; Pan, H.; Zhang, X.; Bi, Y.; Brooks, C.; Wetzel, C.; Sankpal, N.; Fleming, T.; Hawkins, W. G.; Wickline, S. A.; Fields, R. C., Precision delivery of RAS-inhibiting siRNA to KRAS driven cancer via peptide-based nanoparticles. *Oncotarget* **2019,** *10* (46), 4761-4775.

143. Caldorera-Moore, M.; Vela Ramirez, J. E.; Peppas, N. A., Transport and delivery of interferon-alpha through epithelial tight junctions via pH-responsive poly(methacrylic acid-grafted-ethylene glycol) nanoparticles. *J Drug Target* **2019,** *27* (5-6), 582-589.

144. Zhang, L.; Beatty, A.; Lu, L.; Abdalrahman, A.; Makris, T. M.; Wang, G.; Wang, Q., Microfluidic-assisted polymer-protein assembly to fabricate homogeneous functionalnanoparticles. *Mater Sci Eng C Mater Biol Appl* **2020,** *111*, 110768.

145. Knight, F. C.; Gilchuk, P.; Kumar, A.; Becker, K. W.; Sevimli, S.; Jacobson, M. E.; Suryadevara, N.; Wang-Bishop, L.; Boyd, K. L.; Crowe, J. E., Jr.; Joyce, S.; Wilson, J. T., Mucosal Immunization with a pH-Responsive Nanoparticle Vaccine Induces Protective CD8(+) Lung-Resident Memory T Cells. *ACS Nano* **2019,** *13* (10), 10939-10960.

146. Afsharzadeh, M.; Hashemi, M.; Mokhtarzadeh, A.; Abnous, K.; Ramezani, M., Recent advances in co-delivery systems based on polymeric nanoparticle for cancer treatment. *Artif Cells Nanomed Biotechnol* **2018,** *46* (6), 1095-1110.

147. Volpatti, L. R.; Matranga, M. A.; Cortinas, A. B.; Delcassian, D.; Daniel, K. B.; Langer, R.; Anderson, D. G., Glucose-Responsive Nanoparticles for Rapid and Extended Self-Regulated Insulin Delivery. *ACS Nano* **2020,** *14* (1), 488-497.

148. Rideau, E.; Dimova, R.; Schwille, P.; Wurm, F. R.; Landfester, K., Liposomes and polymersomes: a comparative review towards cell mimicking. *Chem Soc Rev* **2018,** *47* (23), 8572-8610.

149. Zelmer, C.; Zweifel, L. P.; Kapinos, L. E.; Craciun, I.; Guven, Z. P.; Palivan, C. G.; Lim, R. Y. H., Organelle-specific targeting of polymersomes into the cell nucleus. *Proc Natl Acad Sci U S A* **2020,** *117* (6), 2770-2778.

150. Liu, X.; Li, C.; Lv, J.; Huang, F.; An, Y.; Shi, L.; Ma, R., Glucose and H_2O_2 Dual-Responsive Polymeric Micelles for the Self-Regulated Release of Insulin. *ACS Appl Bio Mater* **2020,** *3* (3), 1598-1606.

151. Lee, S. W.; Kim, Y. M.; Cho, C. H.; Kim, Y. T.; Kim, S. M.; Hur, S. Y.; Kim, J. H.; Kim, B. G.; Kim, S. C.; Ryu, H. S.; Kang, S. B., An Open-Label, Randomized, Parallel, Phase II Trial to Evaluate the Efficacy and Safety of a Cremophor-Free Polymeric Micelle Formulation of Paclitaxel as First-Line Treatment for Ovarian Cancer: A Korean Gynecologic Oncology Group Study (KGOG-3021). *Cancer Res Treat* **2018,** *50* (1), 195-203.

152. Palmerston Mendes, L.; Pan, J.; Torchilin, V. P., Dendrimers as Nanocarriers for Nucleic Acid and Drug Delivery in Cancer Therapy. *Molecules* **2017,** *22* (9).

153. Sercombe, L.; Veerati, T.; Moheimani, F.; Wu, S. Y.; Sood, A. K.; Hua, S., Advances and Challenges of Liposome Assisted Drug Delivery. *Front Pharmacol* **2015,** *6*, 286.

154. Fenton, O. S.; Olafson, K. N.; Pillai, P. S.; Mitchell, M. J.; Langer, R., Advances in Biomaterials for Drug Delivery. *Adv Mater* **2018**, e1705328.

155. Hou, X.; Zaks, T.; Langer, R.; Dong, Y., Lipid nanoparticles for mRNA delivery. *Nat Rev Mater* **2021,** *6* (12), 1078-1094.

156. Ahmad, A.; Ahsan, H., Lipid-based formulations in cosmeceuticals and biopharmaceuticals. *Biomedical Dermatology* **2020,** *4* (1).

157. Tenchov, R.; Bird, R.; Curtze, A. E.; Zhou, Q., Lipid Nanoparticles-From Liposomes to mRNA Vaccine Delivery, a Landscape of Research Diversity and Advancement. *ACS Nano* **2021**.

158. Zhang, Y.; Huang, L., Liposomal delivery system. In *Nanoparticles for Biomedical Applications*, 2020; pp 145-152.

159. Akbarzadeh, A.; Rezaei-Sadabady, R.; Davaran, S.; Joo, S. W.; Zarghami, N.; Hanifehpour, Y.; Samiei, M.; Kouhi, M.; Koshki, K., Liposome: classification, preparation, and applications. *Nanoscale Research Letters* **2013,** *8* (102), 1-9.

160. Israelachvili, J. N.; Mitchell, D. J.; Ninham, B. W., Theory of self-assembly of hydrocarbon amphiphiles into micelles and bilayers. *Journal of the Chemical Society, Faraday Transactions 2* **1976,** *72*.

161. Has, C.; Sunthar, P., A comprehensive review on recent preparation techniques of liposomes. *J Liposome Res* **2020,** *30* (4), 336-365.

162. Barenholz, Y., Doxil(R) - the first FDA-approved nano-drug: lessons learned. *J Control Release* **2012,** *160* (2), 117-34.

163. Vanic, Z.; Barnert, S.; Suss, R.; Schubert, R., Fusogenic activity of PEGylated pH-sensitive liposomes. *J Liposome Res* **2012,** *22* (2), 148-57.

164. Madkhali, O. A., Perspectives and Prospective on Solid Lipid Nanoparticles as Drug Delivery Systems. *Molecules* **2022,** *27* (5).

165. Basha, S. K.; Dhandayuthabani, R.; Muzammil, M. S.; Kumari, V. S., Solid lipid nanoparticles for oral drug delivery. *Materials Today: Proceedings* **2021,** *36*, 313-324.

166. Limeres, M. J.; Sune-Pou, M.; Prieto-Sanchez, S.; Moreno-Castro, C.; Nusblat, A. D.; Hernandez-Munain, C.; Castro, G. R.; Sune, C.; Sune-Negre, J. M.; Cuestas, M. L., Development and characterization of an improved formulation of cholesteryl oleate-loaded cationic solid-lipid nanoparticles as an efficient non-viral gene delivery system. *Colloids Surf B Biointerfaces* **2019,** *184*, 110533.

167. Hald Albertsen, C.; Kulkarni, J. A.; Witzigmann, D.; Lind, M.; Petersson, K.; Simonsen, J. B., The role of lipid components in lipid nanoparticles for vaccines and gene therapy. *Adv Drug Deliv Rev* **2022,** *188*, 114416.

168. Kurimoto, S.; Yoshinaga, N.; Igarashi, K.; Matsumoto, Y.; Cabral, H.; Uchida, S., PEG-OligoRNA Hybridization of mRNA for Developing Sterically Stable Lipid Nanoparticles toward In Vivo Administration. *Molecules* **2019,** *24* (7).

169. Suzuki, T.; Suzuki, Y.; Hihara, T.; Kubara, K.; Kondo, K.; Hyodo, K.; Yamazaki, K.; Ishida, T.; Ishihara, H., PEG shedding-rate-dependent blood clearance of PEGylated lipid nanoparticles in mice: Faster PEG shedding attenuates anti-PEG IgM production. *Int J Pharm* **2020,** *588*, 119792.

170. Judge, A.; McClintock, K.; Phelps, J. R.; Maclachlan, I., Hypersensitivity and loss of disease site targeting caused by antibody responses to PEGylated liposomes. *Mol Ther* **2006,** *13* (2), 328-37.

171. Cheng, X.; Lee, R. J., The role of helper lipids in lipid nanoparticles (LNPs) designed for oligonucleotide delivery. *Adv Drug Deliv Rev* **2016,** *99* (Pt A), 129-137.

172. Aytar Celik, P.; Erdogan-Gover, K.; Barut, D.; Enuh, B. M.; Amasya, G.; Sengel-Turk, C. T.; Derkus, B.; Cabuk, A., Bacterial Membrane Vesicles as Smart Drug Delivery and Carrier Systems: A New Nanosystems Tool for Current Anticancer and Antimicrobial Therapy. *Pharmaceutics* **2023,** *15* (4).

173. Camussi, G.; Deregibus, M. C.; Bruno, S.; Cantaluppi, V.; Biancone, L., Exosomes/microvesicles as a mechanism of cell-to-cell communication. *Kidney Int* **2010,** *78* (9), 838-48.

174. Hugel, B.; Martínez, M. C.; Kunzelmann, C.; Freyssinet, J.-M., Membrane Microparticles: Two Sides of the Coin. *Physiology* **2005,** *20*, 22-27.

175. Mause, S. F.; Weber, C., Microparticles: protagonists of a novel communication network for intercellular information exchange. *Circ Res* **2010,** *107* (9), 1047-57.

176. Jimenez, J. J.; Jy, W.; Mauro, L. M.; Soderland, C.; Horstman, L. L.; Ahn, Y. S., Endothelial cells release phenotypically and quantitatively distinct microparticles in activation and apoptosis. *Thrombosis Research* **2003,** *109* (4), 175-180.

177. Raposo, G.; Stoorvogel, W., Extracellular vesicles: exosomes, microvesicles, and friends. *J Cell Biol* **2013,** *200* (4), 373-83.

178. Boelens, M. C.; Wu, T. J.; Nabet, B. Y.; Xu, B.; Qiu, Y.; Yoon, T.; Azzam, D. J.; Twyman-Saint Victor, C.; Wiemann, B. Z.; Ishwaran, H.; Ter Brugge, P. J.; Jonkers, J.; Slingerland, J.; Minn, A. J., Exosome transfer from stromal to breast cancer cells regulates therapy resistance pathways. *Cell* **2014,** *159* (3), 499-513.

179. Camacho, L.; Guerrero, P.; Marchetti, D., MicroRNA and protein profiling of brain metastasis competent cell-derived exosomes. *PLoS One* **2013,** *8* (9), e73790.

180. Aheget, H.; Tristan-Manzano, M.; Mazini, L.; Cortijo-Gutierrez, M.; Galindo-Moreno, P.; Herrera, C.; Martin, F.; Marchal, J. A.; Benabdellah, K., Exosome: A New Player in Translational Nanomedicine. *J Clin Med* **2020,** *9* (8).

181. Owens, A. P., 3rd; Mackman, N., Microparticles in hemostasis and thrombosis. *Circ Res* **2011,** *108* (10), 1284-97.

182. Menzies, F. M.; Khan, A. H.; Higgins, C. A.; Nelson, S. M.; Nibbs, R. J., The chemokine receptor CCR2 is not required for successful initiation of labor in mice. *Biol Reprod* **2012,** *86* (4), 118.

183. Cloutier, N.; Tan, S.; Boudreau, L. H.; Cramb, C.; Subbaiah, R.; Lahey, L.; Albert, A.; Shnayder, R.; Gobezie, R.; Nigrovic, P. A.; Farndale, R. W.; Robinson, W. H.; Brisson, A.; Lee, D. M.; Boilard, E., The exposure of autoantigens by microparticles underlies the formation of potent inflammatory components: the microparticle-associated immune complexes. *EMBO Mol Med* **2013,** *5* (2), 235-49.

184. Prakash, P. S.; Caldwell, C. C.; Lentsch, A. B.; Pritts, T. A.; Robinson, B. R., Human microparticles generated during sepsis in patients with critical illness are neutrophil-derived and modulate the immune response. *J Trauma Acute Care Surg* **2012,** *73* (2), 401-6; discussion 406-7.

185. Al-Nedawi, K.; Meehan, B.; Micallef, J.; Lhotak, V.; May, L.; Guha, A.; Rak, J., Intercellular transfer of the oncogenic receptor EGFRvIII by microvesicles derived from tumour cells. *Nat Cell Biol* **2008,** *10* (5), 619-24.

186. Valenti, R.; Huber, V.; Iero, M.; Filipazzi, P.; Parmiani, G.; Rivoltini, L., Tumor-released microvesicles as vehicles of immunosuppression. *Cancer Res* **2007,** *67* (7), 2912-5.

187. Krause, M.; Samoylenko, A.; Vainio, S. J., Exosomes as renal inductive signals in health and disease, and their application as diagnostic markers and therapeutic agents. *Front Cell Dev Biol* **2015,** *3*, 65.

188. Skog, J.; Wurdinger, T.; van Rijn, S.; Meijer, D. H.; Gainche, L.; Sena-Esteves, M.; Curry, W. T., Jr.; Carter, B. S.; Krichevsky, A. M.; Breakefield, X. O., Glioblastoma microvesicles transport RNA and proteins that promote tumour growth and provide diagnostic biomarkers. *Nat Cell Biol* **2008,** *10* (12), 1470-6.

189. Lai, R. C.; Chen, T. S.; Lim, S. K., Mesenchymal stem cell exosome: a novel stem cell-based therapy for cardiovascular disease. *Regen. Med.* **2011,** *6* (4), 481-492.

190. Carnino, J. M.; Lee, H.; Jin, Y., Isolation and characterization of extracellular vesicles from Broncho-alveolar lavage fluid: a review and comparison of different methods. *Respir Res* **2019,** *20* (1), 240.

191. Mulcahy, L. A.; Pink, R. C.; Carter, D. R., Routes and mechanisms of extracellular vesicle uptake. *J Extracell Vesicles* **2014,** *3*.

192. Latifkar, A.; Hur, Y. H.; Sanchez, J. C.; Cerione, R. A.; Antonyak, M. A., New insights into extracellular vesicle biogenesis and function. *J Cell Sci* **2019,** *132* (13).

193. Ravasco, J. M. J. M.; Paiva-Santos, A. C.; Conde, J., Technological challenges of biomembrane-coated top-down cancer nanotherapy. *Nature Reviews Bioengineering* **2023,** *1* (3), 156-158.

194. Krishnan, N.; Peng, F. X.; Mohapatra, A.; Fang, R. H.; Zhang, L., Genetically engineered cellular nanoparticles for biomedical applications. *Biomaterials* **2023,** *296*, 122065.

195. Zhu, J. Y.; Zheng, D. W.; Zhang, M. K.; Yu, W. Y.; Qiu, W. X.; Hu, J. J.; Feng, J.; Zhang, X. Z., Preferential Cancer Cell Self-Recognition and Tumor Self-Targeting by Coating Nanoparticles with Homotypic Cancer Cell Membranes. *Nano Lett* **2016,** *16* (9), 5895-901.

196. Chugh, V.; Vijaya Krishna, K.; Pandit, A., Cell Membrane-Coated Mimics: A Methodological Approach for Fabrication, Characterization for Therapeutic Applications, and Challenges for Clinical Translation. *ACS Nano* **2021**.

197. Cockcroft, S., Mammalian lipids: structure, synthesis and function. *Essays Biochem* **2021,** *65* (5), 813-845.

198. Liu, W. L.; Zou, M. Z.; Qin, S. Y.; Cheng, Y. J.; Ma, Y. H.; Sun, Y. X.; Zhang, X. Z., Recent Advances of Cell Membrane-Coated Nanomaterials for Biomedical Applications. *Advanced Functional Materials* **2020,** *30* (39).

199. Sevencan, C.; McCoy, R. S. A.; Ravisankar, P.; Liu, M.; Govindarajan, S.; Zhu, J.; Bay, B. H.; Leong, D. T., Cell Membrane Nanotherapeutics: From Synthesis to Applications Emerging Tools for Personalized Cancer Therapy. *Advanced Therapeutics* **2020,** *3* (3).

200. Hu, C. M.; Zhang, L.; Aryal, S.; Cheung, C.; Fang, R. H.; Zhang, L., Erythrocyte membrane-camouflaged polymeric nanoparticles as a biomimetic delivery platform. *Proc Natl Acad Sci U S A* **2011,** *108* (27), 10980-5.

201. Gao, W.; Hu, C. M.; Fang, R. H.; Luk, B. T.; Su, J.; Zhang, L., Surface functionalization of gold nanoparticles with red blood cell membranes. *Adv Mater* **2013,** *25* (26), 3549-53.

202. Hu, C. M.; Fang, R. H.; Wang, K. C.; Luk, B. T.; Thamphiwatana, S.; Dehaini, D.; Nguyen, P.; Angsantikul, P.; Wen, C. H.; Kroll, A. V.; Carpenter, C.; Ramesh, M.; Qu, V.; Patel, S. H.; Zhu, J.; Shi, W.; Hofman, F. M.; Chen, T. C.; Gao, W.; Zhang, K.; Chien, S.; Zhang, L., Nanoparticle biointerfacing by platelet membrane cloaking. *Nature* **2015,** *526* (7571), 118-21.

203. Parodi, A.; Quattrocchi, N.; van de Ven, A. L.; Chiappini, C.; Evangelopoulos, M.; Martinez, J. O.; Brown, B. S.; Khaled, S. Z.; Yazdi, I. K.; Enzo, M. V.; Isenhart, L.; Ferrari, M.; Tasciotti, E., Synthetic nanoparticles functionalized with biomimetic leukocyte membranes possess cell-like functions. *Nat Nanotechnol* **2013,** *8* (1), 61-8.

204. Pei, Q.; Hu, X.; Zheng, X.; Liu, S.; Li, Y.; Jing, X.; Xie, Z., Light-Activatable Red Blood Cell Membrane-Camouflaged Dimeric Prodrug Nanoparticles for Synergistic Photodynamic/Chemotherapy. *ACS Nano* **2018,** *12* (2), 1630-1641.

205. Zhang, N.; Li, M.; Sun, X.; Jia, H.; Liu, W., NIR-responsive cancer cytomembrane-cloaked carrier-free nanosystems for highly efficient and self-targeted tumor drug delivery. *Biomaterials* **2018,** *159*, 25-36.

206. Aryal, S.; Hu, C. M.; Fang, R. H.; Dehaini, D.; Carpenter, C.; Zhang, D. E.; Zhang, L., Erythrocyte membrane-cloaked polymeric nanoparticles for controlled drug loading and release. *Nanomedicine (Lond)* **2013,** *8* (8), 1271-80.

207. Su, J.; Sun, H.; Meng, Q.; Zhang, P.; Yin, Q.; Li, Y., Enhanced Blood Suspensibility and Laser-Activated Tumor-specific Drug Release of Theranostic Mesoporous Silica Nanoparticles by Functionalizing with Erythrocyte Membranes. *Theranostics* **2017,** *7* (3), 523-537.

208. Xuan, M.; Shao, J.; Dai, L.; Li, J.; He, Q., Macrophage Cell Membrane Camouflaged Au Nanoshells for in Vivo Prolonged Circulation Life and Enhanced Cancer Photothermal Therapy. *ACS Appl Mater Interfaces* **2016,** *8* (15), 9610-8.

209. Kroll, A. V.; Fang, R. H.; Jiang, Y.; Zhou, J.; Wei, X.; Yu, C. L.; Gao, J.; Luk, B. T.; Dehaini, D.; Gao, W.; Zhang, L., Nanoparticulate Delivery of Cancer Cell Membrane Elicits Multiantigenic Antitumor Immunity. *Adv Mater* **2017,** *29* (47).

210. Dash, P.; Piras, A. M.; Dash, M., Cell membrane coated nanocarriers - an efficient biomimetic platform for targeted therapy. *J Control Release* **2020,** *327*, 546-570.

211. Li, B.; Wang, F.; Gui, L.; He, Q.; Yao, Y.; Chen, H., The potential of biomimetic nanoparticles for tumor-targeted drug delivery. *Nanomedicine (Lond)* **2018**.

212. Abdollah, M. R. A.; Carter, T. J.; Jones, C.; Kalber, T. L.; Rajkumar, V.; Tolner, B.; Gruettner, C.; Zaw-Thin, M.; Baguna Torres, J.; Ellis, M.; Robson, M.; Pedley, R. B.; Mulholland, P.; R, T. M. d. R.; Chester, K. A., Fucoidan Prolongs the Circulation Time of Dextran-Coated Iron Oxide Nanoparticles. *ACS Nano* **2018,** *12* (2), 1156-1169.

213. Luk, B. T.; Fang, R. H.; Hu, C. M.; Copp, J. A.; Thamphiwatana, S.; Dehaini, D.; Gao, W.; Zhang, K.; Li, S.; Zhang, L., Safe and Immunocompatible Nanocarriers Cloaked in RBC Membranes for Drug Delivery to Treat Solid Tumors. *Theranostics* **2016,** *6* (7), 1004-11.

214. Piao, J.-G.; Wang, L.; Gao, F.; You, Y.-Z.; Xiong, Y.; Yang, L., Erythrocyte Membrane Is an Alternative Coating to Polyethylene Glycol for Prolonging the Circulation Lifetime of Gold Nanocages for Photothermal Therapy. *ACS Nano* **2014,** *8* (10), 10414-10425.

215. Wibroe, P. P.; Anselmo, A. C.; Nilsson, P. H.; Sarode, A.; Gupta, V.; Urbanics, R.; Szebeni, J.; Hunter, A. C.; Mitragotri, S.; Mollnes, T. E.; Moghimi, S. M., Bypassing adverse injection reactions to nanoparticles through shape modification and attachment to erythrocytes. *Nat Nanotechnol* **2017,** *12* (6), 589-594.

216. Rao, L.; Bu, L. L.; Xu, J. H.; Cai, B.; Yu, G. T.; Yu, X.; He, Z.; Huang, Q.; Li, A.; Guo, S. S.; Zhang, W. F.; Liu, W.; Sun, Z. J.; Wang, H.; Wang, T. H.; Zhao, X. Z., Red Blood Cell Membrane as a Biomimetic Nanocoating for Prolonged Circulation Time and Reduced Accelerated Blood Clearance. *Small* **2015,** *11* (46), 6225-36.

217. Tsai, R. K.; Discher, D. E., Inhibition of "self" engulfment through deactivation of myosin-II at the phagocytic synapse between human cells. *J Cell Biol* **2008,** *180* (5), 989-1003.

218. Toledano Furman, N. E.; Lupu-Haber, Y.; Bronshtein, T.; Kaneti, L.; Letko, N.; Weinstein, E.; Baruch, L.; Machluf, M., Reconstructed stem cell nanoghosts: a natural tumor targeting platform. *Nano Lett* **2013,** *13* (7), 3248-55.

219. Jiang, Y.; Chekuri, S.; Fang, R. H.; Zhang, L., Engineering biological interactions on the nanoscale. *Curr Opin Biotechnol* **2019,** *58*, 1-8.

220. Fang, R. H.; Hu, C. M.; Luk, B. T.; Gao, W.; Copp, J. A.; Tai, Y.; O'Connor, D. E.; Zhang, L., Cancer cell membrane-coated nanoparticles for anticancer vaccination and drug delivery. *Nano Lett* **2014,** *14* (4), 2181-8.

221. Sun, H.; Su, J.; Meng, Q.; Yin, Q.; Chen, L.; Gu, W.; Zhang, P.; Zhang, Z.; Yu, H.; Wang, S.; Li, Y., Cancer-Cell-Biomimetic Nanoparticles for Targeted Therapy of Homotypic Tumors. *Adv Mater* **2016,** *28* (43), 9581-9588.

222. Tian, H.; Luo, Z.; Liu, L.; Zheng, M.; Chen, Z.; Ma, A.; Liang, R.; Han, Z.; Lu, C.; Cai, L., Cancer Cell Membrane-Biomimetic Oxygen Nanocarrier for Breaking Hypoxia-Induced Chemoresistance. *Advanced Functional Materials* **2017,** *27* (38).

223. Krishnamurthy, S.; Gnanasammandhan, M. K.; Xie, C.; Huang, K.; Cui, M. Y.; Chan, J. M., Monocyte cell membrane-derived nanoghosts for targeted cancer therapy. *Nanoscale* **2016,** *8* (13), 6981-5.

224. Cao, H.; Dan, Z.; He, X.; Zhang, Z.; Yu, H.; Yin, Q.; Li, Y., Liposomes Coated with Isolated Macrophage Membrane Can Target Lung Metastasis of Breast Cancer. *ACS Nano* **2016,** *10* (8), 7738-48.

225. Gao, C.; Lin, Z.; Jurado-Sanchez, B.; Lin, X.; Wu, Z.; He, Q., Stem Cell Membrane-Coated Nanogels for Highly Efficient In Vivo Tumor Targeted Drug Delivery. *Small* **2016,** *12* (30), 4056-62.

226. Bach, J.-F., Immunosuppressive therapy of autoimmune diseases. *TIPS* **1993,** *14* (5), 213-216.

227. Luk, B. T.; Jiang, Y.; Copp, J. A.; Hu, C. J.; Krishnan, N.; Gao, W.; Li, S.; Fang, R. H.; Zhang, L., Biomimetic Targeting of Nanoparticles to Immune Cell Subsets via Cognate Antigen Interactions. *Mol Pharm* **2018,** *15* (9), 3723-3728.

228. Zeng, Z.; Pu, K., Improving Cancer Immunotherapy by Cell Membrane-Camouflaged Nanoparticles. *Advanced Functional Materials* **2020,** *30* (43).

229. Wang, D.; Wang, S.; Zhou, Z.; Bai, D.; Zhang, Q.; Ai, X.; Gao, W.; Zhang, L., White Blood Cell Membrane-Coated Nanoparticles: Recent Development and Medical Applications. *Adv Healthc Mater* **2022,** *11* (7), e2101349.

230. Angsantikul, P.; Thamphiwatana, S.; Zhang, Q.; Spiekermann, K.; Zhuang, J.; Fang, R. H.; Gao, W.; Obonyo, M.; Zhang, L., Coating nanoparticles with gastric epithelial cell membrane for targeted antibiotic delivery against Helicobacter pylori infection. *Adv Ther (Weinh)* **2018,** *1* (2).

231. Pizarro-Cerda, J.; Cossart, P., Bacterial adhesion and entry into host cells. *Cell* **2006,** *124* (4), 715-27.

232. Siboo, I. R.; Chambers, H. F.; Sullam, P. M., Role of SraP, a Serine-Rich Surface Protein of Staphylococcus aureus, in binding to human platelets. *Infect Immun* **2005,** *73* (4), 2273-80.

233. Rodvien, R.; Mielke, C. H., Role of platelets in hemostasis and thrombosis. *West J Med* **1976,** *125*, 181-186.

234. Wei, X.; Ying, M.; Dehaini, D.; Su, Y.; Kroll, A. V.; Zhou, J.; Gao, W.; Fang, R. H.; Chien, S.; Zhang, L., Nanoparticle Functionalization with Platelet Membrane Enables Multifactored Biological Targeting and Detection of Atherosclerosis. *ACS Nano* **2018,** *12* (1), 109-116.

235. Hu, Q.; Qian, C.; Sun, W.; Wang, J.; Chen, Z.; Bomba, H. N.; Xin, H.; Shen, Q.; Gu, Z., Engineered Nanoplatelets for Enhanced Treatment of Multiple Myeloma and Thrombus. *Adv Mater* **2016,** *28* (43), 9573-9580.

236. He, W.; Xing, X.; Wang, X.; Wu, D.; Wu, W.; Guo, J.; Mitragotri, S., Nanocarrier-Mediated Cytosolic Delivery of Biopharmaceuticals. *Advanced Functional Materials* **2020,** *30* (37).

237. Bareford, L. M.; Swaan, P. W., Endocytic mechanisms for targeted drug delivery. *Adv Drug Deliv Rev* **2007,** *59* (8), 748-58.

238. Khalil, I. A.; Kogure, K.; Akita, H.; Harashima, H., Uptake pathways and subsequent intracellular trafficking in nonviral gene delivery. *Pharmacol Rev* **2006,** *58* (1), 32-45.

239. Al-Jamal, W. T.; Al-Jamal, K. T.; Tian, B.; Lacerda, L.; Bomans, P. H.; Frederik, P. M.; Kostarelos, K., Lipid-Quantum Dot Bilayer Vesicles Enhance Tumor Cell Uptake and Retention in Vitro and in Vivo. *ACS Nano* **2008,** *2* (3), 408-418.

240. Babic, M.; Horák, D.; Trchová, M.; Jendelová, P.; Glogarová, K.; Lesný, P.; Herynek, V.; Hájek, M.; Syková, E., Poly(L-lysine)-Modified Iron Oxide Nanoparticles for Stem Cell Labeling. *Bioconjug Chem* **2008,** *19*, 740-750.

241. Herrero, M. A.; Toma, F. M.; Al-Jamal, K. T.; Kostarelos, K.; Bianco, A.; Da Ros, T.; Bano, F.; Casalis, L.; Scoles, G.; Prato, M., Synthesis and Characterization of a Carbon Nanotube-Dendron Series for Efficient siRNA Delivery. *J. Am. Chem. Soc.* **2009,** *131*, 9843-9848.

242. Barba-Bon, A.; Salluce, G.; Lostale-Seijo, I.; Assaf, K. I.; Hennig, A.; Montenegro, J.; Nau, W. M., Boron clusters as broadband membrane carriers. *Nature* **2022,** *603* (7902), 637-642.

243. Taranejoo, S.; Liu, J.; Verma, P.; Hourigan, K., A review of the developments of characteristics of PEI derivatives for gene delivery applications. *Journal of Applied Polymer Science* **2015,** *132* (25), n/a-n/a.

244. Kong, H.; Yi, K.; Zheng, C.; Lao, Y. H.; Zhou, H.; Chan, H. F.; Wang, H.; Tao, Y.; Li, M., Membrane-fusogenic biomimetic particles: a new bioengineering tool learned from nature. *J Mater Chem B* **2022,** *10* (36), 6841-6858.

245. Wickner, W.; Schekman, R., Membrane fusion. *Nat Struct Mol Biol* **2008,** *15* (7), 658-64.

246. Jahn, R.; Lang, T.; Südhof, T. C., Membrane Fusion. *Cell* **2003,** *112*, 519-533.

247. Yang, J.; Bahreman, A.; Daudey, G.; Bussmann, J.; Olsthoorn, R. C.; Kros, A., Drug Delivery via Cell Membrane Fusion Using Lipopeptide Modified Liposomes. *ACS Cent Sci* **2016,** *2* (9), 621-630.

248. Yang, J.; Tu, J.; Lamers, G. E. M.; Olsthoorn, R. C. L.; Kros, A., Membrane Fusion Mediated Intracellular Delivery of Lipid Bilayer Coated Mesoporous Silica Nanoparticles. *Adv Healthc Mater* **2017,** *6* (20).

249. Sun, L.; Gao, Y.; Wang, Y.; Wei, Q.; Shi, J.; Chen, N.; Li, D.; Fan, C., Guiding protein delivery into live cells using DNA-programmed membrane fusion. *Chem Sci* **2018,** *9* (27), 5967-5975.

250. Yang, Y.; Hong, Y.; Nam, G.-H.; Chung, J. H.; Koh, E.; Kim, I.-S., Virus-Mimetic Fusogenic Exosomes for Direct Delivery of Integral Membrane Proteins to Target Cell Membranes. *Advanced Materials* **2017,** *29* (13).

251. Montagna, C.; Petris, G.; Casini, A.; Maule, G.; Franceschini, G. M.; Zanella, I.; Conti, L.; Arnoldi, F.; Burrone, O. R.; Zentilin, L.; Zacchigna, S.; Giacca, M.; Cereseto, A., VSV-G-Enveloped Vesicles for Traceless Delivery of CRISPR-Cas9. *Mol Ther Nucleic Acids* **2018,** *12*, 453-462.

252. Kolasinac, R.; Kleusch, C.; Braun, T.; Merkel, R.; Csiszar, A., Deciphering the Functional Composition of Fusogenic Liposomes. *Int J Mol Sci* **2018,** *19* (2).

253. Liu, X.; Xiang, J.; Zhu, D.; Jiang, L.; Zhou, Z.; Tang, J.; Liu, X.; Huang, Y.; Shen, Y., Fusogenic Reactive Oxygen Species Triggered Charge-Reversal Vector for Effective Gene Delivery. *Adv Mater* **2016,** *28* (9), 1743-52.

254. Tan, H.; Song, Y.; Chen, J.; Zhang, N.; Wang, Q.; Li, Q.; Gao, J.; Yang, H.; Dong, Z.; Weng, X.; Wang, Z.; Sun, D.; Yakufu, W.; Pang, Z.; Huang, Z.; Ge, J., Platelet-Like Fusogenic Liposome-Mediated Targeting Delivery of miR-21 Improves Myocardial Remodeling by Reprogramming Macrophages Post Myocardial Ischemia-Reperfusion Injury. *Adv Sci (Weinh)* **2021,** *8* (15), e2100787.

255. Wang, Q.; Song, Y.; Chen, J.; Li, Q.; Gao, J.; Tan, H.; Zhu, Y.; Wang, Z.; Li, M.; Yang, H.; Zhang, N.; Li, X.; Qian, J.; Pang, Z.; Huang, Z.; Ge, J., Direct in vivo reprogramming with non-viral sequential targeting nanoparticles promotes cardiac regeneration. *Biomaterials* **2021,** *276*, 121028.

256. Pereira-Silva, M.; Chauhan, G.; Shin, M. D.; Hoskins, C.; Madou, M. J.; Martinez-Chapa, S. O.; Steinmetz, N. F.; Veiga, F.; Paiva-Santos, A. C., Unleashing the potential of cell membrane-based nanoparticles for COVID-19 treatment and vaccination. *Expert Opin Drug Deliv* **2021,** *18* (10), 1395-1414.

257. Sun, H.; Su, J.; Meng, Q.; Yin, Q.; Chen, L.; Gu, W.; Zhang, Z.; Yu, H.; Zhang, P.; Wang, S.; Li, Y., Cancer Cell Membrane-Coated Gold Nanocages with Hyperthermia-Triggered Drug Release and Homotypic Target Inhibit Growth and Metastasis of Breast Cancer. *Advanced Functional Materials* **2017,** *27* (3).

258. Min, H.; Wang, J.; Qi, Y.; Zhang, Y.; Han, X.; Xu, Y.; Xu, J.; Li, Y.; Chen, L.; Cheng, K.; Liu, G.; Yang, N.; Li, Y.; Nie, G., Biomimetic Metal-Organic Framework Nanoparticles for Cooperative Combination of Antiangiogenesis and Photodynamic Therapy for Enhanced Efficacy. *Adv Mater* **2019,** *31* (15), e1808200.

259. Guo, Y.; Wang, D.; Song, Q.; Wu, T.; Zhuang, X.; Bao, Y.; Kong, M.; Qi, Y.; Tan, S.; Zhang, Z., Erythrocyte Membrane-Enveloped Polymeric Nanoparticles as Nanovaccine for Induction of Antitumor Immunity against Melanoma. *ACS Nano* **2015,** *9* (7), 6918-6933.

260. Borsig, L.; Wong, R.; Feramisco, J.; Nadeau, D. R.; Varki, N. M.; Varki, A., Heparin and cancer revisited: Mechanistic connections involving platelets, P-selectin, carcinoma mucins, and tumor metastasis. *PNAS* **2001,** *98* (6), 3352-3357.

261. Hu, Q.; Sun, W.; Qian, C.; Wang, C.; Bomba, H. N.; Gu, Z., Anticancer Platelet-Mimicking Nanovehicles. *Adv Mater* **2015,** *27* (44), 7043-50.

262. Lopez-Otin, C.; Blasco, M. A.; Partridge, L.; Serrano, M.; Kroemer, G., The hallmarks of aging. *Cell* **2013,** *153* (6), 1194-217.

263. Gorgoulis, V.; Adams, P. D.; Alimonti, A.; Bennett, D. C.; Bischof, O.; Bishop, C.; Campisi, J.; Collado, M.; Evangelou, K.; Ferbeyre, G.; Gil, J.; Hara, E.; Krizhanovsky, V.; Jurk, D.; Maier, A. B.; Narita, M.; Niedernhofer, L.; Passos, J. F.; Robbins, P. D.; Schmitt, C. A.; Sedivy, J.; Vougas, K.; von Zglinicki, T.; Zhou, D.; Serrano, M.; Demaria, M., Cellular Senescence: Defining a Path Forward. *Cell* **2019,** *179* (4), 813-827.

264. Wiley, C. D.; Campisi, J., The metabolic roots of senescence: mechanisms and opportunities for intervention. *Nat Metab* **2021,** *3* (10), 1290-1301.

265. Khalil, R.; Diab-Assaf, M.; Lemaitre, J. M., Emerging Therapeutic Approaches to Target the Dark Side of Senescent Cells: New Hopes to Treat Aging as a Disease and to Delay Age-Related Pathologies. *Cells* **2023,** *12* (6).

266. Zhu, Y.; Tchkonia, T.; Pirtskhalava, T.; Gower, A. C.; Ding, H.; Giorgadze, N.; Palmer, A. K.; Ikeno, Y.; Hubbard, G. B.; Lenburg, M.; O'Hara, S. P.; LaRusso, N. F.; Miller, J. D.; Roos, C. M.; Verzosa, G. C.; LeBrasseur, N. K.; Wren, J. D.; Farr, J. N.; Khosla, S.; Stout, M. B.; McGowan, S. J.; Fuhrmann-Stroissnigg, H.; Gurkar, A. U.; Zhao, J.; Colangelo, D.; Dorronsoro, A.; Ling, Y. Y.; Barghouthy, A. S.; Navarro, D. C.; Sano, T.; Robbins, P. D.; Niedernhofer, L. J.; Kirkland, J. L., The Achilles' heel of senescent cells: from transcriptome to senolytic drugs. *Aging Cell* **2015,** *14* (4), 644-58.

267. Marin, I.; Boix, O.; Garcia-Garijo, A.; Sirois, I.; Caballe, A.; Zarzuela, E.; Ruano, I.; Attolini, C. S.; Prats, N.; Lopez-Dominguez, J. A.; Kovatcheva, M.; Garralda, E.; Munoz, J.; Caron, E.; Abad, M.; Gros, A.; Pietrocola, F.; Serrano, M., Cellular Senescence Is Immunogenic and Promotes Antitumor Immunity. *Cancer Discov* **2023,** *13* (2), 410-431.

268. Zhu, Y.; Tchkonia, T.; Fuhrmann-Stroissnigg, H.; Dai, H. M.; Ling, Y. Y.; Stout, M. B.; Pirtskhalava, T.; Giorgadze, N.; Johnson, K. O.; Giles, C. B.; Wren, J. D.; Niedernhofer, L. J.; Robbins, P. D.; Kirkland, J. L., Identification of a novel senolytic agent, navitoclax, targeting the Bcl-2 family of anti-apoptotic factors. *Aging Cell* **2016,** *15* (3), 428-435.

269. Vilgelm, A. E.; Pawlikowski, J. S.; Liu, Y.; Hawkins, O. E.; Davis, T. A.; Smith, J.; Weller, K. P.; Horton, L. W.; McClain, C. M.; Ayers, G. D.; Turner, D. C.; Essaka, D. C.; Stewart, C. F.; Sosman, J. A.; Kelley, M. C.;

Ecsedy, J. A.; Johnston, J. N.; Richmond, A., Mdm2 and aurora kinase a inhibitors synergize to block melanoma growth by driving apoptosis and immune clearance of tumor cells. *Cancer Res* **2015,** *75* (1), 181-93.

270. Kirkland, J. L.; Tchkonia, T., Senolytic drugs: from discovery to translation. *J Intern Med* **2020,** *288* (5), 518-536.

271. Fuhrmann-Stroissnigg, H.; Santiago, F. E.; Grassi, D.; Ling, Y.; Niedernhofer, L. J.; Robbins, P. D., SA-beta-Galactosidase-Based Screening Assay for the Identification of Senotherapeutic Drugs. *J Vis Exp* **2019,** (148).

272. Nakagami, H., Cellular senescence and senescence-associated T cells as a potential therapeutic target. *Geriatrics & Gerontology International* **2019,** *20* (2), 97-100.

273. Munoz-Espin, D.; Rovira, M.; Galiana, I.; Gimenez, C.; Lozano-Torres, B.; Paez-Ribes, M.; Llanos, S.; Chaib, S.; Munoz-Martin, M.; Ucero, A. C.; Garaulet, G.; Mulero, F.; Dann, S. G.; VanArsdale, T.; Shields, D. J.; Bernardos, A.; Murguia, J. R.; Martinez-Manez, R.; Serrano, M., A versatile drug delivery system targeting senescent cells. *EMBO Mol Med* **2018,** *10* (9).

274. Rosenberg, S. A.; Yang, J. C.; Restifo, N. P., Cancer immunotherapy: moving beyond current vaccines. *Nat Med* **2004,** *10* (9), 909-915.

275. Liu, H.; Miao, Z.; Zha, Z., Cell membrane-coated nanoparticles for immunotherapy. *Chinese Chemical Letters* **2022,** *33* (4), 1673-1680.

276. Bluestone, J. A.; Bour-Jordan, H., Current and future immunomodulation strategies to restore tolerance in autoimmune diseases. *Cold Spring Harb Perspect Biol* **2012,** *4* (11).

277. Wei, X.; Gao, J.; Fang, R. H.; Luk, B. T.; Kroll, A. V.; Dehaini, D.; Zhou, J.; Kim, H. W.; Gao, W.; Lu, W.; Zhang, L., Nanoparticles camouflaged in platelet membrane coating as an antibody decoy for the treatment of immune thrombocytopenia. *Biomaterials* **2016,** *111*, 116-123.

278. Ott, P. A.; Hu, Z.; Keskin, D. B.; Shukla, S. A.; Sun, J.; Bozym, D. J.; Zhang, W.; Luoma, A.; Giobbie-Hurder, A.; Peter, L.; Chen, C.; Olive, O.; Carter, T. A.; Li, S.; Lieb, D. J.; Eisenhaure, T.; Gjini, E.; Stevens, J.; Lane, W. J.; Javeri, I.; Nellaiappan, K.; Salazar, A. M.; Daley, H.; Seaman, M.; Buchbinder, E. I.; Yoon, C. H.; Harden, M.; Lennon, N.; Gabriel, S.; Rodig, S. J.; Barouch, D. H.; Aster, J. C.; Getz, G.; Wucherpfennig, K.; Neuberg, D.; Ritz, J.; Lander, E. S.; Fritsch, E. F.; Hacohen, N.; Wu, C. J., An immunogenic personal neoantigen vaccine for patients with melanoma. *Nature* **2017,** *547* (7662), 217-221.

279. Wu, L.; Tang, H.; Zheng, H.; Liu, X.; Liu, Y.; Tao, J.; Liang, Z.; Xia, Y.; Xu, Y.; Guo, Y.; Chen, H.; Yang, J., Multiwalled Carbon Nanotubes Prevent Tumor Metastasis Through Switching M2-Polarized Macrophages to M1 via TLR4 Activation. *J Biomed Nanotechnol* **2019,** *15* (1), 138-150.

280. Jin, J.; Krishnamachary, B.; Barnett, J. D.; Chatterjee, S.; Chang, D.; Mironchik, Y.; Wildes, F.; Jaffee, E. M.; Nimmagadda, S.; Bhujwalla, Z. M., Human Cancer Cell Membrane-Coated Biomimetic Nanoparticles Reduce Fibroblast-Mediated Invasion and Metastasis and Induce T-Cells. *ACS Appl Mater Interfaces* **2019,** *11* (8), 7850-7861.

281. Talebian, S.; Conde, J., Why Go NANO on COVID-19 Pandemic? *Matter* **2020,** *3* (3), 598-601.

282. Kostarelos, K., Nanoscale nights of COVID-19. *Nat Nanotechnol* **2020,** *15* (5), 343-344.

283. Chung, Y. H.; Beiss, V.; Fiering, S. N.; Steinmetz, N. F., COVID-19 Vaccine Frontrunners and Their Nanotechnology Design. *ACS Nano* **2020,** *14* (10), 12522-12537.

284. Khurana, A.; Allawadhi, P.; Khurana, I.; Allwadhi, S.; Weiskirchen, R.; Banothu, A. K.; Chhabra, D.; Joshi, K.; Bharani, K. K., Role of nanotechnology behind the success of mRNA vaccines for COVID-19. *Nano Today* **2021,** *38*, 101142.

285. Witika, B. A.; Makoni, P. A.; Mweetwa, L. L.; Ntemi, P. V.; Chikukwa, M. T. R.; Matafwali, S. K.; Mwila, C.; Mudenda, S.; Katandula, J.; Walker, R. B., Nano-Biomimetic Drug Delivery Vehicles: Potential Approaches for COVID-19 Treatment. *Molecules* **2020,** *25* (24).

286. Pinky; Gupta, S.; Krishnakumar, V.; Sharma, Y.; Dinda, A. K.; Mohanty, S., Mesenchymal Stem Cell Derived Exosomes: a Nano Platform for Therapeutics and Drug Delivery in Combating COVID-19. *Stem Cell Rev Rep* **2021,** *17* (1), 33-43.

287. Zhang, Q.; Honko, A.; Zhou, J.; Gong, H.; Downs, S. N.; Vasquez, J. H.; Fang, R. H.; Gao, W.; Griffiths, A.; Zhang, L., Cellular Nanosponges Inhibit SARS-CoV-2 Infectivity. *Nano Lett* **2020,** *20* (7), 5570-5574.

288. Rao, L.; Xia, S.; Xu, W.; Tian, R.; Yu, G.; Gu, C.; Pan, P.; Meng, Q. F.; Cai, X.; Qu, D.; Lu, L.; Xie, Y.; Jiang, S.; Chen, X., Decoy nanoparticles protect against COVID-19 by concurrently adsorbing viruses and inflammatory cytokines. *Proc Natl Acad Sci U S A* **2020,** *117* (44), 27141-27147.

289. Molinaro, R.; Pasto, A.; Taraballi, F.; Giordano, F.; Azzi, J. A.; Tasciotti, E.; Corbo, C., Biomimetic Nanoparticles Potentiate the Anti-Inflammatory Properties of Dexamethasone and Reduce the Cytokine Storm Syndrome: An Additional Weapon against COVID-19? *Nanomaterials (Basel)* **2020,** *10* (11).

290. Grivennikov, S. I.; Greten, F. R.; Karin, M., Immunity, inflammation, and cancer. *Cell* **2010,** *140* (6), 883-99.

291. Zhou, X.; Cao, X.; Tu, H.; Zhang, Z. R.; Deng, L., Inflammation-Targeted Delivery of Celastrol via Neutrophil Membrane-Coated Nanoparticles in the Management of Acute Pancreatitis. *Mol Pharm* **2019,** *16* (3), 1397-1405.

292. Fang, Z.; Fang, J.; Gao, C.; Gao, R.; Lin, P.; Yu, W., Recent trends in platelet membrane-cloaked nanoparticles for application of inflammatory diseases. *Drug Deliv* **2022,** *29* (1), 2805-2814.

293. Lv, W.; Xu, J.; Wang, X.; Li, X.; Xu, Q.; Xin, H., Bioengineered Boronic Ester Modified Dextran Polymer Nanoparticles as Reactive Oxygen Species Responsive Nanocarrier for Ischemic Stroke Treatment. *ACS Nano* **2018,** *12* (6), 5417-5426.

294. Yaghi, S.; Willey, J. Z.; Cucchiara, B.; Goldstein, J. N.; Gonzales, N. R.; Khatri, P.; Kim, L. J.; Mayer, S. A.; Sheth, K. N.; Schwamm, L. H.; American Heart Association Stroke, C.; Council on, C.; Stroke, N.; Council on Clinical, C.; Council on Quality of, C.; Outcomes, R., Treatment and Outcome of Hemorrhagic Transformation After Intravenous Alteplase in Acute Ischemic Stroke: A Scientific Statement for Healthcare Professionals From the American Heart Association/American Stroke Association. *Stroke* **2017,** *48* (12), e343-e361.

295. Hacke, W.; Kaste, M.; Bluhmki, E.; Brozman, M.; Dávalos, A.; Guidetti, D.; Larrue, V.; Lees, K. R.; Medeghri, Z.; Machnig, T.; Schneider, D.; von Kummer, R.; Wahlgren, N.; Toni, D., Thrombolysis with Alteplase 3 to 4.5 Hours after Acute Ischemic Stroke. *NEJM* **2008,** *359* (13), 1317-1329.

296. Correa-Paz, C.; da Silva-Candal, A.; Polo, E.; Parcq, J.; Vivien, D.; Maysinger, D.; Pelaz, B.; Campos, F., New Approaches in Nanomedicine for Ischemic Stroke. *Pharmaceutics* **2021,** *13* (5).

297. Meissner, T. B.; Mandal, P. K.; Ferreira, L. M.; Rossi, D. J.; Cowan, C. A., Genome editing for human gene therapy. *Methods Enzymol* **2014,** *546*, 273-95.

298. Hsu, P. D.; Lander, E. S.; Zhang, F., Development and applications of CRISPR-Cas9 for genome engineering. *Cell* **2014,** *157* (6), 1262-1278.

299. Sander, J. D.; Joung, J. K., CRISPR-Cas systems for editing, regulating and targeting genomes. *Nat Biotechnol* **2014,** *32* (4), 347-55.

300. Lechardeur, D.; Sohn, K.-J.; Haardt, M.; Joshi, P. B.; Monck, M.; Graham, R. W.; Beatty, B.; Squire, J.; O'Brodovich, H.; Lukacs, G. L., Metabolic instability of plasmid DNA in the cytosol: a potential barrier to gene transfer. *Gene Ther* **1999,** *6*, 482-497.

301. Anderson, D. J.; Hetzer, M. W., Nuclear envelope formation by chromatin-mediated reorganization of the endoplasmic reticulum. *Nat Cell Biol* **2007,** *9* (10), 1160-6.

302. Raices, M.; D'Angelo, M. A., Nuclear pore complex composition: a new regulator of tissue-specific and developmental functions. *Nat Rev Mol Cell Biol* **2012,** *13* (11), 687-99.

303. Kay, M. A.; Glorioso, J. C.; Naldini, L., Viral vectors for gene therapy: the art of turning infectious agents into vehicles of therapeutics. *Nat Med* **2001,** *7* (1), 33-40.

304. Levine, R. M.; Pearce, T. R.; Adil, M.; Kokkoli, E., Preparation and characterization of liposome-encapsulated plasmid DNA for gene delivery. *Langmuir* **2013,** *29* (29), 9208-15.

305. Dobson, J., Gene therapy progress and prospects: magnetic nanoparticle-based gene delivery. *Gene Ther* **2006,** *13* (4), 283-7.

306. Pissuwan, D.; Niidome, T.; Cortie, M. B., The forthcoming applications of gold nanoparticles in drug and gene delivery systems. *J Control Release* **2011,** *149* (1), 65-71.

307. Dunbar, C. E.; High, K. A.; Joung, J. K.; Kohn, D. B.; Ozawa, K.; Sadelain, M., Gene therapy comes of age. *Science* **2018,** *359* (6372).

308. Zu, H.; Gao, D., Non-viral Vectors in Gene Therapy: Recent Development, Challenges, and Prospects. *AAPS J* **2021,** *23* (4), 78.

309. Gallops, C.; Ziebarth, J.; Wang, Y., A Polymer Physics Perspective on Why PEI Is an Effective Nonviral Gene Delivery Vector. *ACS Symp. Ser. Am. Chem. Soc.* **2020,** *1350*, 1-12.

310. Tarach, P.; Janaszewska, A., Recent Advances in Preclinical Research Using PAMAM Dendrimers for Cancer Gene Therapy. *Int J Mol Sci* **2021,** *22* (6).

311. Weng, Y.; Xiao, H.; Zhang, J.; Liang, X. J.; Huang, Y., RNAi therapeutic and its innovative biotechnological evolution. *Biotechnol Adv* **2019,** *37* (5), 801-825.

312. https://www.novartis.com/news/media-releases/novartis-receives-eu-approval-leqvio-inclisiran-first-class-sirna-lower-cholesterol-two-doses-year.

313. Buck, J.; Grossen, P.; Cullis, P. R.; Huwyler, J.; Witzigmann, D., Lipid-Based DNA Therapeutics: Hallmarks of Non-Viral Gene Delivery. *ACS Nano* **2019,** *13* (4), 3754-3782.

314. Jinek, M.; Chylinski, K.; Fonfara, I.; Hauer, M.; Doudna, J. A.; Charpentier, E., A Programmable Dual-RNA–Guided DNA Endonuclease in Adaptive Bacterial Immunity. *Science* **2012,** *337*, 816-821.

315. Shmakov, S.; Abudayyeh, O. O.; Makarova, K. S.; Wolf, Y. I.; Gootenberg, J. S.; Semenova, E.; Minakhin, L.; Joung, J.; Konermann, S.; Severinov, K.; Zhang, F.; Koonin, E. V., Discovery and Functional Characterization of Diverse Class 2 CRISPR-Cas Systems. *Mol Cell* **2015,** *60* (3), 385-97.

316. Abudayyeh, O. O.; Gootenberg, J. S.; Konermann, S.; Joung, J.; Slaymaker, I. M.; Cox, D. B.; Shmakov, S.; Makarova, K. S.; Semenova, E.; Minakhin, L.; Severinov, K.; Regev, A.; Lander, E. S.; Koonin, E. V.; Zhang, F., C2c2 is a single-component programmable RNA-guided RNA-targeting CRISPR effector. *Science* **2016,** *353* (6299), aaf5573.

317. Granados-Riveron, J. T.; Aquino-Jarquin, G., CRISPR-Cas13 Precision Transcriptome Engineering in Cancer. *Cancer Res* **2018,** *78* (15), 4107-4113.

318. Huynh, N.; Depner, N.; Larson, R.; King-Jones, K., A versatile toolkit for CRISPR-Cas13-based RNA manipulation in Drosophila. *Genome Biol* **2020,** *21* (1), 279.

319. Soprano, E.; Alvarez, A.; Pelaz, B.; Del Pino, P.; Polo, E., Plasmonic Cell-Derived Nanocomposites for Light-Controlled Cargo Release inside Living Cells. *Adv Biosyst* **2020,** *4* (3), e1900260.

320. Triana-Martinez, F.; Picallos-Rabina, P.; Da Silva-Alvarez, S.; Pietrocola, F.; Llanos, S.; Rodilla, V.; Soprano, E.; Pedrosa, P.; Ferreiros, A.; Barradas, M.; Hernandez-Gonzalez, F.; Lalinde, M.; Prats, N.; Bernado, C.; Gonzalez, P.; Gomez, M.; Ikonomopoulou, M. P.; Fernandez-Marcos, P. J.; Garcia-Caballero, T.; Del Pino, P.; Arribas, J.; Vidal, A.; Gonzalez-Barcia, M.; Serrano, M.; Loza, M. I.; Dominguez, E.; Collado, M., Identification and characterization of Cardiac Glycosides as senolytic compounds. *Nat Commun* **2019,** *10* (1), 4731.

321. Ceballos, M.; Cedrun-Morales, M.; Rodriguez-Perez, M.; Funes-Hernando, S.; Vila-Fungueirino, J. M.; Zampini, G.; Navarro Poupard, M. F.; Polo, E.; Del Pino, P.; Pelaz, B., High-yield halide-assisted synthesis of metal-organic framework UiO-based nanocarriers. *Nanoscale* **2022,** *14* (18), 6789-6801.

322. Morabito, J. V.; Chou, L. Y.; Li, Z.; Manna, C. M.; Petroff, C. A.; Kyada, R. J.; Palomba, J. M.; Byers, J. A.; Tsung, C. K., Molecular encapsulation beyond the aperture size limit through dissociative linker exchange in metal-organic framework crystals. *J Am Chem Soc* **2014,** *136* (36), 12540-3.

323. Bucevičius, J.; Lukinavičius, G.; Gerasimaitė, R., The Use of Hoechst Dyes for DNA Staining and beyond. *Chemosensors* **2018,** *6* (2).

324. Orset, C.; Macrez, R.; Young, A. R.; Panthou, D.; Angles-Cano, E.; Maubert, E.; Agin, V.; Vivien, D., Mouse model of in situ thromboembolic stroke and reperfusion. *Stroke* **2007,** *38* (10), 2771-8.

325. Germain, M.; Caputo, F.; Metcalfe, S.; Tosi, G.; Spring, K.; Aslund, A. K. O.; Pottier, A.; Schiffelers, R.; Ceccaldi, A.; Schmid, R., Delivering the power of nanomedicine to patients today. *J Control Release* **2020,** *326*, 164-171.

326. Beltrán-Gracia, E.; López-Camacho, A.; Higuera-Ciapara, I.; Velázquez-Fernández, J. B.; Vallejo-Cardona, A. A., Nanomedicine review: clinical developments in liposomal applications. *Cancer Nanotechnology* **2019,** *10* (1).

327. Rampado, R.; Caliceti, P.; Agostini, M., Latest Advances in Biomimetic Cell Membrane-Coated and Membrane-Derived Nanovectors for Biomedical Applications. *Nanomaterials (Basel)* **2022,** *12* (9).

328. DeBerardinis, R. J.; Chandel, N. S., We need to talk about the Warburg effect. *Nat Metab* **2020,** *2* (2), 127-129.

329. Mayor, S.; Pagano, R. E., Pathways of clathrin-independent endocytosis. *Nat Rev Mol Cell Biol* **2007,** *8* (8), 603-12.

330. Rothberg, K. G.; Heuser, J. E.; Donzell, W. C.; Ying, Y.; Glenney, J. R.; Anderson, R. G. W., Caveolin, a Protein Component of Caveolae Membrane Coats. *Cell* **1992,** *68*, 673-682.

331. Macia, E.; Ehrlich, M.; Massol, R.; Boucrot, E.; Brunner, C.; Kirchhausen, T., Dynasore, a cell-permeable inhibitor of dynamin. *Dev Cell* **2006,** *10* (6), 839-50.

332. Hu, T. Y.; Frieman, M.; Wolfram, J., Insights from nanomedicine into chloroquine efficacy against COVID-19. *Nat Nanotechnol* **2020,** *15* (4), 247-249.

333. Wang, L.-H.; Rothberg, K. G.; Anderson, R. G. W., Mis-assembly of clathrin lattices on endosomes reveals a regulatory switch for coated pit formation. *J. Cell Biol.* **1993,** *123* (5), 1107-1117.

334. Rodal, S. K.; Skretting, G.; Garred, Ø.; Vilhardt, F.; Van Deurs, B.; Sandvig, K., Extraction of Cholesterol with Methyl-b-Cyclodextrin Perturbs Formation of Clathrin-coated Endocytic Vesicles. *MBoC* **1999,** *10*, 961-974.

335. Narain, A.; Asawa, S.; Chhabria, V.; Patil-Sen, Y., Cell membrane coated nanoparticles: next-generation therapeutics. *Nanomedicine (Lond)* **2017,** *12* (21), 2677-2692.

336. Di Micco, R.; Krizhanovsky, V.; Baker, D.; d'Adda di Fagagna, F., Cellular senescence in ageing: from mechanisms to therapeutic opportunities. *Nat Rev Mol Cell Biol* **2021,** *22* (2), 75-95.

337. Kaur, J.; Farr, J. N., Cellular senescence in age-related disorders. *Transl Res* **2020,** *226*, 96-104.

338. Paez-Ribes, M.; Gonzalez-Gualda, E.; Doherty, G. J.; Munoz-Espin, D., Targeting senescent cells in translational medicine. *EMBO Mol Med* **2019,** *11* (12), e10234.

339. Lagoumtzi, S. M.; Chondrogianni, N., Senolytics and senomorphics: Natural and synthetic therapeutics in the treatment of aging and chronic diseases. *Free Radic Biol Med* **2021,** *171*, 169-190.

340. Hernandez-Segura, A.; Nehme, J.; Demaria, M., Hallmarks of Cellular Senescence. *Trends Cell Biol* **2018,** *28* (6), 436-453.

341. https://covid19.who.int/.

342. Masters, P. S., The molecular biology of coronaviruses. *Adv Virus Res* **2006,** *66*, 193-292.

343. Lin, Y.; Yan, X.; Cao, W.; Wang, C.; Feng, J.; Duan, J.; Xie, S., Probing the structure of the SARS coronavirus using scanning electron microscopy. *Antivir. Ther.* **2004,** *9*, 287-289.

344. Li, F.; Li, W.; Farzan, M.; Harrison, S. C., Structure of SARS Coronavirus Spike Receptor-Binding Domain Complexed with Receptor. *Science* **2005,** *309*, 1864-1868.

345. Gheblawi, M.; Wang, K.; Viveiros, A.; Nguyen, Q.; Zhong, J. C.; Turner, A. J.; Raizada, M. K.; Grant, M. B.; Oudit, G. Y., Angiotensin-Converting Enzyme 2: SARS-CoV-2 Receptor and Regulator of the Renin-Angiotensin System: Celebrating the 20th Anniversary of the Discovery of ACE2. *Circ Res* **2020,** *126* (10), 1456-1474.

346. Tay, M. Z.; Poh, C. M.; Renia, L.; MacAry, P. A.; Ng, L. F. P., The trinity of COVID-19: immunity, inflammation and intervention. *Nat Rev Immunol* **2020,** *20* (6), 363-374.

347. Correa-Paz, C.; Navarro Poupard, M. F.; Polo, E.; Rodriguez-Perez, M.; Migliavacca, M.; Iglesias-Rey, R.; Ouro, A.; Maqueda, E.; Hervella, P.; Sobrino, T.; Castillo, J.; Del Pino, P.; Pelaz, B.; Campos, F., Sonosensitive capsules for brain thrombolysis increase ischemic damage in a stroke model. *J Nanobiotechnology* **2022,** *20* (1), 46.

348. Benjamin, E. J.; Muntner, P.; Alonso, A.; Bittencourt, M. S.; Callaway, C. W.; Carson, A. P.; Chamberlain, A. M.; Chang, A. R.; Cheng, S.; Das, S. R.; Delling, F. N.; Djousse, L.; Elkind, M. S. V.; Ferguson, J. F.; Fornage, M.; Jordan, L. C.; Khan, S. S.; Kissela, B. M.; Knutson, K. L.; Kwan, T. W.; Lackland, D. T.; Lewis, T. T.; Lichtman, J. H.; Longenecker, C. T.; Loop, M. S.; Lutsey, P. L.; Martin, S. S.; Matsushita, K.; Moran, A. E.; Mussolino, M. E.; O'Flaherty, M.; Pandey, A.; Perak, A. M.; Rosamond, W. D.; Roth, G. A.; Sampson, U. K. A.; Satou, G. M.; Schroeder, E. B.; Shah, S. H.; Spartano, N. L.; Stokes, A.; Tirschwell, D. L.; Tsao, C. W.; Turakhia, M. P.; VanWagner, L. B.; Wilkins, J. T.; Wong, S. S.; Virani, S. S.; American Heart Association Council on, E.; Prevention Statistics, C.; Stroke Statistics, S., Heart Disease and Stroke Statistics-2019 Update: A Report From the American Heart Association. *Circulation* **2019,** *139* (10), e56-e528.

349. Correa-Paz, C.; Navarro Poupard, M. F.; Polo, E.; Rodriguez-Perez, M.; Taboada, P.; Iglesias-Rey, R.; Hervella, P.; Sobrino, T.; Vivien, D.; Castillo, J.; Del Pino, P.; Campos, F.; Pelaz, B., In vivo ultrasound-activated delivery of recombinant tissue plasminogen activator from the cavity of sub-micrometric capsules. *J Control Release* **2019,** *308*, 162-171.

350. Guo, X.; Hong, T.; Zang, J.; Shao, R.; Hou, X.; Wang, K.; Liu, W.; Su, F.; He, B., Thrombus-specific/responsive biomimetic nanomedicine for spatiotemporal thrombolysis and alleviation of myocardial ischemia/reperfusion injury. *J Nanobiotechnology* **2022,** *20* (1), 531.

351. Wang, S.; Duan, Y.; Zhang, Q.; Komarla, A.; Gong, H.; Gao, W.; Zhang, L., Drug Targeting via Platelet Membrane-Coated Nanoparticles. *Small Struct* **2020,** *1* (1).

352. Li, M.; Li, J.; Chen, J.; Liu, Y.; Cheng, X.; Yang, F.; Gu, N., Platelet Membrane Biomimetic Magnetic Nanocarriers for Targeted Delivery and in Situ Generation of Nitric Oxide in Early Ischemic Stroke. *ACS Nano* **2020,** *14* (2), 2024-2035.

353. Olsson, M.; Bruhns, P.; Frazier, W. A.; Ravetch, J. V.; Oldenborg, P. A., Platelet homeostasis is regulated by platelet expression of CD47 under normal conditions and in passive immune thrombocytopenia. *Blood* **2005,** *105* (9), 3577-82.

354. Du, X., Signaling and regulation of the platelet glycoprotein Ib–IX–V complex. *Curr Opin Hematol* **2007,** *14*, 262-269.

355. Liu, Y.; Jennings, N. L.; Dart, A. M.; Du, X. J., Standardizing a simpler, more sensitive and accurate tail bleeding assay in mice. *World J Exp Med* **2012,** *2* (2), 30-6.

356. Heissig, B.; Salama, Y.; Takahashi, S.; Osada, T.; Hattori, K., The multifaceted role of plasminogen in inflammation. *Cell Signal* **2020,** *75*, 109761.

357. Mingarro, G.; Del Olmo, M. L., Improvements in the genetic editing technologies: CRISPR-Cas and beyond. *Gene* **2022**, 147064.

358. Troder, S. E.; Zevnik, B., History of genome editing: From meganucleases to CRISPR. *Lab Anim* **2022,** *56* (1), 60-68.

359. Khalil, A. M., The genome editing revolution: review. *J Genet Eng Biotechnol* **2020,** *18* (1), 68.

360. Kavuri, N. R.; Ramasamy, M.; Qi, Y.; Mandadi, K., Applications of CRISPR/Cas13-Based RNA Editing in Plants. *Cells* **2022,** *11* (17).

361. Bulcha, J. T.; Wang, Y.; Ma, H.; Tai, P. W. L.; Gao, G., Viral vector platforms within the gene therapy landscape. *Signal Transduct Target Ther* **2021,** *6* (1), 53.

362. Du, X.; Wang, J.; Zhou, Q.; Zhang, L.; Wang, S.; Zhang, Z.; Yao, C., Advanced physical techniques for gene delivery based on membrane perforation. *Drug Deliv* **2018,** *25* (1), 1516-1525.

363. Hejabi, F.; Abbaszadeh, M. S.; Taji, S.; O'Neill, A.; Farjadian, F.; Doroudian, M., Nanocarriers: A novel strategy for the delivery of CRISPR/Cas systems. *Front Chem* **2022,** *10*, 957572.

364. Soprano, E.; Migliavacca, M.; Lopez-Ferreiro, M.; Pelaz, B.; Polo, E.; Del Pino, P., Fusogenic Cell-Derived nanocarriers for cytosolic delivery of cargo inside living cells. *J Colloid Interface Sci* **2023,** *648*, 488-496.

365. Kushawah, G.; Hernandez-Huertas, L.; Abugattas-Nunez Del Prado, J.; Martinez-Morales, J. R.; DeVore, M. L.; Hassan, H.; Moreno-Sanchez, I.; Tomas-Gallardo, L.; Diaz-Moscoso, A.; Monges, D. E.; Guelfo, J. R.; Theune, W. C.; Brannan, E. O.; Wang, W.; Corbin, T. J.; Moran, A. M.; Sanchez Alvarado, A.; Malaga-Trillo, E.; Takacs, C. M.; Bazzini, A. A.; Moreno-Mateos, M. A., CRISPR-Cas13d Induces Efficient mRNA Knockdown in Animal Embryos. *Dev Cell* **2020,** *54* (6), 805-817 e7.

366. Csiszar, A.; Hersch, N.; Dieluweit, S.; Biehl, R.; Merkel, R.; Hoffmann, B., Novel Fusogenic Liposomes for Fluorescent Cell Labeling and Membrane Modification. *Bioconjug Chem* **2010,** *21*, 537-543.

367. Abbott, T. R.; Dhamdhere, G.; Liu, Y.; Lin, X.; Goudy, L.; Zeng, L.; Chemparathy, A.; Chmura, S.; Heaton, N. S.; Debs, R.; Pande, T.; Endy, D.; La Russa, M. F.; Lewis, D. B.; Qi, L. S., Development of CRISPR as an Antiviral Strategy to Combat SARS-CoV-2 and Influenza. *Cell* **2020,** *181* (4), 865-876 e12.

368. Maestre, A. M.; Garzon, A.; Rodriguez, D., Equine torovirus (BEV) induces caspase-mediated apoptosis in infected cells. *PLoS One* **2011,** *6* (6), e20972.

369. Ujike, M.; Taguchi, F., Recent Progress in Torovirus Molecular Biology. *Viruses* **2021,** *13* (3).

370. Roth, J. C.; Curiel, D. T.; Pereboeva, L., Cell vehicle targeting strategies. *Gene Ther* **2008,** *15* (10), 716-29.

371. Cedrun-Morales, M.; Ceballos, M.; Polo, E.; Del Pino, P.; Pelaz, B., Nanosized metal-organic frameworks as unique platforms for bioapplications. *Chem Commun (Camb)* **2023,** *59* (20), 2869-2887.

372. Wu, J.; Shaw, C. M.; Martin, D. C., Electron Microscopy of Organic Materials. In *Polymer Science: A Comprehensive Reference*, 2012; pp 509-525.

373. Yeung, T.; Gilbert, G. E.; Shi, J.; Silvius, J.; Kapus, A.; Grinstein, S., Membrane Phosphatidylserine Regulates Surface Charge and Protein Localization. *Sci Rep* **2008,** *319*, 210-213.

Appendices – Rights & Permissions

Appendix I: Conflict of interest

Martina Migliavacca, the doctoral candidate, declares that there is no conflict of interest associated with this Doctoral Thesis.

Santiago de Compostela, October 4th, 2023.

Appendix II: PhD list of publications and permissions

Part of the results from Chapters 2 will be published in:

"Thrombolytic therapy based on lyophilized platelet-derived nanocarriers for ischemic stroke". *Journal of Nanobiotechnology*. (Submitted in **2023**)

Martina Migliavacca[1#], Clara Correa-Paz[2#], María Pérez-Mato[2], Patrick-Brian Bielawski[3], Issan Zhang[3], Pablo Hervella[2], Marina Rubio[4], Dusica Maysinger[3], Denis Vivien[4,5], Pablo del Pino[1], Beatriz Pelaz[1*], Ester Polo[1*], Francisco Campos[2*]

[1]Center for Research in Biological Chemistry and Molecular Materials (CiQUS), University of Santiago de Compostela, 15705 Santiago de Compostela, Spain. [2]Clinical Neurosciences Research Laboratory (LINC), Health Research Institute of Santiago de Compostela (IDIS), 15706 Santiago de Compostela, Spain. [3]Department of Pharmacology and Therapeutics, McGill University, Montreal, QC, H3G 1Y6, Canada. [4]Normandie University, UNICAEN, INSERM UMR-S U1237, Physiopathology and Imaging of Neurological Disorders (PhIND), GIP Cyceron, Institute Blood and Brain @ Caen-Normandie (BB@C), 14000 Caen, France. [5]Department of Clinical Research, Caen Normandie University Hospital, Caen, France.

Contributions: preparation, optimization, and characterization of the materials; writing – original draft.

Impact Factor: 10.2. Q1 in Nanoscience & Nanotechnology. No written permission from Spriger Nature is necessary. Copyright 2023. ISSN 1477-3155

Rights and permissions

Part of the results from Chapters 3 and 4 has been published in:

"Fusogenic Cell-Derived nanocarriers for cytosolic delivery of cargo inside living cells". *Journal of Colloid and Interface Science*, **2023**, *648*, 488-496.

doi.org/10.1016/j.jcis.2023.06.015

Enrica Soprano, Martina Migliavacca, Miriam Lopez-Ferreiro, Beatriz Pelaz, Ester Polo*, Pablo del Pino*.

Centro Singular de Investigacion en Química Bioloxica e Materiais Moleculares (CiQUS), Universidade de Santiago de Compostela. Rúa Jenaro de la Fuente s/n, 15705, Santiago de Compostela, Spain.

Contributions: preparation and characterization of the materials; *in vitro* experiments; writing – original draft.

Impact Factor: 9.9. Q1 in Chemistry, Physical. No written permission from Elsevier is necessary. Copyright 2023. ISSN 0021-9797.

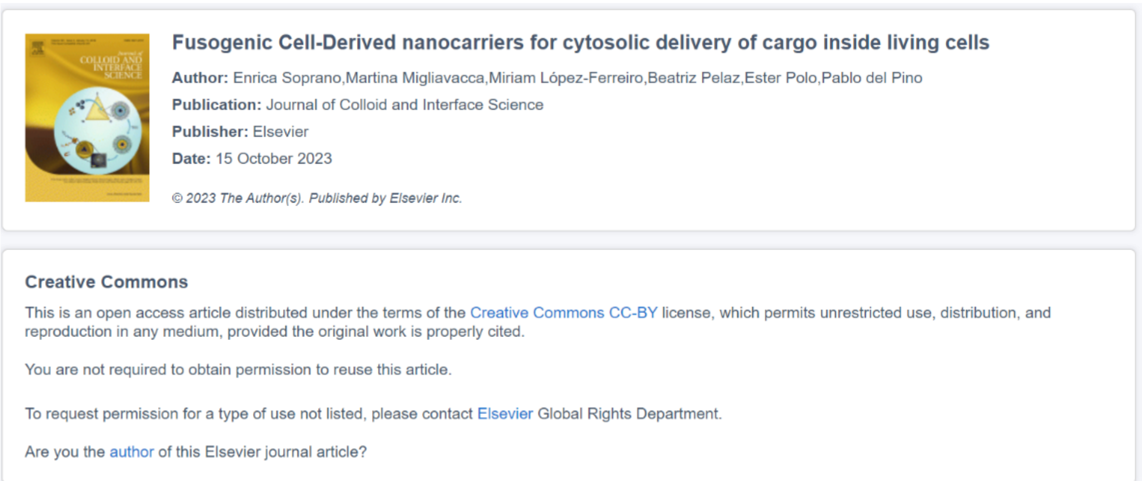

Fusogenic Cell-Derived nanocarriers for cytosolic delivery of cargo inside living cells

Author: Enrica Soprano,Martina Migliavacca,Miriam López-Ferreiro,Beatriz Pelaz,Ester Polo,Pablo del Pino

Publication: Journal of Colloid and Interface Science

Publisher: Elsevier

Date: 15 October 2023

Appendix III: Permissions to publish images, tables, and figures

<table>
<tr><th colspan="2">IMAGES AND FIGURES: RIGHTS AND PERMISSIONS</th></tr>
<tr><td>Figure 1-6</td><td>
ACS Publications
Most Trusted. Most Cited. Most Read.

Best Practices for the Synthesis, Activation, and Characterization of Metal–Organic Frameworks
Author: Ashlee J. Howarth, Aaron W. Peters, Nicolaas A. Vermeulen, et al
Publication: Chemistry of Materials
Publisher: American Chemical Society
Date: Jan 1, 2017
Copyright © 2017, American Chemical Society

PERMISSION/LICENSE IS GRANTED FOR YOUR ORDER AT NO CHARGE

This type of permission/license, instead of the standard Terms and Conditions, is sent to you because no fee is being charged for your order. Please note the following:

- Permission is granted for your request in both print and electronic formats, and translations.
- If figures and/or tables were requested, they may be adapted or used in part.
- Please print this page for your records and send a copy of it to your publisher/graduate school.
- Appropriate credit for the requested material should be given as follows: "Reprinted (adapted) with permission from {COMPLETE REFERENCE CITATION}. Copyright {YEAR} American Chemical Society." Insert appropriate information in place of the capitalized words.
- One-time permission is granted only for the use specified in your RightsLink request. No additional uses are granted (such as derivative works or other editions). For any uses, please submit a new request.

If credit is given to another source for the material you requested from RightsLink, permission must be obtained from that source.
BACK CLOSE WINDOW
</td></tr>
<tr><td>Figure 1-8</td><td>
<table>
<tr><td>License Number</td><td>5593540087881</td></tr>
<tr><td>License date</td><td>Jul 21, 2023</td></tr>
<tr><td>Licensed Content Publisher</td><td>Springer Nature</td></tr>
<tr><td>Licensed Content Publication</td><td>Nature Reviews Bioengineering</td></tr>
<tr><td>Licensed Content Title</td><td>Technological challenges of biomembrane-coated top-down cancer nanotherapy</td></tr>
<tr><td>Licensed Content Author</td><td>João M. J. M. Ravasco et al</td></tr>
<tr><td>Licensed Content Date</td><td>Jan 31, 2023</td></tr>
<tr><td>Type of Use</td><td>Thesis/Dissertation</td></tr>
<tr><td>Requestor type</td><td>academic/university or research institute</td></tr>
<tr><td>Format</td><td>print and electronic</td></tr>
<tr><td>Portion</td><td>figures/tables/illustrations</td></tr>
<tr><td>Number of figures/tables/illustrations</td><td>1</td></tr>
<tr><td>Will you be translating?</td><td>no</td></tr>
<tr><td>Circulation/distribution</td><td>1 - 29</td></tr>
<tr><td>Author of this Springer Nature content</td><td>no</td></tr>
<tr><td>Title</td><td>Engineering smart biomimetic nanocarriers for biological application</td></tr>
<tr><td>Institution name</td><td>University of Santiago de Compostela</td></tr>
<tr><td>Expected presentation date</td><td>Oct 2023</td></tr>
<tr><td>Portions</td><td>Figure 1</td></tr>
<tr><td>Requestor Location</td><td>Ms. Martina Migliavacca
Rua Jenaro de la Fuente s/n

Santiago de Compostela, 15782
Spain
Attn: Ms. Martina Migliavacca</td></tr>
<tr><td>Total</td><td>0.00 EUR</td></tr>
</table>
</td></tr>
<tr><td>Figure 1-10</td><td>
Order Details

1. Journal of materials chemistry. B, Materials for biology and medicine — Billing Status: Open
Article: Membrane-fusogenic biomimetic particles: a new bioengineering tool learned from nature
Print License
<table>
<tr><td>Order License ID</td><td>1377950-1</td><td>Type of Use</td><td>Republish in a thesis/dissert...</td></tr>
<tr><td>Order detail status</td><td>Completed</td><td>Publisher</td><td>Royal Society of Chemistry</td></tr>
<tr><td>ISSN</td><td>2050-7518</td><td>Portion</td><td>Image/photo/illustration</td></tr>
</table>
0,00 EUR
Republication Permission
View Details

Total Items: 1 — Subtotal: 0,00 EUR
Order Total: 0,00 EUR
</td></tr>
</table>

<table>
<tr>
<td>Figure 1-15</td>
<td>
<h3>Rights and permissions</h3>
Open Access This article is licensed under a Creative Commons Attribution 4.0 International License, which permits use, sharing, adaptation, distribution and reproduction in any medium or format, as long as you give appropriate credit to the original author(s) and the source, provide a link to the Creative Commons licence, and indicate if changes were made. The images or other third party material in this article are included in the article's Creative Commons licence, unless indicated otherwise in a credit line to the material. If material is not included in the article's Creative Commons licence and your intended use is not permitted by statutory regulation or exceeds the permitted use, you will need to obtain permission directly from the copyright holder. To view a copy of this licence, visit http://creativecommons.org/licenses/by/4.0/. The Creative Commons Public Domain Dedication waiver (http://creativecommons.org/publicdomain/zero/1.0/) applies to the data made available in this article, unless otherwise stated in a credit line to the data.
Reprints and Permissions
<h3>About this article</h3>
Check for updates
Cite this article
Huynh, N., Depner, N., Larson, R. et al. A versatile toolkit for CRISPR-Cas13-based RNA manipulation in Drosophila. Genome Biol 21, 279 (2020). https://doi.org/10.1186/s13059-020-02193-y
Download citation
Received
21 May 2020
Accepted
04 November 2020
Published
17 November 2020
DOI
https://doi.org/10.1186/s13059-020-02193-y
Share this article
Anyone you share the following link with will be able to read this content:
Get shareable link
Provided by the Springer Nature SharedIt content-sharing initiative
</td>
</tr>
<tr>
<td>Figure 2-3</td>
<td>
Ashley Waldron (Addgene)
Jul 19, 2023, 9:16 AM EDT
Dear Martina,
Thank you for contacting Addgene. Per our copyright terms you are welcome to use any information and figures from our website or blog for informational, non-commercial use.
To cite content on Addgene's website:
"Source: www.addgene.org, accessed [Date]."
To cite content on Addgene's blog:
"Author. “Article Title.” URL. Posted [Date]. Accessed [Date]."
To cite our eBooks:

Addgene. "CRISPR 101: A Desktop Resource." https://info.addgene.org/download-addgenes-ebook-crispr-101-3rd-edition. Posted January 2021. Accessed [Date].
Addgene. "Fluorescent Proteins 101: A Desktop Resource." http://info.addgene.org/download-addgenes-fluorescent-proteins-101-ebook Posted August 2017. Accessed [Date].
Addgene. "Plasmids 101: A Desktop Resource." http://info.addgene.org/download-addgenes-ebook-plasmids-101-3rd-edition Posted March 2017. Accessed [Date].

To cite the use of SnapGene generated plasmid maps:
"Image generated by SnapGene software (from GSL Biotech; available at snapgene.com)"
Please let me know if I can be of any further assistance!
Best Regards,
Ashley
</td>
</tr>
</table>

Figure 3-13	License Number: 5593690598767 License date: Jul 21, 2023 Licensed Content Publisher: Springer Nature Licensed Content Publication: Nature Reviews Molecular Cell Biology Licensed Content Title: Pathways of clathrin-independent endocytosis Licensed Content Author: Satyajit Mayor et al Licensed Content Date: Dec 31, 1969 Type of Use: Thesis/Dissertation Requestor type: academic/university or research institute Format: print and electronic Portion: figures/tables/illustrations Number of figures/tables/illustrations: 1 Will you be translating?: no Circulation/distribution: 1 - 29 Author of this Springer Nature content: no Title: Engineering smart biomimetic nanocarriers for biological application Institution name: University of Santiago de Compostela Expected presentation date: Oct 2023 Portions: Figure 1 Requestor Location: Ms. Martina Migliavacca Rua Jenaro de la Fuente s/n Santiago de Compostela, 15782 Spain Attn: Ms. Martina Migliavacca Total: **0.00 EUR**
Figure 3-24	License Number: 5594140322220 License date: Jul 22, 2023 Licensed Content Publisher: Elsevier Licensed Content Publication: Elsevier Books Licensed Content Title: Advances in Virus Research Licensed Content Author: Paul S. Masters Licensed Content Date: Jan 1, 2006 Licensed Content Pages: 100 Type of Use: reuse in a thesis/dissertation Portion: figures/tables/illustrations Number of figures/tables/illustrations: 1 Format: both print and electronic Are you the author of this Elsevier chapter?: No Will you be translating?: No Title: Engineering smart biomimetic nanocarriers for biological application Institution name: University of Santiago de Compostela Expected presentation date: Oct 2023 Portions: Figure 1 Requestor Location: Ms. Martina Migliavacca Rua Jenaro de la Fuente s/n Santiago de Compostela, 15782 Spain Attn: Ms. Martina Migliavacca Publisher Tax ID: GB 494 6272 12 Total: **0.00 EUR**
Figure 3-24	CCC RightsLink — Home · Help · Live Chat · Sign in · Create Account Sage **Probing the Structure of the Sars Coronavirus Using Scanning Electron Microscopy** **Author:** Yun Lin, Xiyun Yan, Wuchun Cao, Chaoying Wang, et al. **Publication:** Antiviral Therapy **Publisher:** SAGE Publications **Date:** 2004-02-01 *Copyright © 2004, © SAGE Publications* **Gratis Reuse** Permission is granted at no cost for use of content in a Master's Thesis and/or Doctoral Dissertation, subject to the following limitations. You may use a single excerpt or up to 3 figures tables. If you use more than those limits, or intend to distribute or sell your Master's Thesis/Doctoral Dissertation to the general public through print or website publication, please return to the previous page and select 'Republish in a Book/Journal' or 'Post on intranet/password-protected website' to complete your request. BACK · CLOSE WINDOW

Figure 3-42

CCC | RightsLink

? Help | Live Chat

The multifaceted role of plasminogen in inflammation

Author: Beate Heissig,Yousef Salama,Satoshi Takahashi,Taro Osada,Koichi Hattori
Publication: Cellular Signalling
Publisher: Elsevier
Date: November 2020

© 2020 The Authors. Published by Elsevier Inc.

Creative Commons

This is an open access article distributed under the terms of the Creative Commons CC-BY license, which permits unrestricted use, distribution, and reproduction in any medium, provided the original work is properly cited.

You are not required to obtain permission to reuse this article.

To request permission for a type of use not listed, please contact Elsevier Global Rights Department.

Are you the author of this Elsevier journal article?

Figure 3-57

Dear Ms. Martina Migliavacca,

Good evening!

We hereby grant you permission to reprint the material below at no charge in your thesis subject to the following conditions:

RE: Development of CRISPR as an Antiviral Strategy to Combat SARS-CoV-2 and Influenza, Cell, Volume 181, Issue 4, 14 May 2020, Pages 865-876.e12, 1 Figure.

Proposed use: Thesis/Dissertation.

1. If any part of the material to be used (for example, figures) has appeared in our publication with credit or acknowledgement to another source, permission must also be sought from that source. If such permission is not obtained then that material may not be included in your publication/copies.

2. Suitable acknowledgment to the source must be made, either as a footnote or in a reference list at the end of your publication, as follows:
"This article was published in Publication title, Vol number, Author(s), Title of article, Page Nos, Copyright Elsevier (or appropriate Society name) (Year)."

3. Your thesis may be submitted to your institution in either print or electronic form.

4. Reproduction of this material is confined to the purpose for which permission is hereby given

5. This permission is granted for non-exclusive world English rights only. For other languages please reapply separately for each one required. Permission excludes use in an electronic form other than submission. Should you have a

specific electronic project in mind please reapply for permission.

6. Should your thesis be published commercially, please reapply for permission.

This includes permission for the Library and Archives of Canada to supply single copies, on demand, of the complete thesis. Should your thesis be published commercially, please reapply for permission- Canada
This includes permission for UMI to supply single copies, on demand, of the complete thesis. Should your thesis be published commercially, please reapply for permission-ROW

7. Posting of the full article online is not permitted. You may post an abstract with a link to the Elsevier website www.elsevier.com, or to the article on ScienceDirect if it is available on that platform.

8. Article can used be in the University library if it is embedded in the thesis and not used commercially.

Best wishes on your thesis!

Kind regards,

Thomas Rexson Yesudoss
Copyrights Specialist
ELSEVIER | HCM - Health Content Management

Visit Elsevier Permissions

Figure 3-58	**MDPI Open Access Information and Policy** All articles published by MDPI are made immediately available worldwide under an open access license. This means: • everyone has free and unlimited access to the full-text of *all* articles published in MDPI journals; • everyone is free to re-use the published material if proper accreditation/citation of the original publication is given; • open access publication is supported by the authors' institutes or research funding agencies by payment of a comparatively low **Article Processing Charge (APC)** for accepted articles. **Permissions** No special permission is required to reuse all or part of article published by MDPI, including figures and tables. For articles published under an open access Creative Common CC BY license, any part of the article may be reused without permission provided that the original article is clearly cited. Reuse of an article does not imply endorsement by the authors or MDPI.

TABLES: RIGHTS AND PERMISSIONS	
Table 3-18	**MDPI Open Access Information and Policy** All articles published by MDPI are made immediately available worldwide under an open access license. This means: • everyone has free and unlimited access to the full-text of *all* articles published in MDPI journals; • everyone is free to re-use the published material if proper accreditation/citation of the original publication is given; • open access publication is supported by the authors' institutes or research funding agencies by payment of a comparatively low **Article Processing Charge (APC)** for accepted articles. **Permissions** No special permission is required to reuse all or part of article published by MDPI, including figures and tables. For articles published under an open access Creative Common CC BY license, any part of the article may be reused without permission provided that the original article is clearly cited. Reuse of an article does not imply endorsement by the authors or MDPI.

Appendix IV: All the other images, tables, and figures

Martina Migliavacca, the doctoral candidate, declares that all the other images, tables, and figures shown in this Doctoral Thesis have been personally elaborated.

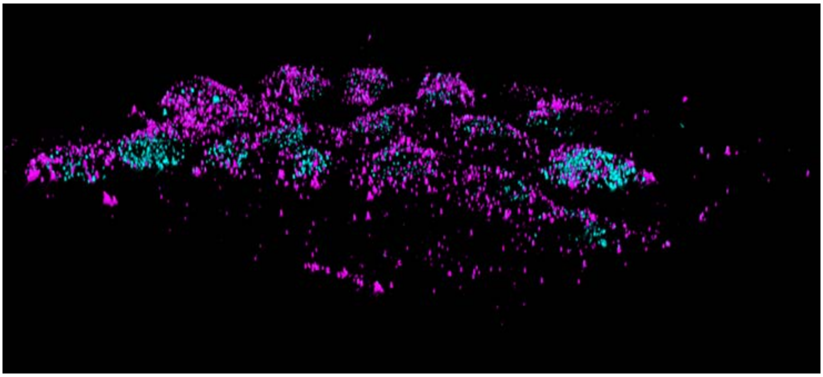

The experimental results presented in this Doctoral Thesis shed light on the versatility and promising potential of cell-derived nanovesicles as a novel platform for addressing key challenges in modern medicine, ranging from targeted drug delivery to gene therapy. The exploration of cellsomes' biomimetic properties has demonstrated their capacity as innovative nanocarriers for molecules and drugs, as well as advanced biomimetic coating for other types of nanoparticles, capitalizing both on their tissue-specific targeting capabilities and on the possibility to engineer these nanocarriers to enhance the intracellular delivery.